University of Alberta
Department of Civil &
Environmental Engineering

Shear Lag in Bolted Cold-Formed Steel Angles and Channels in Tension

by

Amy Sin-Man Yip

and

J.J.R. Cheng

September, 2000

Shear Lab in Bolted Cold-Formed Steel Angles and Channels in Tension

by

Amy Sin-Man Yip

and

J.J. Roger Cheng

Structural Engineering Report 133

Department of Civil and Environmental Engineering
University of Alberta
Edmonton, Alberta, Canada

September 2000

ABSTRACT

Highly non-uniform stresses will be generated near the connection of a tension member when the member is not connected through all of the elements of the cross section. Thus, the whole cross-section may not be fully utilized, which causes a reduction in the net section efficiency. This loss of efficiency of the section is termed as "shear lag". This phenomenon has been studied extensively and design provisions are available in most of the steel design standards. However, most of these researches, on which the current design standards are based, used hot-rolled steel sections. There is relatively little information available about the shear lag effects in the design of cold-formed tension members, which are more slender than hot-rolled sections. An investigation was therefore undertaken to study the shear lag effect in angle and channel cold-formed tension members with bolted connection.

An experimental program, consisting of 23 angle and channel specimens, was conducted to study the shear lag effect. The connection length and cross sectional geometry are two major parameters studied in the program. With the test results, the net section efficiency and the behavior of the specimens were discussed. Finite element method was used to model and analyze the test specimens. A good correlation between the numerical results and test results was found. A parametric study was also set up using the developed finite element models to investigate the factors affecting the net section efficiency of angle and channel sections.

With the results obtained from the parametric study, it was concluded that the current design equations give inconsistent predictions on the net section efficiency of cold-formed tension members. It was found that the net section efficiency does not only depend on the connection length and eccentricity, but also the flat width-to- thickness and flat width-to-bolt diameter ratios. Based on this observation, new net section efficiency equations were developed using non-linear regression analysis for both angle and channel sections. It is shown that the prediction calculated by the formulae is in good agreement with the available test data. A design recommendation for cold-formed tension members has also been developed based on the formulae proposed.

TABLE OF CONTENTS

LIST OF TABLES

LIST OF FIGURES

LIST OF SYMBOLS

A	cross-sectional area of the tension coupon at rupture
A_0	initial cross-sectional area of the tension coupon
A_c	net cross-sectional area of the connected leg
A_g	gross area of cross-section
A_{gv}	gross shear area
A_{gt}	gross tension area
A_{nv}	net shear area
A_{nt}	net tension area
A_n	net area of cross-section
A_{ne}	effective net area of cross-section
A'_{ne}	effective net cross-sectional area accounting for shear lag
A_u	gross cross-sectional area of the unconnected leg
b'	width of the flange
B	width of the flange for channel/unconnected leg for angle
B_r	factored bearing capacity
Bl_r	factored block shear resistance
C	constant for bearing resistance
d	diameter of the bolt hole
d_1, d_2	location of strain gauges
D	depth of the section
E_{ave}	average modulus of elasticity obtained from the tension coupons at the flat portions
F_{ub}	tensile strength of the material in bearing
F_p	nominal bearing stress
F_u	ultimate tensile strength of the material
F_y	yield strength of the material
k	ratio of A_c to A_u
K_1	ductility factor
K_2	fabrication factor

K_3	geometry factor
K_4	shear lag factor
L	connection length
L'	distance from the point of loading to the innermost bolt
L_c	width of the connected leg
L_e	distance along the line of force from the edge of the connected part to the center of a standard hole
L_n	failure path length normal to force
L_o	width of the unconnected leg
L_s	failure path length parallel to force (ie, in shear)
m	number of holes across the connected leg
m'	number of holes across the web
n	number of bolts per line
P	maximum load obtained from the coarse or intermediate mesh model
P_{AISI}	net section capacity of the member calculated based on AISI Specification
P_{AISC}	net section capacity of the member calculated based on AISC Specification
P_b	predicted bearing capacity of the member
P_{block}	predicted block shear capacity of the member
P_f	maximum load obtained from the fine mesh model
P_{FEA}	maximum load obtained from the finite element analysis
P_{net}	net section tensile strength of the member
P_{pred}	predicted capacity of the member
P_{S136}	net section capacity of the member calculated based on CSA-S136-94
$P_{S16.1}$	net section capacity of the member calculated based on CSA-S16.1-94
P_{Test}	dynamic ultimate strength of the test
P_u	ultimate capacity of the member
P_{UMR}	net section capacity of the member calculated based on the equations suggested by University of Missouri-Rolla
Q	percent reduction in the area of a standard test coupon (51 mm gauge length)
r	force transmitted by the bolt or bolts at the section considered, divided by the tension force in the member at that section

R	inner corner radius
R^2	coefficient of determination
RD	relative difference in maximum load
s	distance along the line of force between centers of holes
s'	spacing of bolts perpendicular to the line of stress
t	thickness of the section
T_r	factored tensile resistance of the member
U	net section efficiency, reduction factor
w	flat width of the section
$\bar{x}$	eccentricity, distance from the face of the connection to the center of gravity of the member
β	factor that accounts for the effect of connection length
$\Delta P/\Delta \varepsilon$	the slope of the Load-Deformation curve for the tension coupon at the corner
ϕ	resistance factor
ϕ_u	tensile fracture resistance factor
ϕ_{ub}	resistance factor for bolts in bearing-type connections

1. INTRODUCTION

1.1 General

Tension members are frequently used in fabricated steel structures. Common uses for tension members are in bracing members, chords and web members of trusses, hangers for floors and roofs, and in other similar applications. The most widely used structural shapes are the angle section and the channel section. For practical reasons, it is unusual to connect the entire cross-section at the connections. As a result, highly non-uniform stresses will be generated near the connection and this can cause localized yielding in parts of the cross-section. Thus, the whole cross-section may not be fully utilized which causes a reduction in the net section efficiency. This behavior of loss of efficiency of the section is termed "shear lag".

Generally, the ratio of the ultimate capacity to the net section tensile strength of the member is used to evaluate the efficiency of a cross-section. When fasteners are used, this ratio is referred to as net section efficiency (U). Thus, for the case under examination, the net section efficiency is:

$$U = \frac{P_u}{P_{net}} \qquad [1.1]$$

where P_u = ultimate capacity of the member

P_{net} = net section tensile strength of the member

= $A_n F_u$

A_n = net area of cross-section =gross area − hole area

F_u = tensile strength of the material

1

1.2 Statement of the Problem

Most design provisions, including Canadian Standard CAN/CSA-S16.1-94 (1994) for fabricated steel tension members, are based on the work done by Munse and Chesson (1963) and subsequent work that was performed in an attempt to simplify the design procedure. However, the work of Munse and Chesson and subsequent work on shear lag effect in tension members made use of hot-rolled steel sections, which are much more stocky than cold-formed steel sections. Therefore, these results may not be applicable to cold-formed steel members in tension.

In the current CSA-S136-94 (1994) Standard, Cold-Formed Steel Structural Members, the method proposed by Marsh (1969) is used to consider shear lag effects in designing cold-formed tension members. This method considers a partially connected tension member as an eccentrically loaded member; however, it does not consider the geometry of the bolted connection and does not make any distinction between bolted and welded connections. Therefore, more information from both physical tests and numerical analyses of cold-formed steel tension members having different types of end connections is desirable. Thus, there is a need to conduct research on the shear lag effect in cold-formed angles and channels in tension.

1.3 Objectives

The objectives of this program are to:

1. Conduct physical tests of single angle and channel tension members in order to examine the shear lag effect;

2

2. Expand the data base of test results on cold-formed tensile steel member with bolted connection;

3. Examine the validity of the current design criteria for cold-formed steel members in tension;

4. Develop finite element models that can be used in future studies to obtain the capacity of single angles and channels numerically;

5. Propose design criteria for cold-formed steel members in tension.

1.4 Methodology Used in the Research

In order to investigate the shear lag effect on bolted cold-formed tension members, an experimental program, which consists of three different sizes of unstiffened cold-formed angles and channels with various connection lengths, was first conducted. Based on the test results, finite element method would be applied to model and analyze the test specimens under tension. A parametric study was then conducted using the validated finite element models. With the results obtained from the parametric study, new net section efficiency equations for both angle and channel sections were developed using non-linear regression analysis, and design recommendations for cold-formed tension members were proposed.

1.5 Outline of the Thesis

Chapter 2 presents of a literature review on the net section efficiency of bolted tension members. The review includes research done on hot-rolled and cold-formed steel sections. The design specifications currently used for both hot-rolled and cold-formed

3

steel members in tension are also listed. Chapter 3 contains a description of the experimental program in which specimen description, instrumentation, test set-up and procedures are described. Chapter 4 presents the results of the test program. The finite element method is used in Chapter 5 to predict the test results. Chapter 6 presents a parametric study performed using the finite element model developed in Chapter 5. Based on the results of the parametric study and non-linear regression analysis, design equations for cold-formed steel tension members are proposed and design provisions are developed. Finally, the summary, conclusions and recommendations are presented in Chapter 7.

2. LITERATURE REVIEW

2.1 Previous Studies on Shear Lag of Tension Members

In 1906 and 1907, McKibben tested 18 single angle sections with various types of end connections. The net section efficiencies obtained in these tests ranged from 75 to 83 percent, with a mean of 80 percent. In 1935, Young studied the results obtained by McKibben and proposed the net section efficiency (U) for a single angle member to be calculated as:

$$U = 1.0 - 0.18 \frac{L_o}{L_c} \qquad [2.1]$$

where L_c = width of the connected leg

   L_o = width of the unconnected leg

Nelson conducted an experiment using 18 single angles connected at their ends by bolts in 1953. Both equal and unequal leg angles were tested. For the angles with unequal legs, both connecting to the long leg and connecting to the short leg were studied. The net section efficiencies found in these tests ranged from 64 to 84 percent with a mean of 75 percent. Besides the number of bolts per line used, Nelson found that the ratio of unconnected leg area to connected leg net area was also a factor that would affect the efficiency of the angle section. Based on these test results, he proposed an empirical equation for the net section efficiency that took the following form:

$$U = \frac{1}{1 + \dfrac{k}{n}} \qquad [2.2]$$

where n = number of bolts per line

$$k = \frac{A_u}{A_c}$$

A_u = gross cross-sectional area of the unconnected leg

A_c = net cross-sectional area of the connected leg

In 1963, Munse and Chesson investigated a wide range of truss-type tension members using both test results obtained from their own experiments and from others. The parameters studied included different cross-sectional configurations, connections, materials, and fabrication methods. Both riveted and bolted connections were examined. An empirical equation to calculate the net section efficiency was proposed.

Munse and Chesson found that the net section efficiency of tension members with bolted or riveted end connections was a function of a number of factors and it can be expressed as follows:

$$A_{ne} = K_1 K_2 K_3 K_4 A_n \qquad\qquad [2.3]$$

where A_{ne} = effective net area of cross-section

A_n = net area of cross-section

K_1 = 0.82 + 0.0032Q < 1 (Q is described below)

K_2 = 0.85 for members with punched holes

= 1.0 for members with drilled holes

$$K_3 = 1.6 - 0.7\frac{A_n}{A_g}$$

A_g = gross area of cross-section

6

$$K_4 = 1 - \frac{\overline{x}}{L} \quad (\overline{x} \text{ and } L \text{ are described in the following})$$

K_1 is the factor that accounts for the ductility of material, in which, the term Q is the percent reduction in the area at rupture of a standard tensile test coupon (51 mm gauge length). K_2 is the fabrication factor that accounts for the reduction in efficiency due to the effect of punching the holes. K_3 is a geometry factor that accounts for the effect of hole spacing on the connection. Finally, K_4 is the shear lag factor. This factor takes into account both the eccentricity in the connected part and the connection length. In the expression for K_4, $\overline{x}$ refers to the distance from the face of the connection to the center of gravity of the member, and L represents the connection length and is taken as the distance between extreme fasteners.

In 1969, the influence of the edge distance and the end distance on net section efficiency was investigated by Kennedy and Sinclair. In this investigation, 721 single angle, single bolted connections were tested. In order to simulate the fabrication of members in field conditions, all the specimens were cut to length by shearing and all holes were punched. The test results showed that minimum edge and end distances were required to develop the yield strength of the cross-section.

A series of tests on single angle members in tension and compression were conducted by Marsh in 1969. The effects of plastic behavior were studied during ultimate loading of the sections. Marsh stated that as the extreme fibres of the section yield, the line of action of the load would move, as well as the eccentricity. Based on

7

these observations, he proposed that the net effective area (A_{ne}) could be calculated as follows:

$$A_{ne} = \frac{(L_c^2 + L_o t)t}{L_c - 0.04L'} - dt$$ [2.4]

where L_c = width of the connected leg

L_o = width of the unconnected leg

t = thickness of the section

L' = distance from the point of loading to the innermost bolt

d = diameter of the bolt hole

For unequal leg angles, this formula gives a good prediction if the long leg is connected. However, the prediction is rather optimistic if the short leg is connected.

In 1993, an experimental program was conducted by Wu and Kulak to investigate the shear lag effect on single and double angle tension members. The parameters studied included:

- Length of the member;

- Length of the connection;

- Size and disposition of the cross-section, including angle thickness and whether the long or short leg is connected;

- Out-of-plane stiffness of the gusset plate for the single angle cases.

Based on the test results, the following design formula was proposed:

$$T_r = 0.85\phi(F_u A_c + \beta F_y A_u)$$ [2.5]

where T_r = factored resistance of the member

8

$\phi = 0.90$

F_u = ultimate tensile strength of the material

F_y = yield strength of the material

A_c = net area of the connected leg at the critical cross-section, computed by taking

the diameter of holes 2 mm larger than the nominal size if the holes are

punched

A_u = gross area of the connected leg

$\beta = 1.0$ for members with four or more transverse lines of fasteners

$= 0.5$ for members with fewer than four transverse lines of fasteners

Alternatively, as a convenience in the design process, a simplified equation was

also proposed and is stated as follows:

$$A_{ne} = UA_n \qquad [2.6]$$

and
$$T_r = 0.85\phi F_u A_{ne} \qquad [2.7]$$

where $U = 0.80$ if the connection has four or more fasteners per line

$= 0.60$ if the connection has fewer than four fasteners per line

A_n = net area of the critical cross-section, calculated by taking the hole diameter

2 mm larger than the nominal size if the holes are punched

2.2 Specific Studies on Cold-Formed Tension Steel Members

Since 1950, Winter conducted a series of tests on cold-formed steel with bolted

connections and the tests were mainly focused on the flat sheet connections with washers.

Based on his findings, he derived empirical relationships to predict the ultimate capacity

9

and mode of failure for bolted connections. Four basic types of failure modes, as shown in Fig. 2.1, were identified as follows:

1. Longitudinal shearing (block shear failure) of the sheet (Fig. 2.1a)

2. Bearing failure, leading to a visible bulge in front of the bolt or bolts (Fig. 2.1b)

3. Net section fracture (Fig. 2.1c)

4. Bolt shear fracture (Fig. 2.1d)

In 1975, Chong and Matlock studied the strength of bolted connections without washers in cold-formed steel sheets. The procedures they used followed closely to those being used by Winter. In their test results, they observed the same four types of failure modes described by Winter. They also derived relationships in the same format as Winter for the ultimate capacity for the bolted connections without washers.

In 1993, an experimental and analytical study was initiated by La-Boube and Yu at the University of Missouri-Rolla to expand the knowledge and understanding of the behavior of cold-formed steel bolted connections. This research consisted of two parts. The first part concentrated on the tensile capacity, bearing capacity and the interaction of tension and bearing capacities of flat sheet cold-formed steel bolted connections. For the specimens that failed in bearing, the results showed that the AISI specification was a good predictor of the ultimate strength while the AISC specification was not. For the specimens that failed in net section, both the AISI and AISC specifications were deemed to be good predictors. In the second part, the tensile capacity and bearing capacity of

bolted connections of flat sheet, angle and channel cold-formed steel members were addressed. For the angle and channel sections that failed by net section fracture, the studies showed that the current AISC specification formulation for addressing the influence of shear lag is unacceptable for cold-formed steel connections. Based on the tests results, the equations that could estimate the degrading influence of shear lag on the tensile capacity of bolted connections were derived for cold-formed angle and channel cold-formed sections and are stated as follows:

(i)   for angle sections

$$U = 1 - 1.2\frac{\overline{x}}{L} \leq 0.9 \qquad \text{but} \geq 0.4 \qquad [2.8]$$

(ii)   for channel sections

$$U = 1 - 0.357\frac{\overline{x}}{L} \leq 0.9 \qquad \text{but} \geq 0.5 \qquad [2.9]$$

where U = net section efficiency

$\overline{x}$ = distance from the face of the connection to the center of gravity of the member

L = connection length

Between 1994 and 1998, a total of eighteen tests were conducted by Cheng *et al.* at the University of Alberta to study the shear lag effects on bolted cold-formed sections in tension. Among those cold-formed steel tests, there were seven unstiffened angles, five stiffened angles, and six unstiffened channels. Test results showed that the shear lag effects must be considered in the design of bolted cold-formed steel angles in tension

11

while the shear lag effect is negligible for channel sections. The results also showed that the stiffener has no effect on the net section efficiency.

2.3 Current Design Specifications

2.3.1 American Iron and Steel Institute (AISI, 1996)

2.3.1.1 <u>Tensile Strength</u>

According to the specification, the tensile resistance of the net section connected by fasteners shall be the lesser of:

(i) $T_r = \phi A_n F_y$ [2.10]

$\phi = 0.95$

(ii)   When washers are provided under both the bolt head and the nut

$T_r = \phi(1.0 - 0.9r + 3rd/s') F_u A_n \leq \phi F_u A_n$ [2.11]

$\phi = 0.65$ for double shear

$\phi = 0.55$ for single shear

(iii)   Either washers are not provided under the bolt head and nut, or only one

washer is provided under either the bolt head or nut

$T_r = \phi(1.0 - r + 2.5rd/s') F_u A_n \leq \phi F_u A_n$ [2.12]

$\phi = 0.65$

where A_n = net area of the connected part

r = force transmitted by the bolt or bolts at the section considered,

divided by the tension force in the member at that section. If r

is less than 0.2, it shall be permitted to be taken equal to zero

s' = spacing of bolts perpendicular to the line of stress; in the case

of a single bolt, s = gross width of sheet

d = diameter of bolt hole

F_y = yield strength of the material

F_u = ultimate tensile strength of the material

2.3.1.2 <u>Bearing Capacity</u>

The factored bearing capacity, B_r, of a bolted section shall be taken as:

$$B_r = \phi dt F_p \qquad [2.13]$$

where d = diameter of bolt hole

t = thickness of the section

F_p = nominal bearing stress as given in Tables 2.1 and 2.2

ϕ = resistance factor, given in Tables 2.1 and 2.2

2.3.2 American Institute of Steel Construction (AISC, 1993)

2.3.2.1 <u>Tensile Strength</u>

This specification indicates that for fracture in the net section, the factored tensile strength shall be the lesser of the followings:

(i) $T_r = \phi F_y A_g$ $\qquad [2.14]$

(ii) $T_r = \phi_u F_u A_{ne}$ $\qquad [2.15]$

where T_r = factored tensile resistance

F_y = yield strength of the material

F_u = ultimate tensile strength of material

A_g = gross cross-sectional area

A_{ne} = effective net area = UA_n

A_n = net area of the specimen

U = reduction coefficient

ϕ = 0.90

ϕ_u = 0.75

In the Eqn. 2.15, the reduction coefficient varies depending on the type of member and the number of bolts in the connection. According to the 1993 AISC Commentary, the reduction coefficient shall be taken as follows:

(a) for connections with two bolts in the line of stress,

$$U = 0.75$$

(b) for connections with three bolts in the line of stress,

$$U = 0.85$$

However, the specification makes no provision for members connected with only one bolt. In addition, the 1993 specification introduced the following calculation of the reduction coefficient U:

$$U = 1 - \overline{X}/L \leq 0.9 \qquad [2.16]$$

where $\overline{X}$ = connection eccentricity

L = length of the connection parallel to the line of stress

2.3.2.2 Bearing Capacity

According to Section J3.10, the factored bearing strength, B_r, at bolt holes shall be taken as follows:

(i) When $L_e \geq 1.5d$ and $s \geq 3d$ and there are two or more bolts in line of stress:

    a) when deformation around the bolt holes is a design consideration

$$B_r = 2.4\phi dtF_u \qquad [2.17]$$

    b) when deformation around the bolt holes is not a design consideration

        (1) for the bolt nearest the edge

$$B_r = \phi L_e t F_u \leq 3.0\phi dtF_u \qquad [2.18]$$

        (2) for the remaining bolts

$$B_r = \phi(s-0.5d)tF_u \leq 3.0\phi dtF_u \qquad [2.19]$$

(ii) When $L_e < 1.5d$ and $s < 3d$ or for a single bolt in the line of force:

    (1) for a single bolt hole or the bolt nearest the edge when there are two or more bolt holes in the line of force

$$B_r = \phi L_e t F_u \leq 2.4\phi dtF_u \qquad [2.20]$$

    (2) for the remaining bolts

$$B_r = \phi(s-0.5d)tF_u \leq 2.4\phi dtF_u \qquad [2.21]$$

where L_e = distance along the line of force from the edge of the connected part to the center of a standard hole

      s = distance along the line of force between centers of standard holes

      d = diameter of bolt hole

      F_u = ultimate strength of the material

      t = material thickness

ϕ = resistance factor, taken as 0.75

2.3.2.3 Block Shear

The block shear strength is determined by the sum of the shear strength on a failure path parallel to the force direction and the tensile strength on a perpendicular segment. When tensile strength on the net section is used to determine the resistance on one segment, yielding on the gross section shall be used on the perpendicular segment. The factored block shear resistance, Bl_r, shall be determined as follows:

(i)   when $F_uA_{nt} > 0.6F_uA_{nv}$

$$Bl_r = \phi[0.6F_yA_{gv} + F_uA_{nt}]$$ [2.22]

(ii)   when $0.6F_uA_{nv} > F_uA_{nt}$

$$Bl_r = \phi[0.6F_uA_{nv} + F_yA_{gt}]$$ [2.23]

where A_{gv} = gross shear area

A_{gt} = gross tension area

A_{nv} = net area subject to shear

A_{nt} = net area subject to tension

F_y = yield strength of the material

F_u = ultimate tensile strength of the material

ϕ = resistance factor, taken as 0.75

2.3.3 CSA Standard S16.1-94

2.3.3.1 <u>Tensile Strength</u>

The factored resistance of a tension member, T_r, developed by a member subjected to an axial tensile force shall be taken as the lesser of:

(i) $\quad T_r = \phi A_g F_y$ [2.24]

(ii) $\quad T_r = 0.85 \phi A_{ne} F_u$ [2.25]

(iii) $\quad T_r = 0.85 \phi A'_{ne} F_u$ [2.26]

where T_r = factored tensile resistance

ϕ = resistance factor, taken as 0.9 for tension members

A_g = gross cross-sectional area

A_{ne} = effective net area

A'_{ne} = effective net cross-sectional area accounting for shear lag

F_y = yield strength of the material

F_u = ultimate strength of the material

The first equation is based on the yield strength of the gross section and the rest are based on the ultimate tensile strength of the effective net section of the member. In the case where the member capacity is governed by the net section rupture, there is the additional multiplier of 0.85 to the regular reduction factor of 0.9. This additional multiplier is to increase the safety index for this mode of failure because it was found that in the case where the net section fractures before the gross section yields, failure occurs with little deformation and little warning.

In the equation (iii) stated above, the effective net area of the section is reduced to account for the effect of shear lag. According to Clause 12.3.3.2 (b) and (c), the reduced effective net area shall be taken as follows:

(a) for angles connected by only one leg with

(i) four or more transverse lines of fasteners,

$$A'_{ne} = 0.8 \ A_{ne}$$

(ii) fewer than four transverse lines of fasteners,

$$A'_{ne} = 0.60 \ A_{ne}$$

(b) for structural shapes other than I shapes, shapes made from I shapes, and angle sections connected with

(i) three or more transverse lines of fasteners:

$$A'_{ne} = 0.85 \ A_{ne} \ \text{or}$$

(ii) with two transverse lines of fasteners:

$$A'_{ne} = 0.75 \ A_{ne}$$

2.3.3.2 Bearing Capacity

The factored bearing resistance of a member with bolted connections shall be taken as:

$$B_r = 3\phi_b tdnF_u \qquad [2.27]$$

where t = material thickness

d = diameter of bolt hole

n = number of bolts in the connection

F_u = ultimate tensile strength of the material

ϕ_{ub} = performance factor for bolts in bearing-type connections, taken as 0.67

2.3.3.3 Block Shear

The factored block shear strength, Bl_r, of a member shall be calculated as:

$$Bl_r = 0.85\phi_u[0.6L_s + L_n]tF_u \qquad [2.28]$$

where L_s = failure path length parallel to force (ie, in shear)

L_n = failure path length normal to force

F_u = ultimate strength of the material

ϕ_u = tensile fracture resistance factor, taken as 0.75

2.3.4 CSA Standard S136-94

2.3.4.1 Tensile Strength

For single angles with unstiffened legs connected by fasteners in one leg, the tensile resistance shall be the lesser of:

(i) $T_r = \phi A_g F_y$ [2.29]

(ii) $T_r = \phi_u[A_g - (0.7L_o + md)t]F_u$ [2.30]

where L_o = width of unconnected leg

d = diameter of bolt hole

m = number of holes across the connected leg

ϕ = resistance factor for tension member, taken as 0.90

ϕ_u = tensile fracture resistance factor, taken as 0.75

For single channels with unstiffened flanges connected by fasteners in the web, the tensile resistance shall be the lesser of:

(i) $T_r = \phi A_g F_y$ [2.31]

(ii) $T_r = \phi_u[A_g - (b' + m'd)t]F_u$ [2.32]

where b' = width of the flange

d = diameter of bolt hole

m' = number of holes across the web

ϕ_u = tensile fracture resistance factor, taken as 0.75

2.3.4.2 Bearing Capacity

In addition to the above criteria, the failure by load bearing around the bolts should also be considered. The bearing capacity of a member is given as:

$B_r = \phi_u C t d n F_u$ [2.33]

where C = a constant, which is a function of the material thickness

= 3   if $d/t \leq 10$

= 30t/d   if $10 < d/t < 15$

= 2   if $d/t \geq 15$

t = material thickness

d = diameter of the bolt hole

n = number of bolts in the connection

F_u = tensile strength of the material in bearing

ϕ_u = performance factor for tensile strength, taken as 0.75

20

2.3.4.3 Block Shear

According to Clause 6.3.1 in S136-94, the block shear strength of a member with single line of bolt is given as:

$$BL_r = \phi_u[0.6L_s + L_n]tF_u \qquad [2.34]$$

where t = material thickness

L_s = net failure path length parallel to force (ie, in shear)

L_n = net failure path length normal to force

F_u = specified minimum ultimate tensile strength

ϕ_u = tensile fracture resistance factor, taken as 0.75

2.4 Comparison of Previous Test Results with Current Specifications

In this section, the test data on bolted cold-formed tension members obtained by the other researchers are compared with the current Specifications and net section efficiency equations proposed by La-Boube and Yu (Equation 2.8 and 2.9). The sources of the test data for angle and channel sections can be seen in Tables 2.3 and 2.4, respectively. Only the specimens that were associated with the net section failure mode are included since this mode of failure is more critical. Angle and channel members bolted through both flanges have been excluded. The resistance factors used in those Specifications were taken as unity in this comparison. As can be seen, none of the specifications can predict the net section efficiency of angle and channel sections accurately; therefore, this project was conducted to investigate the net section efficiency in cold-formed tension members.

21

Table 2.1 Nominal Bearing Stress for Bolted Connections with Washers under Both Bolt Head and Nut

Thickness of connected part, t [mm]	Type of Joint	F_u/F_y ratio of connected part	ϕ	Nominal bearing stress, F_p
0.61 ≤ t < 4.76	Inside sheet of double shear connection	≥ 1.08	0.55	3.33 F_u
		<1.08	0.65	3.00 F_u
	Single shear and outside sheets of double shear connection	No limit	0.60	3.00 F_u
t ≥ 4.76	See AISC Specifications			

Table 2.2 Nominal Bearing Stress for Bolted Connections without Washers Under Both Bolt Head and Nut, or With Only One Washer

Thickness of connected part, t [mm]	Type of joint	F_u/F_y ratio of connected part	ϕ	Nominal bearing stress, F_p
0.61< t < 4.76	Inside sheet of double shear connection	≥ 1.08	0.65	3.00 F_u
	Single shear and outside sheets of double shear connection	≥ 1.08	0.70	2.22 F_u
t ≥ 4.76	See AISC Specifications			

22

Table 2.3 Comparison of Others' Test Results with Current Specifications for Angle Sections

Data Source	Specimen	Size [mm x mm x mm]	No. of bolts	Bolt Dia [mm]	$\bar{x}$ [mm]	L [mm]	P_{max} [kN]	P_{max}/P_{AISI}	P_{max}/P_{AISC}	$P_{max}/P_{S16.1}$	P_{max}/P_{S136}	P_{max}/P_{UMR}
University of Alberta (1997)	12-2	102x102x2.657	2	19.1	26.8	95.5	135.8	0.76	0.77	0.93	0.91	0.84
	12-3	102x102x2.657	3	19.1	26.8	191	154.7	0.77	0.74	1.05	1.03	0.76
	12-4	102x102x2.657	3	19.1	26.8	191	158.3	0.79	0.75	1.08	1.06	0.78
	14-2	50.8x50.8x1.897	2	15.9	13.6	63.3	35.7	0.80	0.91	1.19	1.22	0.96
	14-3	50.8x50.8x1.897	3	15.9	13.6	126.6	43.0	0.93	0.96	1.43	1.47	0.99
	16-2	38.1x38.1x1.519	2	12.7	10.3	38.1	20.3	0.78	0.98	1.19	1.23	1.06
	16-3	38.1x38.1x1.519	3	12.7	10.3	76.2	24.4	0.91	0.99	1.43	1.48	1.03
University of Missouri-Rolla, UMR (1995)	LBN11-1	41.3x41.3x1.067	2	12.7	11.1	36.37	15.8	0.68	0.86	1.00	1.03	0.94
	LBN11-2	41.3x41.3x1.067	2	12.7	11.1	36.3	16.2	0.69	0.88	1.02	1.06	0.97
	LBN11-3	41.3x41.3x1.067	2	12.7	11.1	36.47	15.9	0.68	0.87	1.01	1.04	0.95
	LCN11-1	41.3x41.3x1.067	3	12.7	11.1	72.75	19.6	0.80	0.88	1.24	1.28	0.91
	LCN11-2	41.3x41.3x1.067	3	12.7	11.1	72.69	20.0	0.82	0.90	1.26	1.31	0.93
	LCN11-3	41.3x41.3x1.067	3	12.7	11.1	72.69	20.9	0.86	0.94	1.32	1.36	0.97
	LBN12-1	41.3x82.5x1.067	2	12.7	28.7	36.32	17.9	0.47	1.97	0.69	0.89	0.83
	LBN12-2	41.3x82.5x1.067	2	12.7	28.7	36.32	19.3	0.51	2.12	0.75	0.96	0.90
	LBN12-3	41.3x82.5x1.067	2	12.7	28.7	36.32	18.2	0.48	2.00	0.71	0.90	0.85
	LCN12-1	41.3x82.5x1.067	3	12.7	28.6	72.64	21.9	0.55	0.84	0.85	1.08	0.96
	LCN12-2	41.3x82.5x1.067	3	12.7	28.6	72.64	22.8	0.57	0.87	0.88	1.13	1.00
	LBN13-1	41.3x82.5x1.067	2	12.7	7.5	36.4	25.3	0.85	0.74	0.98	0.79	0.78
	LBN13-2	41.3x82.5x1.067	2	12.7	7.51	36.32	24.4	0.82	0.71	0.94	0.76	0.75
	LCN13-1	41.3x82.5x1.067	3	12.7	7.5	72.64	29.8	0.87	0.77	1.15	0.93	0.79
	LCN13-2	41.3x82.5x1.067	3	12.7	7.51	72.59	31.7	0.93	0.82	1.23	0.99	0.84

23

Table 2.3 Comparison of Others' Test Results with Current Specifications for Angle Sections (Continued)

Data Source	Specimen	Size [mm x mm x mm]	No. of bolts	Bolt Dia [mm]	$\bar{x}$ [mm]	L [mm]	P_{max} [kN]	P_{max} / P_{AISI}	P_{max} / P_{AISC}	P_{max} / $P_{S16.1}$	P_{max} / P_{S136}	P_{max} / P_{UMR}
	LBN31-1	41.3x41.3x3.048	2	12.7	12.3	36.42	49.0	0.83	1.11	1.23	1.34	1.24
	LBN31-2	41.3x41.3x3.048	2	12.7	12.3	36.55	48.3	0.82	1.09	1.21	1.32	1.21
	LCN31-1	41.3x41.3x3.048	3	12.7	12.2	73	58.5	0.95	1.05	1.46	1.58	1.09
University	LCN31-2	41.3x41.3x3.048	3	12.7	12.2	72.9	56.7	0.92	1.02	1.41	1.53	1.06
of	LBN32-1	41.3x82.5x3.048	2	12.7	30	36.37	52.0	0.52	2.62	0.77	1.03	0.92
Missouri-	LBN32-2	41.3x82.5x3.048	2	12.7	30	36.53	56.0	0.56	2.77	0.83	1.11	1.00
Rolla,	LCN32-1	41.3x82.5x3.048	3	12.7	30	72.95	62.9	0.61	0.95	0.93	1.25	1.10
UMR	LCN32-2	41.3x82.5x3.048	3	12.7	30	72.95	60.2	0.58	0.91	0.89	1.19	1.05
(1995)	LBN33-1	41.3x82.5x3.048	2	12.7	8.42	36.5	80.9	1.03	0.93	1.19	0.98	0.99
	LBN33-2	41.3x82.5x3.048	2	12.7	8.45	36.37	79.6	1.02	0.92	1.18	0.96	0.98
	LCN33-1	41.3x82.5x3.048	3	12.7	8.48	72.64	88.3	0.99	0.89	1.31	1.08	0.92
	LCN33-2	41.3x82.5x3.048	3	12.7	8.45	72.59	90.9	1.02	0.91	1.35	1.10	0.94

24

Table 2.4 Comparison of Others' Test Results with Current Specifications for Channel Sections

Data Source	Specimen	Size [mm x mm x mm]	No. of bolts	Bolt Dia [mm]	$\bar{x}$ [mm]	L [mm]	P_{max} [kN]	P_{max}/P_{AISI}	P_{max}/P_{AISC}	$P_{max}/P_{S16.1}$	P_{max}/P_{S136}	P_{max}/P_{UMR}
University of Alberta (1998)	C50x2	51.0x31.0x1.803	2	12.7	9.4	38.1	40.1	1.20	1.07	1.07	1.18	0.89
	C50x3	51.0x31.0x1.803	3	12.7	9.4	76.2	48.7	1.46	1.26	1.26	1.43	1.09
	C75x3	76.0x31.0x1.803	3	15.9	7.8	126.6	63.8	1.55	1.34	1.34	1.39	1.15
	C100x3	101.5x31.0x1.803	3	19.1	6.7	191	77.7	1.58	1.36	1.36	1.36	1.17
University Missouri-Rolla, UMR (1995)	CBN11-1	41.3x31.0x1.067	2	12.7	10.3	36.32	24.5	1.15	1.03	0.98	1.16	0.82
	CBN11-2	41.3x31.0x1.067	2	12.7	10.4	36.35	24.2	1.14	1.03	0.98	1.15	0.82
	CCN11-1	41.3x31.0x1.067	3	12.7	10.3	72.75	30.7	1.43	1.22	1.22	1.44	1.02
	CCN11-2	41.3x31.0x1.067	3	12.7	10.3	73.05	31.1	1.46	1.24	1.24	1.47	1.04
	CBN31-1	41.3x31.0x3.048	2	12.7	11.7	36.4	73.7	1.33	1.35	1.22	1.53	1.03
	CBN31-2	41.3x31.0x3.048	2	12.7	11.6	36.42	71.3	1.27	1.29	1.17	1.45	0.99
	CCN31-1	41.3x31.0x3.048	3	12.7	11.6	73.2	82.9	1.48	1.23	1.23	1.69	1.13
	CCN31-2	41.3x31.0x3.048	3	12.7	11.6	72.85	83.2	1.48	1.23	1.23	1.70	1.14

25
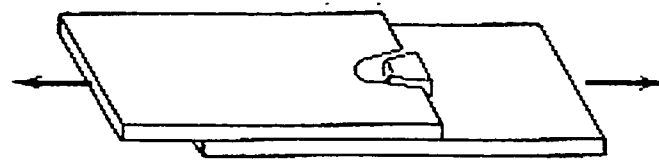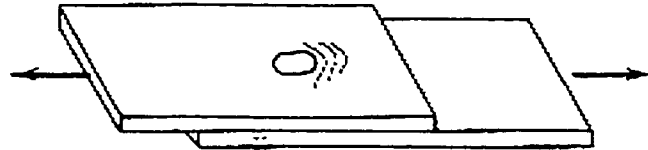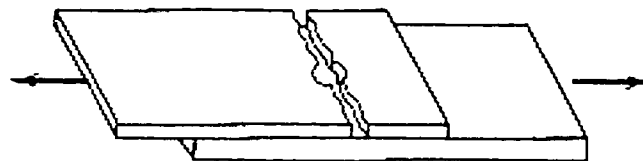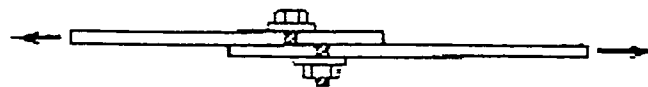
Figure 2.1 Failure Modes of Bolted Connections

3. EXPERIMENTAL PROGRAM

3.1 General

The purpose of this experimental program is to investigate the effect of shear lag on the net section fracture of bolted cold-formed steel angle and channel tension members. The parameters that were considered in this program were:

- number of transverse lines of bolts/ length of connections

- size of cross-section

- presence of washers

Besides the net section strength of the member, the strain distributions at the critical section and the deformations of the specimens were also examined. A total of twenty-three specimens were tested. Three different sizes of both angle and channel sections were used. Only one line of bolts was considered and the number of transverse lines of bolts tested varied from one to four. All tests were performed at the University of Alberta using MTS 1000kN Universal Testing Machine.

3.2 Tension Coupons

The material properties of the angle and channel sections were obtained using tension coupon tests. A total of eight tests were conducted. The coupons were taken from 305 mm leftovers from the delivered 3050 mm sections. For the angle section, three coupons were taken from the flat portion of one leg and one from the corner of the 102 mm angle. For the channel section, one coupon was taken from the flange, two

coupons were taken from the web and one coupon was taken from the corner of the 102 mm channel. The locations of tension coupons cut from the angle and channel sections are shown in Fig. 3.1. A gauge length of 50 mm was used for the coupons. The tension coupons were prepared in accordance with the requirements of American Society for Testing and Materials (ASTM) A370 (1997).

The load and the deformation were obtained as a read-out from the MTS testing machine. An extensometer with a 50 mm gauge length was used to measure the strain in the coupon. Elongation over the coupon gauge length at rupture was measured after rupture.

3.3 Specimens Description

The specimens were prepared from 12 individual pieces of angle and channel. Each of the pieces was about 3000 mm long. They were produced from the same roll of sheet steel and were formed by brake forming. Two specimens were cut from each piece and the length of each specimen was about 1200 mm long. The description of the specimens is presented in Table 3.1 and shown in Fig. 3.2.

A system of identification was used to differentiate between the various specimens. A three letter/digits name was given to each specimen. The first letter represents the geometry that being either an angle (A) or a channel (C). The second digit signifies the size of the specimen in inches. The third digit to the right of the hyphen designates the number of bolts used in the connections. Washers were used in all the

specimens, except A2-2N. N represents the specimen without washer. In addition, duplicated tests were made for specimen A3-1 and C3-1. An asterisk is placed in front of the first digit in order to distinguish the duplicated tests. As shown in Table 3.1, all test specimens had the same thickness.

All holes were drilled to a diameter of 20.6 mm and these accommodated 19.1 mm dia. ASTM A325 bolts in a bearing-type connection. Gusset plates were prepared from steel meeting CAN/CSA G40.21-M Grade 350W (1997). The gusset plates had a thickness of 12.7 mm and a width of 50.8 mm within the tension grips and 101.6 mm beyond the tension grips. One set of gusset plates was used throughout the entire phase of the test set-ups since only one set of bolt spacing was used.

3.4 Test Set-up and Instrumentation

The gusset plates were held in the tension grips with bolts. Shims were inserted between the tension grips and the crosshead to prevent any in-plane rotation of the gusset plates. The test set-up is shown in Fig. 3.3.

Electrical resistance strain gauges were used to measure the strain distribution at the critical section of the member (Section A) and the mid-length of one of the angle and channel sections (Section B). All gauges were oriented to measure the strains in the load direction. The strain gauge locations for the angle and channel sections are shown in Fig. 3.4 and Fig. 3.5, respectively.

The total elongation of a specimen was measured by stroke of the testing machine. Two tests were repeated in order to verify the stroke measurement. They were 76 mm channel and angle sections with one bolt at the connection. In these two tests, two linear variable differential transformers (LVDT's) were used to measure the elongation of the specimen on the connected element. The locations of LVDT's are shown in Fig. 3.6, one was connected to the head of the bolts while the other was tied to the gusset plates at the bolt locations.

3.5 Test Procedure

The top and bottom gusset plates were first installed in the tension grips. After alignment was considered to be satisfactory, the specimen was bolted to the gusset plates with one washer on the specimen side for each bolt (except specimen A2-2N). The bolts were lightly tightened but not yet at the so-called "snug-tight" condition. A tensile load of 2 kN was then applied to the system such that the bolts were bearing against the gusset plate and the specimen. In this way, major slip of the connections during the loading was unlikely. While the load was being held, the bolts were turned to "snug-tight" condition, the load on the MTS was then returned to zero.

With all instrumentation zeroed, the tensile load was then applied using the MTS set on the stroke control mode. At regular intervals, the stroke was held constant such that the specimen was allowed to redistribute the stress and static load readings were obtained. Readings of strain gauges and LVDTs were taken continually during the

loading process. An x-y plotter was used to monitor the load versus elongation behavior

of the test.

Table 3.1 Specimens Description

Specimen	Size [mm]	Thickness [mm]	Number of bolt holes	Bolt Size [mm]	Corner Radius [mm]	Gross Area [mm^2]	Net Area [mm^2]	Member Length [mm]
A2-1	51x51x1.214	1.214	1	19.05	2.38	120.3	94.8	1216
A2-2	51x51x1.214	1.214	2	19.05	2.38	120.3	94.8	1217
A2-2N	51x51x1.214	1.214	2	19.05	2.38	120.3	94.8	1219
A2-3	51x51x1.214	1.214	3	19.05	2.38	120.3	94.8	1217
A3-1	76x76x1.214	1.214	1	19.05	2.38	182.0	156.4	1218
*A3-1	76x76x1.214	1.214	1	19.05	2.38	182.0	156.4	1218
A3-2	76x76x1.214	1.214	2	19.05	2.38	182.0	156.4	1220
A3-3	76x76x1.214	1.214	3	19.05	2.38	182.0	156.4	1218
A4-1	102x102x1.214	1.214	1	19.05	2.38	243.7	218.1	1221
A4-2	102x102x1.214	1.214	2	19.05	2.38	243.7	218.1	1216
A4-3	102x102x1.214	1.214	3	19.05	2.38	243.7	218.1	1222
A4-4	102x102x1.214	1.214	4	19.05	2.38	243.7	218.1	1215
C2-1	51x29x1.214	1.214	1	19.05	2.38	125.0	99.4	1217
C2-2	51x29x1.214	1.214	2	19.05	2.38	125.0	99.4	1217
C2-3	51x29x1.214	1.214	3	19.05	2.38	125.0	99.4	1218
C3-1	76x29x1.214	1.214	1	19.05	2.38	155.8	130.3	1219
*C3-1	76x29x1.214	1.214	1	19.05	2.38	155.8	130.3	1219
C3-2	76x29x1.214	1.214	2	19.05	2.38	155.8	130.3	1218
C3-3	76x29x1.214	1.214	3	19.05	2.38	155.8	130.3	1218
C4-1	102x29x1.214	1.214	1	19.05	2.38	186.7	161.1	1217
C4-2	102x29x1.214	1.214	2	19.05	2.38	186.7	161.1	1216
C4-3	102x29x1.214	1.214	3	19.05	2.38	186.7	161.1	1220
C4-4	102x29x1.214	1.214	4	19.05	2.38	186.7	161.1	1218

32
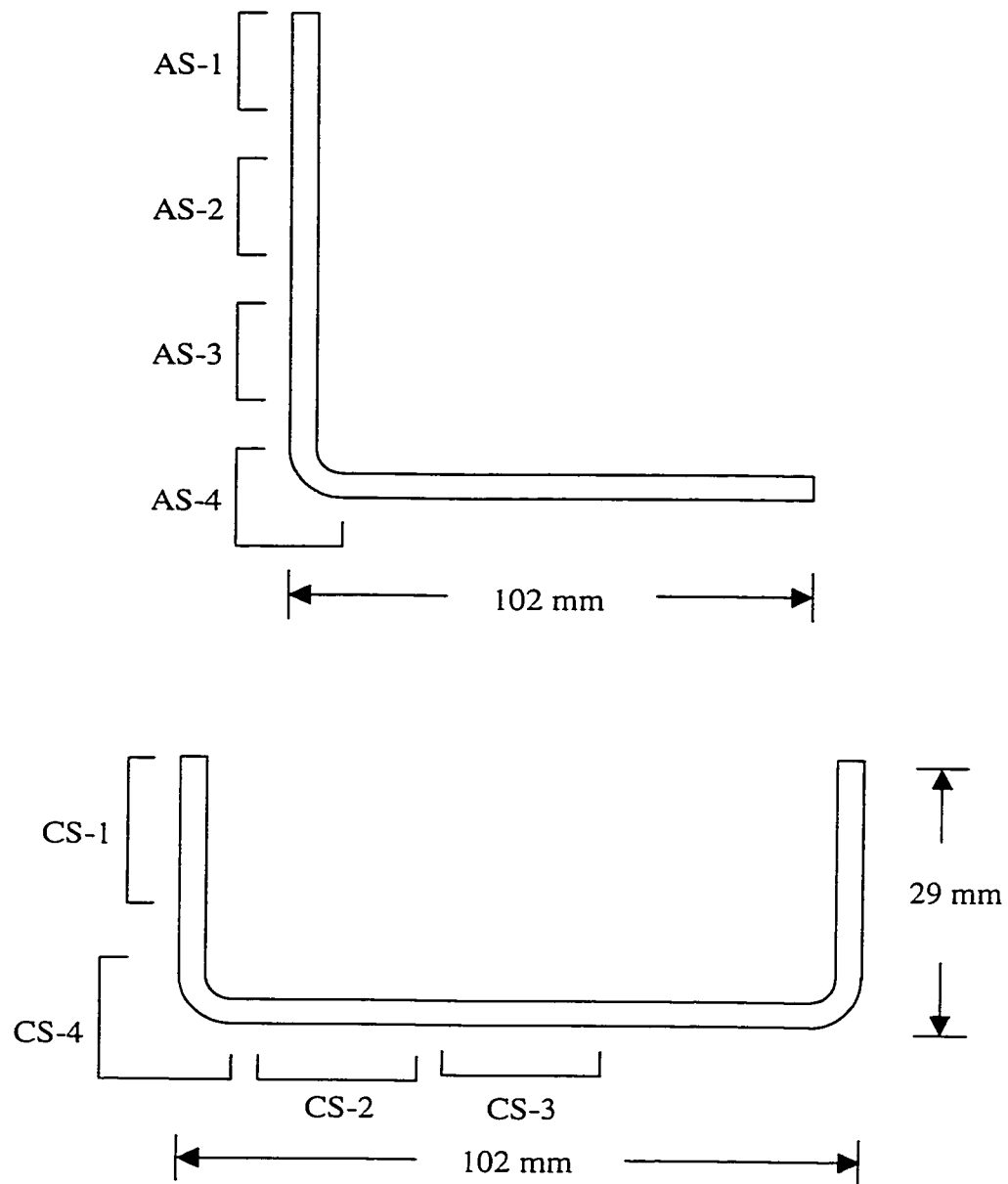
Figure 3.1 Tension Coupons Locations for Angle and Channel Sections

1200 mm

(n-1) at 63.5 mm

D

e

D

R=2.38 mm

t

B

D

D

R=2.38 mm

t
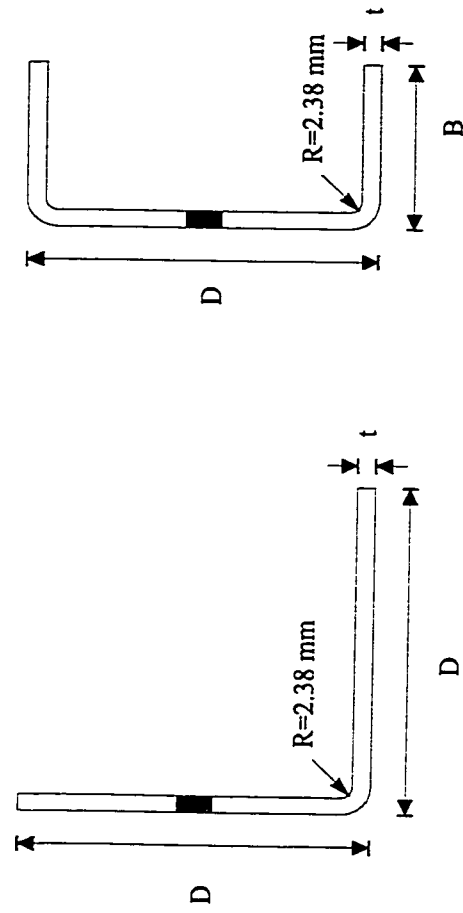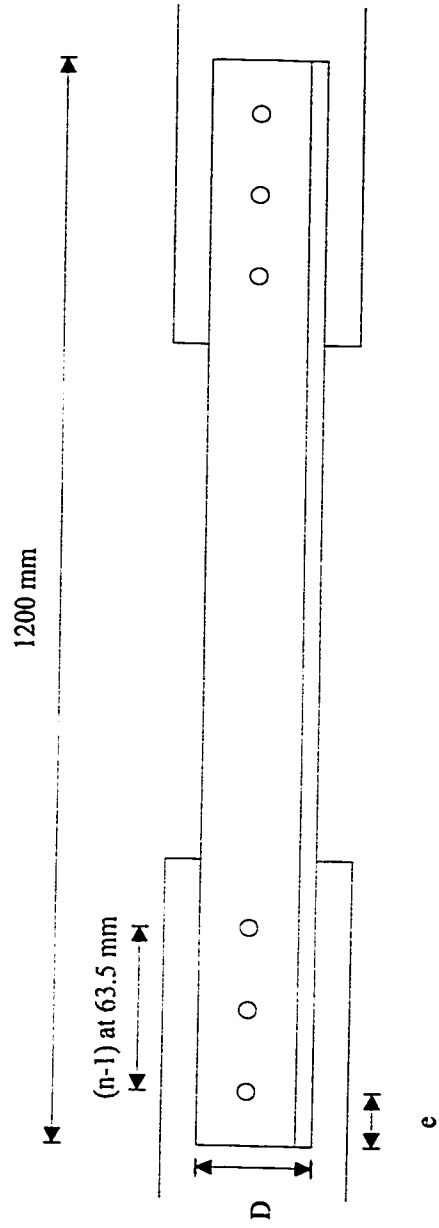
Figure 3.2 Specimen Dimensions

34

Figure 3.3 Test Set-up

51 mm angles: d_1=0 mm
$\quad\quad\quad\quad\quad$ d_2=18 mm
76 mm angles: d_1=25 mm
$\quad\quad\quad\quad\quad$ d_2=25 mm
102 mm angles: d_1=35 mm
$\quad\quad\quad\quad\quad$ d_2=35 mm

Section A $\quad\quad$ Section B

C.L.

Section B

(for A3-2 only)

d_2 $\quad$ d_2

d_2 $\quad$ d_2

Section A

d_2 $\quad$ d_2

d_1 $\quad$ d_1
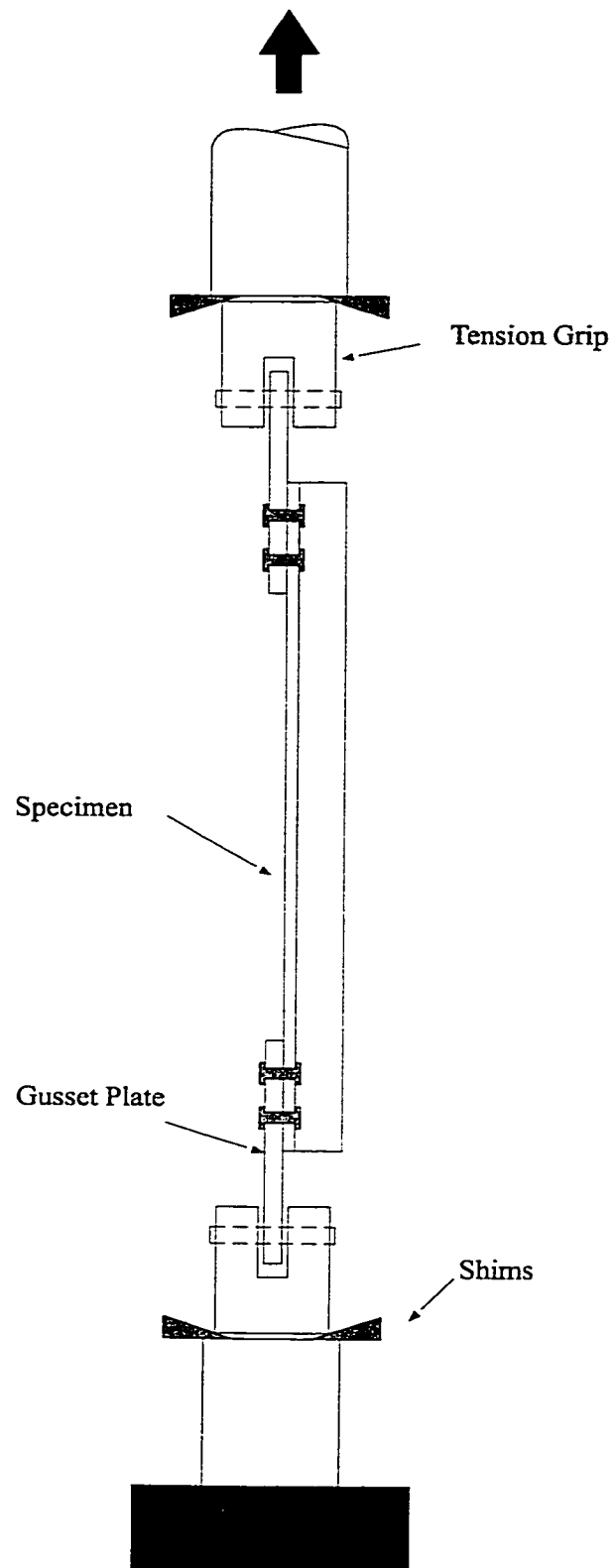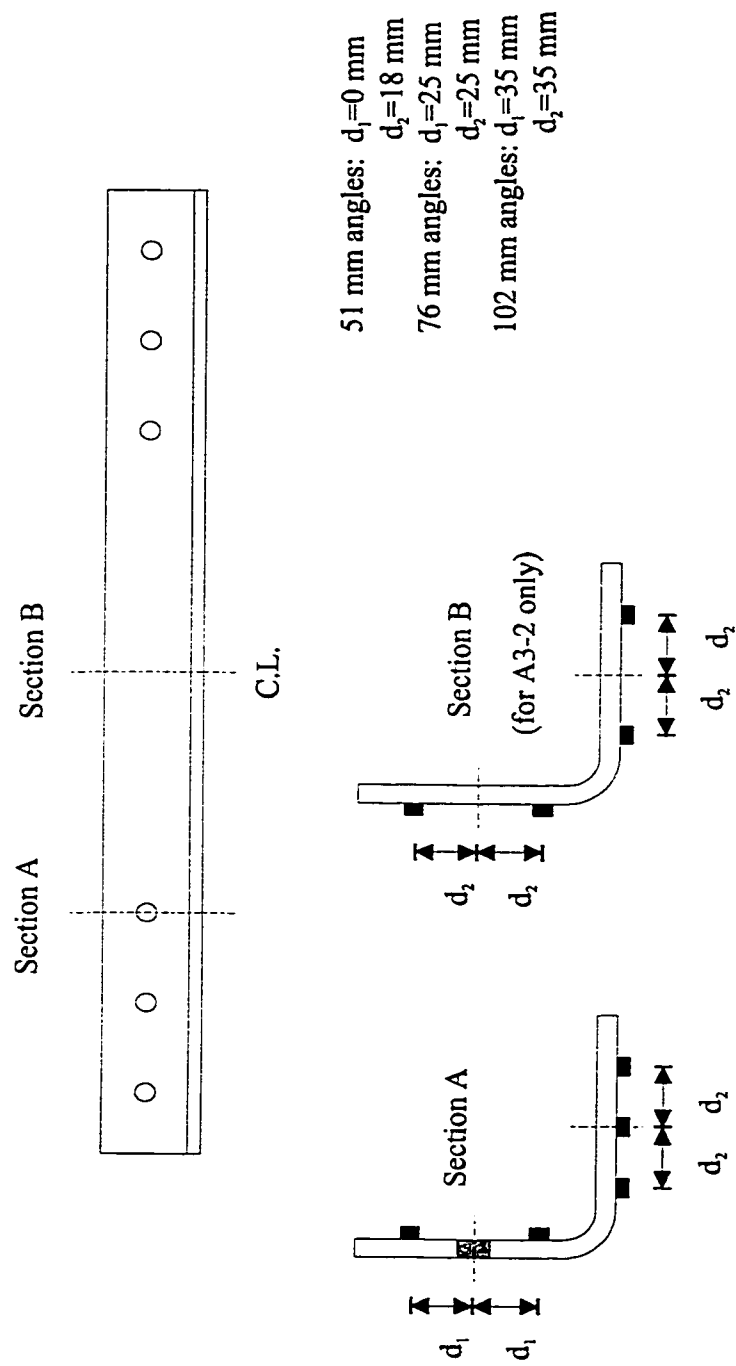
Figure 3.4 Strain Gauge Locations for Angle Sections

36

Section B

Section A

C.L.

51 mm channel: $d_1=d_2=0$ mm
76 mm channel: $d_1=27$ mm
$d_2=0$ mm
102 mm channel: $d_1=27$ mm
$d_2=10$ mm

10mm

Section B

(for C3-2 only)

10mm

10mm 10mm

Section A

10mm 10mm

d_2 d_1 d_1 d_2
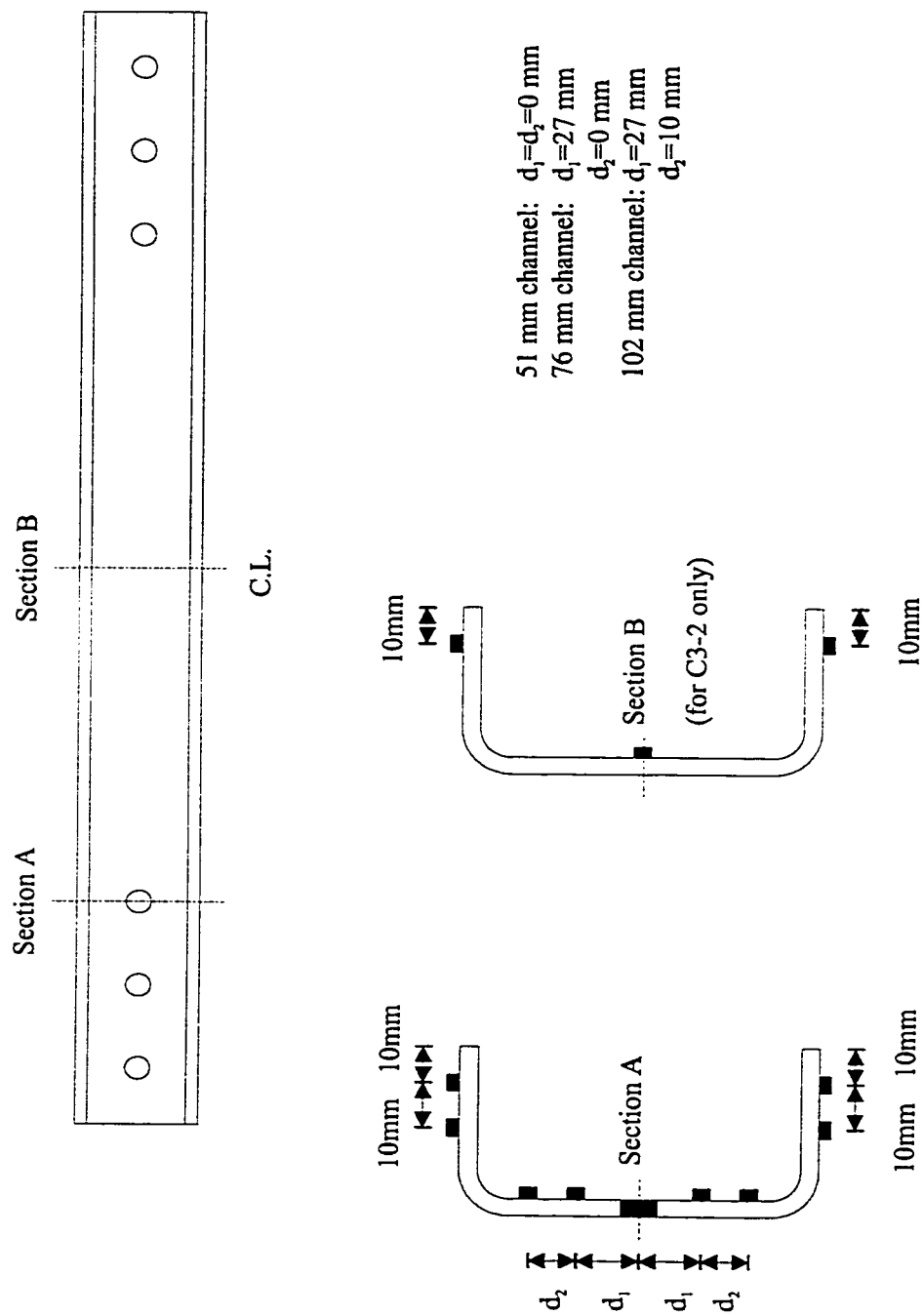
Figure 3.5 Strain Gauge Locations for Channel Sections

37
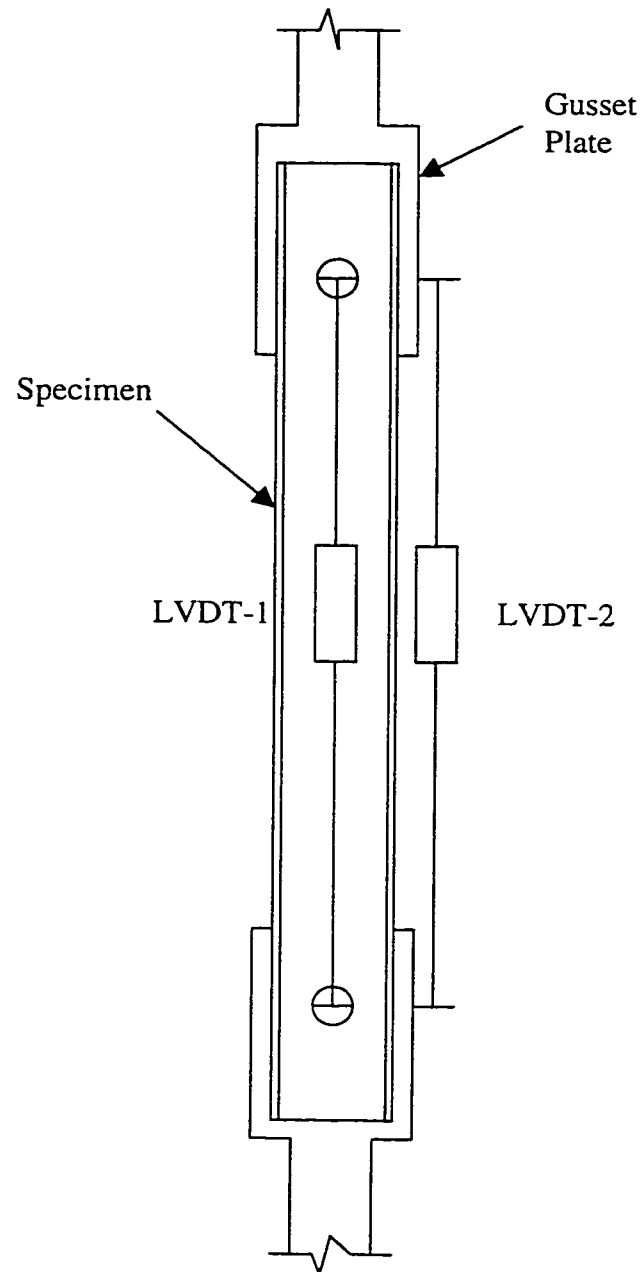
Figure 3.6 Locations of LVDT's

4. TEST RESULTS

4.1 Tension Coupon Tests

The material properties of the tension coupons taken from the angle and channel sections are reported in Table 4.1. The average modulus of elasticity, static yield strength, dynamic yield strength, static ultimate strength, and dynamic ultimate strength for the flat coupons from the angle and channel sections are shown in Table 4.2. The material properties of the corner coupons were calculated by assuming the modulus of elasticity is the same as the flat coupons, the initial cross-sectional area for corner coupons, A_0, can then be calculated using the following formula:

$$A_0 = \frac{\Delta P}{\Delta \varepsilon} \times \frac{1}{E_{ave}} \qquad [4.1]$$

where $\Delta P / \Delta \varepsilon$ = the slope of the Load-Deformation curve for the tension coupon at the

corner

E_{ave} = average modulus of elasticity obtained from the tension coupons at the flat

portions

The modulus of elasticity of tension coupon CS-3 is significantly lower than that of CS-1 and CS-2. The reason is probably due to the error in extensometer; therefore, the result of tension coupon CS-3 is not considered. The rupture strain for both corner coupons AS-4 and CS-4 are not available due to the non-uniform distortion at the corner of the coupon at rupture. The average values calculated in Table 4.2 for each section are based on the values of the coupons taken from the flat portion. The stress-strain diagrams for the coupons of angle and channel sections are shown in Fig. 4.1 and Fig. 4.2, respectively.

39

4.2 Full Scale Tests

4.2.1 Test results

The dynamic ultimate strength, P_{Test}, and the failure mode of the specimens are presented in Table 4.3. The net section efficiency (N.S.E.) of the member was calculated based on the dynamic ultimate load and the measured dynamic ultimate strength of the tension coupon material.

$$N.S.E. = \frac{P_{Test}}{F_u x A_n}$$ [4.2]

From a design point of view, usually static strength is used to calculate the predicted load; however, dynamic strength is used in this report because using the dynamic strength would give a lower value of net section efficiency, as a result, a conservative result would then be obtained. In addition, the load obtained from the test was in dynamic, therefore the dynamic strength should be used to calculate the predicted load. Table 4.3 shows that the net section efficiency increases as the connection length increases.

4.2.2 General observations

During the loading process, the gusset plates used for all angle and channel sections remained straight. As the load increased, the unconnected portion at the two ends of the specimens from the end of specimens to the last line of bolt gradually separated from the gusset plates. As a result, a gap was formed between free ends and the gusset plate due to the eccentricity about the centroid of the section, which is termed as global bending. The width of the gap varied from one specimen to another, with the maximum observed value of 10 mm. The width of this type of gap increased as the connection length decreased, as the end distance increased, and as the size of the

40

specimen increased. In addition, as shown in Fig. 4.3, local bending of the angle about the bolt was observed after the fracture occurred. The magnitude of in-plane deflection due to the local bending varied from one angle to another, and the maximum value observed was 15 mm. However, this type of bending was not found in channel sections due to the symmetry of the cross-section. Generally, the larger deflections were observed with those cases of shorter connection lengths.

There was no major slip of the connections observed, except specimen C3-1 (76 mm x 29 mm x 1.214 mm channel, one-bolt connection). All the specimens failed at the critical cross-section as the ultimate load was reached. For the specimens that failed in bearing, piling up of material and elongation of bolt hole were observed at the critical section, as can be seen in Fig. 4.4 and Fig. 4.5. This type of failure was observed for all the test specimens with one bolt and some with two bolts in the connections, depending on the size of the specimens. The rest of the specimens with two or more transverse lines of bolts failed by net section fracture. Necking at the critical section was observed for this type of failure. At the failure load, the unconnected leg of the angle sections and the flanges of the channel sections at the connections had moved in considerably due to the second order effects, as shown in Fig. 4.6 and Fig. 4.7. The magnitude of this deformation (or second order buckling) effect became more severe as the size of specimen increased. It was noted that all the bolts were still tight after completion of the tests. This indicates that the bolts were not highly stressed during the tests.

4.2.3 Load-deformation relationship

In this section, the effects of the size of cross-section, the connection length and the presence of washers on the load-deformation behavior, and the comparison between the repeated tests are discussed. The load-versus-deformation curves for all specimens were attached in Appendix A for reference. The elongation of the specimen reported herein was the stroke reported by the MTS machine.

The effect of different connection lengths can be illustrated in the load versus elongation curves in Fig. 4.10 and Fig. 4.11. In Fig. 4.10, specimens A4-2, A4-3, and A4-4 were all 102 mm x 102 mm x 1.214 mm angle specimens, which had two, three, and four bolts, respectively, at the connection. Specimens C4-2, C4-3, and C4-4 shown in Fig. 4.11 are all 102 mm x 102 mm x 1.214 mm channel specimens with two, three, and four bolts, respectively, at the connection. As expected, the specimen A4-2 and C4-2 with the shortest connection had the lowest ultimate strength. The ultimate strengths for the four-bolted connection and the three-bolted connection in both cases were very close to each other, however the deformation of the specimens with long connection were less than that of the specimens with short connection. This situation can be due to the distribution of shear forces among the bolts. Since the deformation of the specimen is mainly contributed from the elongation of the first bolt. If the number of bolt used increases, each bolt would carry less amount of load; as a result, elongation of the bolt hole would decrease.

The behavior of specimen with washer at the connection (A2-2) and without washer (A2-2N) is shown in Fig. 4.12. Each of these specimens was identical in all respects except for the use of washer. With the use of washers at the connection, the maximum load was increased by 16 percent. In both cases, the elongations are relatively the same. This phenomenon can be attributed to the better clamping force provided by the washers. The better clamping force would reduce the stress concentration at the connection. Therefore, the stress distribution at the critical section would become more uniform; consequently, the capacity of the section would increase.

The load-deformation relations for the repeated channel section tests, C3-1 and *C3-1 (76 mm x 76 mm x 1.214 mm, one-bolt connection) are showed in Fig. 4.13. As can be seen, the maximum load obtained in *C3-1 was about 50 percent higher than C3-1. The large discrepancy was most likely due to the inconsistent clamping force applied during when tightening the bolts. Since tension control was not applied in the test, the clamping force may vary from test to test and causing such a variation. A slip was observed for specimen C3-1. For specimen *C3-1, the increase indicated that the high clamping force produced by the bolt introduced a frictional resistance between the plates and the specimen and causing the connection to become a frictional type of connection. More discussion about this postulation will be covered in Chapter 5.

4.2.4 Strain distribution

The typical strain distribution for angle and channel sections is discussed in this section. The load versus strain curves at the critical section for specimen A4-4 (102 mm

x 102 mm x 1.214 mm angle, four-bolt connection) are shown in Fig 4.14. As shown in the figure, the strain was largest at edge of the connected leg and smallest at the edge of the outstanding leg. The edge of the outstanding leg was in compression throughout the whole loading process and the strain reached a value close to the compressive yield strain after the ultimate load was reached. The strain at the middle of the unconnected leg was in compression under loads up to about 95 percent of the ultimate load; after that it shifted to tension. The same behavior was observed for angles with short connections. As shown in Fig. 4.15, the edge of the outstanding leg of A3-2 (76 mm x 76 mm x 1.214 mm angle, two-bolt connection) was in compression throughout and the strain measured at the edge of the outstanding leg reached a value close to the compressive yield strain. The load versus strain curves for the mid-length section of A3-2 (76 mm x 76 mm x 1.214 mm angle, two-bolt connection) are shown in Fig 4.16. Similar to the strain at the critical section, the strain close to the edge of the outstanding leg was in compression throughout the whole loading process.

Due to the stress concentration around the bolt holes, the strains measured on the critical section of the connected leg usually had wide variations for the angles. However, limited number of strain gauges were used at the connected leg, therefore, the strain distribution at the connected leg could not be obtained. On the other hand, the strain distribution of the outstanding leg at the critical section showed some regular patterns. These can be seen in Fig. 4.17, where the strain distributions A3-2 are shown for different levels of load. The strain distribution of A3-2 was linear on the unconnected leg during the entire loading history. This type of linear strain distribution pattern described was

typical for all angle members. This linear strain distribution throughout the loading process reflected the bending deformation perpendicular to the gusset plate, as described in Section 4.2.2 in terms of global bending and local bending.

Among the channel specimens, there were two different strain distributions found: one for specimens with short connection length, and one for specimens with long connection length. For channels with short connection length, the flanges were in compression throughout the loading process. As shown in Fig. 4.18, the strain at the edge of the flanges of specimen C4-2 (102 mm x 29 mm x 1.214 mm, two-bolt connection) reached a value close to the compressive yield strain after the ultimate load was reached. Figure 4.19 shows the strain distribution at the critical section of C4-2. At low load level, the strain distribution was relatively uniform; however, after the yield strength was reached, the distribution became highly non-uniform, especially for the strain around the bolt hole due to the stress concentration.

For specimen having long connection length, as illustrated in Figs. 4.20 and 4.21 for specimen C4-4, the strains in the flanges and web were in tension throughout. Similar to specimens with short connection length, the strain distribution was uniform at the beginning of the loading stage (Fig. 4.22); however, as the load increased, the strain distribution at the web became non-uniform due to the stress concentration around the bolt hole.

Figure 4.23 shows the load versus strain curves for the mid-section of specimen C3-2 (76 mm x 29 mm x 1.214 mm angle, two-bolt connection). It showed that the strains at two flanges were very close to each other and the strain at the web was about twice as much as that at the flanges. As seen in Fig. 4.24, the shapes of the strain distribution at the mid-section of specimen of C3-2 remained relatively the same at different load levels.

Table 4.1 Material Properties

Specimen	Modulus of Elasticity [MPa]	Static Yield Strength [MPa]	Dynamic Yield Strength [MPa]	Static Ultimate Strength [MPa]	Dynamic Ultimate Strength [MPa]	Strain at Rupture [%]
AS-1	199000	275	291	315	341	50.7
AS-2	201000	279	295	319	342	50.4
AS-3	192000	275	290	314	338	25.1
AS-4	197000	341	367	382	407	N/A
CS-1	200000	282	300	327	350	47.1
CS-2	196000	280	297	322	346	43.7
CS-3	173000	283	300	322	346	23.2
CS-4	198000	343	362	379	406	N/A

Table 4.2 Average Material Properties of Angle and Channel Sections

Material	Modulus of Elasticity [MPa]	Static Yield Strength [MPa]	Dynamic Yield Strength [MPa]	Static Ultimate Strength [MPa]	Dynamic Ultimate Strength [MPa]
Angle	197000	276	292	316	340
Channel	198000	281	299	324	347

47

Table 4.3 Test Results

Specimen	Size [mm]	Number of bolt per line	P_{Test} [kN]	P_{Net} [kN]	P_{Test} / P_{Net}	Mode of failure
A2-1	51x51x1.214	1	15.5	29.9	0.52	Bearing and fracture
A2-2	51x51x1.214	2	27.9	29.9	0.93	Net section fracture
A2-2N	51x51x1.214	2	24.0	29.9	0.80	Net section fracture
A2-3	51x51x1.214	3	31.1	29.9	1.04	Net section fracture
A3-1	76x76x1.214	1	21.9	49.4	0.44	Bearing and fracture
*A3-1	76x76x1.214	1	23.5	49.4	0.48	Bearing
A3-2	76x76x1.214	2	32.8	49.4	0.66	Net section fracture
A3-3	76x76x1.214	3	37.7	49.4	0.76	Net section fracture
A4-1	102x102x1.214	1	18.3	68.9	0.27	Bearing
A4-2	102x102x1.214	2	34.0	68.9	0.49	Bearing
A4-3	102x102x1.214	3	45.1	68.9	0.65	Net section fracture
A4-4	102x102x1.214	4	49.4	68.9	0.72	Net section fracture
C2-1	51x29x1.214	1	23.0	32.2	0.71	Bearing
C2-2	51x29x1.214	2	36.8	32.2	1.14	Net section fracture
C2-3	51x29x1.214	3	37.6	32.2	1.17	Net section fracture
C3-1	76x29x1.214	1	18.1	42.2	0.43	Bearing
*C3-1	76x29x1.214	1	27.0	42.2	0.64	Bearing
C3-2	76x29x1.214	2	36.3	42.2	0.86	Bearing and fracture
C3-3	76x29x1.214	3	48.1	42.2	1.14	Net section fracture
C4-1	102x29x1.214	1	19.6	52.2	0.38	Bearing
C4-2	102x29x1.214	2	40.5	52.2	0.78	Bearing
C4-3	102x29x1.214	3	52.5	52.2	1.01	Net section fracture
C4-4	102x29x1.214	4	55.8	52.2	1.07	Net section fracture
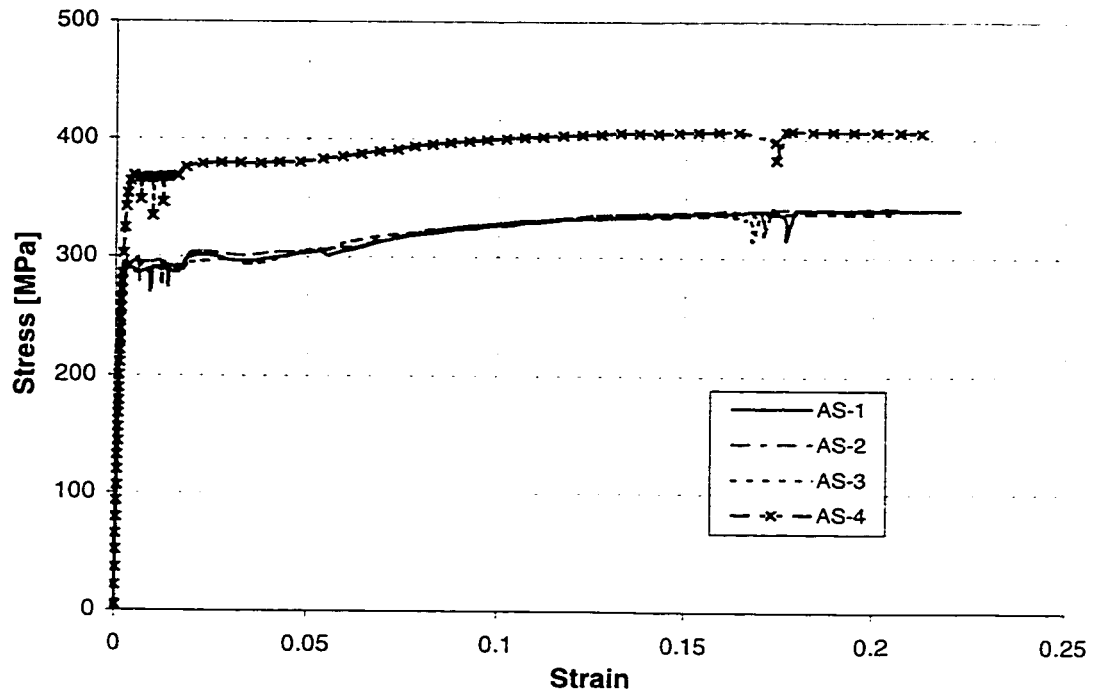
Figure 4.1 Stress vs. Strain for Tension Coupons cut from Angle Sections
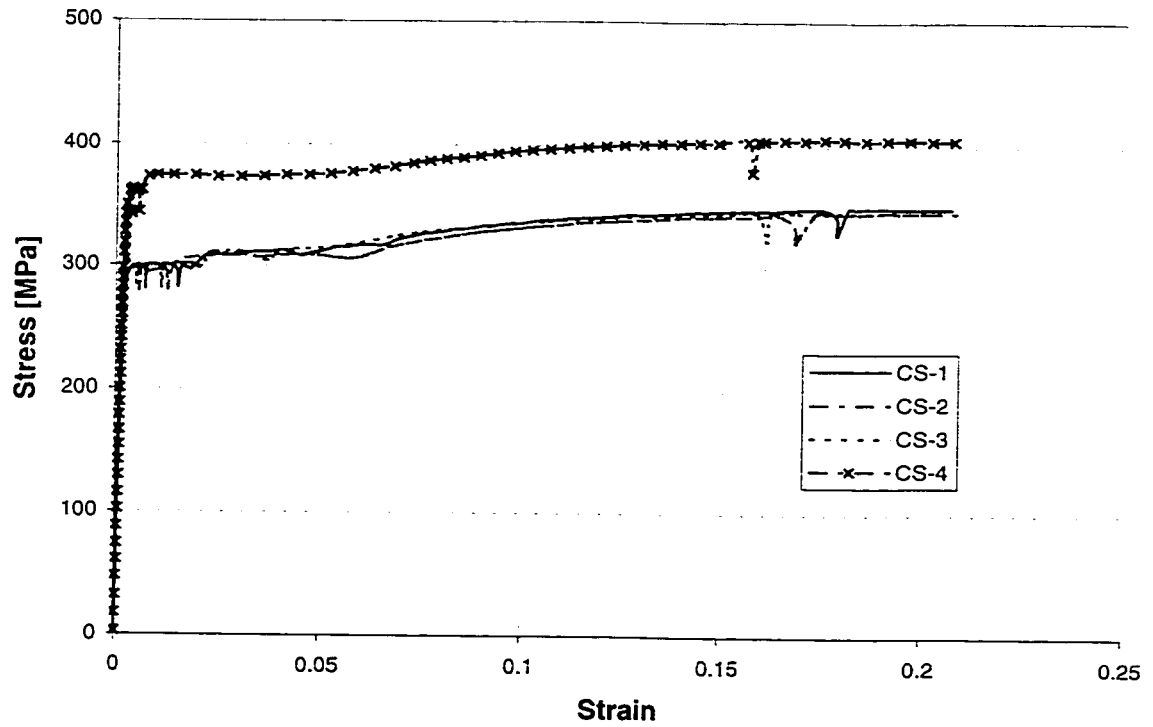
Figure 4.2 Stress vs. Strain for Tension Coupons cut from Channel Sections

49
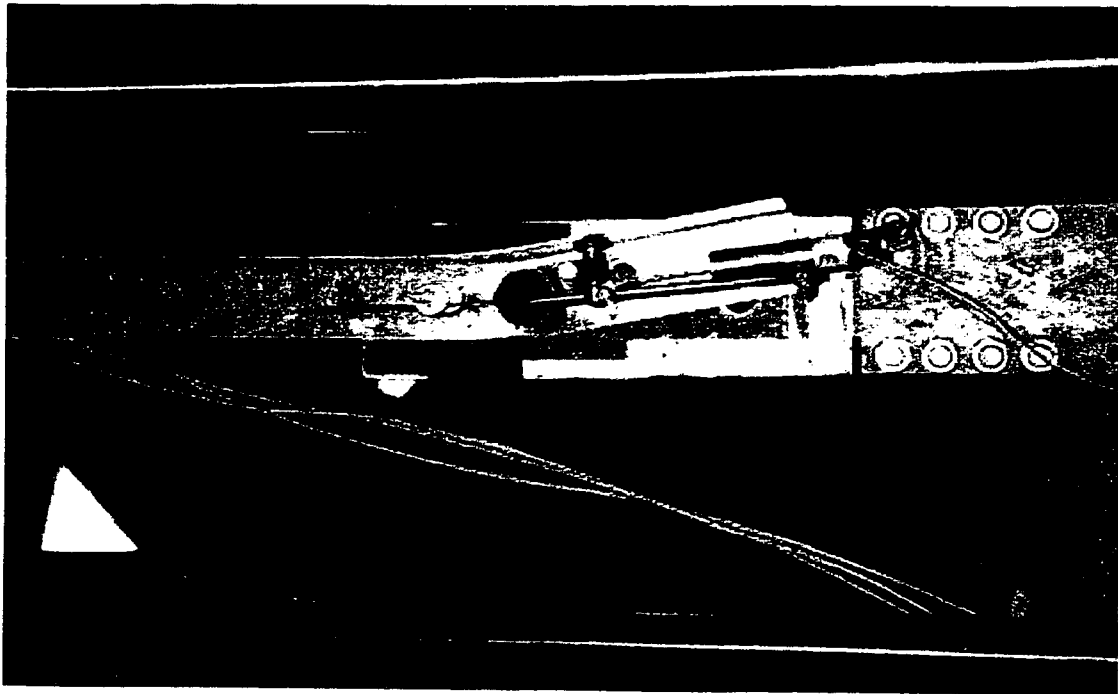
Figure 4.3 Local Bending

Figure 4.4 Deformed Angles Failed in Bearing
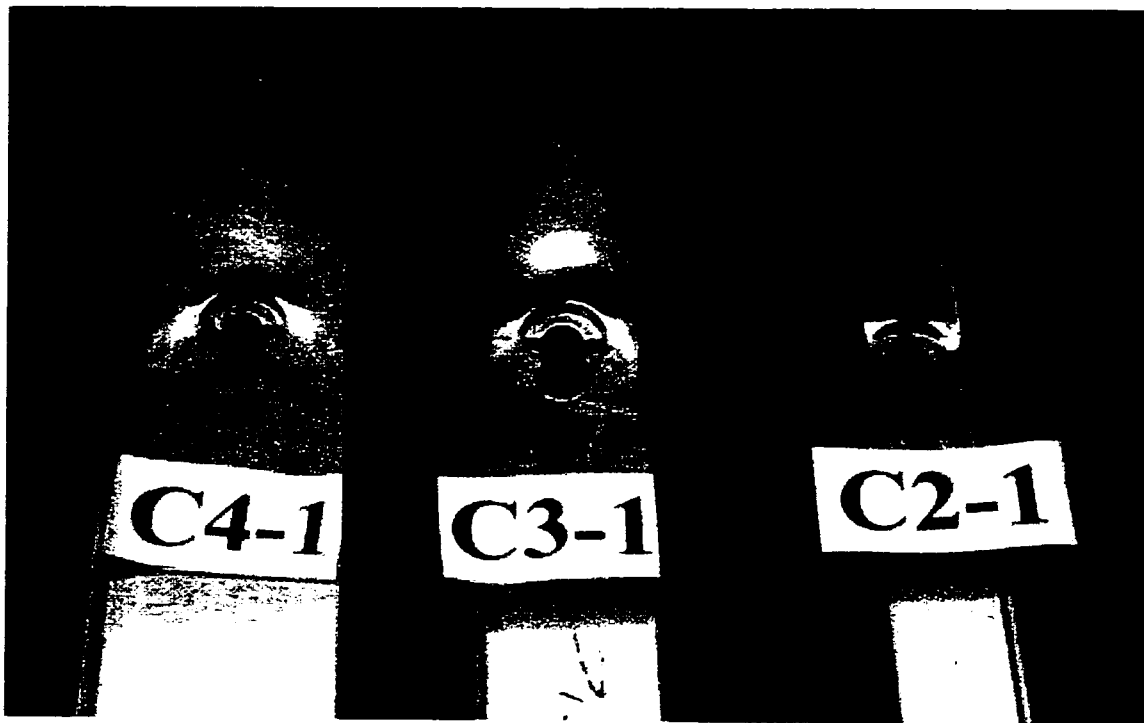
Figure 4.5 Deformed Channels Failed in Bearing
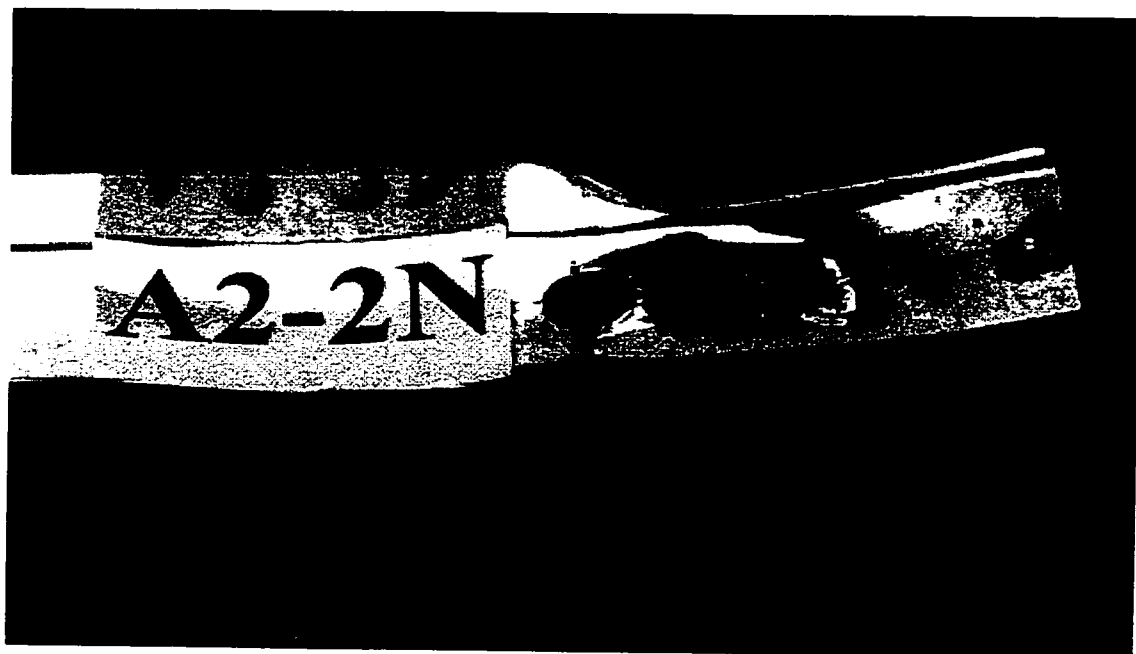
Figure 4.6 Deformed Angle Failed by Net Section Rupture

51
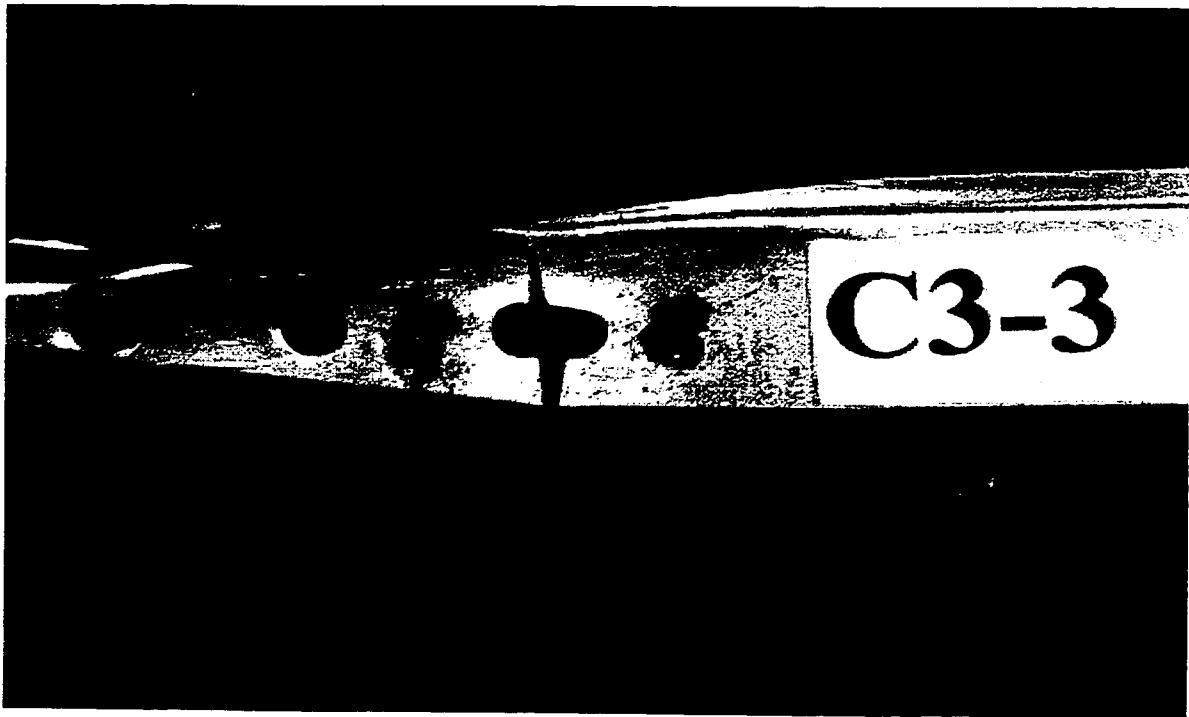
Figure 4.7 Deformed Channel Failed by Net Section Rupture
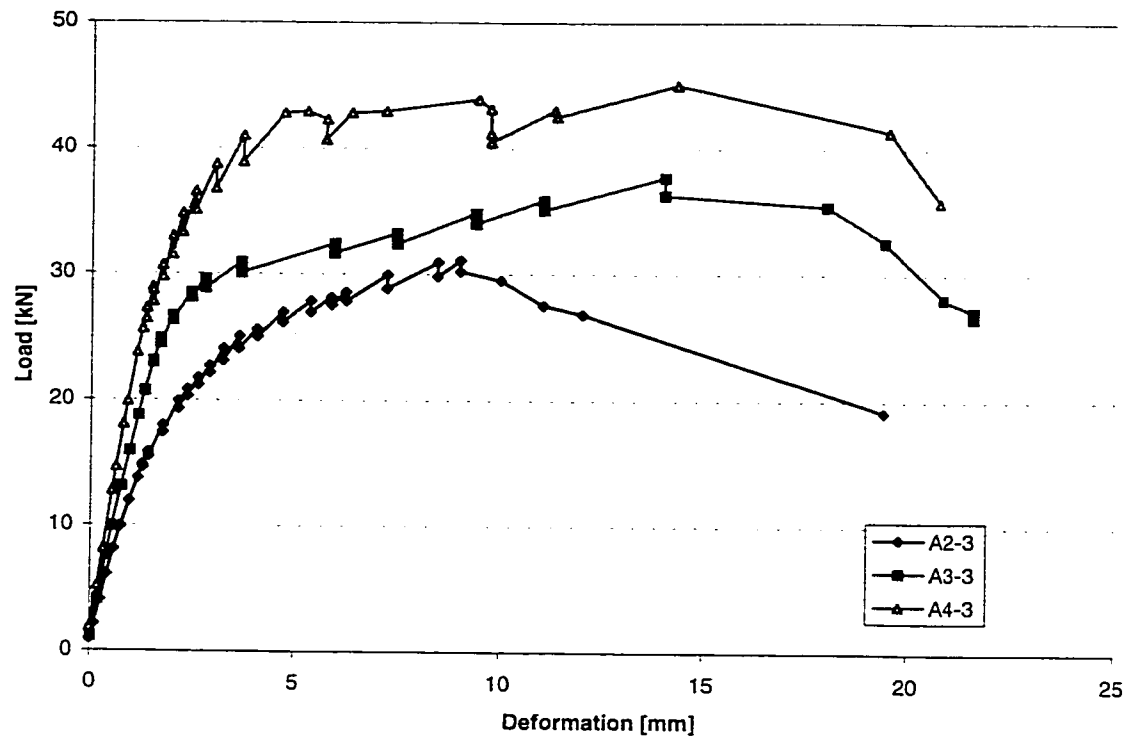
Figure 4.8 Load vs. Deformation for A2-3, A3-3 and A4-3
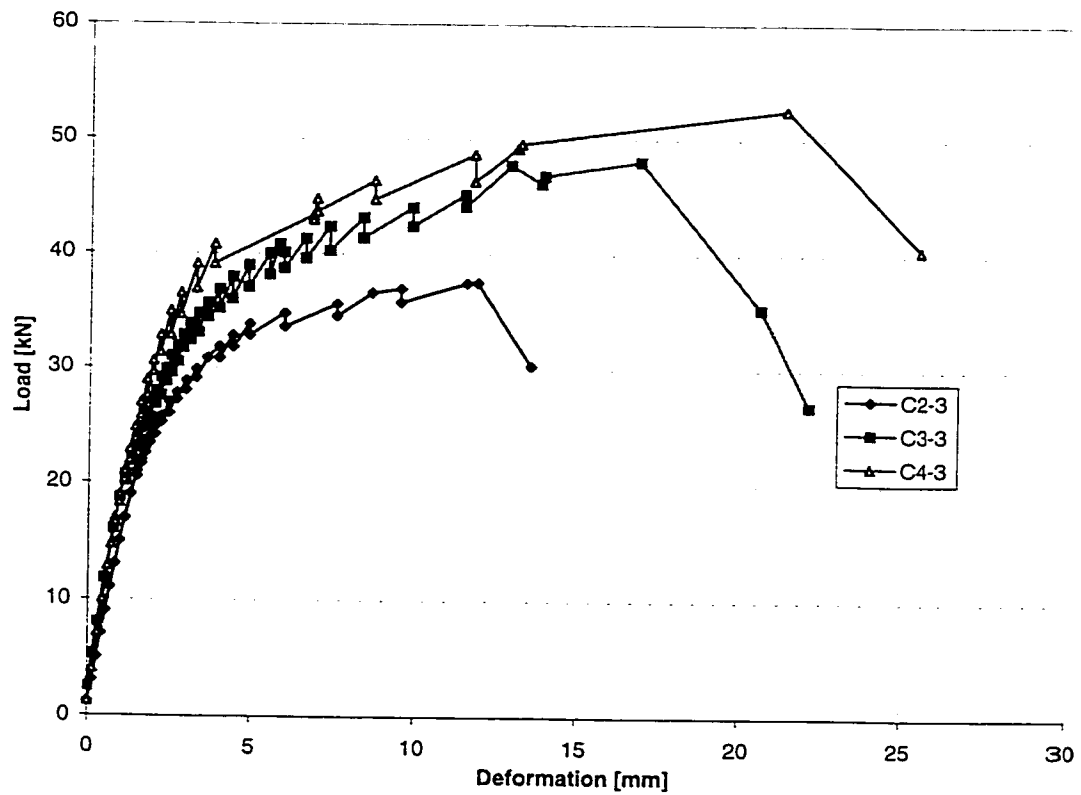
Figure 4.9 Load vs. Deformation for C2-3, C3-3 and C4-3
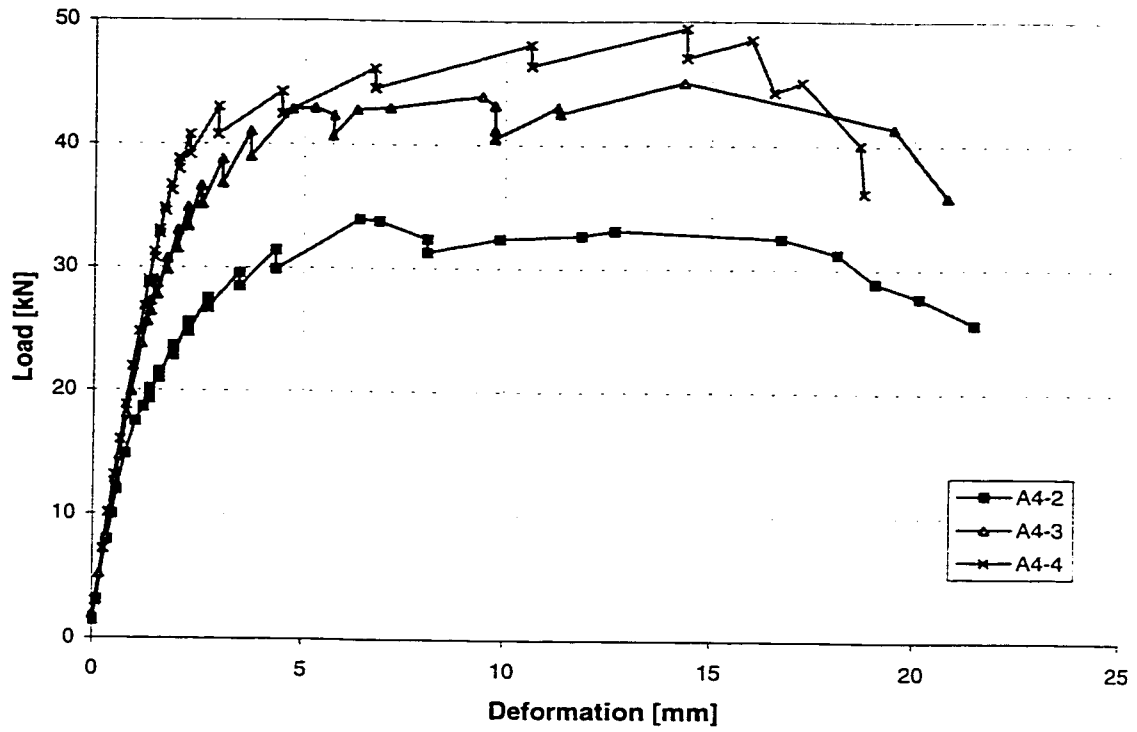
Figure 4.10 Load vs. Deformation for A4-2, A4-3 and A4-4
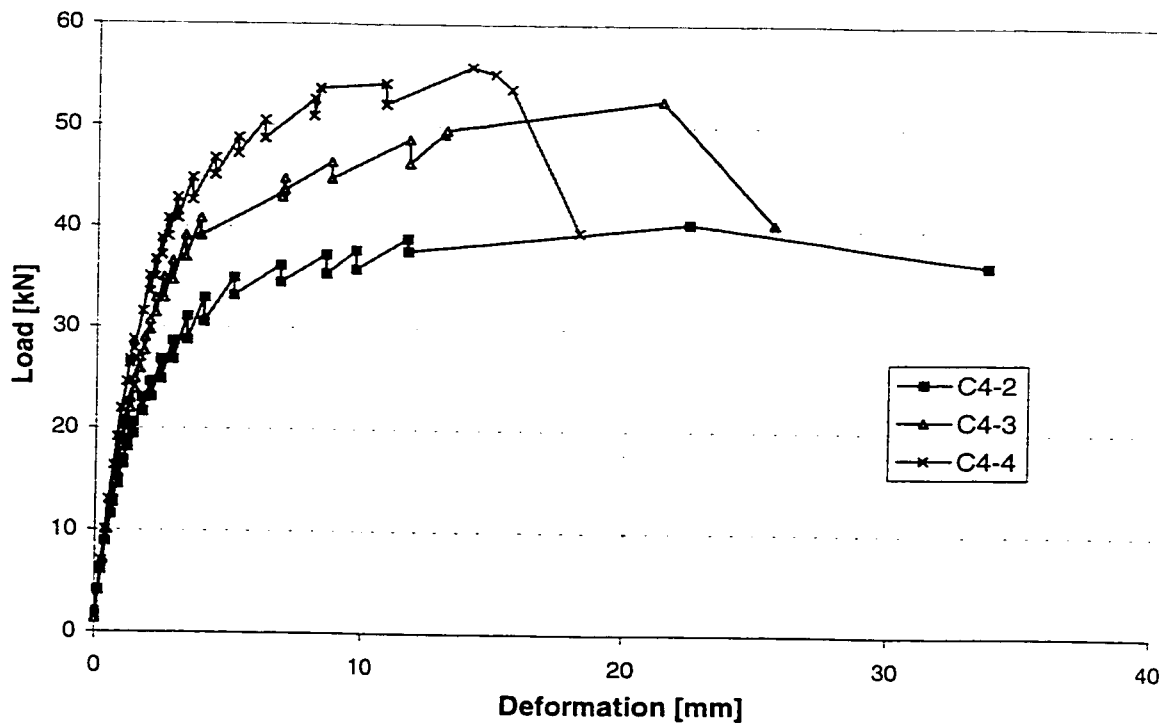
Figure 4.11 Load vs. Deformation for C4-2, C4-3 and C4-4

54
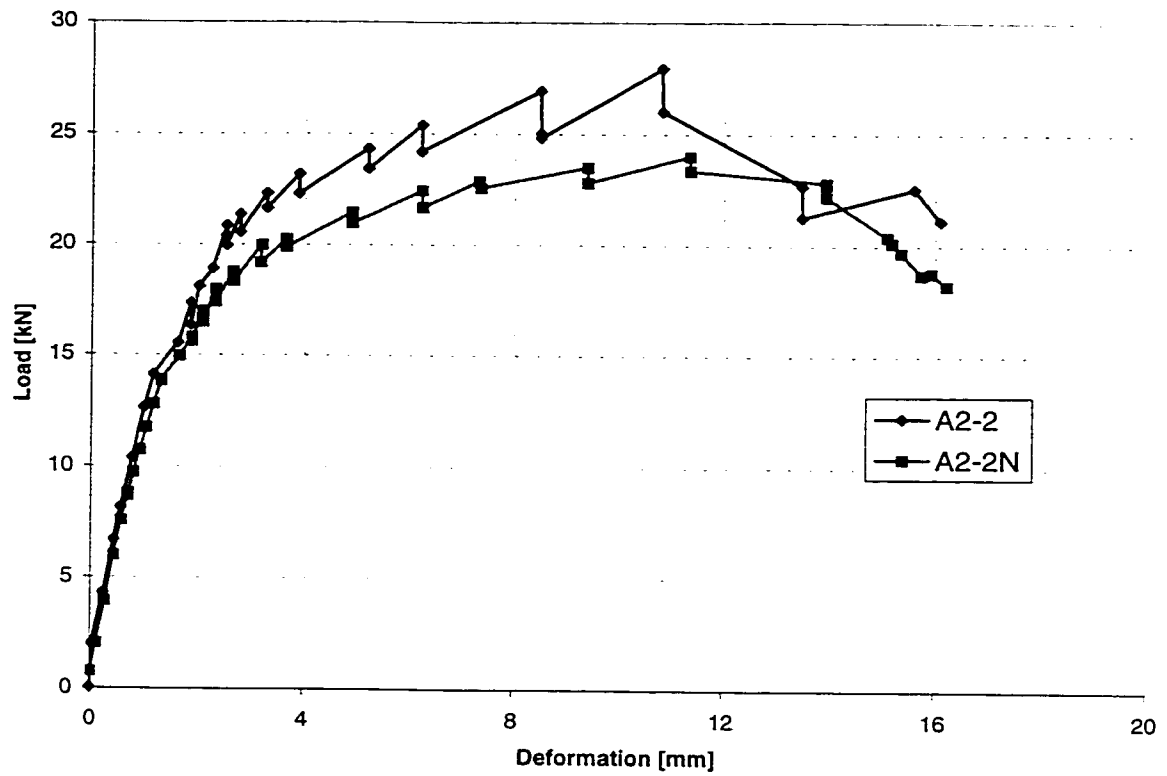
Figure 4.12 Load vs. Deformation for A2-2 and A2-2N
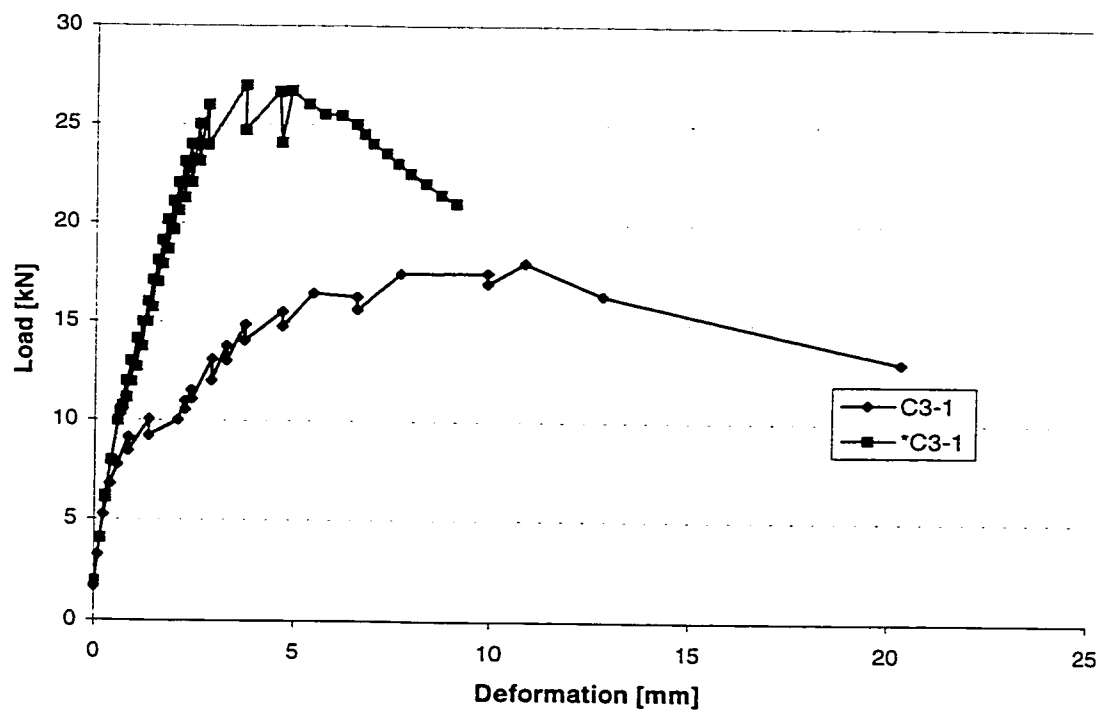
Figure 4.13 Load vs. Deformation for C3-1 and *C3-1

55
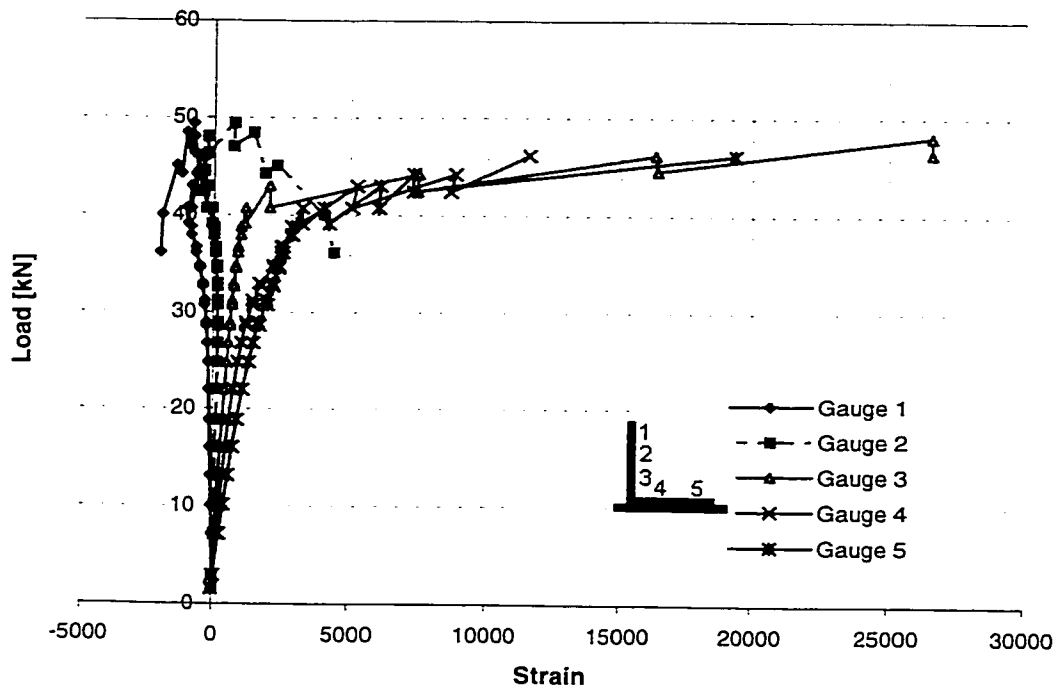
Figure 4.14 Load vs. Strain at the Critical Section for A4-4
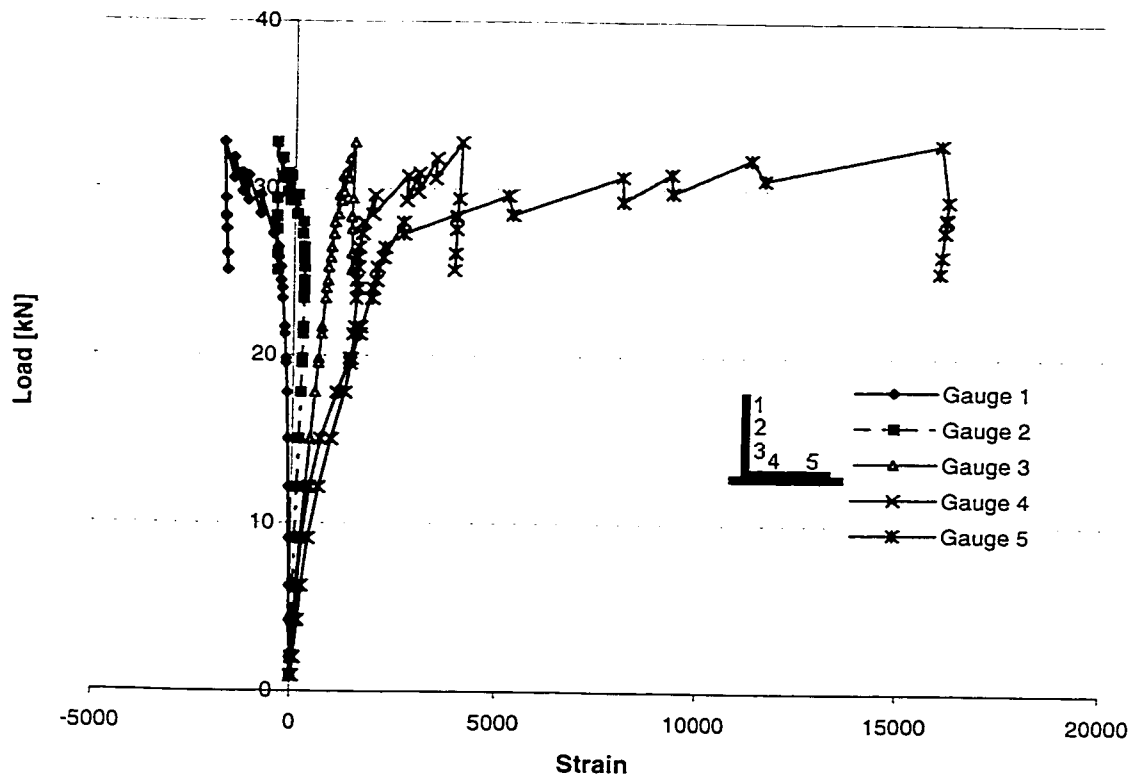
Figure 4.15 Load vs. Strain at the Critical Section for A3-2

56
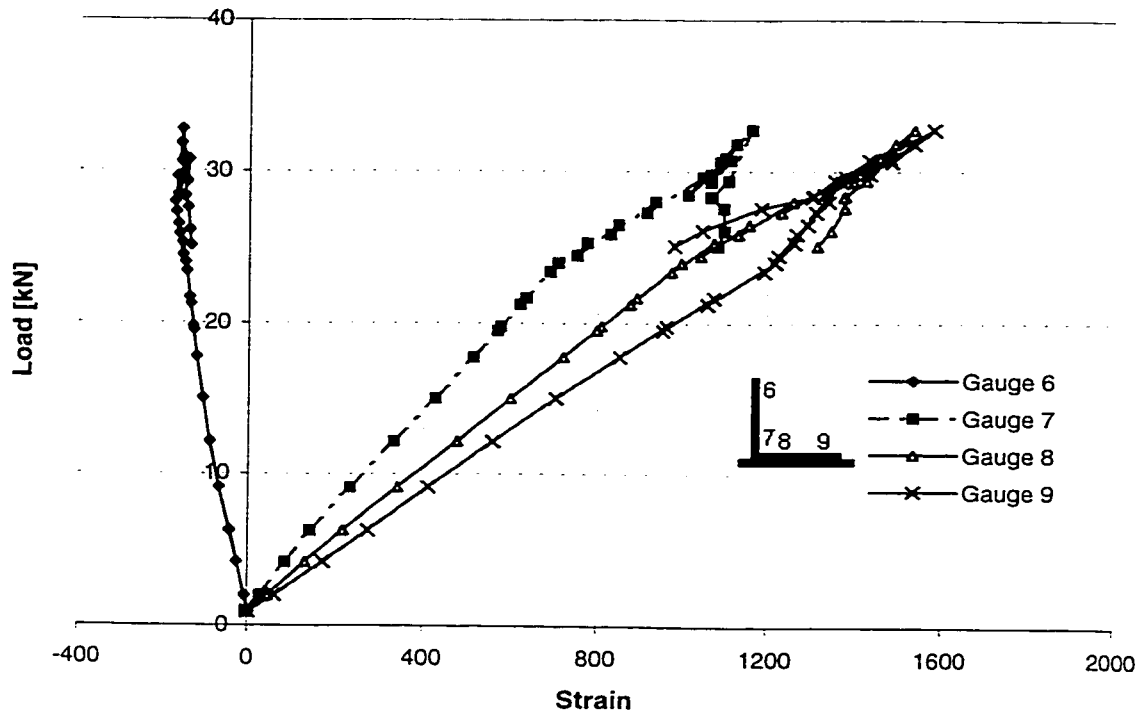
Figure 4.16 Load vs. Strain at the Mid-length of A3-2
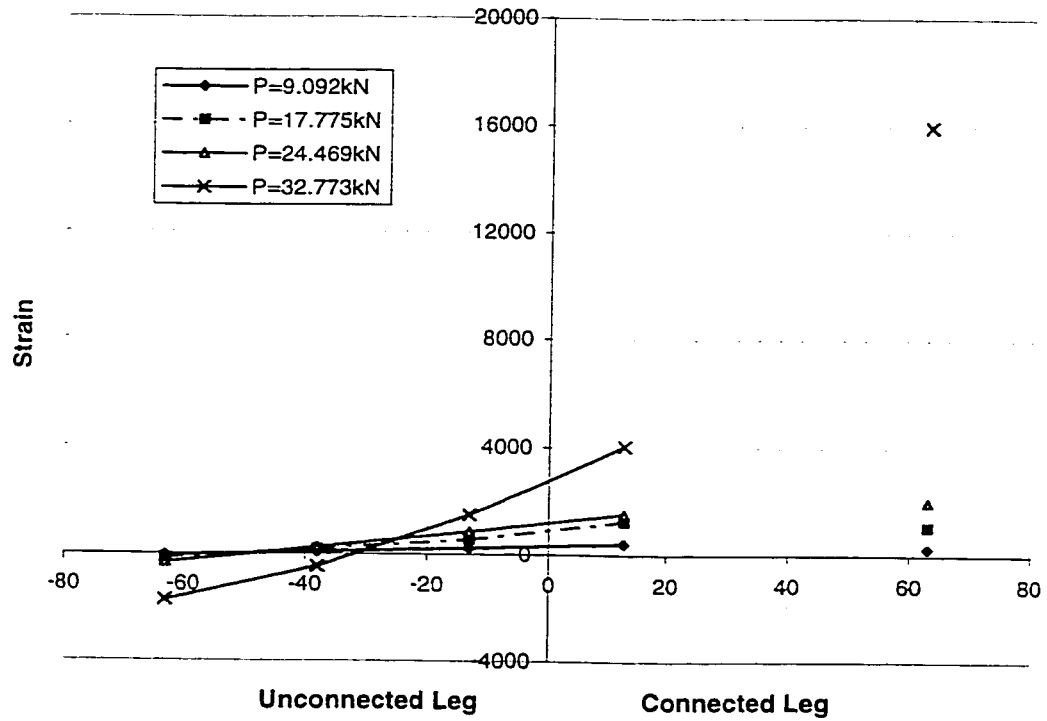
Figure 4.17 Stain Distribution at Critical Section of A3-2

57
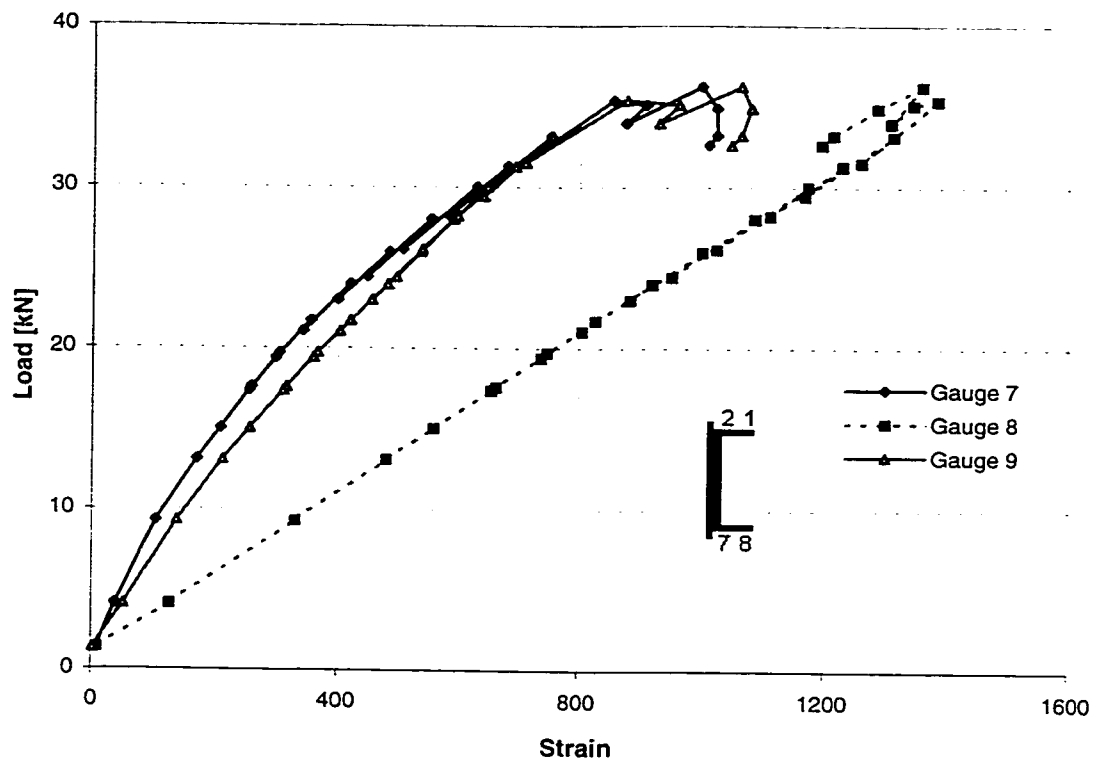
Figure 4.18 Load vs. Strain at the Flanges at Critical Section of C4-2
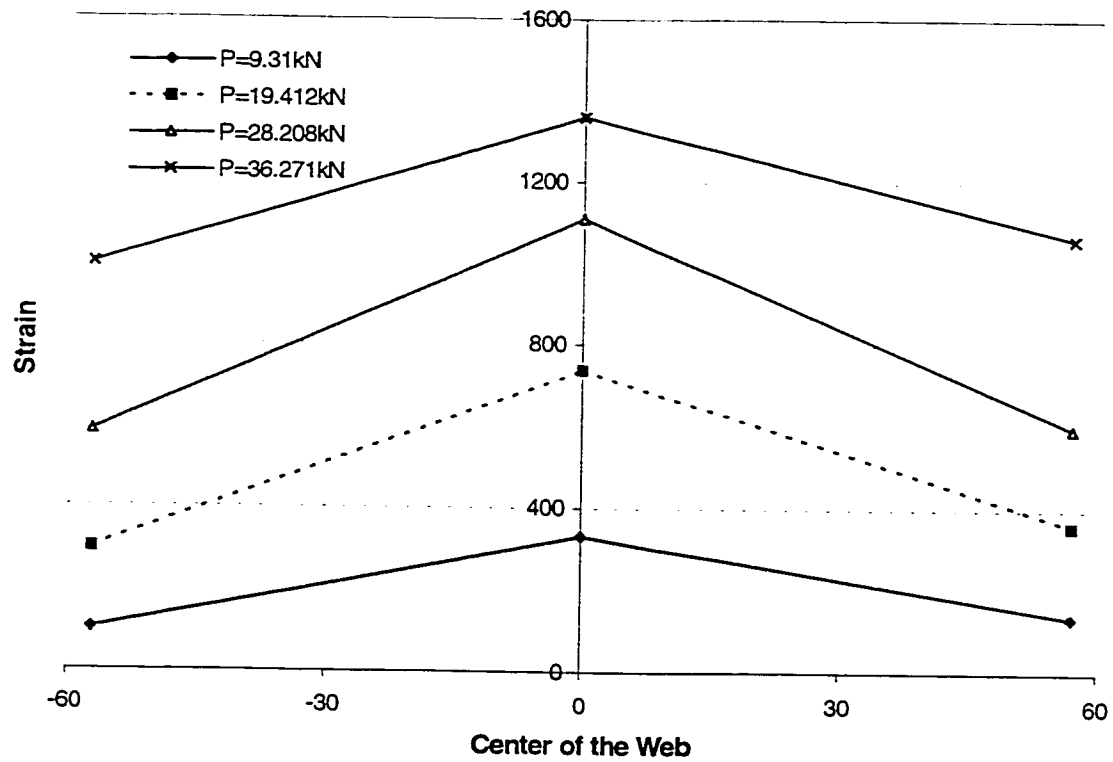
Figure 4.19 Strain Distribution at the web at Critical Section of C4-2

58
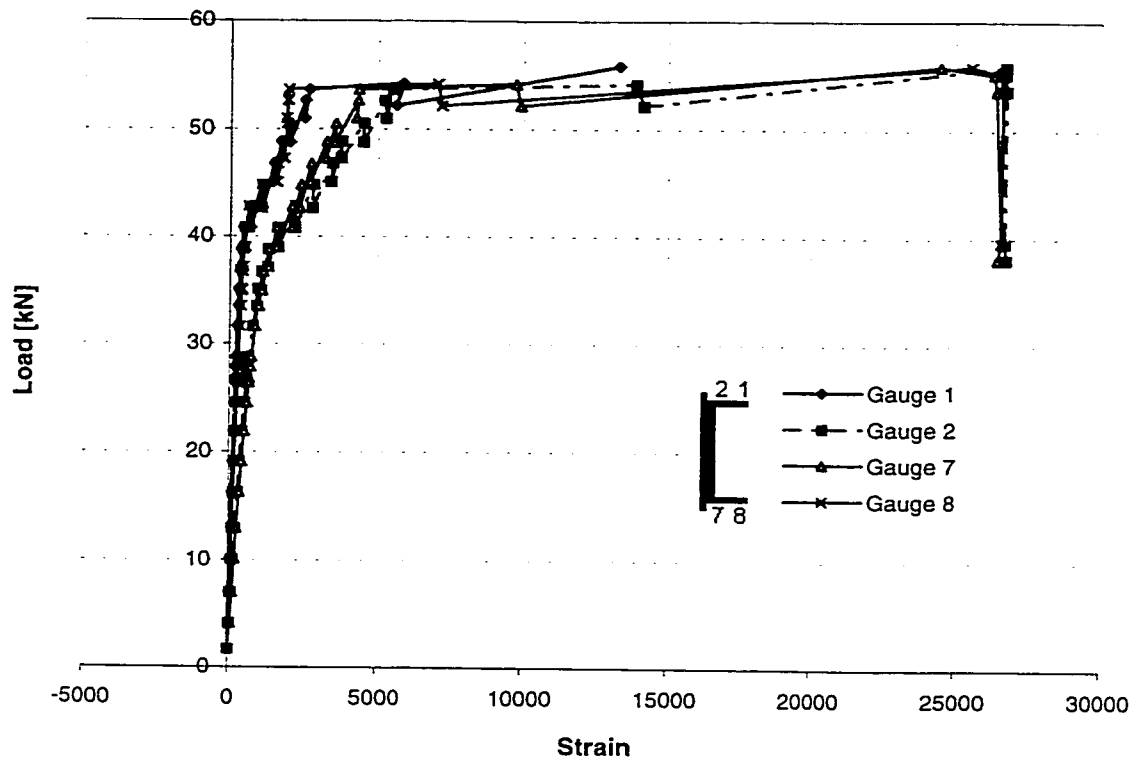
Figure 4.20 Load vs. Strain at the Critical Section at the Flanges of C4-4
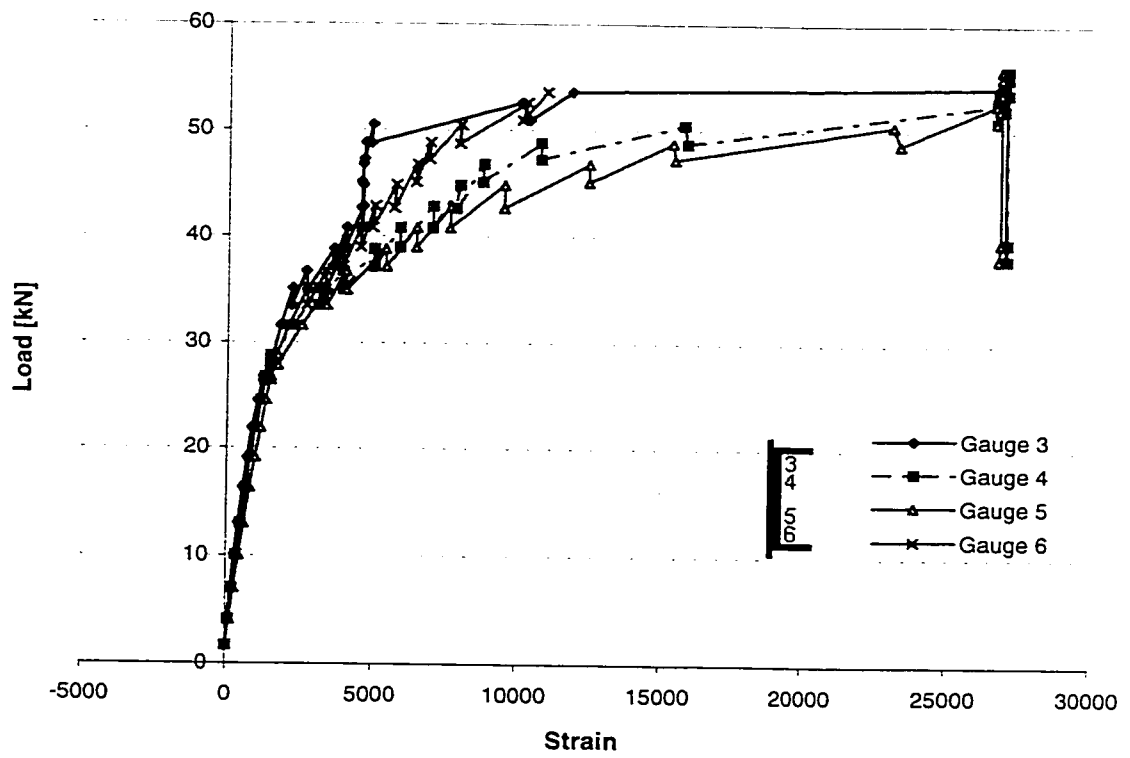
Figure 4.21 Load vs. Strain at the Critical Section at the Web of C4-4
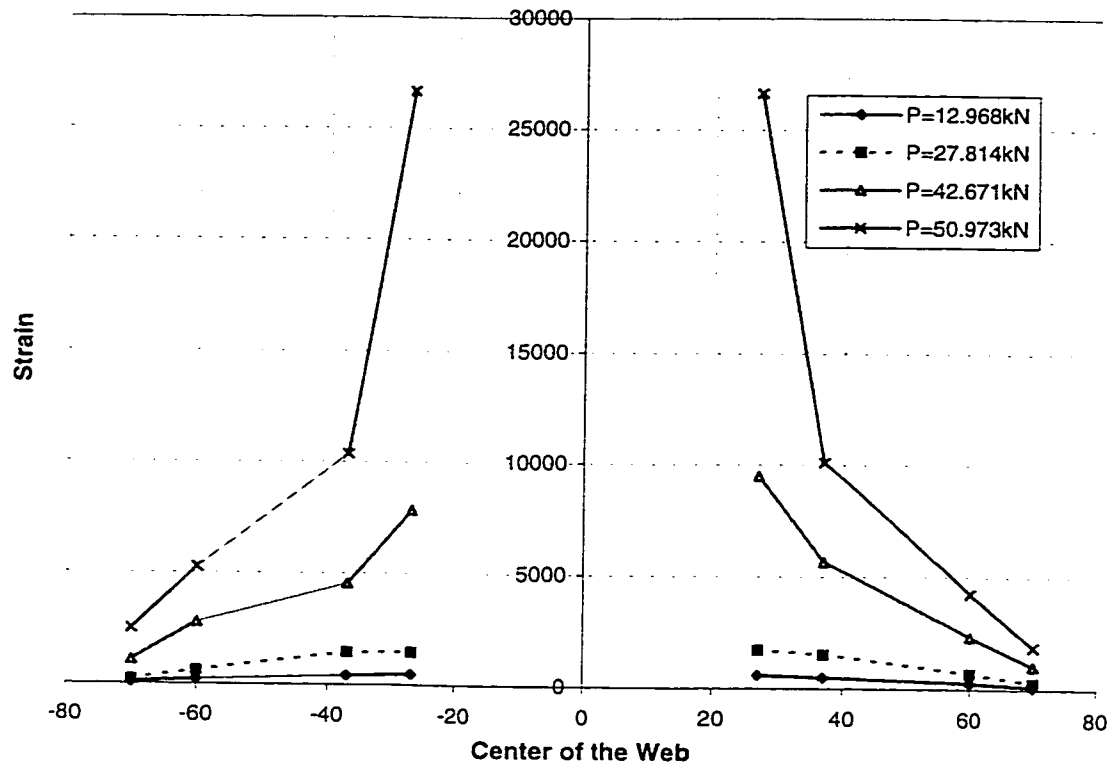
Figure 4.22 Strain Distribution at Critical Section of the Web for C4-4
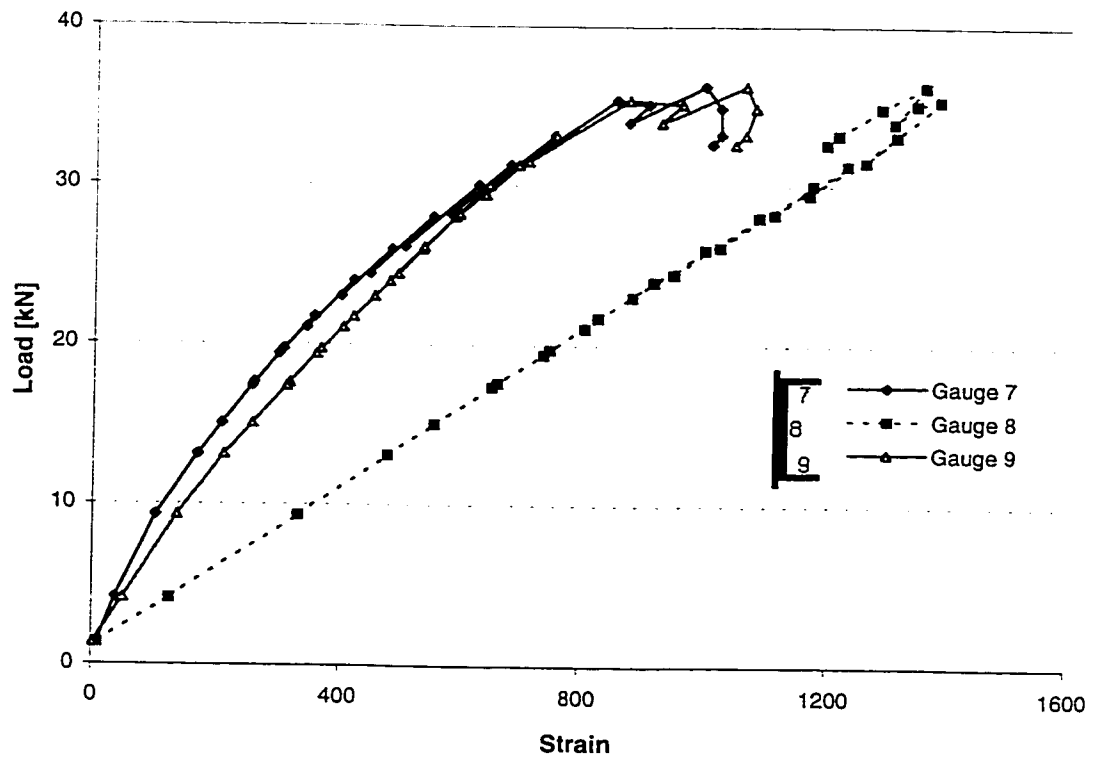
Figure 4.23 Load vs. Strain at Mid-section of C3-2

60
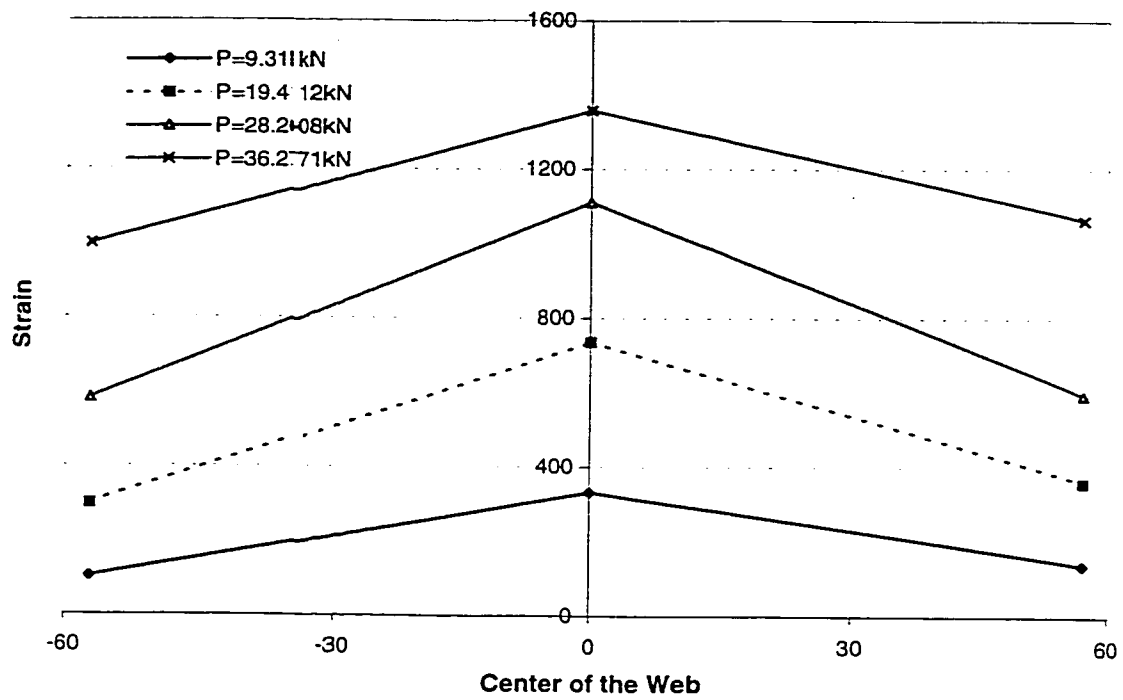
Figure 4.24 Strain Distribution at Mid-length for C3-2

5. FINITE ELEMENT ANALYSIS

5.1 General

The goal of the finite element analysis was to develop a model that could study the shear lag behavior of cold-formed steel tension member. In order to test the validity of the model, the results obtained from the analysis were used to compare with the test results from the experiments. The validated model was then used to conduct a parametric study, which can determine the effect of parameters that were not investigated specifically in the test program.

The finite element analysis was performed using the commercial finite element program ABAQUS, version 5.7 (Hibbitt et al., 1997). The analysis was conducted on a SUN SPARC workstation.

5.2 Numerical Model

The ABAQUS S4R element was used to model the tension member. It is a four-node, doubly curved quadratic shell element. This element has six degrees of freedom at each of the four nodes: three translational components and three rotational components. The S4R element allows for changes in element thickness and accounts for finite membrane strains. It has one integration point at the centroid of the element. The cross-sectional behavior of this element is integrated at five points across the thickness of the element (Hibbitt et al., 1997). Finite elements were not used to model the gusset plate because of the relatively large stiffness of these elements comparing to the test specimen.

Instead, appropriate boundary conditions were placed in the model to simulate the effects of the gusset plate on the specimens.

In order to find the optimal mesh configuration, a mesh study was performed. Optimal mesh is the coarsest mesh that would lead to an accurate result. Three different meshes were used: coarse mesh, intermediate mesh, and fine mesh. The number of elements and element size for coarse mesh was 551 and 12.7 mm by 16 mm, for intermediate mesh was 1334 and 6.35 mm by 5 mm, and for fine mesh was 3271 and 3.18 mm by 5 mm. The meshes are shown in Fig. 5.1. The maximum load obtained from the analysis was 21.8 kN for coarse mesh, 15.6 kN for the intermediate mesh, and 15.2 kN for the fine mesh. The relative difference in maximum load, RD, was calculated using the following formula:

$$RD = \frac{P - P_f}{P_f} \times 100\% \tag{5.1}$$

where P = maximum load obtained from the coarse or intermediate mesh model

P_f = maximum load obtained from the fine mesh model

The difference between the load predicted using the coarse mesh and the fine mesh was 43.4 percent, while the difference between the loads predicted using the intermediate mesh and the fine mesh was 2.63 percent. It showed that the intermediate mesh has converged to the exact solution and it was chosen as the mesh used in this study.

Using the mesh chosen above, a typical undeformed finite element mesh of the modeled angles and channels were developed, as shown in Fig. 5.2 and Fig. 5.3 respectively. As can be seen in these figures, only half of the length of the member was

modeled in the finite element analysis due to symmetry of the test specimens. At the mid-length cross-section of the member, the 2 and 3-direction rotational degrees of freedom were fixed. In the analysis, the axes 1, 2, and 3 were equivalent to axes x, y and z, respectively.

In the finite element models, the shear deformation of the bolts was ignored. The load was assumed to transfer from the gusset plate to the angle fully by the bearing of the bolts. Therefore, one-half of the circumference of each bolt hole in the model, which was supposed to bear against the bolt in the tests, was fixed in the 1 and 2 translational degrees of freedom. Since the bolts had been tightened before loading and the bolts were still tight after tests, all nodes in the first two circumferences around the bolt holes of the specimen were fixed in the 3 translational degree of freedom.

5.3 Material Model

In the analysis, the materials were assumed to behave according to the incremental isotropic hardening material. The material properties used at corner area of the specimen were different from that at the flat area. This is to account for the influence of cold working. The material properties used in the analysis were true stress and strain converted from the average stress-strain data obtained from the coupon tests. Figures 5.4 and 5.5 show the material model used to model the angle sections and channel sections, respectively. Failure was assumed to occur when the most highly strained elements in the specimen around the first bolt reached the rupture strain. The rupture strains used for

angle and channel sections are 0.5 and 0.45, respectively. These two values were obtained from the tension coupon tests based on the following equation:

$$\text{Rupture Strain} = \text{Ln}(\frac{A_o}{A})$$

[5.2]

where A = cross sectional area of the tension coupon at rupture

A_0 = initial cross sectional area of the tension coupon

5.4 Numerical Results

5.4.1 Experimental-to-analytical ratio

Table 5.1 presents the summary of the results obtained from the finite element analysis. It also shows the comparison of the experimental results with the analytical results. The ratio of ultimate load from the experiments to that from the analysis ranges from 0.97 to 1.31 with mean value of 1.11 and coefficient of variation of 0.093 for the angle sections, and from 0.95 to 1.31 with mean value of 1.09 and coefficient of variation of 0.096 for the channel sections. Good agreement was obtained, except for couple of specimens, between the numerical predictions and test results. The reason of discrepancy can be attributed to the conservative assumptions, such as neglecting the frictional forces between the gusset plates and the specimen, used in the finite element model.

5.4.2 Mode of failure

The typical deformed shape obtained from the analysis for the angle and channel sections, which failed in net section fracture, along with that obtained from the experiment are shown in Fig. 5.6 and Fig. 5.7, respectively. Similar to the experimental results, the unconnected leg of the angle and the flanges of the channel moved in towards

the bolt line. The in-plane bending at the connecting length of the angle specimens observed in the test (as shown in Fig. 5.6) is due to the eccentric force generated after the fracture of the section at the first line of bolts. Fig. 5.8 and Fig. 5.9 show the deformed shape obtained from the test and the analysis for the angle and channel sections that failed in bearing. Similar to the test specimens, piling of material at the bolt hole was observed in the analysis. In addition, Fig. 5.10 shows the side view of the typical deformed shape of specimen, the bending of the free end agreed with what has been observed in the experimental program. As illustrated in those figures above-mentioned, the numerical analysis gave a good prediction in the failure mode and deformed shape.

5.4.3 Load-deformation relationship

The load versus elongation behavior obtained from the finite element analysis can be compared with that observed in the experiment. The comparison for specimen A2-1 (51 mm x 51 mm x 1.214 mm angle, one-bolt connection) for the angle section and specimen C2-3 (51 mm x 29 mm x 1.214 mm channel, three-bolt connection) for the channel section are plotted in Fig. 5.11 and Fig. 5.12, respectively, where it can be seen that the curves from analysis were very similar to the test results. For the other specimens, the analytical behavior also agreed with the test results in the general sense, except that the limit elongation reached at the limit point of the analytical curves were different from that of the test results. This is due to the simplified assumption of the rupture strains used in the analyses. Other load-versus-elongation curves are included in Appendix B.

Although the maximum load was similar, discrepancy between the analytical and test results for specimen C3-1 was observed in terms of the deformation due to the slip, therefore, a repeated test, designated as *C3-1, was done. However, the tested load for the *C3-1 was 50 percent higher than that of C3-1. As discussed in Section 4.2.3, the increase was possibly due to the high clamping force produced when tightening the bolts, in order to verify this, a slightly different finite element model was used for *C3-1. At the connection, the bolt hole of *C3-1 was filled in order to eliminate the stress concentration at the edge during the loading process. So that, instead of having bearing type of connection, the frictional type of connection would be obtained. Figure 5.13 shows the analytical and experimental results for both specimen C3-1 and *C3-1. It shows that the analytical results correlate with the experimental results in terms of ultimate load for both cases. In addition, from the comparison of the analytical result with the experimental result for *C3-1, it confirmed that the 50 percent increase of load in the test was due to the change in connection type from bearing to frictional. Therefore, it proved that the amount of bolt tension applied does affect the ultimate load capacity of the connection.

5.4.4 Strain and stress distributions

The typical strain distributions at the critical section obtained from the analysis for the angle and channel section are shown in Figs. 5.14 and 5.15, respectively. Similar to the test results, the strain around the bolt hole was highest in both the angle and channel section. At the unconnected leg of the angle section and the flanges of the channel section, the strains were in compression, which correlated with the test results.

Moreover, in agreement with the test results, at low load level, the strain distributions in both cases remained relatively uniform at the critical section. In Figs. 5.16 and 5.17, the strain distributions at the mid-section of A3-2 and C3-2, respectively, are plotted. As it can be seen, similar distributions were obtained as compared with the test results.

Figures 5.18 and 5.19 show the typical stress contour of the analyzed angle A4-2 (102 mm x 102 mm x 1.214 mm angle with two bolt at the connection) and channel C4-2 (102 mm x 29 mm x 1.214 mm channel with two bolt at the connection), respectively, at the last load step. The lighter color indicates the specimen was in compression while the darker was in tension. It can be seen that the unconnected leg of the angle and the flanges of the channel were in compression. The stress distributions of specimens A4-2 and C4-2 at the critical section, with three load levels, are shown in Figs 5.20 and 5.21, respectively. They show stress redistribution at the unconnected leg for the angle section and the web of the channel section. The high compression stresses at the tip of the unconnected leg of the angle and at the flanges of the channel, observed closed to the ultimate load, agreed with the buckling behavior from the tests. Figures 5.22 and 5.23, and Figs. 5.24 and 5.25 show the stress contour and stress distributions at the critical section of specimen A4-4 (102 mm x 102 mm x 1.214 mm angle, four-bolt connection) and specimen C4-4 (102 mm x 102 mm x 1.214 mm channel, four-bolt connection), respectively. As shown in these figures, the compression stresses at the unconnected leg of the angle and the flanges of the channel were not as high as those specimens with short connected length.

Table 5.1 Summary of Analytical Results

Specimen	Size [mm]	Ultimate Load [kN] Test	Ultimate Load [kN] Analysis	Test / Analysis
A2-1	51 x 51 x 1.214	15.48	15.55	1.00
A2-2	51 x 51 x 1.214	27.92	21.32	1.31
A2-2N	51 x 51 x 1.214	24.01	21.32	1.13
A2-3	51 x 51 x 1.214	31.09	25.76	1.21
A3-1	76 x 76 x 1.214	21.94	21.71	1.01
*A3-1	76 x 76 x 1.214	23.49	21.71	1.08
A3-2	76 x 76 x 1.214	32.77	27.59	1.19
A3-3	76 x 76 x 1.214	37.72	33.31	1.13
A4-1	102 x 102 x 1.214	18.28	18.87	0.97
A4-2	102 x 102 x 1.214	33.95	33.51	1.01
A4-3	102 x 102 x 1.214	45.08	39.39	1.14
A4-4	102 x 102 x 1.214	49.44	41.45	1.19
C2-1	51x29x1.214	22.97	23.58	0.97
C2-2	51x29x1.214	36.84	28.11	1.31
C2-3	51x29x1.214	37.56	32.85	1.14
C3-1	76x29x1.214	18.05	19.01	0.95
*C3-1	76x29x1.214	26.99	26.24[+]	1.03
C3-2	76x29x1.214	36.27	31.98	1.13
C3-3	76x29x1.214	48.12	40.76	1.18
C4-1	102x29x1.214	19.64	18.98	1.03
C4-2	102x29x1.214	40.52	39.59	1.02
C4-3	102x29x1.214	52.54	45.20	1.16
C4-4	102x29x1.214	55.81	50.62	1.10

[+]Obtained from different model mentioned in Section 5.4.3
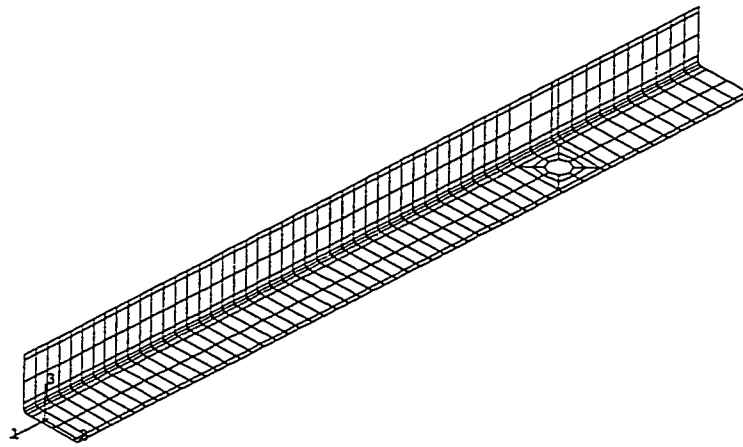
a) Coarse Mesh
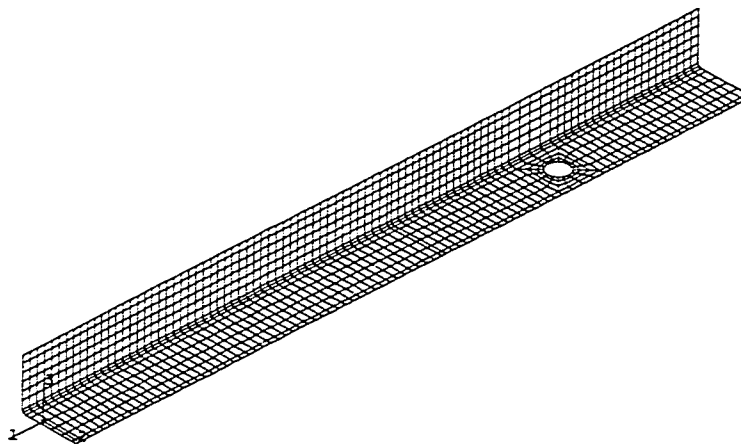
b) Intermediate Mesh
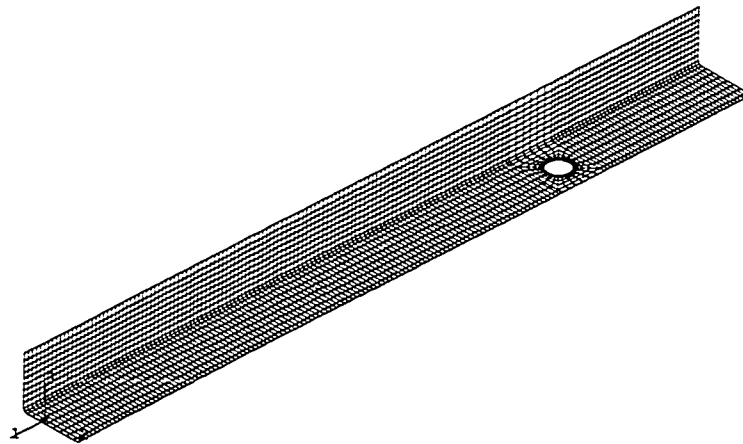
c) Fine Mesh

Figure 5.1 Mesh for A2-1 Specimen
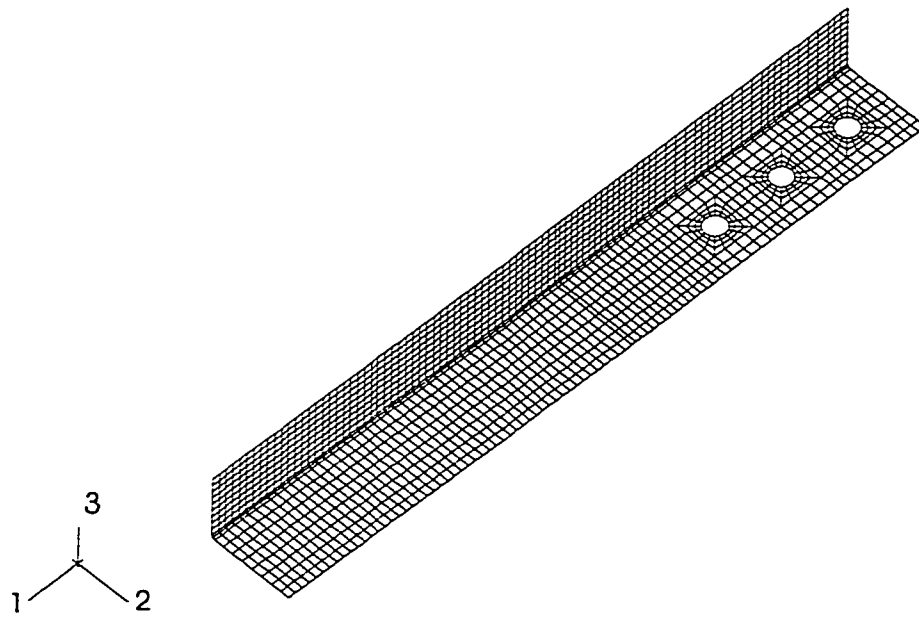
Figure 5.2 Typical Finite Element Mesh for Specimen A3-3
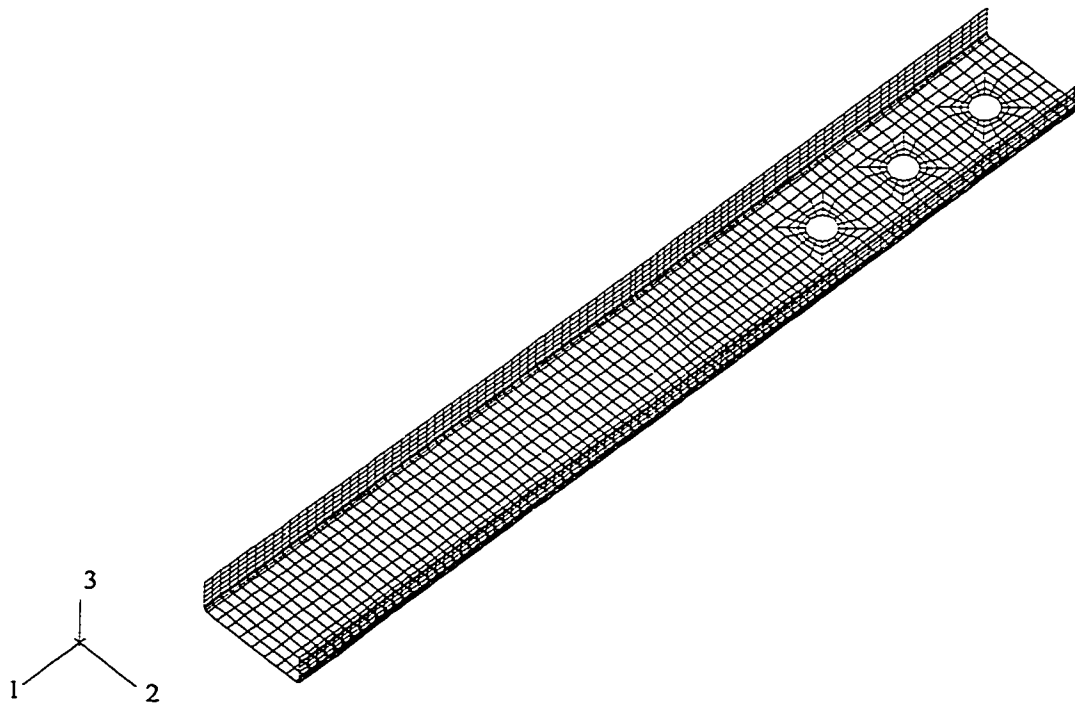
Figure 5.3 Typical Finite Element Mesh for Specimen C3-3
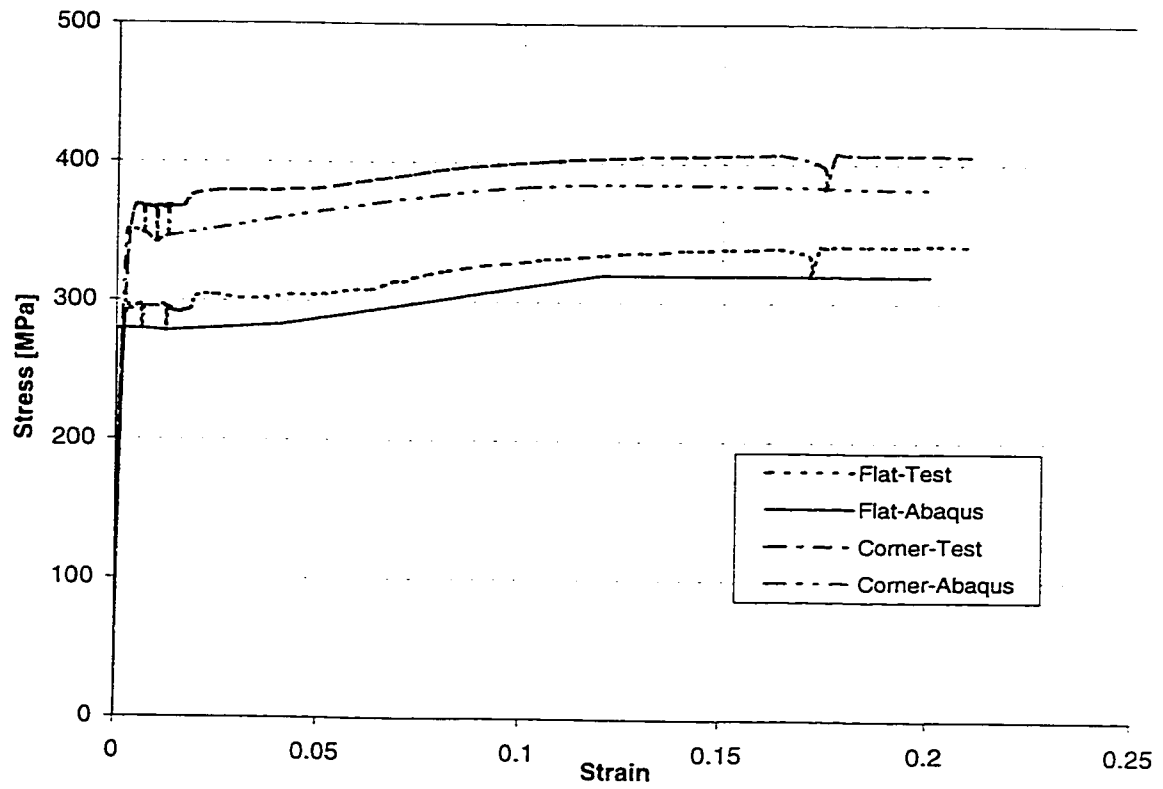
Figure 5.4 Material Model for Angle Sections
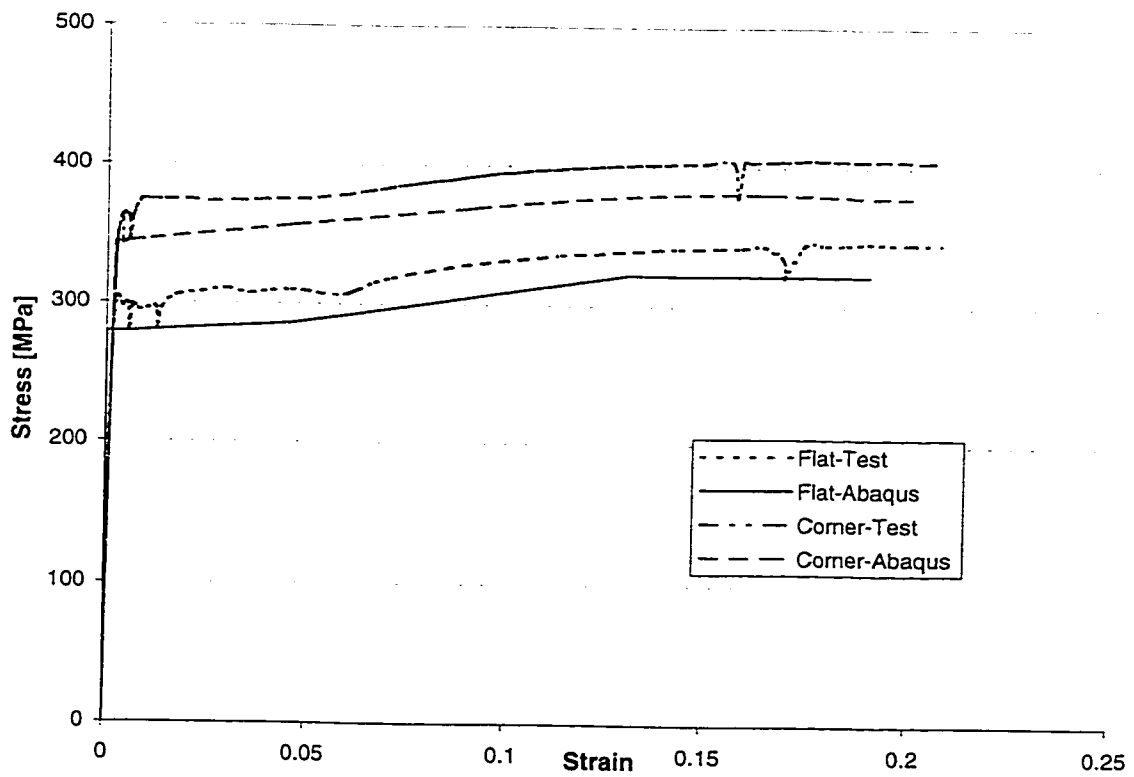
Figure 5.5 Material Model for Channel Sections
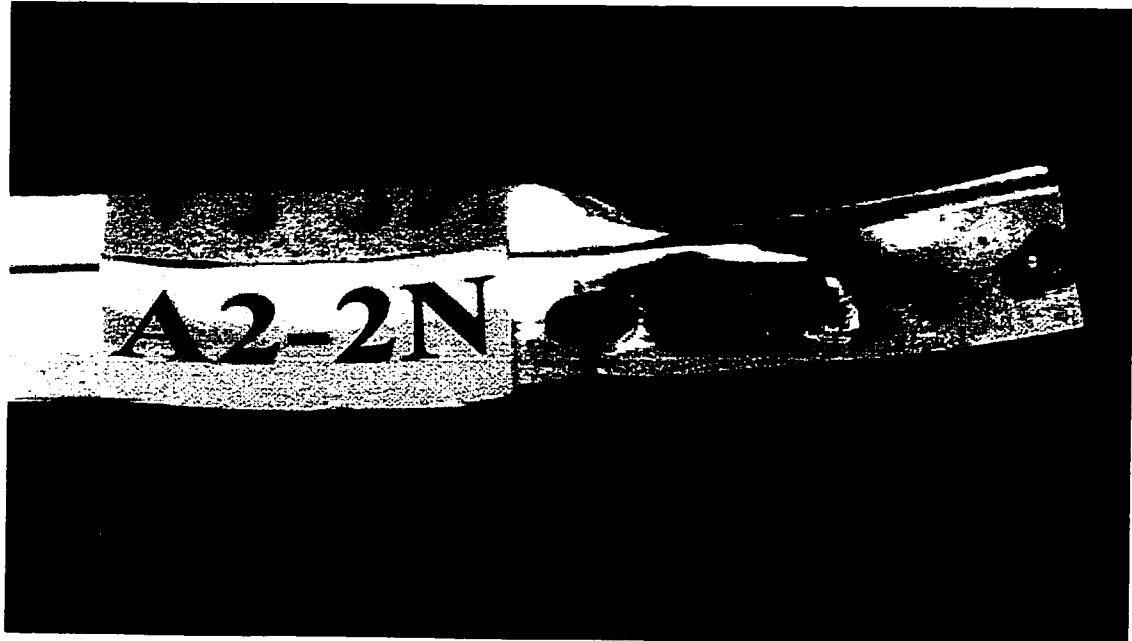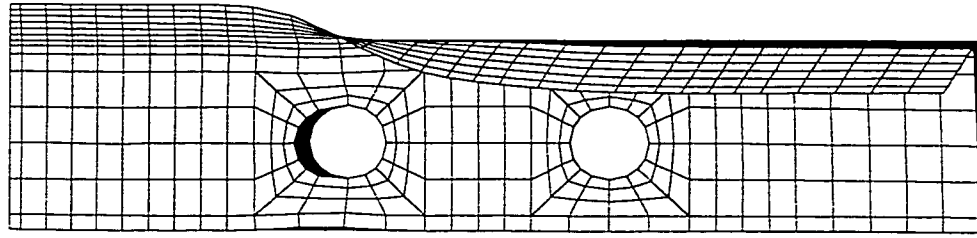
Figure 5.6 Predicted and Observed Deformation for Specimen A2-2N
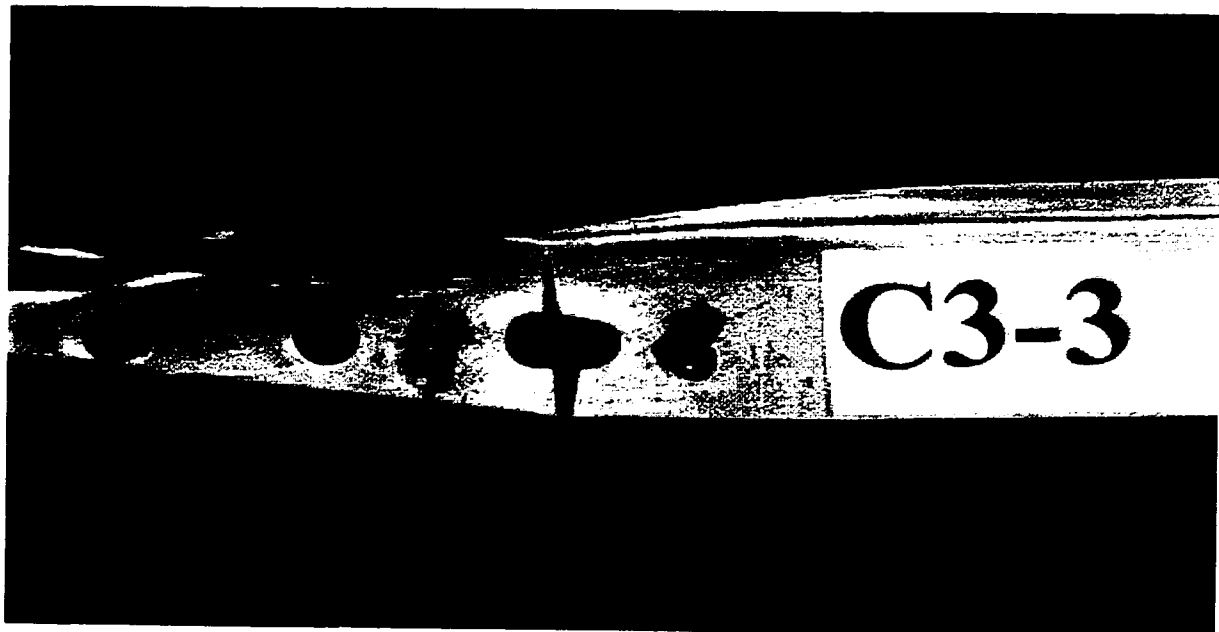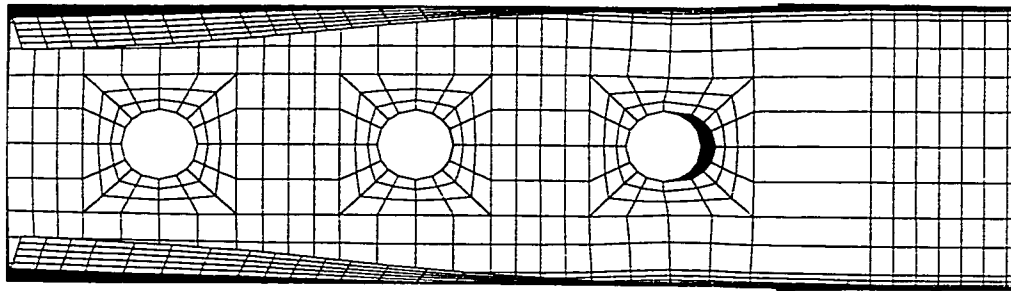
Figure 5.7 Predicted and Observed Deformation for Specimen C3-3
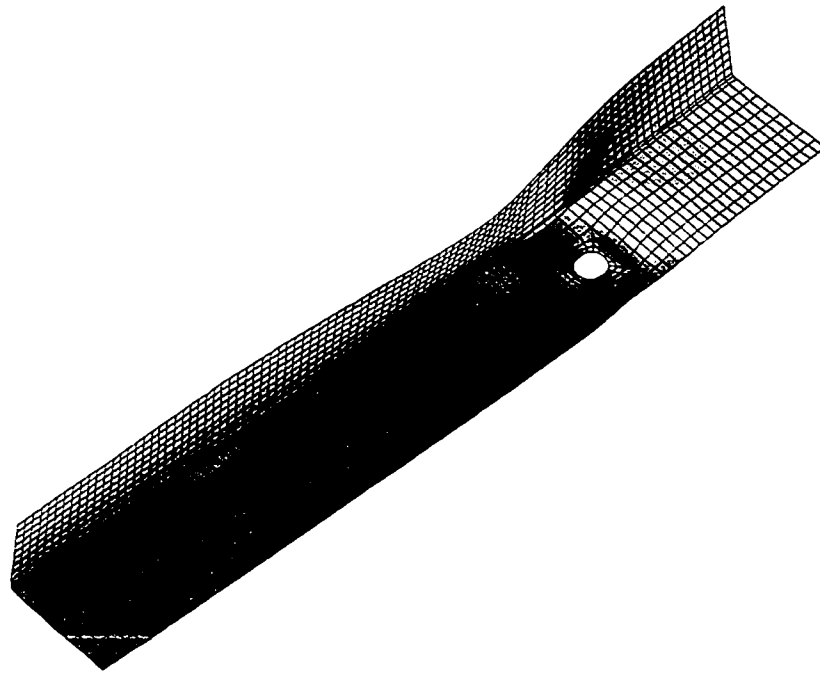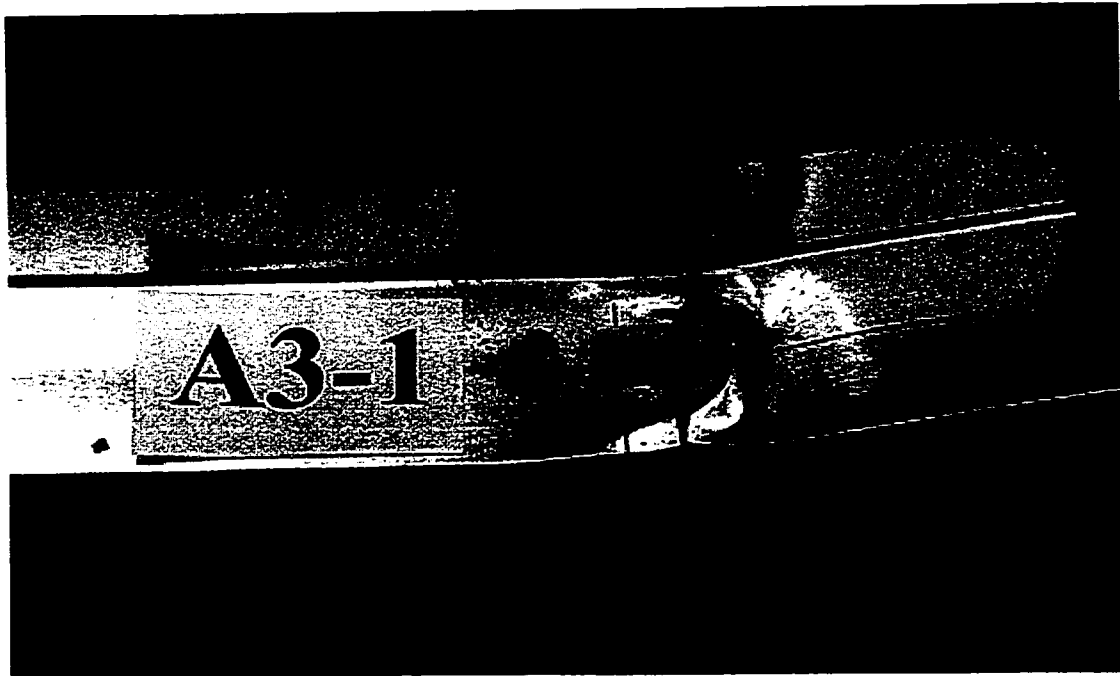
Figure 5.8 Observed and Predicted Deformed Shape for Specimen A3-1
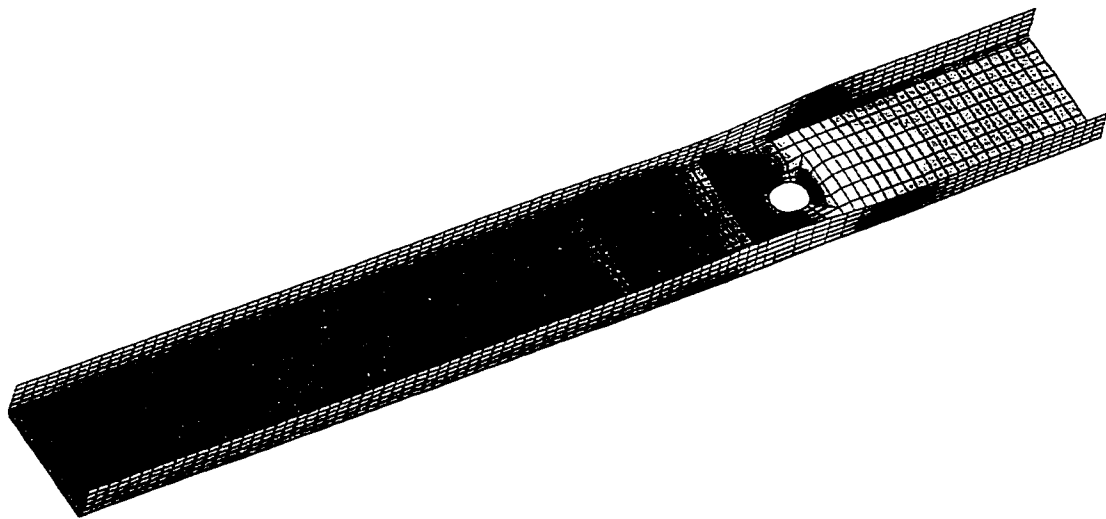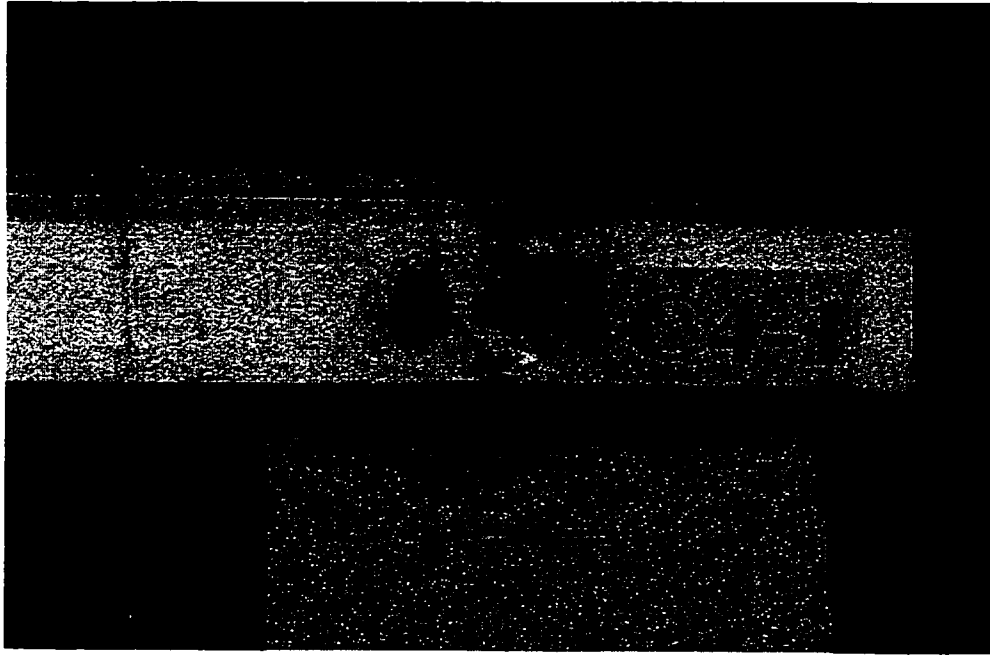
Figure 5.9 Observed and Predicted Deformed Shape for Specimen C4-1

Figure 5.10 Side View of Typical Predicted Deformed Specimen C3-2
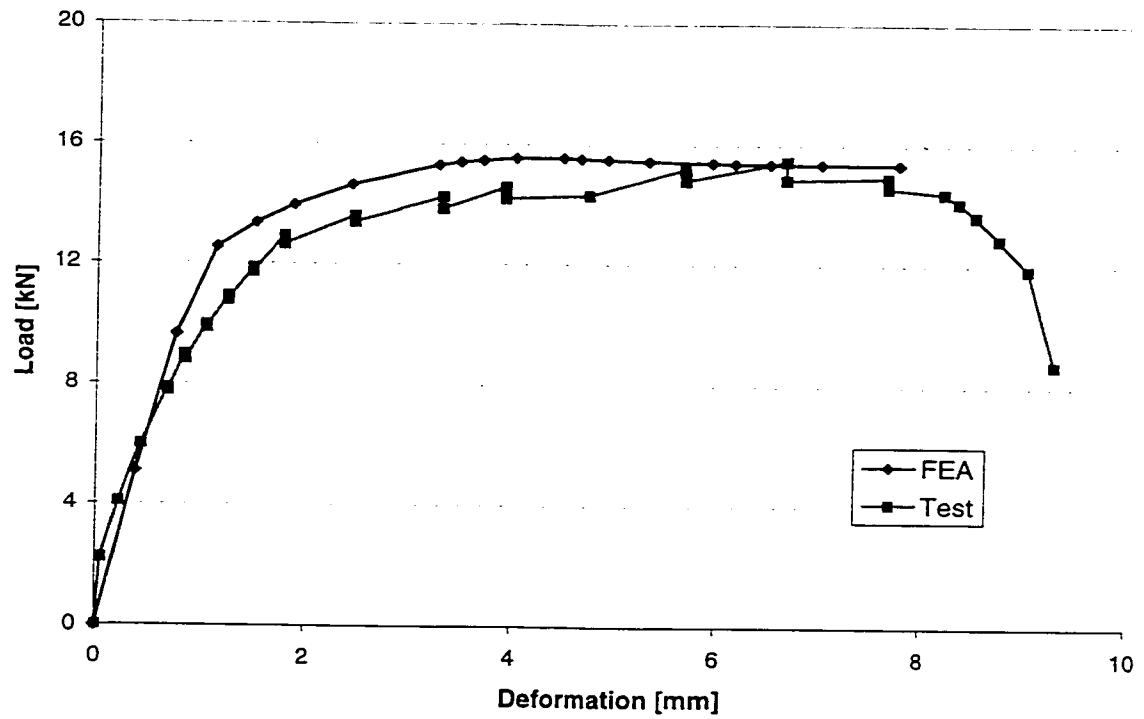
Figure 5.11 Comparison of Load vs. Deformation for A2-1
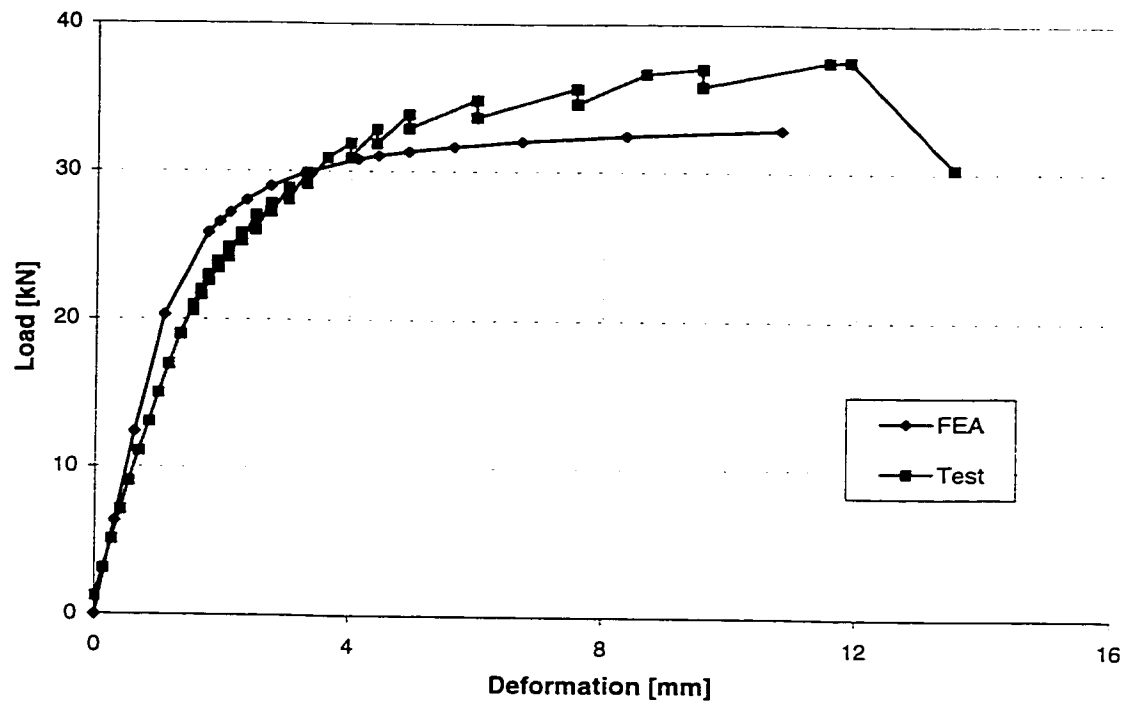
Figure 5.12 Comparison of Load vs. Deformation for C2-3
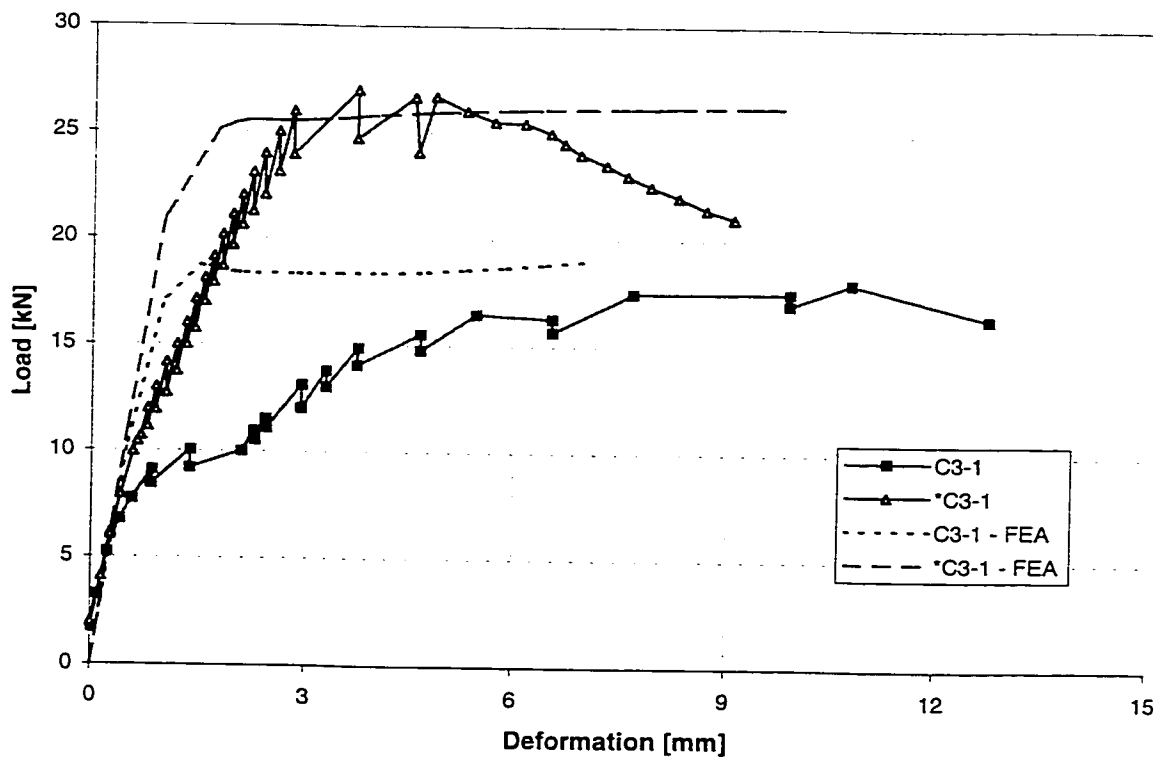
Figure 5.13 Comparison of Load vs. Deformation for C3-1 and *C3-1
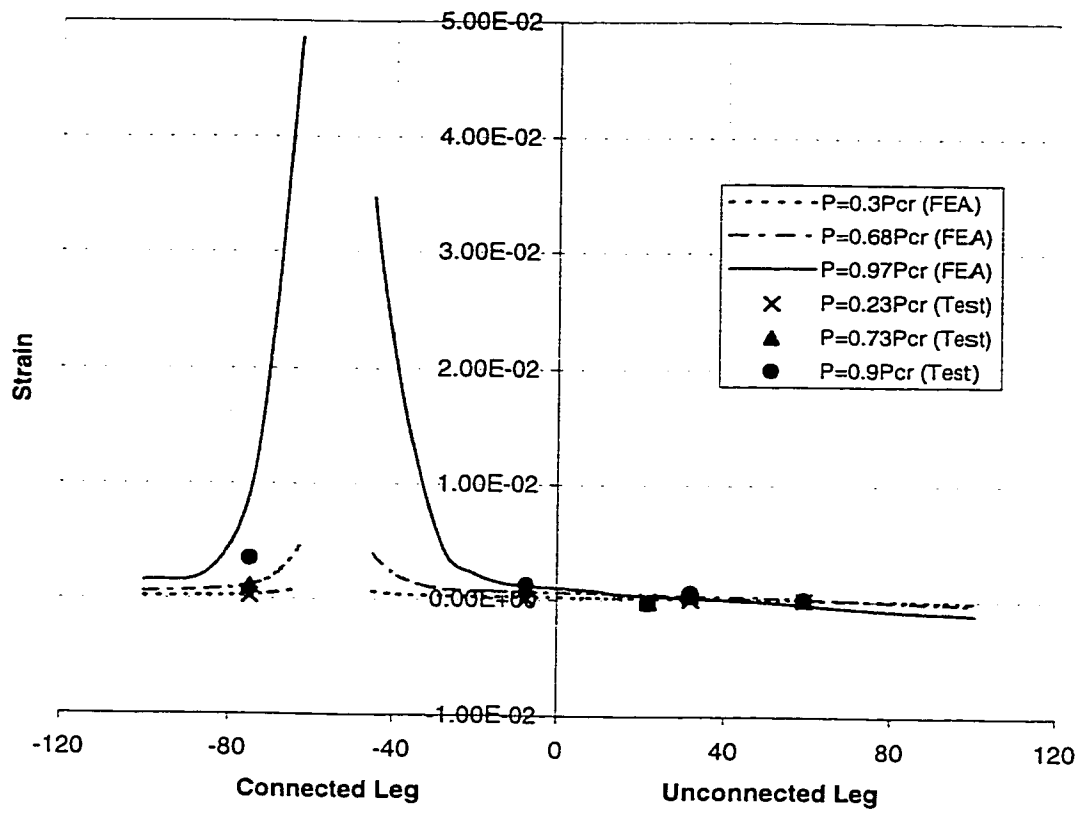
Figure 5.14 Strain Distributions of Specimen A4-2 at Critical Section
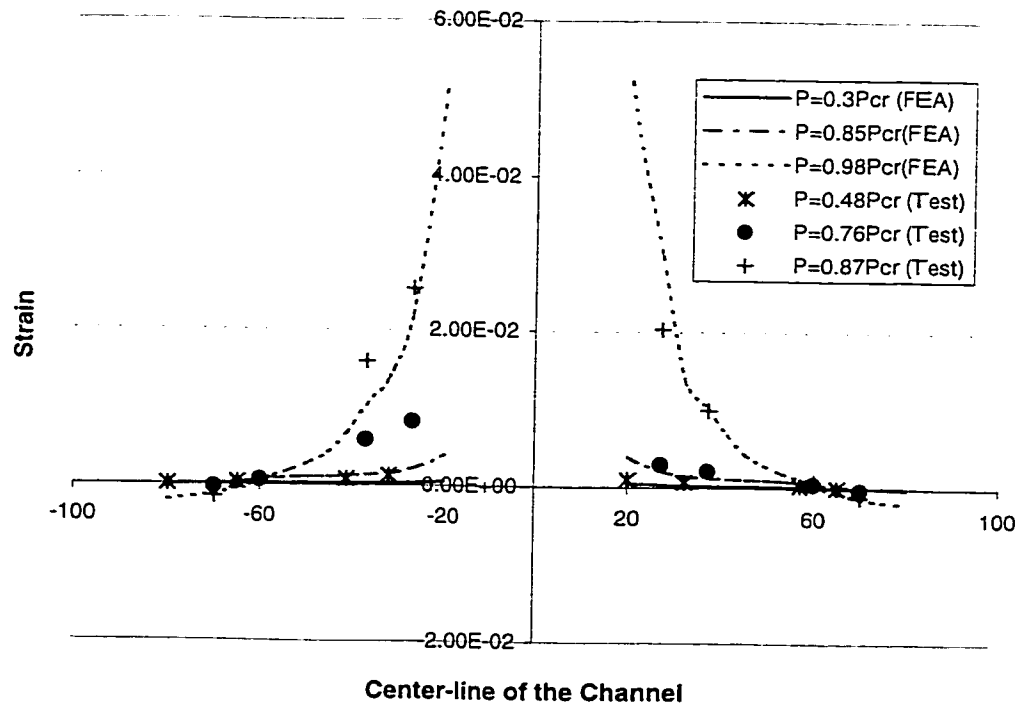
Figure 5.15 Strain Distributions of Specimen C4-2 at Critical Section
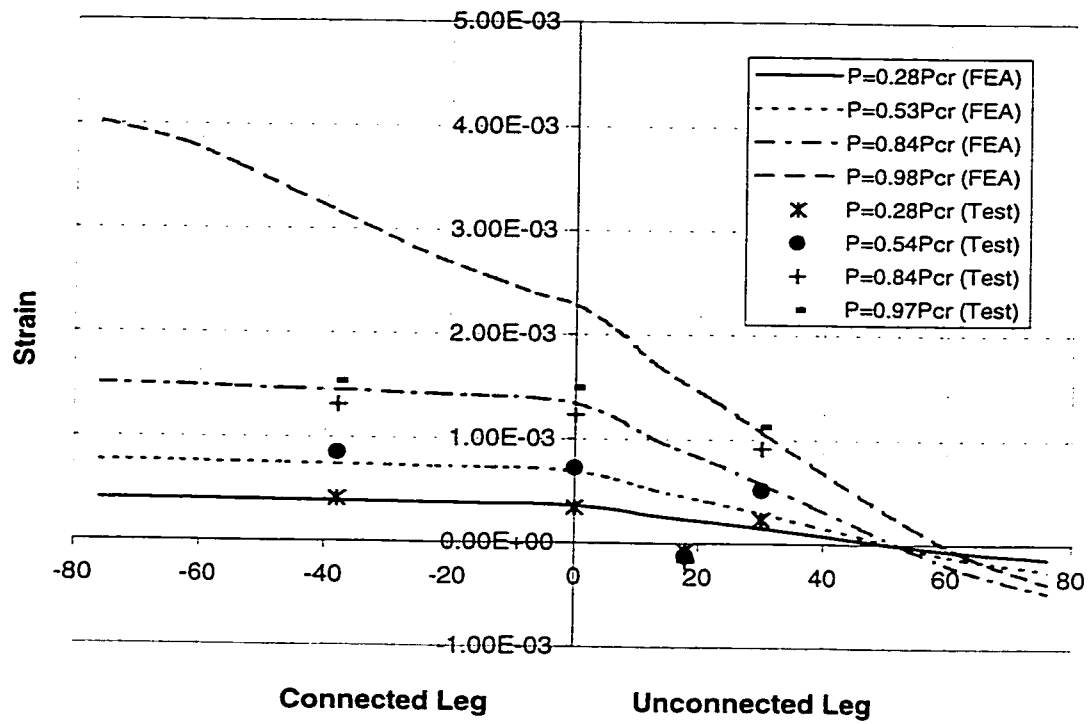
Figure 5.16 Strain Distribution of Specimen A3-2 at Mid-Section
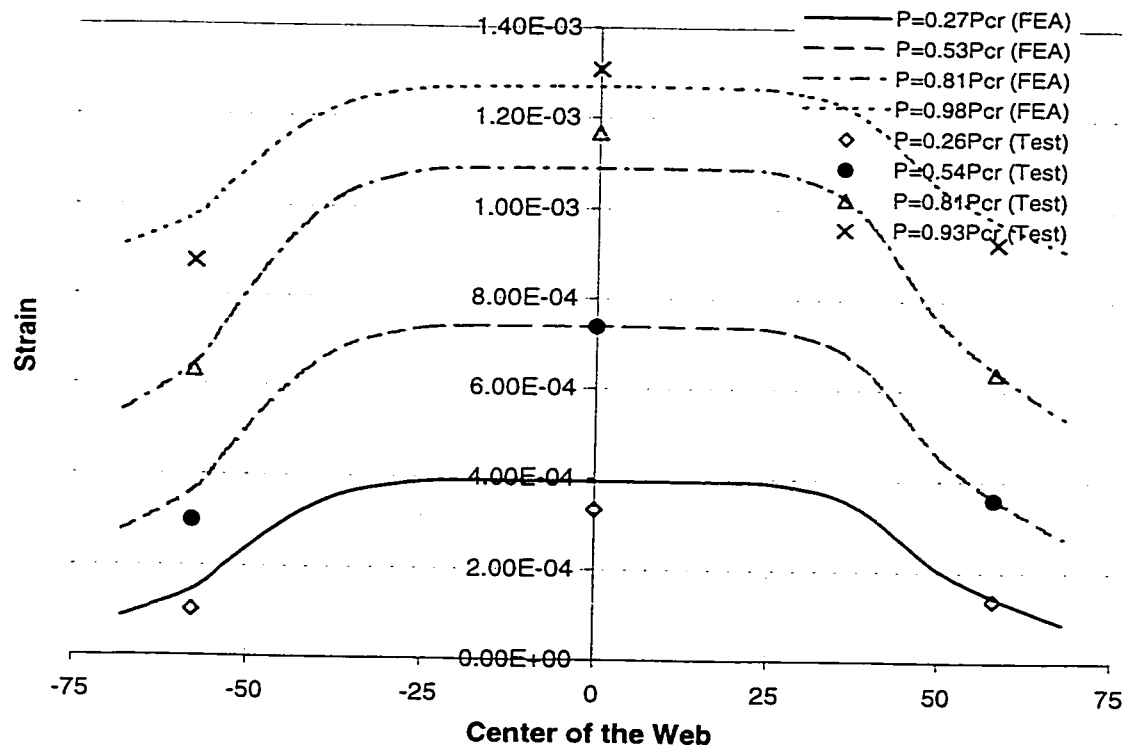
Figure 5.17 Strain Distribution of Specimen C3-2 at Mid-Section
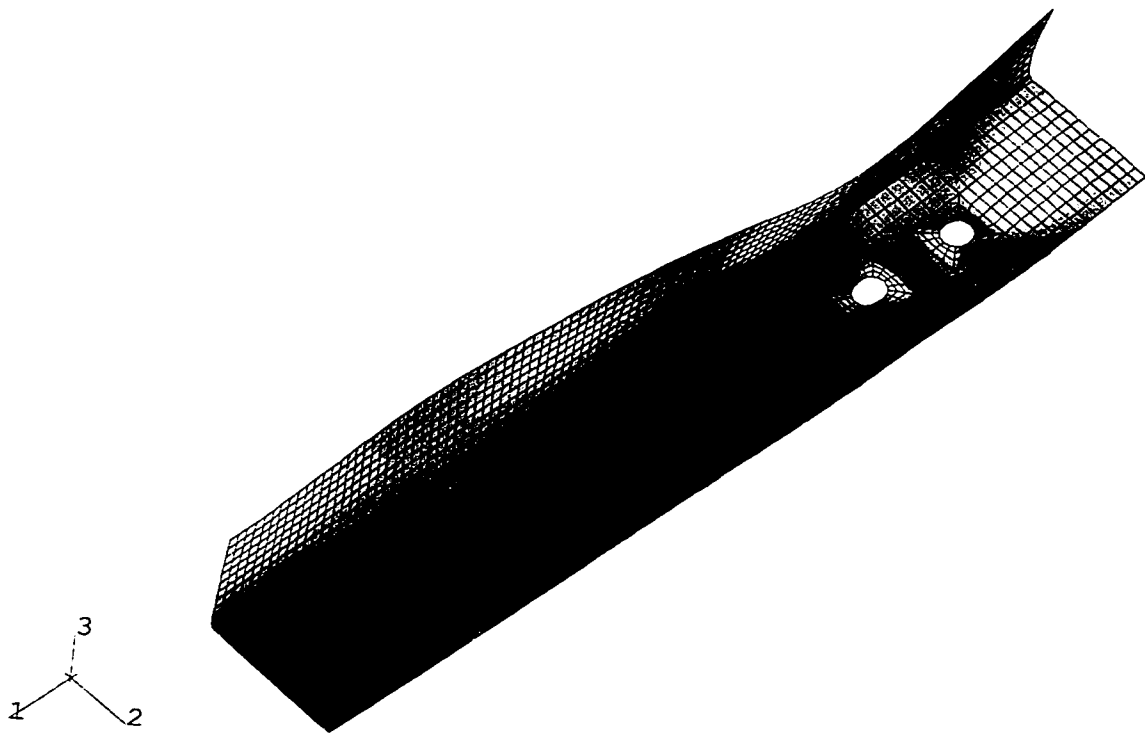
Figure 5.18 Stress (in Load Direction) Contour of Specimen A4-2 at the Ultimate Load
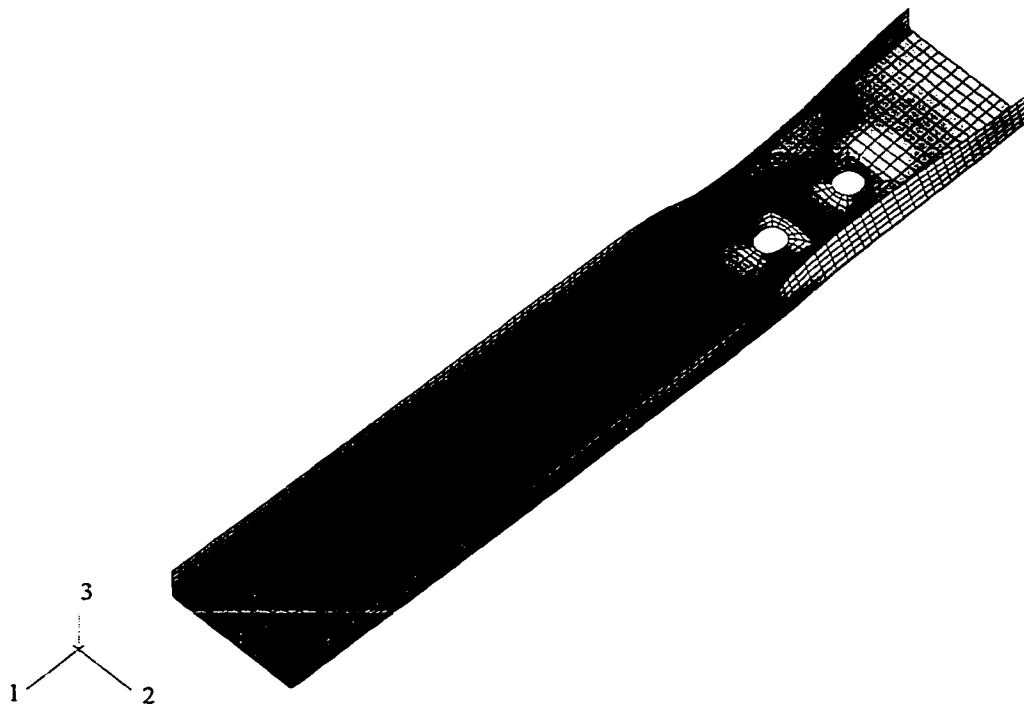
Figure 5.19 Stress (in Load Direction) Contour of Specimen C4-2 at the Ultimate Load
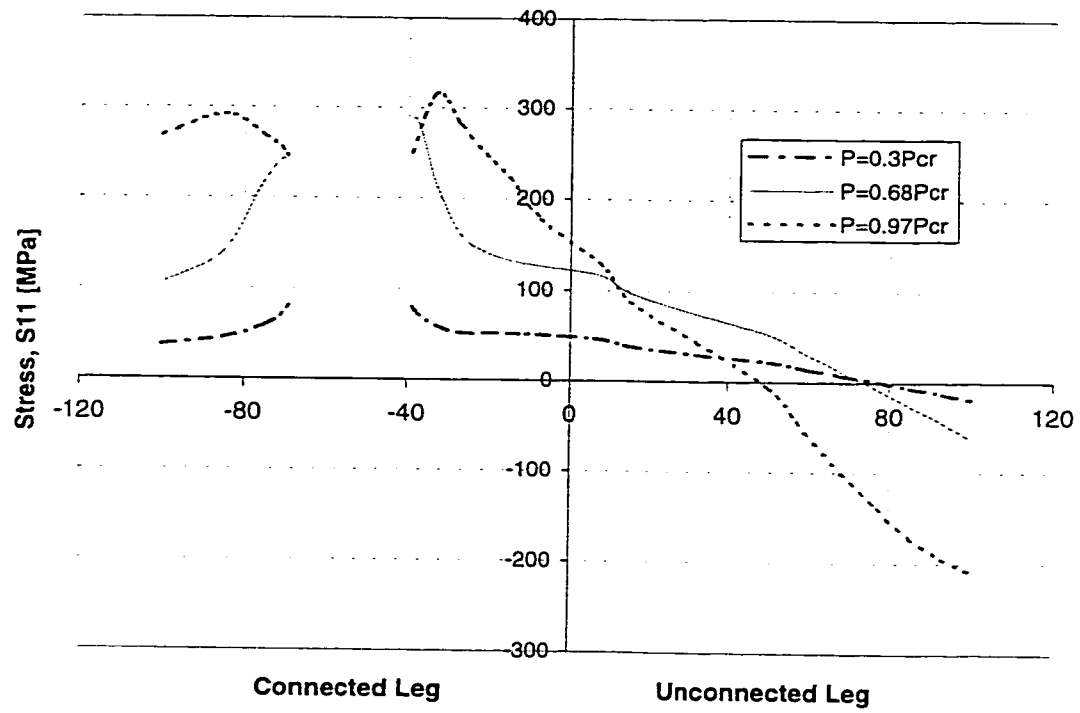
Figure 5.20 Stress Distributions of Specimen A4-2 at the Critical Section
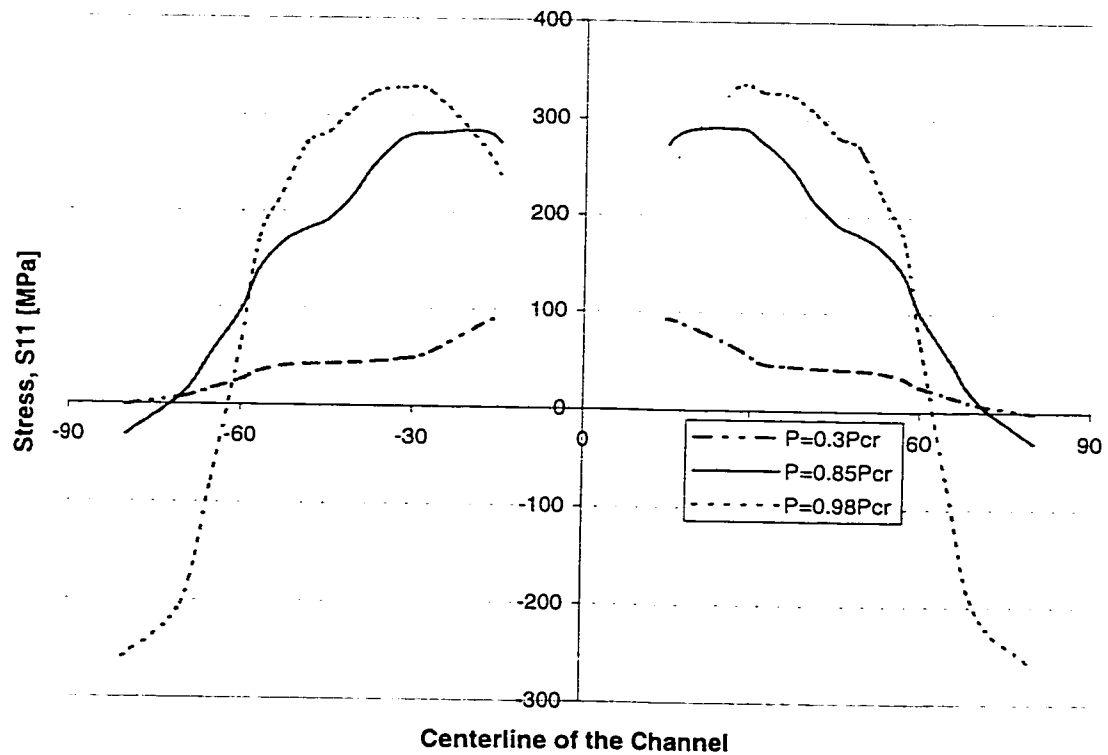
Figure 5.21 Stress Distributions of Specimen C4-2 at the Critical Section

82
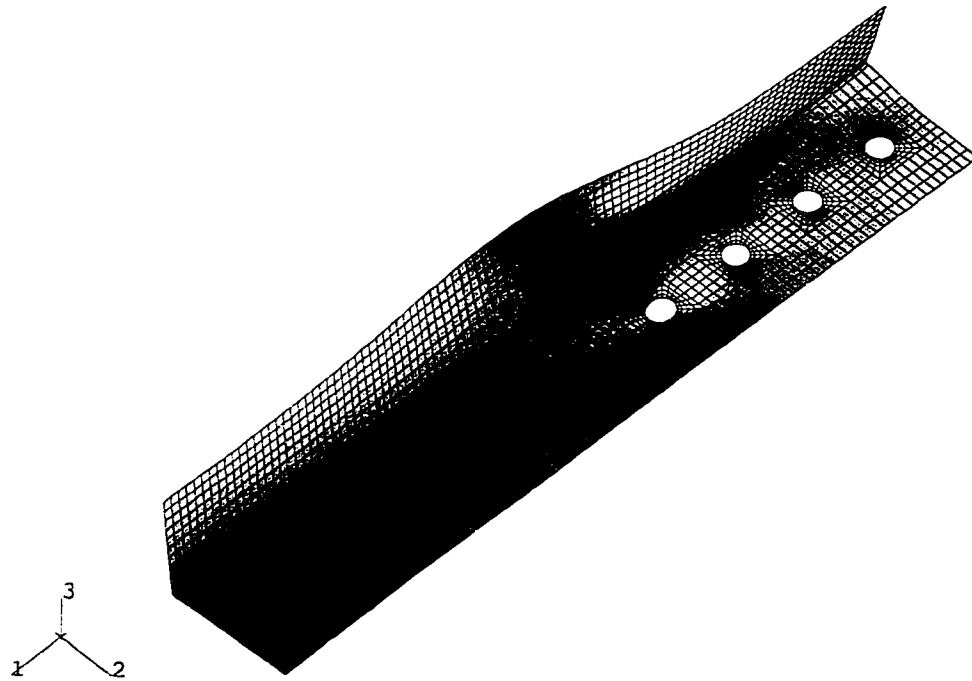
Figure 5.22 Stress Contour (in Load Direction) of Specimen A4-4 at the Ultimate Load
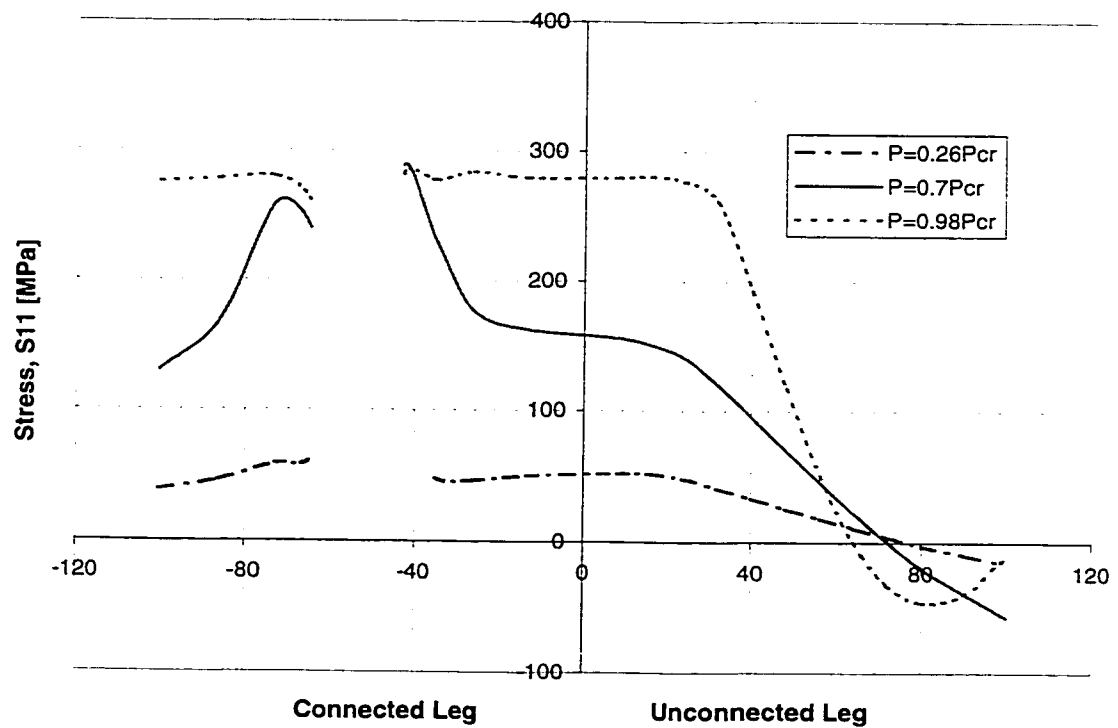
Figure 5.23 Stress Distributions of Specimen A4-4 at the Critical Section
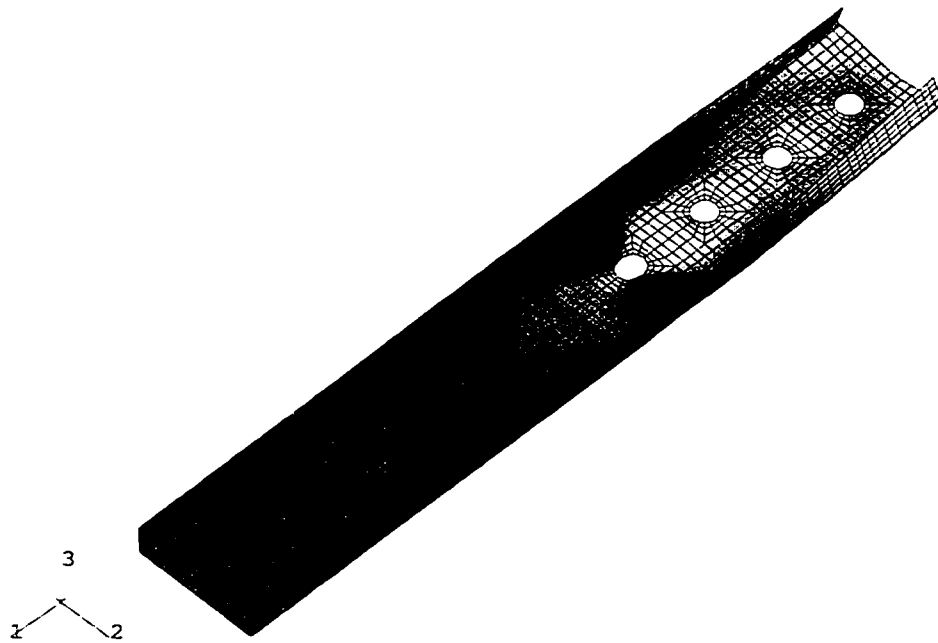
Figure 5.24 Stress Contour (in Load Direction) of Specimen C4-4 at the Ultimate Load
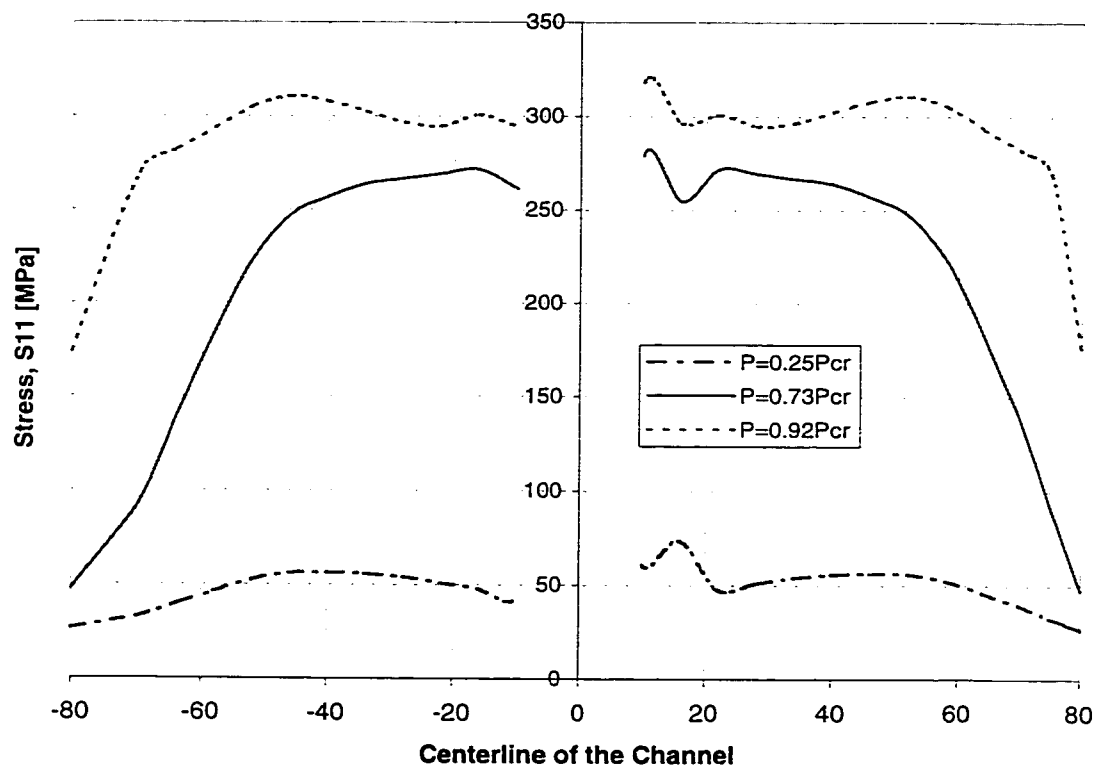
Figure 5.25 Stress Distribution in Specimen C4-4 at the Ultimate Load

6. PARAMETRIC STUDIES

6.1 General

The finite element models developed in the previous chapter were used to investigate the net section strength of angle and channel cold-formed tension members. The parameters that were considered in the analysis included the material property, the eccentricity, the number of bolts used at the connection, the flat width-to-thickness ratio and the flat width-to-bolt diameter ratio.

The results obtained from the finite element analyses were then discussed with respect to the above-mentioned parameters that were considered to have a possible effect on the net section efficiency. A net section efficiency formula for each section based on the parametric studies was proposed and the formulae were verified with the test results obtained in this project and from the others.

6.2 Design of Parametric Studies

6.2.1 Scope of the study

6.2.1.1 <u>Angle Sections</u>

For the angle sections, only equal leg angles without stiffeners and single line of bolts are considered. Ranges of the parameters considered are listed as follows:

Size: 50 mm x 50 mm, 76 mm x 76 mm, and 102 mm x 102 mm

Thickness, t (Gage number): 2.667 mm (G12), 1.905 mm (G14), 1.524 mm

(G16), and 1.219 mm (G18)

Number of bolts: 1 to 4

Spacing between bolts: 63.5 mm

Diameter of bolt: 19.1 mm

Material constant (F_u/F_y): 1.15 (310 MPa/270 MPa), 1.35 (310 MPa/230 MPa)

and 1.50 (345 MPa/230 MPa)

6.2.1.2 Channel Sections

For the channel sections, only unstiffened channels with single line of bolts

connected at the web are considered. Ranges of the parameters considered are listed as

follows:

Size (web depth x flange width): 50 mm x 29 mm, 76 mm x 29 mm, and 102 mm

x 29 mm

Thickness, t (Gage number): 2.667 mm (G12), 1.905 mm (G14), 1.524 mm

(G16), and 1.219 mm (G18)

Number of bolts: 1 to 4

Spacing between bolts: 63.5 mm

Diameter of bolt: 19.1 mm

Material constant (F_u/F_y): 1.15 (310 MPa/270 MPa), 1.35 (310 MPa/230 MPa)

and 1.50 (345 MPa/230 MPa)

A total of 100 finite element analyses were performed for angle and channel

sections. For all the analyses, the analysis was stopped when the strain of the element

86

reached the rupture strain, and the rupture strain used in this analysis was assumed to be 50%.

6.2.2 Designation of the numerical models

A system of identification is used to differentiate between the various numerical models. The first digit represents the geometry that being either an angle (a) or a channel (c). The second digit signifies the gage number of the specimen. The third digit designates the size of the model in inches and the fourth digit designates the number of bolts used in the connections. Some of the models have an extra number at the end of the designation, this number signifies the end distance of the model in millimeters. For those models having a material constant other than 1.35, an extra letter is inserted at the end of the designation: 'x' represents the model having a material constant of 1.15 while 'y' represented the model having a material constant of 1.5. The descriptions of models used in this study for angle and channel sections are listed in Tables 6.1 and 6.2, respectively.

6.3 Results of Parametric Studies

The results for the angle sections and channel sections are showed in Tables 6.3 and 6.4, respectively. The ratio of the results obtained from the finite element analysis to the predicted load was calculated for each mode of failure. The predicted loads for net section strength, bearing failure, and block shear fracture were calculated according to Eqs. 2.25, 2.33, and 2.34 discussed in Section 2.3, respectively, except the resistance factors of 0.85ϕ in Eq. 2.25 and ϕ in Eqs. 2.33 and 2.34 were taken as unity. Only the

models that were associated with the net section failure mode were considered in further discussion.

In order to differentiate the net section fracture from bearing and block shear failures, assumption regarding the finite element-to-predicted load ratio has been made. The formulas of the predicted load for bearing and block shear (Eqs. 2.33 and 2.34) were assumed to be accurate. That means if the finite element result-to-predicted load ratios for bearing and block shear were greater than or equal to 1.0, then the section would fail in bearing and block shear, respectively. Otherwise, the section was failed in net section fracture. The governing mode of failure for each section is shown in "bold" in Tables 6.3 and 6.4.

6.4 Discussion of Parametric Study Results

6.4.1 Effect of material property

To study the effect of ultimate tensile-to-yield strength ratio on the net section efficiency (N. S. E.), 76 mm x 76 mm x 1.905 mm angle and 102 mm x 28.6 mm x 1.905 mm channel sections were used. Three types of material properties were considered. The rupture strain was assumed to be 50%. Tables 6.5 and 6.6 show the details and results for this analysis. The effect of material property on the net section efficiency for angle and channel sections is shown in Fig. 6.1 and Fig. 6.2, respectively. As shown in these figures, as the ultimate tensile-to-yield strength ratio, F_u/F_y, increases, the net section efficiency decreases. It also means that higher the ductility the lower net section efficiency.

Besides net section fracture, as mentioned in Chapter 2, there is another design criteria that has to be considered when designing tension members: gross section yield, which is limited by yielding at the gross section. For those sections with higher ultimate tensile-to-yield strength ratio, the probability for them to be governed by yielding at gross section is higher, and this can be shown in Fig. 6.3. In this figure, by assuming the net section area equal to the gross section area, gross section yield would occur when the net section efficiencies for the section with material constant of 1.15, 1.35, and 1.50 are above 0.87, 0.74, and 0.67, respectively. The values of these critical net section efficiencies are derived by equating the net section strength to the gross section yielding:

$$UA_nF_u = A_gF_y$$

$$U = \frac{A_gF_y}{A_nF_u}$$

By assuming $A_g = A_n$,

$$U = \frac{F_y}{F_u}$$

As seen in this figure, gross section yield is obtained for the section with F_u/F_y ratio of 1.35 and 1.5 when four or more bolts are used at the connection. Although the net section efficiency for these sections is lower, a greater value of elongation can be obtained since the ductility is higher for these sections. For the angle models with four bolts at the connection, the load vs. deformation curves of different material properties are plotted in Fig. 6.4. As illustrated in this figure, the elongation for the section with F_u/F_y ratio of 1.5 is greater than that with F_u/F_y ratio of 1.15; while the ultimate load for that section is lower than that with F_u/F_y ratio of 1.15.

Another contributing factor to the net section fracture is the rupture strain. Generally, a material with higher F_u/F_y ratio gives higher rupture strain. For the ease of analysis, however, the same rupture strain is used for all the models without considering the difference in limiting strain, the ultimate load predictions for the section with higher ductility are therefore lower. Since large variations in the material properties exist, the intermediate material constant (F_u/F_y = 1.35) with 50% rupture strain was used as the material properties for the rest of the parametric analysis.

6.4.2 Effect of eccentricity, $\bar{x}$

The eccentricity is one of the factors influencing the net section efficiency. According to Munse and Chesson (1963), the efficiency of a section would decrease as the eccentricity increases. The eccentricity highly depends on the shape of the cross section. Tables 6.7 and 6.8 summarize all the sectional properties, including eccentricity, flat width-to-thickness ratio (w/t), and flat width-to-bolt diameter ratio (w/d), along with the net section efficiency for the angle and channel sections, respectively. As can be seen in the tables, the net section efficiency for channel models was generally higher than that for the angle models. For instance, considering the a14-4 series of the angle sections and c14-4 series of the channel sections, both series have the w/t ratio of 50 and w/d ratio of 5, while the eccentricity of the angle sections are as twice much as that for the channel sections. By comparing the two series, the net section efficiency of the angle sections are significantly lower than that of the channel sections due to the difference in eccentricity, therefore, it implies that the shear lag effect in channel sections was not as severe as that in angle sections.

In addition, the effect of eccentricity on net section efficiency for angle sections and channel sections is shown in Figs. 6.5 and 6.6, respectively. The sections considered in both cases were those with 3 bolts at the connection and gage thickness of 14 to 18. As shown in Fig. 6.5, the net section efficiency decreases significantly as the eccentricity increases for the angle sections. The decrease of net section efficiency may also be contributed from the flat width-to-thickness ratio. However, by comparing the G16 and G18 series with G14 series, same significant drop in efficiency is also observed. The main difference between the three series is the value of flat width-to-thickness ratio; however, the net section efficiency remains almost the same for the sections with the same eccentricity. It implies that the eccentricity is the most important factor for the net section efficiency of angle section. In contrast, different observation is found for the channel sections. Figure 6.6 shows that the net section efficiency increases as the eccentricity increases; however, the increase is not significant. It implies that the eccentricity is not the main factor affecting the net section efficiency of the channel sections. This can be contributed to the practical geometric limitation of channel sections. In this study, the flange to web ratio of channel sections was limited to the range of from 0.25 to 0.56. This limitation practically eliminates the significance of the eccentricity on channel sections.

6.4.3 Effect of number of bolts

As discussed in Chapter 2, the net section strength is strongly affected by the connection length, designated as 'L'. The connection length was calculated using the following formula:

$$L = \text{Bolt spacing} \times (\text{Number of bolts} - 1)$$

Since there was only one bolt spacing used in this parametric study, the effect of the number of bolts used at the connection was simply equivalent to the effect of the connection length. The results of the gage 14 angle and channel sections are used to study the effect of the number of bolts on the net section efficiency. There are twelve angle and twelve channel sections with six different section shapes considered in this comparison. 1, 2, 3 and 4 bolts were used at the connections.

Figures 6.7 and 6.8 show the relation between the net section efficiency and the number of bolts used at the connection for gage 14 angle and channel models, respectively. From these figures, it shows that the net section efficiency increases with the increase in number of bolts used. In addition, for those angle and channel sections with flat width-to-thickness ratio, w/t, less than 25, and channel sections with w/t ratio less than 50, the net section efficiency of the sections with four transverse lines of bolts gave about the same values as those with three transverse lines of bolts. It implies that effect of the number of bolts used at the connection, as well as the effect of the connection length, upon the net section efficiency is not significant when three transverse lines of bolts were used for those sections. Similar observations are found as well for the angle and channel sections with different thickness.

6.4.4 Effect of flat width-to-thickness ratio

Flat width, w, is usually used when defining the width of connected element. It is the width of the straight portion of the connected element and does not include the bent

portion of the element. It is usually non-dimensionalized with the thickness, t, of the section to form the flat width-to-thickness ratio, w/t, which has been proved to be an influential factor for net section efficiency.

In order to study the effect of flat width-to-thickness ratio on net section efficiency, nine angle and nine channel sections with three different section sizes were considered in this comparison. The number of bolts at the connection is 2 for the angle sections and 3 for the channel section. The results are shown in Figs. 6.9 and 6.10 for the angle and channel sections, respectively. The values of the eccentricity and the flat width-to-bolt diameter ratio are the same for the sections used in each curve. These figures show that as the flat width-to-thickness ratio increases, the net section efficiency decreases.

6.4.5 Effect of flat width-to-bolt diameter ratio

As mentioned above, the flat width could also be non-dimensionalized with the diameter of the bolt hole, d, to form the flat width-to-bolt diameter ratio, w/d, which reflects the shear lag effect across the width. In order to illustrate the effect of the w/d ratio on the net section efficiency, sections with about the same values of eccentricity and w/t ratio were chosen. For the angle sections, the series of a12-4 and a14-3 were considered since both of these series have the values of eccentricity around 25 and the w/t ratio around 36. Similarly, for the channel sections, the series of c12-6 and c14-4 were considered. Both of these series have the values of eccentricity around 7.0 and the w/t ratio around 50. The results for the angle and channel section are shown in Figs. 6.11 and

6.12, respectively. As shown in these figures, the net section efficiency decreases as the w/d ratio increases; however, the decrease in the net section efficiency for the angle sections is not as significant as that in the channel sections.

6.5 Proposed Net Section Strength Formula

6.5.1 Evaluation of the $(1-\bar{x}/L)$ rule

The net section efficiency based on $(1-\bar{x}/L)$ for the angle and channel sections used in the parametric study are calculated and shown in Tables 6.9 and 6.10, respectively. Only those angle and channel sections with two or more bolts in the line of force and with the net section failure mode were considered. Illustrated from the tables, the $(1-\bar{x}/L)$ rule does not accurately predict the net section efficiency for angles and channels. As discussed in Section 6.4, there are two other factors affecting the net section efficiency, and they are flat width-to-thickness ratio and flat width-to-bolt diameter ratio. For the angle sections with flat width-to-thickness ratio, w/t, less than 30, and the flat width-to-bolt diameter ratio, w/d, less than 2.5, the $(1-\bar{x}/L)$ rule is a fair predictor of the net section efficiency; however, for those angle sections with w/t ratio greater than 30 and w/d ratio greater than 2.5, this rule does not provide good results. For the channel sections, the $(1-\bar{x}/L)$ rule only gives a good correlation to the results obtained from the parametric study for those channel sections with flat width-to-thickness ratio, w/t, less than 40 and flat width-to-bolt diameter ratio, w/d, less than 5.

94

6.5.2 Proposed net section efficiency formula

Based on the above-mentioned observations, in addition to the factor $(1-\bar{x}/L)$, geometric factors such as the flat width-to-thickness ratio and the flat width-to-bolt diameter ratio also have the effect on the net section efficiency. Therefore, new net section efficiency factor, U, equations for both angle and channel sections are developed to include the effects of eccentricity $(\bar{x})$, connection length (L), flat width-to-thickness ratio (w/t), and flat width-to-bolt diameter ratio (w/d). In order to establish the form of the equation, regression analyses (including linear and non-linear regression analysis) have been performed and the commercially available statistical software SigmaPlot 5.0 (SPSS, 1999) is used. In the analysis, the form of the predicted equation was first chosen and the optimal values of the unknown coefficients were then calculated. In SigmaPlot, the coefficients are obtained by minimizing the residual errors using the least squares method. In order to determine the most suitable form of equation to describe the net section efficiency of a section, the coefficient of determination, R^2 is used. It is the most common measure of how well the regression model describes the data. If R^2 values are close to 1, the equation is a good description of the relation between the independent and dependent variables.

Different forms of net section efficiency equations have been tried and the equation with the following form was found to give the greatest value of R^2:

$$U = 1 - a(\frac{\bar{x}}{L})^b (\frac{w}{t})^c (\frac{w}{d})^g$$

[6.1]

where a, b, c and g are the regression coefficients obtained by performing regression analysis. The data used in the analysis were those having two or more fasteners in the

line of force since the $\overline{x}/L$ term for those sections with only one bolt was not available. Only sections with net section failure were considered.

For the angle sections, obtaining the optimal values of the regression coefficients gives:

$$U = 1 - 0.085(\frac{\overline{x}}{L})^{0.41}(\frac{w}{t})^{0.36}(\frac{w}{d})^{0.51}$$

[6.2]

and the R^2 of this equation is 0.89. Similarly, for the channel sections, the net section efficiency equation obtained by performing the regression analysis is shown below:

$$U = 1 - 0.04(\frac{\overline{x}}{L})^{0.85}(\frac{w}{t})^{0.54}(\frac{w}{d})^{1.02}$$

[6.3]

where the R^2 of this equation is 0.92.

In addition, the results obtained for the form with a lower R^2 are presented here as the reference. This form is similar to Eq. 6.1 except there is no flat width-to-bolt diameter ratio present in the equation. For the angle sections, the net section efficiency equation was

$$U = 1 - 0.08(\frac{\overline{x}}{L})^{0.5}(\frac{w}{t})^{0.6}$$

[6.4]

with the R^2 value of 0.82; while for the channel sections, the equation was

$$U = 1 - 0.01(\frac{\overline{x}}{L})(\frac{w}{t})^{1.39}$$

[6.5]

with the R^2 value of 0.82. As compared with Eqs. 6.4 and 6.5, the R^2 values in Eqs. 6.2 and 6.3 are higher which implies a better prediction of the net section efficiency can be obtained based on these two equations, therefore, they are chosen as the equations to

obtain the net section efficiency in this report herein for cold-formed angle and channel sections.

For those connections with only one fastener, since the $\bar{x}/L$ term was not available, non-linear regression analysis was performed using the equation with the form similar to Eq. 6.1 with no $\bar{x}/L$ term applied. Again, only sections with net section failure were considered. For the angle sections, the net section efficiency equation was

$$U = 1 - 0.11(\frac{w}{t})^{0.3}(\frac{w}{d})^{0.42}$$

[6.6]

with the R^2 value of 0.99; while for the channel sections, the equation was

$$U = 1 - 0.11(\frac{w}{t})^{0.4}(\frac{w}{d})^{0.07}$$

[6.7]

with the R^2 value of 1.0.

In Tables 6.11 and 6.12, the net section efficiency predicted by using Eqs. 6.2 and 6.6, and Eqs. 6.3 and 6.7 are compared with the net section efficiency obtained from the parametric study for angle and channel sections, respectively. The average ratio of the predicted values to the results obtained from the finite element analysis is 1.01 with a standard deviation of 0.07 for the angle section and 1.00 with a standard deviation of 0.05 for the channel section. This indicates that Eqs. 6.2 and 6.6, and Eq. 6.3 and 6.7 provide a better prediction on the net section efficiency than the $(1-\bar{x}/L)$ rule did. Therefore, Eqs. 6.2 and 6.6, and Eqs. 6.3 and 6.7 are proposed to predict the net section efficiency of bolted equal leg angle and channel sections, respectively.

6.6 Recommended Design Method

6.6.1 Design recommendations

With the results obtained from the above discussion, it is recommended that for cold-formed equal leg angle members with one line of bolts connected at one leg and channel members with one line of bolts connected at the web, the factored tensile resistance, T_r, can be taken as the least of

a) $T_r = \phi A_g F_y$ [6.8]

b) $T_r = \phi_u A_{ne} F_u$ [6.9]

where ϕ = resistance factor, taken as 0.9 for tension members

ϕ_u = tensile fracture resistance factor, taken as 0.75

F_y = specified yield strength

F_u = specified ultimate strength

A_g = gross cross-sectional area

A_{ne} = effective net area accounting for shear lag

In Eq. 6.9, the effective net area can be calculated as follows:

$A_{ne} = UA_n$ [6.10]

where A_n = critical net area of connected part, calculated by taking the hole diameter 2 mm larger than the nominal size

U = shear lag reduction factor to be determined as follows:

a) For angle members connected by one leg

(i) with one bolt in the line of force

$$U = 1 - 0.11(\frac{w}{t})^{0.3} (\frac{w}{d})^{0.42} \le 1.0$$

[6.11]

(ii) with two or more bolts in the line of force

$$U = 1 - 0.085(\frac{\overline{x}}{L})^{0.41} (\frac{w}{t})^{0.36} (\frac{w}{d})^{0.51} \le 1.0$$

[6.12]

b) For channel members connected by the web

(i) with one bolt in the line of force

$$U = 1 - 0.11(\frac{w}{t})^{0.4} (\frac{w}{d})^{0.07} \le 1.0$$

[6.13]

(ii) with two or more bolts in the line of force

$$U = 1 - 0.04(\frac{\overline{x}}{L})^{0.85} (\frac{w}{t})^{0.54} (\frac{w}{d})^{1.02} \le 1.0$$

[6.14]

6.6.2 Evaluation of design recommendations with test results

Tables 6.13 and 6.14 show the comparison between unfactored tensile resistance of a member and the test results obtained in this project and by the others (by University of Alberta from 1994 to 1997 (Cheng *et al*), and University of Missouri-Rolla (La-Boube and Yu, 1995)) and the results are plotted in Fig. 6.13 and Fig. 6.14 for the angle and channel sections, respectively. In order to calculate the unfactored tensile resistance of a section, Eq. 6.9 was used without any ϕ-factor applied. For the angle sections, only those having equal leg and failed in net section fracture are being considered while for the channel sections, only those sections connected on the web and having net section failure were considered. It was found that the mean ratio of the test results to the predictions based on Eq. 6.9 is 1.01 with a standard deviation of 0.17 for the angle sections and 1.08 with a standard deviation of 0.13 for the channel sections. All the calculated data is

within 20% of the tested data. Also, most of the ratios are above 1.0. (It is unconservative if the ratio is less than 1.0.) Therefore, it can be concluded that the net section efficiency can be predicted well using Eqs. 6.11 to 14 directly and the factored tensile resistance of a net section of the cold-formed steel angle and channel sections can be calculated based on the recommendation suggested in this section.

6.6.3 Further discussion of proposed methods

The design recommendations proposed above, based on the test data and parametric study results obtained from this report, can be applicable to those equal leg angles and channels with flange-to-web ratio ranging from 0.25 to 0.625, which have one line of bolts at the connection. Tables 6.15 and 6.16 illustrate the applicability of the proposed methods on those angle and channel sections, respectively, which were not considered in this study. The source of the data for angle sections was from University of Alberta (1997) and University of Missouri-Rolla (1995) while the data for channel sections was from the University of Missouri-Rolla (1995). As can be seen from the Table 6.15, good correlation is found between the efficiencies obtained from the test and the proposed method for the stiffened angle sections. For the unequal leg angles, the proposed method is unconservative when the short leg is connected but conservative when the long leg is connected. In the situation where both legs of the angle sections or both the flanges of the channel sections are connected, the proposed methods become non-applicable. Therefore, further tests and analyses are desirable in order to investigate the shear lag effect on unequal leg angles and sections with more than one element connected. In addition, when designing the sections with two lines of bolts, the proposed

100

recommendations should provide a conservative predicted load since the net section efficiency increases with the increase in the number of bolt line across the connection; however, this assumption should be confirmed with future investigation.

Table 6.1 Description of Angle Models in the Parametric Study

Model Name	D [mm]	B [mm]	t [mm]	R [mm]	End Dist [mm]	Bolt Spacing [mm]	No. of Bolts	Bolt Size [mm]	Gross Area [mm²]	Net Area [mm²]	Fy [MPa]	Fu [MPa]	Fu/Fy	x̄ [mm]	w/t Ratio	w/d Ratio
a12-4-1	101.6	101.6	2.667	4.763	60	63.5	1	19	528	472	230	310	1.35	26.7	35.8	5.03
a12-4-2	101.6	101.6	2.667	4.763	60	63.5	2	19	528	472	230	310	1.35	26.7	35.8	5.03
a12-4-2-90	101.6	101.6	2.667	4.763	90	63.5	2	19	528	472	230	310	1.35	26.7	35.8	5.03
a12-4-3	101.6	101.6	2.667	4.763	60	63.5	3	19	528	472	230	310	1.35	26.7	35.8	5.03
a12-4-3-90	101.6	101.6	2.667	4.763	90	63.5	3	19	528	472	230	310	1.35	26.7	35.8	5.03
a12-4-4	101.6	101.6	2.667	4.763	60	63.5	4	19	528	472	230	310	1.35	26.7	35.8	5.03
a14-4-1	101.6	101.6	1.905	2.381	60	63.5	1	19	381	341	230	310	1.35	26.3	51.6	5.17
a14-4-2	101.6	101.6	1.905	2.381	60	63.5	2	19	381	341	230	310	1.35	26.3	51.6	5.17
a14-4-2-90	101.6	101.6	1.905	2.381	90	63.5	2	19	381	341	230	310	1.35	26.3	51.6	5.17
a14-4-3	101.6	101.6	1.905	2.381	60	63.5	3	19	381	341	230	310	1.35	26.3	51.6	5.17
a14-4-3-90	101.6	101.6	1.905	2.381	90	63.5	3	19	381	341	230	310	1.35	26.3	51.6	5.17
a14-4-4	101.6	101.6	1.905	2.381	60	63.5	4	19	381	341	230	310	1.35	26.3	51.6	5.17
a16-4-1	101.6	101.6	1.524	2.381	60	63.5	1	19	305	273	230	310	1.35	26.1	64.6	5.18
a16-4-2	101.6	101.6	1.524	2.381	60	63.5	2	19	305	273	230	310	1.35	26.1	64.6	5.18
a16-4-3	101.6	101.6	1.524	2.381	60	63.5	3	19	305	273	230	310	1.35	26.1	64.6	5.18
a16-4-4	101.6	101.6	1.524	2.381	60	63.5	4	19	305	273	230	310	1.35	26.1	64.6	5.18
a14-3-1-x	76.2	76.2	1.905	2.381	60	63.5	1	19	284	244	270	310	1.15	20.0	38.3	3.84
a14-3-2-x	76.2	76.2	1.905	2.381	60	63.5	2	19	284	244	270	310	1.15	20.0	38.3	3.84
a14-3-3-x	76.2	76.2	1.905	2.381	90	63.5	3	19	284	244	270	310	1.15	20.0	38.3	3.84
a14-3-4-x	76.2	76.2	1.905	2.381	60	63.5	4	19	284	244	270	310	1.15	20.0	38.3	3.84
a14-3-1	76.2	76.2	1.905	2.381	60	63.5	1	19	284	244	230	310	1.35	20.0	38.3	3.84
a14-3-2	76.2	76.2	1.905	2.381	60	63.5	2	19	284	244	230	310	1.35	20.0	38.3	3.84
a14-3-2-90	76.2	76.2	1.905	2.381	90	63.5	2	19	284	244	230	310	1.35	20.0	38.3	3.84
a14-3-3	76.2	76.2	1.905	2.381	60	63.5	3	19	284	244	230	310	1.35	20.0	38.3	3.84
a14-3-4	76.2	76.2	1.905	2.381	60	63.5	4	19	284	244	230	310	1.35	20.0	38.3	3.84
a14-3-1y	76.2	76.2	1.905	2.381	60	63.5	1	19	284	244	230	345	1.50	20.0	38.3	3.84
a14-3-2-y	76.2	76.2	1.905	2.381	60	63.5	2	19	284	244	230	345	1.50	20.0	38.3	3.84
a14-3-3-y	76.2	76.2	1.905	2.381	60	63.5	3	19	284	244	230	345	1.50	20.0	38.3	3.84
a14-3-4-y	76.2	76.2	1.905	2.381	60	63.5	4	19	284	244	230	345	1.50	20.0	38.3	3.84

Table 6.1 Description of Angle Models in the Parametric Study (Continued)

Model Name	D [mm]	B [mm]	t [mm]	R [mm]	End Dist [mm]	Bolt Spacing [mm]	No. of Bolts	Bolt Size [mm]	Gross Area [mm²]	Net Area [mm²]	Fy [MPa]	Fu [MPa]	Fu/Fy	x̄ [mm]	w/t Ratio	w/d Ratio
a16-3-1	76.2	76.2	1.524	2.381	60	63.5	1	19	228	196	230	310	1.35	19.8	47.9	3.85
a16-3-2	76.2	76.2	1.524	2.381	60	63.5	2	19	228	196	230	310	1.35	19.8	47.9	3.85
a16-3-3	76.2	76.2	1.524	2.381	60	63.5	3	19	228	196	230	310	1.35	19.8	47.9	3.85
a16-3-4	76.2	76.2	1.524	2.381	60	63.5	4	19	228	196	230	310	1.35	19.8	47.9	3.85
a18-3-1	76.2	76.2	1.219	2.381	60	63.5	1	19	183	157	230	310	1.35	19.7	60.0	3.85
a18-3-1-30	76.2	76.2	1.219	2.381	30	63.5	1	19	183	157	230	310	1.35	19.7	60.0	3.85
a18-3-2	76.2	76.2	1.219	2.381	60	63.5	2	19	183	157	230	310	1.35	19.7	60.0	3.85
a18-3-3	76.2	76.2	1.219	2.381	60	63.5	3	19	183	157	230	310	1.35	19.7	60.0	3.85
a18-3-4	76.2	76.2	1.219	2.381	60	63.5	4	19	183	157	230	310	1.35	19.7	60.0	3.85
a14-2-1	50.8	50.8	1.905	2.381	60	63.5	1	19	187	147	230	310	1.35	13.6	24.9	2.50
a14-2-2	50.8	50.8	1.905	2.381	60	63.5	2	19	187	147	230	310	1.35	13.6	24.9	2.50
a14-2-3	50.8	50.8	1.905	2.381	60	63.5	3	19	187	147	230	310	1.35	13.6	24.9	2.50
a14-2-4	50.8	50.8	1.905	2.381	60	63.5	4	19	187	147	230	310	1.35	13.6	24.9	2.50
a16-2-1	50.8	50.8	1.524	2.381	60	63.5	1	19	150	118	230	310	1.35	13.5	31.3	2.51
a16-2-2	50.8	50.8	1.524	2.381	60	63.5	2	19	150	118	230	310	1.35	13.6	31.3	2.51
a16-2-3	50.8	50.8	1.524	2.381	60	63.5	3	19	150	118	230	310	1.35	13.6	31.3	2.51
a16-2-4	50.8	50.8	1.524	2.381	60	63.5	4	19	150	118	230	310	1.35	13.6	31.3	2.51
a18-2-1	50.8	50.8	1.219	2.381	60	63.5	1	19	121	95	230	310	1.35	13.5	39.2	2.52
a18-2-2	50.8	50.8	1.219	2.381	60	63.5	2	19	121	95	230	310	1.35	13.5	39.2	2.52
a18-2-3	50.8	50.8	1.219	2.381	60	63.5	3	19	121	95	230	310	1.35	13.5	39.2	2.52
a18-2-4	50.8	50.8	1.219	2.381	60	63.5	4	19	121	95	230	310	1.35	13.5	39.2	2.52

Table 6.2 Description of Channel Models in the Parametric Study

Model Name	D [mm]	B [mm]	t [mm]	R [mm]	End Dist [mm]	Bolt Spacing [mm]	No. of Bolts	Bolt Size [mm]	Gross Area [mm²]	Net Area [mm²]	Fy [MPa]	Fu [MPa]	Fu/Fy	x̄ [mm]	w/t Ratio	w/d Ratio
c12-6-1	152.4	38.1	2.67	4.76	60	63.5	1	19	581	525	230	310	1.35	7.6	52.6	7.38
c12-6-2	152.4	38.1	2.67	4.76	60	63.5	2	19	581	525	230	310	1.35	7.6	52.6	7.38
c12-6-2-90	152.4	38.1	2.67	4.76	90	63.5	2	19	581	525	230	310	1.35	7.6	52.6	7.38
c12-6-3	152.4	38.1	2.67	4.76	60	63.5	3	19	581	525	230	310	1.35	7.6	52.6	7.38
c12-6-3-90	152.4	38.1	2.67	4.76	90	63.5	3	19	581	525	230	310	1.35	7.6	52.6	7.38
c12-6-4	152.4	38.1	2.67	4.76	60	63.5	4	19	581	525	230	310	1.35	7.6	52.6	7.38
c14-6-1	152.4	38.1	1.91	2.38	60	63.5	1	19	423	382	230	310	1.35	7.2	76.5	7.67
c14-6-2	152.4	38.1	1.91	2.38	60	63.5	2	19	423	382	230	310	1.35	7.2	76.5	7.67
c14-6-2-90	152.4	38.1	1.91	2.38	90	63.5	2	19	423	382	230	310	1.35	7.2	76.5	7.67
c14-6-3	152.4	38.1	1.91	2.38	60	63.5	3	19	423	382	230	310	1.35	7.2	76.5	7.67
c14-6-3-90	152.4	38.1	1.91	2.38	90	63.5	3	19	423	382	230	310	1.35	7.2	76.5	7.67
c14-6-4	152.4	38.1	1.91	2.38	60	63.5	4	19	423	382	230	310	1.35	7.2	76.5	7.67
c16-6-1	152.4	38.1	1.52	2.38	60	63.5	1	19	339	307	230	310	1.35	7.0	95.9	7.69
c16-6-2	152.4	38.1	1.52	2.38	60	63.5	2	19	339	307	230	310	1.35	7.0	95.9	7.69
c16-6-3	152.4	38.1	1.52	2.38	60	63.5	3	19	339	307	230	310	1.35	7.0	95.9	7.69
c16-6-4	152.4	38.1	1.52	2.38	60	63.5	4	19	339	307	230	310	1.35	7.0	95.9	7.69
c14-4-1-x	101.6	28.6	1.91	2.38	60	63.5	1	19	290	250	270	310	1.15	6.0	49.8	5.00
c14-4-2-x	101.6	28.6	1.91	2.38	60	63.5	2	19	290	250	270	310	1.15	6.0	49.8	5.00
c14-4-3-x	101.6	28.6	1.91	2.38	90	63.5	3	19	290	250	270	310	1.15	6.0	49.8	5.00
c14-4-4-x	101.6	28.6	1.91	2.38	60	63.5	4	19	290	250	270	310	1.15	6.0	49.8	5.00
c14-4-1	101.6	28.6	1.91	2.38	60	63.5	1	19	290	250	230	310	1.35	6.0	49.8	5.00
c14-4-2	101.6	28.6	1.91	2.38	60	63.5	2	19	290	250	230	310	1.35	6.0	49.8	5.00
c14-4-2-90	101.6	28.6	1.91	2.38	90	63.5	2	19	290	250	230	310	1.35	6.0	49.8	5.00
c14-4-3	101.6	28.6	1.91	2.38	60	63.5	3	19	290	250	230	310	1.35	6.0	49.8	5.00
c14-4-4	101.6	28.6	1.91	2.38	60	63.5	4	19	290	250	230	310	1.35	6.0	49.8	5.00
c14-4-1-y	101.6	28.6	1.91	2.38	60	63.5	1	19	290	250	230	345	1.50	6.0	49.8	5.00
c14-4-2-y	101.6	28.6	1.91	2.38	60	63.5	2	19	290	250	230	345	1.50	6.0	49.8	5.00
c14-4-3-y	101.6	28.6	1.91	2.38	60	63.5	3	19	290	250	230	345	1.50	6.0	49.8	5.00
c14-4-4-y	101.6	28.6	1.91	2.38	60	63.5	4	19	290	250	230	345	1.50	6.0	49.8	5.00

Table 6.2 Description of Channel Models in the Parametric Study (Continued)

Model Name	D [mm]	B [mm]	t [mm]	R [mm]	End Dist [mm]	Bolt Spacing [mm]	No. of Bolts	Bolt Size [mm]	Gross Area [mm²]	Net Area [mm²]	F_y [MPa]	F_u [MPa]	F_u/F_y	$\bar{x}$ [mm]	w/t Ratio	w/d Ratio
c16-4-1	101.6	28.6	1.52	2.38	60	63.5	1	19	233	201	230	310	1.35	6.8	62.5	5.02
c16-4-2	101.6	28.6	1.52	2.38	60	63.5	2	19	233	201	230	310	1.35	6.8	62.5	5.02
c16-4-3	101.6	28.6	1.52	2.38	60	63.5	3	19	233	201	230	310	1.35	6.8	62.5	5.02
c16-4-4	101.6	28.6	1.52	2.38	60	63.5	4	19	233	201	230	310	1.35	6.8	62.5	5.02
c18-4-1	101.6	28.6	1.22	2.38	60	63.5	1	19	188	162	230	310	1.35	6.7	78.4	5.03
c18-4-1-30	101.6	28.6	1.22	2.38	30	63.5	1	19	188	162	230	310	1.35	6.7	78.4	5.03
c18-4-2	101.6	28.6	1.22	2.38	60	63.5	2	19	188	162	230	310	1.35	6.7	78.4	5.03
c18-4-3	101.6	28.6	1.22	2.38	60	63.5	3	19	188	162	230	310	1.35	6.7	78.4	5.03
c18-4-4	101.6	28.6	1.22	2.38	60	63.5	4	19	188	162	230	310	1.35	6.7	78.4	5.03
c14-2-1	50.8	28.6	1.91	2.38	60	63.5	1	19	193	153	230	310	1.35	8.5	23.2	2.32
c14-2-2	50.8	28.6	1.91	2.38	60	63.5	2	19	193	153	230	310	1.35	8.5	23.2	2.32
c14-2-3	50.8	28.6	1.91	2.38	60	63.5	3	19	193	153	230	310	1.35	8.5	23.2	2.32
c14-2-4	50.8	28.6	1.91	2.38	60	63.5	4	19	193	153	230	310	1.35	8.5	23.2	2.32
c16-2-1	50.8	28.6	1.52	2.38	60	63.5	1	19	155	123	230	310	1.35	8.4	29.2	2.34
c16-2-2	50.8	28.6	1.52	2.38	60	63.5	2	19	155	123	230	310	1.35	8.4	29.2	2.34
c16-2-3	50.8	28.6	1.52	2.38	60	63.5	3	19	155	123	230	310	1.35	8.4	29.2	2.34
c16-2-4	50.8	28.6	1.52	2.38	60	63.5	4	19	155	123	230	310	1.35	8.4	29.2	2.34
c18-2-1	50.8	28.6	1.22	2.38	60	63.5	1	19	126	100	230	310	1.35	8.2	36.8	2.36
c18-2-2	50.8	28.6	1.22	2.38	60	63.5	2	19	126	100	230	310	1.35	8.2	36.8	2.36
c18-2-3	50.8	28.6	1.22	2.38	60	63.5	3	19	126	100	230	310	1.35	8.2	36.8	2.36
c18-2-4	50.8	28.6	1.22	2.38	60	63.5	4	19	126	100	230	310	1.35	8.2	36.8	2.36

Table 6.3 Results for Angle Models

Model Name	P_{Net} [kN]	P_b [kN]	P_{block} [kN]	P_{FEA} [kN]	P_{FEA}/P_{net}	P_{FEA}/P_b	P_{FEA}/P_{block}	Mode of Failure
a12-4-1	146.2	47.2	49.1	50.0	0.34	1.06	1.02	Bearing
a12-4-2	146.2	94.5	91.2	78.4	0.54	0.83	0.86	Net Section Fracture
a12-4-2-90	146.2	94.5	121.0	79.9	0.55	0.85	0.66	Net Section Fracture
a12-4-3	146.2	141.7	133.3	87.5	0.60	0.62	0.66	Net Section Fracture
a12-4-3-90	146.2	141.7	163.1	87.9	0.60	0.62	0.54	Net Section Fracture
a12-4-4	146.2	189.0	175.4	95.7	0.65	0.51	0.55	Net Section Fracture
a14-4-1	105.6	33.7	35.1	31.8	0.30	0.94	0.91	Net Section Fracture
a14-4-2	105.6	67.5	65.1	52.0	0.49	0.77	0.80	Net Section Fracture
a14-4-2-90	105.6	67.5	86.4	52.7	0.50	0.78	0.61	Net Section Fracture
a14-4-3	105.6	101.2	95.2	60.2	0.57	0.59	0.63	Net Section Fracture
a14-4-3-90	105.6	101.2	116.5	60.7	0.57	0.60	0.52	Net Section Fracture
a14-4-4	105.6	135.0	125.3	65.8	0.62	0.49	0.53	Net Section Fracture
a16-4-1	84.7	21.6	28.0	23.7	0.28	1.10	0.85	Bearing
a16-4-2	84.7	43.2	52.1	39.2	0.46	0.91	0.75	Net Section Fracture
a16-4-3	84.7	64.8	76.2	46.4	0.55	0.72	0.61	Net Section Fracture
a16-4-4	84.7	86.4	100.2	51.2	0.60	0.59	0.51	Net Section Fracture
a14-3-1x	75.6	33.7	35.1	33.3	0.44	0.99	0.95	Bearing
a14-3-2x	75.6	67.5	65.1	46.3	0.61	0.69	0.71	Net Section Fracture
a14-3-3x	75.6	101.2	95.2	53.7	0.71	0.53	0.56	Net Section Fracture
a14-3-4x	75.6	135.0	125.3	59.8	0.79	0.44	0.48	Net Section Fracture
a14-3-1	75.6	33.7	35.1	30.9	0.41	0.91	0.88	Net Section Fracture
a14-3-2	75.6	67.5	65.1	43.4	0.57	0.64	0.67	Net Section Fracture
a14-3-2-90	75.6	67.5	86.4	44.0	0.58	0.65	0.51	Net Section Fracture
a14-3-3	75.6	101.2	95.2	50.8	0.67	0.50	0.53	Net Section Fracture
a14-3-4	75.6	135.0	125.3	56.7	0.75	0.42	0.45	Net Section Fracture
a14-3-1y	84.1	37.6	39.0	31.7	0.38	0.84	0.81	Net Section Fracture
a14-3-2y	84.1	75.1	72.5	45.7	0.54	0.61	0.63	Net Section Fracture
a14-3-3y	84.1	112.7	106.0	54.1	0.64	0.48	0.51	Net Section Fracture
a14-3-4y	84.1	150.2	139.5	60.6	0.72	0.40	0.43	Net Section Fracture
a16-3-1	60.7	21.6	28.0	22.5	0.37	1.04	0.80	Bearing
a16-3-2	60.7	43.2	52.1	33.2	0.55	0.77	0.64	Net Section Fracture
a16-3-3	60.7	64.8	76.2	39.3	0.65	0.61	0.52	Net Section Fracture
a16-3-4	60.7	86.4	100.2	43.8	0.72	0.51	0.44	Net Section Fracture
a18-3-1	48.7	14.4	22.4	17.0	0.35	1.18	0.76	Bearing
a18-3-1-30	48.7	14.4	8.8	16.1	0.33	1.12	1.82	Bearing
a18-3-2	48.7	28.8	41.7	25.3	0.52	0.88	0.61	Net Section Fracture
a18-3-3	48.7	43.2	60.9	30.6	0.63	0.71	0.50	Net Section Fracture
a18-3-4	48.7	57.6	80.2	34.1	0.70	0.59	0.43	Net Section Fracture
a14-2-1	45.6	33.7	35.1	26.9	0.59	0.80	0.77	Net Section Fracture
a14-2-2	45.6	67.5	65.1	33.4	0.73	0.49	0.51	Net Section Fracture
a14-2-3	45.6	101.2	95.2	41.0	0.90	0.41	0.43	Net Section Fracture
a14-2-4	45.6	135.0	125.3	43.1	0.95	0.32	0.34	Net Section Fracture
a16-2-1	36.7	21.6	28.0	20.1	0.55	0.93	0.72	Net Section Fracture
a16-2-2	36.7	43.2	52.1	25.8	0.70	0.60	0.50	Net Section Fracture
a16-2-3	36.7	64.8	76.2	31.9	0.87	0.49	0.42	Net Section Fracture
a16-2-4	36.7	86.4	100.2	34.2	0.93	0.40	0.34	Net Section Fracture
a18-2-1	29.5	14.4	22.4	14.6	0.50	1.02	0.65	Bearing
a18-2-2	29.5	28.8	41.7	20.0	0.68	0.69	0.48	Net Section Fracture
a18-2-3	29.5	43.2	60.9	24.5	0.83	0.57	0.40	Net Section Fracture
a18-2-4	29.5	57.6	80.2	27.0	0.91	0.47	0.34	Net Section Fracture

Table 6.4 Results for Channel Models

Model Name	P_{net} [kN]	P_b [kN]	P_{block} [kN]	P_{FEA} [kN]	P_{FEA} / P_{net}	P_{FEA} / P_b	P_{FEA} / P_{block}	Mode of Failure
c12-6-1	162.8	47.2	49.1	55.2	0.34	1.17	1.12	Bearing
c12-6-2	162.8	94.5	91.2	90.1	0.55	0.95	0.99	Net Section Fracture
c12-6-2-90	162.8	94.5	121.0	91.4	0.56	0.97	0.76	Net Section Fracture
c12-6-3	162.8	141.7	133.3	117.7	0.72	0.83	0.88	Net Section Fracture
c12-6-3-90	162.8	141.7	163.1	119.6	0.73	0.84	0.73	Net Section Fracture
c12-6-4	162.8	189.0	175.4	138.3	0.85	0.73	0.79	Net Section Fracture
c14-6-1	118.6	33.7	35.1	33.1	0.28	0.98	0.94	Net Section Fracture
c14-6-2	118.6	67.5	65.1	60.0	0.51	0.89	0.92	Net Section Fracture
c14-6-2-90	118.6	67.5	86.4	60.9	0.51	0.90	0.70	Net Section Fracture
c14-6-3	118.6	101.2	95.2	78.1	0.66	0.77	0.82	Net Section Fracture
c14-6-3-90	118.6	101.2	116.5	79.5	0.67	0.79	0.68	Net Section Fracture
c14-6-4	118.6	135.0	125.3	91.6	0.77	0.68	0.73	Net Section Fracture
c16-6-1	95.3	21.6	28.0	24.5	0.26	1.13	0.87	Bearing
c16-6-2	95.3	43.2	52.1	45.9	0.48	1.06	0.88	Bearing
c16-6-3	95.3	64.8	76.2	59.4	0.62	0.92	0.78	Net Section Fracture
c16-6-4	95.3	86.4	100.2	71.1	0.75	0.82	0.71	Net Section Fracture
c14-4-1x	77.4	33.7	35.1	34.2	0.44	1.01	0.97	Bearing
c14-4-2x	77.4	67.5	65.1	56.1	0.73	0.83	0.86	Net Section Fracture
c14-4-3x	77.4	101.2	95.2	75.3	0.97	0.74	0.79	Net Section Fracture
c14-4-4x	77.4	135.0	125.3	77.4	1.00	0.57	0.62	Net Section Fracture
c14-4-1	77.4	33.7	35.1	32.1	0.41	0.95	0.91	Net Section Fracture
c14-4-2	77.4	67.5	65.1	52.2	0.67	0.77	0.80	Net Section Fracture
c14-4-2-90	77.4	67.5	86.4	53.4	0.69	0.79	0.62	Net Section Fracture
c14-4-3	77.4	101.2	95.2	69.5	0.90	0.69	0.73	Net Section Fracture
c14-4-4	77.4	135.0	125.3	73.6	0.95	0.54	0.59	Net Section Fracture
c14-4-1y	86.1	37.6	39.0	33.9	0.39	0.90	0.87	Net Section Fracture
c14-4-2y	86.1	75.1	72.5	54.8	0.64	0.73	0.76	Net Section Fracture
c14-4-3y	86.1	112.7	106.0	74.1	0.86	0.66	0.70	Net Section Fracture
c14-4-4y	86.1	150.2	139.5	77.7	0.90	0.52	0.56	Net Section Fracture
c16-4-1	62.3	21.6	28.0	23.9	0.38	1.11	0.85	Bearing
c16-4-2	62.3	43.2	52.1	39.5	0.63	0.91	0.76	Net Section Fracture
c16-4-3	62.3	64.8	76.2	54.0	0.87	0.83	0.71	Net Section Fracture
c16-4-4	62.3	86.4	100.2	57.6	0.93	0.67	0.57	Net Section Fracture
c18-4-1	50.2	14.4	22.4	17.8	0.35	1.24	0.79	Bearing
c18-4-1-30	50.2	14.4	8.8	17.2	0.34	1.19	1.94	Bearing
c18-4-2	50.2	28.8	41.7	30.1	0.60	1.05	0.72	Bearing
c18-4-3	50.2	43.2	60.9	40.9	0.81	0.95	0.67	Net Section Fracture
c18-4-4	50.2	57.6	80.2	45.5	0.91	0.79	0.57	Net Section Fracture
c14-2-1	47.4	33.7	35.1	28.2	0.59	0.83	0.80	Net Section Fracture
c14-2-2	47.4	67.5	65.1	44.1	0.93	0.65	0.68	Net Section Fracture
c14-2-3	47.4	101.2	95.2	47.8	1.01	0.47	0.50	Net Section Fracture
c14-2-4	47.4	135.0	125.3	48.2	1.02	0.36	0.38	Net Section Fracture
c16-2-1	38.3	21.6	28.0	21.0	0.55	0.97	0.75	Net Section Fracture
c16-2-2	38.3	43.2	52.1	34.2	0.89	0.79	0.66	Net Section Fracture
c16-2-3	38.3	64.8	76.2	37.8	0.99	0.58	0.50	Net Section Fracture
c16-2-4	38.3	86.4	100.2	38.6	1.01	0.45	0.38	Net Section Fracture
c18-2-1	31.0	14.4	22.4	15.7	0.51	1.09	0.70	Bearing
c18-2-2	31.0	28.8	41.7	26.6	0.86	0.92	0.64	Net Section Fracture
c18-2-3	31.0	43.2	60.9	30.1	0.97	0.70	0.49	Net Section Fracture
c18-2-4	31.0	57.6	80.2	30.9	0.99	0.54	0.39	Net Section Fracture

Table 6.5 Details and Results of Angle Sections categorized in accordance with Material Constant

Model Name	D [mm]	t [mm]	Bolt Spacing [mm]	No. of Bolts	Bolt Size [mm]	F_y [MPa]	F_u [MPa]	F_u/F_y	Net Section Efficiency
a14-3-1x	76.2	1.91	63.5	1	19	270	310	1.15	0.44
a14-3-2x	76.2	1.91	63.5	2	19	270	310	1.15	0.61
a14-3-3x	76.2	1.91	63.5	3	19	270	310	1.15	0.71
a14-3-4x	76.2	1.91	63.5	4	19	270	310	1.15	0.79
a14-3-1	76.2	1.91	63.5	1	19	230	310	1.35	0.41
a14-3-2	76.2	1.91	63.5	2	19	230	310	1.35	0.57
a14-3-3	76.2	1.91	63.5	3	19	230	310	1.35	0.67
a14-3-4	76.2	1.91	63.5	4	19	230	310	1.35	0.75
a14-3-1y	76.2	1.91	63.5	1	19	230	345	1.50	0.38
a14-3-2y	76.2	1.91	63.5	2	19	230	345	1.50	0.54
a14-3-3y	76.2	1.91	63.5	3	19	230	345	1.50	0.64
a14-3-4y	76.2	1.91	63.5	4	19	230	345	1.50	0.72

Table 6.6 Details and Results of Channel Sections categorized in accordance with Material Constant

Model Name	D [mm]	B [mm]	t [mm]	Bolt Spacing [mm]	No. of Bolts	Bolt Size [mm]	F_y [MPa]	F_u [MPa]	F_u/F_y	Net Section Efficiency
c14-4-2x	101.6	28.6	1.91	63.5	2	19	270	310	1.15	0.73
c14-4-3x	101.6	28.6	1.91	63.5	3	19	270	310	1.15	0.97
c14-4-4x	101.6	28.6	1.91	63.5	4	19	270	310	1.15	1.00
c14-4-1	101.6	28.6	1.91	63.5	1	19	230	310	1.35	0.41
c14-4-2	101.6	28.6	1.91	63.5	2	19	230	310	1.35	0.67
c14-4-3	101.6	28.6	1.91	63.5	3	19	230	310	1.35	0.90
c14-4-4	101.6	28.6	1.91	63.5	4	19	230	310	1.35	0.95
c14-4-1y	101.6	28.6	1.91	63.5	1	19	230	345	1.50	0.39
c14-4-2y	101.6	28.6	1.91	63.5	2	19	230	345	1.50	0.64
c14-4-3y	101.6	28.6	1.91	63.5	3	19	230	345	1.50	0.86
c14-4-4y	101.6	28.6	1.91	63.5	4	19	230	345	1.50	0.90

Table 6.7 Summary of the Sectional Properties and Results for Angle Sections That
Failed in Net Section Fracture

Model Name	D [mm]	t [mm]	R [mm]	End Dist [mm]	Bolt Spacing [mm]	No. of Bolts	Bolt Size [mm]	$\bar{x}$ [mm]	w/t Ratio	w/d Ratio	N. S. E.
a12-4-2	101.6	2.67	4.76	60	63.5	2	19	26.7	35.8	5.03	0.54
a12-4-3	101.6	2.67	4.76	60	63.5	3	19	26.7	35.8	5.03	0.60
a12-4-4	101.6	2.67	4.76	60	63.5	4	19	26.7	35.8	5.03	0.65
a14-4-1	101.6	1.91	2.38	60	63.5	1	19	26.3	51.6	5.17	0.30
a14-4-2	101.6	1.91	2.38	60	63.5	2	19	26.3	51.6	5.17	0.49
a14-4-3	101.6	1.91	2.38	60	63.5	3	19	26.3	51.6	5.17	0.57
a14-4-4	101.6	1.91	2.38	60	63.5	4	19	26.3	51.6	5.17	0.62
a16-4-2	101.6	1.52	2.38	60	63.5	2	19	26.1	64.6	5.18	0.46
a16-4-3	101.6	1.52	2.38	60	63.5	3	19	26.1	64.6	5.18	0.55
a16-4-4	101.6	1.52	2.38	60	63.5	4	19	26.1	64.6	5.18	0.60
a14-3-1	76.2	1.91	2.38	60	63.5	1	19	20.0	38.3	3.84	0.41
a14-3-2	76.2	1.91	2.38	60	63.5	2	19	20.0	38.3	3.84	0.57
a14-3-3	76.2	1.91	2.38	60	63.5	3	19	20.0	38.3	3.84	0.67
a14-3-4	76.2	1.91	2.38	60	63.5	4	19	20.0	38.3	3.84	0.75
a16-3-2	76.2	1.52	2.38	60	63.5	2	19	19.8	47.9	3.85	0.55
a16-3-3	76.2	1.52	2.38	60	63.5	3	19	19.8	47.9	3.85	0.65
a16-3-4	76.2	1.52	2.38	60	63.5	4	19	19.8	47.9	3.85	0.72
a18-3-2	76.2	1.22	2.38	60	63.5	2	19	19.7	60.0	3.85	0.52
a18-3-3	76.2	1.22	2.38	60	63.5	3	19	19.7	60.0	3.85	0.63
a18-3-4	76.2	1.22	2.38	60	63.5	4	19	19.7	60.0	3.85	0.70
a14-2-1	50.8	1.91	2.38	60	63.5	1	19	13.6	24.9	2.50	0.59
a14-2-2	50.8	1.91	2.38	60	63.5	2	19	13.6	24.9	2.50	0.73
a14-2-3	50.8	1.91	2.38	60	63.5	3	19	13.6	24.9	2.50	0.90
a14-2-4	50.8	1.91	2.38	60	63.5	4	19	13.6	24.9	2.50	0.95
a16-2-1	50.8	1.52	2.38	60	63.5	1	19	13.5	31.3	2.51	0.55
a16-2-2	50.8	1.52	2.38	60	63.5	2	19	13.6	31.3	2.51	0.70
a16-2-3	50.8	1.52	2.38	60	63.5	3	19	13.6	31.3	2.51	0.87
a16-2-4	50.8	1.52	2.38	60	63.5	4	19	13.6	31.3	2.51	0.93
a18-2-2	50.8	1.22	2.38	60	63.5	2	19	13.5	39.2	2.52	0.68
a18-2-3	50.8	1.22	2.38	60	63.5	3	19	13.5	39.2	2.52	0.83
a18-2-4	50.8	1.22	2.38	60	63.5	4	19	13.5	39.2	2.52	0.91

Table 6.8 Summary of the Sectional Properties and Results for Channel Sections That
Failed in Net Section Fracture

Model Name	D [mm]	B [mm]	t [mm]	R [mm]	End Dist [mm]	Bolt Spacing [mm]	No. of Bolts	Bolt Size [mm]	x̄ [mm]	w/t Ratio	w/d Ratio	N. S. E.
c12-6-2	152.4	38.1	2.667	4.76	60	63.5	2	19	7.6	52.6	7.38	0.55
c12-6-3	152.4	38.1	2.667	4.76	60	63.5	3	19	7.6	52.6	7.38	0.72
c12-6-4	152.4	38.1	2.667	4.76	60	63.5	4	19	7.6	52.6	7.38	0.85
c14-6-1	152.4	38.1	1.905	2.38	60	63.5	1	19	7.2	76.5	7.67	0.28
c14-6-2	152.4	38.1	1.905	2.38	60	63.5	2	19	7.2	76.5	7.67	0.51
c14-6-3	152.4	38.1	1.905	2.38	60	63.5	3	19	7.2	76.5	7.67	0.66
c14-6-4	152.4	38.1	1.905	2.38	60	63.5	4	19	7.2	76.5	7.67	0.77
c16-6-3	152.4	38.1	1.524	2.38	60	63.5	3	19	7.0	95.9	7.69	0.62
c16-6-4	152.4	38.1	1.524	2.38	60	63.5	4	19	7.0	95.9	7.69	0.75
c14-4-1	101.6	28.6	1.905	2.38	60	63.5	1	19	6.0	49.8	5.00	0.41
c14-4-2	101.6	28.6	1.905	2.38	60	63.5	2	19	6.0	49.8	5.00	0.67
c14-4-3	101.6	28.6	1.905	2.38	60	63.5	3	19	6.0	49.8	5.00	0.90
c14-4-4	101.6	28.6	1.905	2.38	60	63.5	4	19	6.0	49.8	5.00	0.95
c16-4-2	101.6	28.6	1.524	2.38	60	63.5	2	19	6.8	62.5	5.02	0.63
c16-4-3	101.6	28.6	1.524	2.38	60	63.5	3	19	6.8	62.5	5.02	0.87
c16-4-4	101.6	28.6	1.524	2.38	60	63.5	4	19	6.8	62.5	5.02	0.93
c18-4-3	101.6	28.6	1.219	2.38	60	63.5	3	19	6.7	78.4	5.03	0.81
c18-4-4	101.6	28.6	1.219	2.38	60	63.5	4	19	6.7	78.4	5.03	0.91
c14-2-1	50.8	28.6	1.905	2.38	60	63.5	1	19	8.5	23.2	2.32	0.59
c14-2-2	50.8	28.6	1.905	2.38	60	63.5	2	19	8.5	23.2	2.32	0.93
c14-2-3	50.8	28.6	1.905	2.38	60	63.5	3	19	8.5	23.2	2.32	1.01
c14-2-4	50.8	28.6	1.905	2.38	60	63.5	4	19	8.5	23.2	2.32	1.02
c16-2-1	50.8	28.6	1.524	2.38	60	63.5	1	19	8.4	29.2	2.34	0.55
c16-2-2	50.8	28.6	1.524	2.38	60	63.5	2	19	8.4	29.2	2.34	0.89
c16-2-3	50.8	28.6	1.524	2.38	60	63.5	3	19	8.4	29.2	2.34	0.99
c16-2-4	50.8	28.6	1.524	2.38	60	63.5	4	19	8.4	29.2	2.34	1.01
c18-2-2	50.8	28.6	1.219	2.38	60	63.5	2	19	8.2	36.8	2.36	0.86
c18-2-3	50.8	28.6	1.219	2.38	60	63.5	3	19	8.2	36.8	2.36	0.97
c18-2-4	50.8	28.6	1.219	2.38	60	63.5	4	19	8.2	36.8	2.36	0.99

Table 6.9 Comparison of $(1 - \frac{\bar{x}}{L})$ and the Finite Element Result for Angle Sections

Specimen	No. of bolts	Bolt Diameter [mm]	D [mm]	t [mm]	R [mm]	L [mm]	w [mm]	w/t Ratio	w/d Ratio	$(1-\bar{x}/L)$	N. S. E.
a12-4-2	2	19.1	101.6	2.667	4.76	63.5	95.5	35.81	5.01	0.58	0.54
a12-4-2-90	2	19.1	101.6	2.667	4.76	63.5	95.5	35.81	5.01	0.58	0.55
a12-4-3	3	19.1	101.6	2.667	4.76	127	95.5	35.81	5.01	0.79	0.60
a12-4-3-90	3	19.1	101.6	2.667	4.76	127	95.5	35.81	5.01	0.79	0.60
a12-4-4	4	19.1	101.6	2.667	4.76	190.5	95.5	35.81	5.01	0.86	0.65
a14-4-2	2	19.1	101.6	1.905	2.38	63.5	98.3	51.58	5.16	0.59	0.49
a14-4-2-90	2	19.1	101.6	1.905	2.38	63.5	98.3	51.58	5.16	0.59	0.50
a14-4-3	3	19.1	101.6	1.905	2.38	127	98.3	51.58	5.16	0.79	0.57
a14-4-3-90	3	19.1	101.6	1.905	2.38	127	98.3	51.58	5.16	0.79	0.57
a14-4-4	4	19.1	101.6	1.905	2.38	190.5	98.3	51.58	5.16	0.86	0.62
a16-4-2	2	19.1	101.6	1.524	2.38	63.5	98.5	64.60	5.17	0.59	0.46
a16-4-3	3	19.1	101.6	1.524	2.38	127	98.5	64.60	5.17	0.79	0.55
a16-4-4	4	19.1	101.6	1.524	2.38	190.5	98.5	64.60	5.17	0.86	0.60
a14-3-2	2	19.1	76.2	1.905	2.38	63.5	72.9	38.25	3.83	0.69	0.57
a14-3-2-90	2	19.1	76.2	1.905	2.38	63.5	72.9	38.25	3.83	0.69	0.58
a14-3-3	3	19.1	76.2	1.905	2.38	127	72.9	38.25	3.83	0.84	0.67
a14-3-4	4	19.1	76.2	1.905	2.38	190.5	72.9	38.25	3.83	0.90	0.75
a16-3-2	2	19.1	76.2	1.524	2.38	63.5	73.1	47.94	3.84	0.69	0.55
a16-3-3	3	19.1	76.2	1.524	2.38	127	73.1	47.94	3.84	0.84	0.65
a16-3-4	4	19.1	76.2	1.524	2.38	190.5	73.1	47.94	3.84	0.90	0.72
a18-3-2	2	19.1	76.2	1.219	2.38	63.5	73.2	60.05	3.84	0.69	0.52
a18-3-3	3	19.1	76.2	1.219	2.38	127	73.2	60.05	3.84	0.85	0.63
a18-3-4	4	19.1	76.2	1.219	2.38	190.5	73.2	60.05	3.84	0.90	0.70
a14-2-2	2	19.1	50.8	1.905	2.38	63.5	47.5	24.92	2.49	0.79	0.73
a14-2-3	3	19.1	50.8	1.905	2.38	127	47.5	24.92	2.49	0.89	0.90
a14-2-4	4	19.1	50.8	1.905	2.38	190.5	47.5	24.92	2.49	0.93	0.95
a16-2-2	2	19.1	50.8	1.524	2.38	63.5	47.7	31.27	2.50	0.79	0.70
a16-2-3	3	19.1	50.8	1.524	2.38	127	47.7	31.27	2.50	0.89	0.87
a16-2-4	4	19.1	50.8	1.524	2.38	190.5	47.7	31.27	2.50	0.93	0.93
a18-2-2	2	19.1	50.8	1.219	2.38	63.5	47.8	39.21	2.51	0.79	0.68
a18-2-3	3	19.1	50.8	1.219	2.38	127	47.8	39.21	2.51	0.89	0.83
a18-2-4	4	19.1	50.8	1.219	2.38	190.5	47.8	39.21	2.51	0.93	0.91

Table 6.10 Comparison of $(1 - \dfrac{\bar{x}}{L})$ with Finite Element Result for Channel Sections

Model Name	No. of bolts	Bolt Dia. [mm]	D [mm]	B [mm]	t [mm]	R [mm]	L [mm]	w [mm]	w/t Ratio	w/d Ratio	$(1-\bar{x}/L)$	N. S. E.
c12-6-2	2	19.1	152.4	38.1	2.67	4.76	63.5	140.2	52.57	7.36	0.88	0.55
c12-6-2-90	2	19.1	152.4	38.1	2.67	4.76	63.5	140.2	52.57	7.36	0.88	0.56
c12-6-3	3	19.1	152.4	38.1	2.67	4.76	127.0	140.2	52.57	7.36	0.94	0.72
c12-6-3-90	3	19.1	152.4	38.1	2.67	4.76	127.0	140.2	52.57	7.36	0.94	0.73
c12-6-4	4	19.1	152.4	38.1	2.67	4.76	190.5	140.2	52.57	7.36	0.96	0.85
c14-6-2	2	19.1	152.4	38.1	1.91	2.38	63.5	145.7	76.50	7.65	0.89	0.51
c14-6-2-90	2	19.1	152.4	38.1	1.91	2.38	63.5	145.7	76.50	7.65	0.89	0.51
c14-6-3	3	19.1	152.4	38.1	1.91	2.38	127.0	145.7	76.50	7.65	0.94	0.66
c14-6-3-90	3	19.1	152.4	38.1	1.91	2.38	127.0	145.7	76.50	7.65	0.94	0.67
c14-6-4	4	19.1	152.4	38.1	1.91	2.38	190.5	145.7	76.50	7.65	0.96	0.77
c16-6-3	3	19.1	152.4	38.1	1.52	2.38	127.0	146.1	95.88	7.67	0.94	0.62
c16-6-4	4	19.1	152.4	38.1	1.52	2.38	190.5	146.1	95.88	7.67	0.96	0.75
c14-4-2	2	19.1	101.6	28.575	1.91	2.38	63.5	94.9	49.83	4.98	0.91	0.67
c14-4-2-90	2	19.1	101.6	28.575	1.91	2.38	63.5	94.9	49.83	4.98	0.91	0.69
c14-4-3	3	19.1	101.6	28.575	1.91	2.38	127.0	94.9	49.83	4.98	0.95	0.90
c14-4-4	4	19.1	101.6	28.575	1.91	2.38	190.5	94.9	49.83	4.98	0.97	0.95
c16-4-2	2	19.1	101.6	28.575	1.52	2.38	63.5	95.3	62.54	5.00	0.89	0.63
c16-4-3	3	19.1	101.6	28.575	1.52	2.38	127.0	95.3	62.54	5.00	0.95	0.87
c16-4-4	4	19.1	101.6	28.575	1.52	2.38	190.5	95.3	62.54	5.00	0.96	0.93
c18-4-3	3	19.1	101.6	28.575	1.22	2.38	127.0	95.6	78.43	5.02	0.95	0.81
c18-4-4	4	19.1	101.6	28.575	1.22	2.38	190.5	95.6	78.43	5.02	0.96	0.91
c14-2-2	2	19.1	50.8	28.575	1.91	2.38	63.5	44.1	23.17	2.32	0.87	0.93
c14-2-3	3	19.1	50.8	28.575	1.91	2.38	127.0	44.1	23.17	2.32	0.93	1.01
c14-2-4	4	19.1	50.8	28.575	1.91	2.38	190.5	44.1	23.17	2.32	0.96	1.02
c16-2-2	2	19.1	50.8	28.575	1.52	2.38	63.5	44.5	29.21	2.34	0.87	0.89
c16-2-3	3	19.1	50.8	28.575	1.52	2.38	127.0	44.5	29.21	2.34	0.93	0.99
c16-2-4	4	19.1	50.8	28.575	1.52	2.38	190.5	44.5	29.21	2.34	0.96	1.01
c18-2-2	2	19.1	50.8	28.575	1.22	2.38	63.5	44.8	36.76	2.35	0.87	0.86
c18-2-3	3	19.1	50.8	28.575	1.22	2.38	127.0	44.8	36.76	2.35	0.94	0.97
c18-2-4	4	19.1	50.8	28.575	1.22	2.38	190.5	44.8	36.76	2.35	0.96	0.99

Table 6.11 Comparison of the Proposed Net Section Efficiency Formulae to the Finite Element Analysis for Angle Sections

Model Name	U_{calc} Eqs. 6.2 and 6.6	U_{FEA}	U_{FEA} / U_{calc}
a12-4-2	0.51	0.54	1.05
a12-4-2-90	0.51	0.55	1.07
a12-4-3	0.63	0.60	0.95
a12-4-3-90	0.63	0.60	0.95
a12-4-4	0.69	0.65	0.95
a14-4-1	0.28	0.30	1.07
a14-4-2	0.43	0.49	1.13
a14-4-2-90	0.43	0.50	1.15
a14-4-3	0.57	0.57	0.99
a14-4-3-90	0.57	0.57	1.00
a14-4-4	0.64	0.62	0.97
a16-4-2	0.39	0.46	1.19
a16-4-3	0.54	0.55	1.02
a16-4-4	0.61	0.60	0.99
a14-3-1	0.42	0.41	0.98
a14-3-2	0.61	0.57	0.94
a14-3-2-90	0.61	0.58	0.95
a14-3-3	0.71	0.67	0.95
a14-3-4	0.75	0.75	1.00
a16-3-2	0.58	0.55	0.94
a16-3-3	0.68	0.65	0.95
a16-3-4	0.73	0.72	0.99
a18-3-2	0.54	0.52	0.96
a18-3-3	0.66	0.63	0.96
a18-3-4	0.71	0.70	0.99
a14-2-1	0.58	0.55	0.95
a14-2-2	0.77	0.73	0.95
a14-2-3	0.83	0.90	1.09
a14-2-4	0.85	0.95	1.11
a16-2-1	0.55	0.59	1.07
a16-2-2	0.75	0.70	0.94
a16-2-3	0.81	0.87	1.07
a16-2-4	0.84	0.93	1.11
a18-2-2	0.73	0.68	0.93
a18-2-3	0.80	0.83	1.04
a18-2-4	0.83	0.91	1.10

Table 6.12 Comparison of the Proposed Net Section Efficiency Formulae to the Finite
Element Analysis for Channel Sections

Model Name	U_{calc} Eqs. 6.3 and 6.7	U_{FEA}	U_{FEA} / U_{calc}
c12-6-2	0.57	0.55	0.97
c12-6-2-90	0.57	0.56	0.98
c12-6-3	0.76	0.72	0.95
c12-6-3-90	0.76	0.73	0.96
c12-6-4	0.83	0.85	1.02
c14-6-1	0.28	0.28	1.00
c14-6-2	0.48	0.51	1.05
c14-6-2-90	0.48	0.51	1.07
c14-6-3	0.71	0.66	0.93
c14-6-3-90	0.71	0.67	0.94
c14-6-4	0.80	0.77	0.97
c16-6-3	0.68	0.62	0.92
c16-6-4	0.77	0.75	0.97
c14-4-1	0.41	0.41	1.00
c14-4-2	0.77	0.67	0.87
c14-4-2-90	0.77	0.69	0.89
c14-4-3	0.87	0.90	1.03
c14-4-4	0.91	0.95	1.04
c16-4-2	0.71	0.63	0.89
c16-4-3	0.84	0.87	1.03
c16-4-4	0.89	0.93	1.04
c18-4-3	0.82	0.81	0.99
c18-4-4	0.87	0.91	1.04
c14-2-1	0.59	0.59	1.00
c14-2-2	0.91	0.93	1.03
c14-2-3	0.95	1.01	1.06
c14-2-4	0.96	1.02	1.06
c16-2-1	0.55	0.55	1.00
c16-2-2	0.90	0.89	1.00
c16-2-3	0.94	0.99	1.05
c16-2-4	0.96	1.01	1.05
c18-2-2	0.88	0.86	0.97
c18-2-3	0.93	0.97	1.04
c18-2-4	0.95	0.99	1.04

Table 6.13 Evaluation of Equation 6.9 with the Test Results for Angle Sections

Data Source	Specimen	Size [mm]	No. of bolts	Bolt Size [mm]	D [mm]	B [mm]	t [mm]	R [mm]	F_u [MPa]	P_calc [kN]	P_test [kN]	P_test / P_calc
University of Alberta (1997)	12-2	102x102x2.657	2	19.1	102	102	2.657	4.76	516	143.4	135.8	0.95
	12-3	102x102x2.657	3	19.1	102	102	2.657	4.76	516	168.5	154.7	0.92
	12-4	102x102x2.657	3	19.1	102	102	2.657	4.76	516	168.5	158.3	0.94
	14-2	50.8x50.8x1.897	2	15.875	50.8	50.8	1.897	4.76	327	37.9	35.7	0.94
	14-3	50.8x50.8x1.897	3	15.875	50.8	50.8	1.897	4.76	327	40.8	43.0	1.05
	16-2	38.1x38.1x1.519	2	12.7	38.1	38.1	1.519	2.38	317	21.1	20.3	0.96
	16-3	38.1x38.1x1.519	3	12.7	38.1	38.1	1.519	2.38	317	22.8	24.4	1.07
University of Alberta (1999)	A2-2	51x51x1.214	2	19.1	50.8	50.8	1.214	2.38	316	22.0	27.9	1.27
	A2-2N	51x51x1.214	2	19.1	50.8	50.8	1.214	2.38	316	22.0	24.0	1.09
	A2-3	51x51x1.214	3	19.1	50.8	50.8	1.214	2.38	316	24.0	31.1	1.30
	A3-2	76x76x1.214	2	19.1	76.2	76.2	1.214	2.38	316	27.0	32.8	1.21
	A3-3	76x76x1.214	3	19.1	76.2	76.2	1.214	2.38	316	32.6	37.7	1.16
	A4-2	102x102x1.214	2	19.1	101.6	101.6	1.214	2.38	316	23.4	34.0	1.45
	A4-3	102x102x1.214	3	19.1	101.6	101.6	1.214	2.38	316	34.7	45.1	1.30
	A4-4	102x102x1.214	4	19.1	101.6	101.6	1.214	2.38	316	39.9	49.4	1.24
University of Missouri Rolla	LAN11-1	41.3x41.3x1.067	1	12.7	41.3	41.3	1.067	5.56	385	13.7	12.8	0.93
	LAN11-2	41.3x41.3x1.067	1	12.7	41.3	41.3	1.067	5.56	385	13.7	12.2	0.89
	LAN11-3	41.3x41.3x1.067	1	12.7	41.3	41.3	1.067	5.56	385	13.7	12.0	0.88
	LBN11-1	41.3x41.3x1.067	2	12.7	41.3	41.3	1.067	5.56	385	18.3	15.8	0.86
	LBN11-2	41.3x41.3x1.067	2	12.7	41.3	41.3	1.067	5.56	385	18.3	16.2	0.88
	LBN11-3	41.3x41.3x1.067	2	12.7	41.3	41.3	1.067	5.56	385	18.3	15.9	0.87
	LCN11-1	41.3x41.3x1.067	3	12.7	41.3	41.3	1.067	5.56	385	20.3	19.6	0.96
	LCN11-2	41.3x41.3x1.067	3	12.7	41.3	41.3	1.067	5.56	385	20.3	20.0	0.99
	LCN11-3	41.3x41.3x1.067	3	12.7	41.3	41.3	1.067	5.56	385	20.3	20.9	1.03
	LAN31-1	41.3x41.3x3.048	1	12.7	41.3	41.3	3.048	9.53	366	46.6	32.6	0.70
	LAN31-2	41.3x41.3x3.048	1	12.7	41.3	41.3	3.048	9.53	366	46.6	32.7	0.70
	LBN31-1	41.3x41.3x3.048	2	12.7	41.3	41.3	3.048	10.32	366	54.6	49.0	0.90
	LBN31-2	41.3x41.3x3.048	2	12.7	41.3	41.3	3.048	10.32	366	54.6	48.3	0.88
	LCN31-1	41.3x41.3x3.048	3	12.7	41.3	41.3	3.048	9.53	366	57.7	58.5	1.01
	LCN31-2	41.3x41.3x3.048	3	12.7	41.3	41.3	3.048	9.53	366	57.7	56.7	0.98

Table 6.14 Evaluation of Equation 6.9 with the Test Results for Channel Sections

Data Source	Specimen	Size [mm]	No. of bolts	Bolt Size [mm]	D [mm]	B [mm]	t [mm]	R [mm]	F_u [MPa]	P_{calc} [kN]	P_{test} [kN]	P_{test}/P_{calc}
University of Alberta (1998)	C50x2	51.0x31.0x1.803	2	12.7	51	31.0	1.80	2.38	301	38.7	40.1	1.04
	C50x3	51.0x31.0x1.803	3	12.7	51	31.0	1.80	2.38	301	43.9	48.7	1.11
	C75x3	76.0x31.0x1.803	3	15.9	76	31.0	1.80	2.38	301	55.1	63.8	1.16
	C100x3	101.5x31.0x1.803	3	19.1	102	31.0	1.80	2.38	301	67.1	77.7	1.16
University of Alberta (1999)	C2-2	51x29x1.214	2	19.1	50.8	28.6	1.21	2.38	324	28.6	36.8	1.29
	C2-3	51x29x1.214	3	19.1	50.8	28.6	1.21	2.38	324	30.2	37.6	1.24
	C3-2	76x29x1.214	2	19.1	76.2	28.6	1.21	2.38	324	34.0	36.3	1.07
	C3-3	76x29x1.214	3	19.1	76.2	28.6	1.21	2.38	324	37.6	48.1	1.28
	C4-2	102x29x1.214	2	19.1	101.6	28.6	1.21	2.38	324	37.7	40.5	1.07
	C4-3	102x29x1.214	3	19.1	101.6	28.6	1.21	2.38	324	44.2	52.5	1.19
	C4-4	102x29x1.214	4	19.1	101.6	28.6	1.21	2.38	324	46.5	55.8	1.20
University of Missouri - Rolla	CBN11-1	41.3x31.0x1.067	2	12.7	41.3	31.0	1.07	6.35	385	27.8	24.5	0.88
	CBN11-2	41.3x31.0x1.067	2	12.7	41.3	31.0	1.07	6.76	385	27.9	24.2	0.87
	CCN11-1	41.3x31.0x1.067	3	12.7	41.3	31.0	1.07	5.94	385	30.2	30.7	1.02
	CCN11-2	41.3x31.0x1.067	3	12.7	41.3	31.0	1.07	6.35	385	30.2	31.1	1.03
	CBN31-1	41.3x31.0x3.048	2	12.7	41.3	31.0	3.05	10.32	365	77.3	73.7	0.95
	CBN31-2	41.3x31.0x3.048	2	12.7	41.3	31.0	3.05	9.53	365	77.5	71.3	0.92
	CCN31-1	41.3x31.0x3.048	3	12.7	41.3	31.0	3.05	9.53	365	79.2	82.9	1.05
	CCN31-2	41.3x31.0x3.048	3	12.7	41.3	31.0	3.05	9.53	365	79.2	83.2	1.05

Table 6.15 Comparison of Test Data with Equation 6.9 for Angle Sections That were Beyond the Scope of This Study

Data Source		Specimen	Size [mm]	No. of bolts per line	Bolt Size [mm]	D [mm]	B [mm]	t [mm]	Lip Size [mm]	R [mm]	P_{Test} [kN]	P_{Net} [kN]	P_{Test}/P_{Net}	U_{calc}
University of Alberta (1997)	Stiffened Angles	St12-3	102x102x2.657	3	19.1	102	102	2.657	24.4	4.76	203	276	0.66	0.59
		St14-2	50.8x50.8x1.897	2	15.9	50.8	50.8	1.897	16.4	4.76	68.6	95.28	0.70	0.77
		St14-3	50.8x50.8x1.897	3	15.9	50.8	50.8	1.897	16.4	4.76	75.7	95.28	0.77	0.81
		St16-3	38.1x38.1x1.519	3	12.7	38.1	38.1	1.519	14.2	2.38	44.9	56.3	0.74	0.83
University of Missouri-Rolla (1995)	Connected to short leg	LAN12-1	41.3x82.5x1.067	1	12.7	41.3	82.5	1.1	-	6.8	11.3	43.1	0.26	0.54
		LAN12-2	41.3x82.5x1.067	1	12.7	41.3	82.5	1.1	-	6.8	11.0	43.1	0.26	0.54
		LBN12-1	41.3x82.5x1.067	2	12.7	41.3	82.5	1.1	-	6.8	17.9	43.1	0.42	0.56
		LBN12-2	41.3x82.5x1.067	2	12.7	41.3	82.5	1.1	-	6.8	19.3	43.1	0.45	0.56
		LBN12-3	41.3x82.5x1.067	2	12.7	41.3	82.5	1.1	-	6.8	18.2	43.1	0.42	0.56
		LCN12-1	41.3x82.5x1.067	3	12.7	41.3	82.5	1.1	-	6.4	21.9	43.2	0.51	0.67
		LCN12-2	41.3x82.5x1.067	3	12.7	41.3	82.5	1.1	-	6.4	22.8	43.2	0.53	0.67
	Connected to long leg	LAN13-1	41.3x82.5x1.067	1	12.7	82.5	41.3	1.1	-	6.4	13.1	43.2	0.30	0.17
		LAN13-2	41.3x82.5x1.067	1	12.7	82.5	41.3	1.1	-	6.8	13.1	43.1	0.30	0.17
		LBN13-1	41.3x82.5x1.067	2	12.7	82.5	41.3	1.1	-	6.4	25.3	43.2	0.59	0.49
		LBN13-2	41.3x82.5x1.067	2	12.7	82.5	41.3	1.1	-	6.8	24.4	43.1	0.57	0.49
		LCN13-1	41.3x82.5x1.067	3	12.7	82.5	41.3	1.1	-	6.4	29.8	43.2	0.69	0.62
		LCN13-2	41.3x82.5x1.067	3	12.7	82.5	41.3	1.1	-	6.8	31.7	43.1	0.74	0.62
	Connected to both legs	LAN14-1	41.3x82.5x1.067	1	12.7	41.3	82.5	1.1	-	6.4	30.2	37.1	0.81	N/A
		LAN14-2	41.3x82.5x1.067	1	12.7	41.3	82.5	1.1	-	6.8	26.0	37.1	0.70	N/A
		LBN14-1	41.3x82.5x1.067	2	12.7	41.3	82.5	1.1	-	6.4	35.6	37.1	0.96	N/A
		LBN14-2	41.3x82.5x1.067	2	12.7	41.3	82.5	1.1	-	6.4	36.1	37.1	0.97	N/A
		LCN14-1	41.3x82.5x1.067	3	12.7	41.3	82.5	1.1	-	6.8	36.0	37.1	0.97	N/A
		LCN14-2	41.3x82.5x1.067	3	12.7	41.3	82.5	1.1	-	6.8	36.2	37.1	0.98	N/A
	Connected to short leg	LAN32-1	41.3x82.5x3.048	1	12.7	41.3	82.5	3.0	-	11.1	42.9	112	0.38	0.71
		LAN32-2	41.3x82.5x3.048	1	12.7	41.3	82.5	3.0	-	10.3	32.4	112	0.29	0.70
		LAN32-3	41.3x82.5x3.048	1	12.7	41.3	82.5	3.0	-	10.3	31.0	112	0.28	0.70
		LBN32-1	41.3x82.5x3.048	2	12.7	41.3	82.5	3.0	-	10.3	52.0	112	0.46	0.74
		LBN32-2	41.3x82.5x3.048	2	12.7	41.3	82.5	3.0	-	10.3	56.0	112	0.50	0.74
		LCN32-1	41.3x82.5x3.048	3	12.7	41.3	82.5	3.0	-	10.3	62.9	112	0.56	0.80
		LCN32-2	41.3x82.5x3.048	3	12.7	41.3	82.5	3.0	-	10.3	60.2	112	0.53	0.80
	Connected to long leg	LBN33-1	41.3x82.5x3.048	2	12.7	82.5	41.3	3.0	-	9.5	80.9	113	0.72	0.66
		LBN33-2	41.3x82.5x3.048	2	12.7	82.5	41.3	3.0	-	10.3	79.6	112	0.71	0.66
		LCN33-1	41.3x82.5x3.048	3	12.7	82.5	41.3	3.0	-	11.1	88.3	112	0.79	0.75
		LCN33-2	41.3x82.5x3.048	3	12.7	82.5	41.3	3.0	-	10.3	90.9	112	0.81	0.74
	Connected to both legs	LAN34-2	41.3x82.5x3.048	1	12.7	41.3	82.5	3.0	-	10.3	82.7	96.1	0.86	N/A
		LBN34-1	41.3x82.5x3.048	2	12.7	41.3	82.5	3.0	-	11.1	93.9	95.7	0.98	N/A
		LBN34-2	41.3x82.5x3.048	2	12.7	41.3	82.5	3.0	-	10.3	99.7	96.1	1.04	N/A
		LCN34-1	41.3x82.5x3.048	3	12.7	41.3	82.5	3.0	-	10.3	100	96.1	1.04	N/A
		LCN34-2	41.3x82.5x3.048	3	12.7	41.3	82.5	3.0	-	10.3	100	96.1	1.04	N/A
		LCN34-3	41.3x82.5x3.048	3	12.7	41.3	82.5	3.0	-	10.3	110	96.1	1.15	N/A

117

Table 6.16 Comparison of Test Data with Equation 6.9 for Channel Sections That were Beyond the Scope of This Study

	Specimen	Size [mm]	No. of bolts per line	Bolt Size [mm]	D [mm]	B [mm]	t [mm]	R [mm]	P_{Test} [kN]	P_{Net} [kN]	P_{Test}/P_{Net}	U
Connected to 2 flanges	CAN12-1	51.0x41.3x1.067	1	12.7	51.0	41.3	1.07	6.35	24.5	39.8	0.61	N/A
	CBN12-1	51.0x41.3x1.067	2	12.7	51.0	41.3	1.07	6.35	37.7	39.8	0.95	N/A
	CBN12-2	51.0x41.3x1.067	2	12.7	51.0	41.3	1.07	6.35	39.9	39.8	1.00	N/A
	CCN12-1	51.0x41.3x1.067	3	12.7	51.0	41.3	1.07	6.35	38.7	39.8	0.97	N/A
	CCN12-2	51.0x41.3x1.067	3	12.7	51.0	41.3	1.07	6.35	39.8	39.8	1.00	N/A
	CCN14-1	152x41.3x1.067	3	12.7	152	41.3	1.07	6.75	56.2	80.8	0.69	N/A
	CCN14-2	152x41.3x1.067	3	12.7	152	41.3	1.07	6.75	51.4	80.8	0.64	N/A
	CCN14-3	152x41.3x1.067	3	12.7	152	41.3	1.07	6.75	52.7	80.8	0.65	N/A
	CAN32-1	51.0x41.3x3.048	1	12.7	51.0	41.3	3.05	9.53	65.4	98.7	0.66	N/A
	CAN32-2	51.0x41.3x3.048	1	12.7	51.0	41.3	3.05	9.53	62.9	98.7	0.64	N/A
	CBN32-1	51.0x41.3x3.048	2	12.7	51.0	41.3	3.05	11.1	106.7	97.2	1.10	N/A
	CBN32-2	51.0x41.3x3.048	2	12.7	51.0	41.3	3.05	11.1	103.8	97.2	1.07	N/A
	CCN32-1	51.0x41.3x3.048	3	12.7	51.0	41.3	3.05	11.1	107.4	97.2	1.10	N/A
	CCN32-2	51.0x41.3x3.048	3	12.7	51.0	41.3	3.05	11.1	103.6	97.2	1.07	N/A
	CBN34-1	152x41.3x3.048	2	12.7	152	41.3	3.05	10.3	112.5	210.5	0.53	N/A
	CBN34-2	152x41.3x3.048	2	12.7	152	41.3	3.05	10.3	115.6	210.5	0.55	N/A
	CCN34-1	152x41.3x3.048	3	12.7	152	41.3	3.05	10.3	172.6	210.5	0.82	N/A
	CCN34-2	152x41.3x3.048	3	12.7	152	41.3	3.05	9.53	173.5	211.3	0.82	N/A
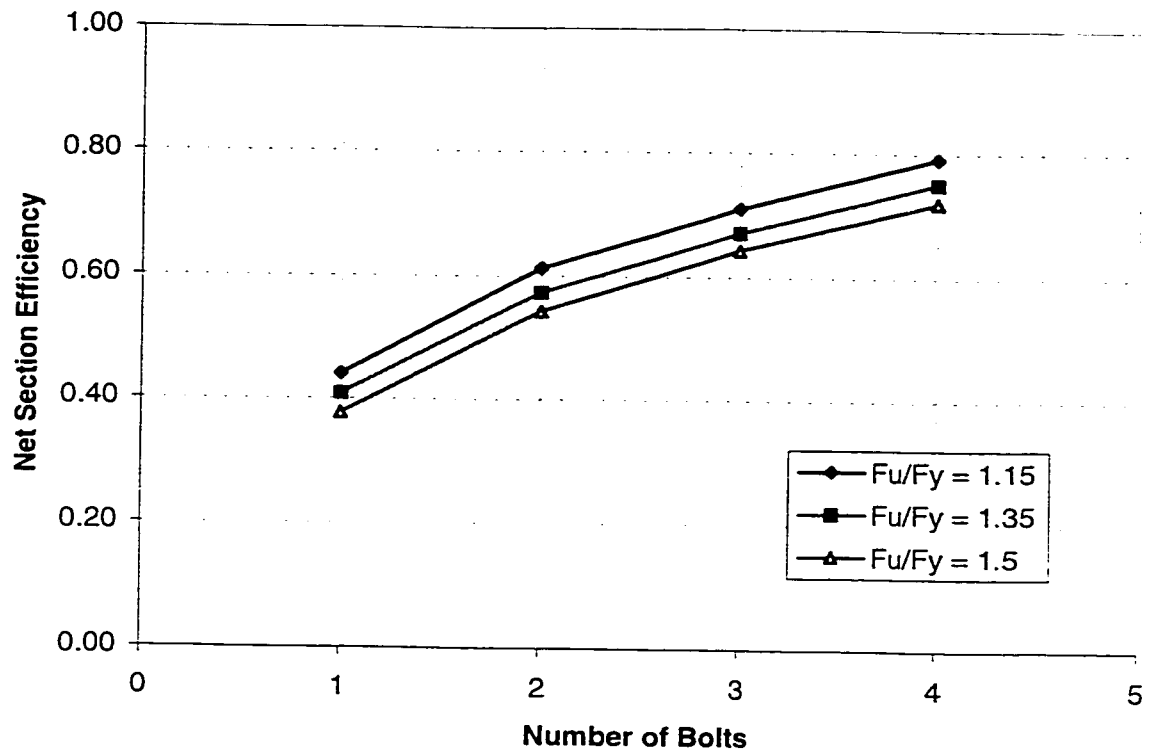
Figure 6.1 Effect of Material Properties on Net Section Efficiency of Angle Sections
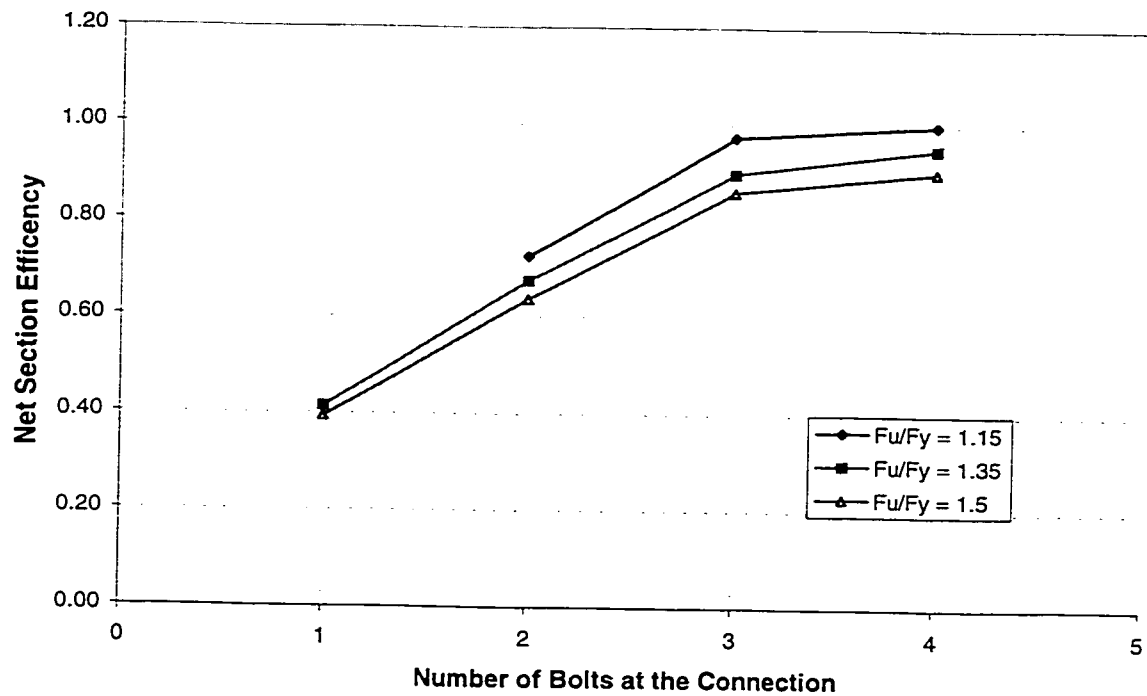
Figure 6.2 Effect of Material Properties on Net Section Efficiency of Channel Sections

119
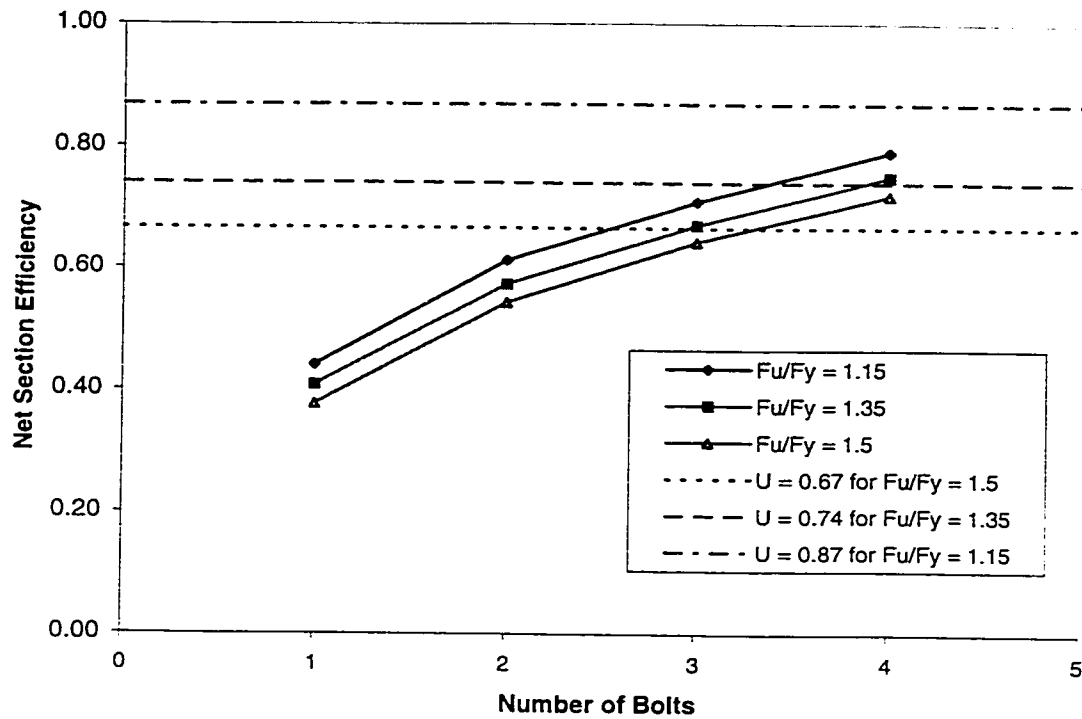
Figure 6.3 Effect of Material Properties on Net Section Efficiency of Angle Sections with Consideration of Gross Section Yielding
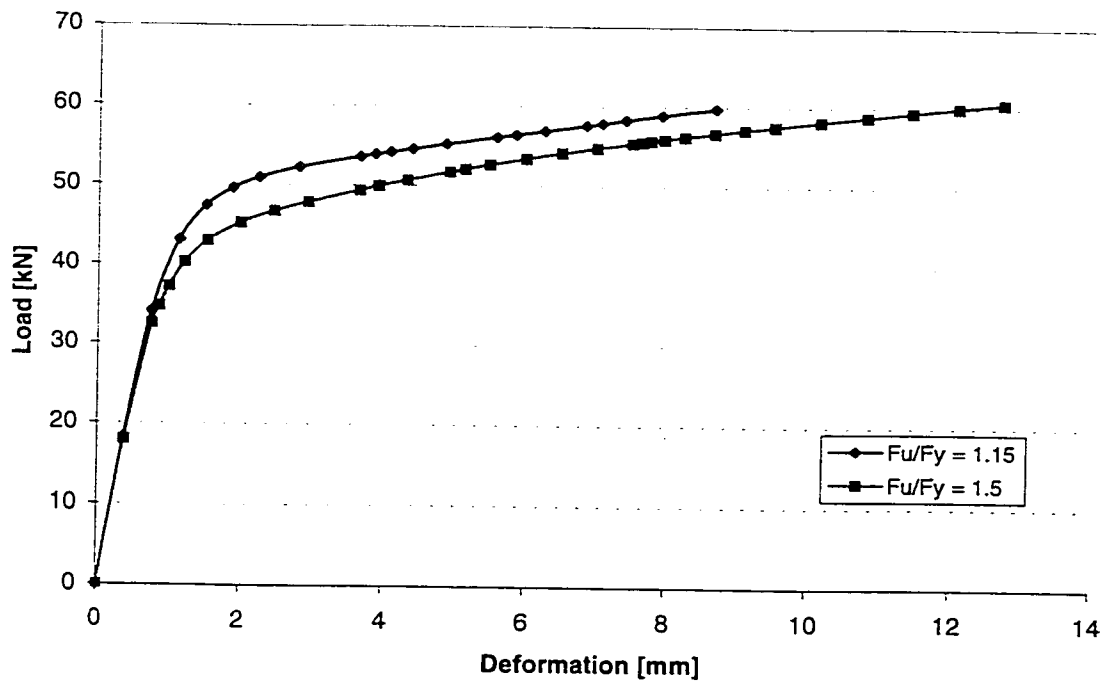
Figure 6.4 Load vs. Deformation Curves for Angle Sections with Different Material Constant, Number of bolts = 4
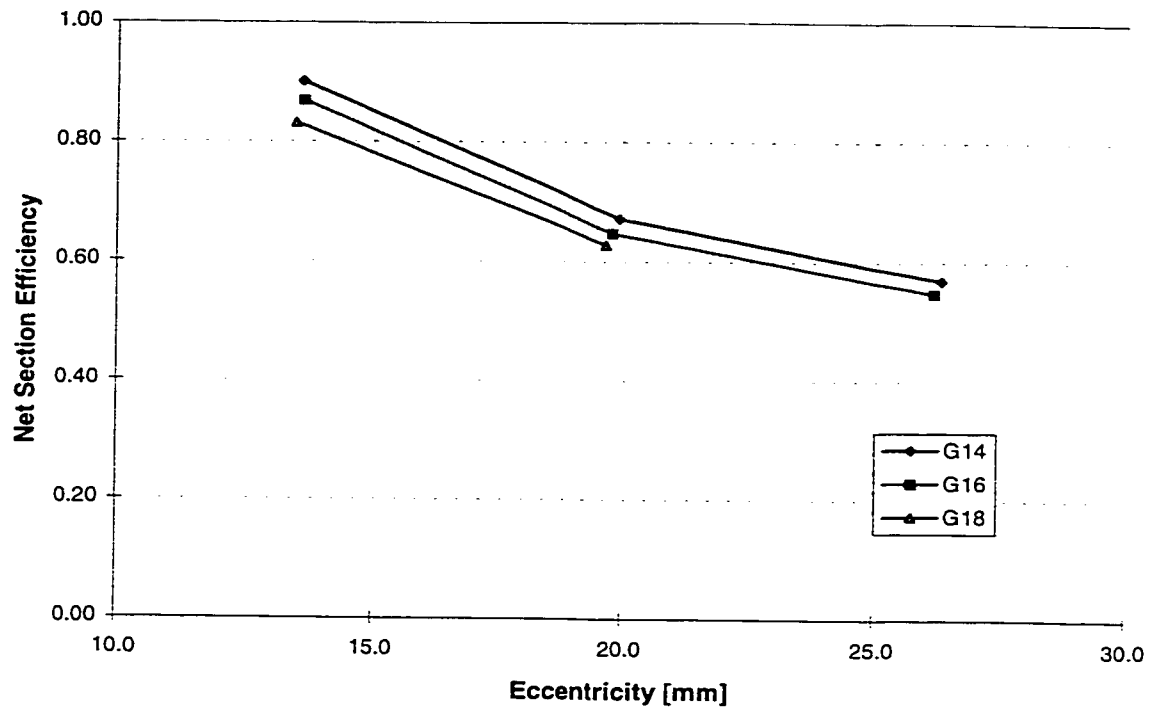
Figure 6.5 Effect of Eccentricity on Net Section Efficiency Angle Sections
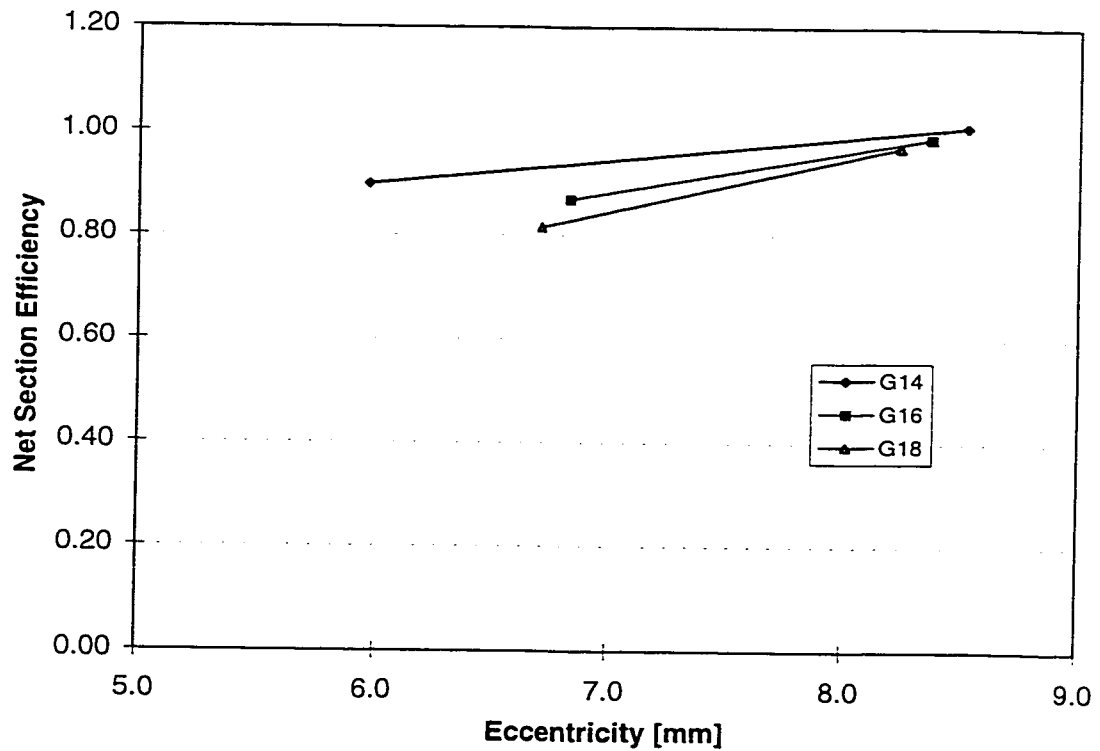
Figure 6.6 Effect of Eccentricity on Net Section Efficiency Channel Sections
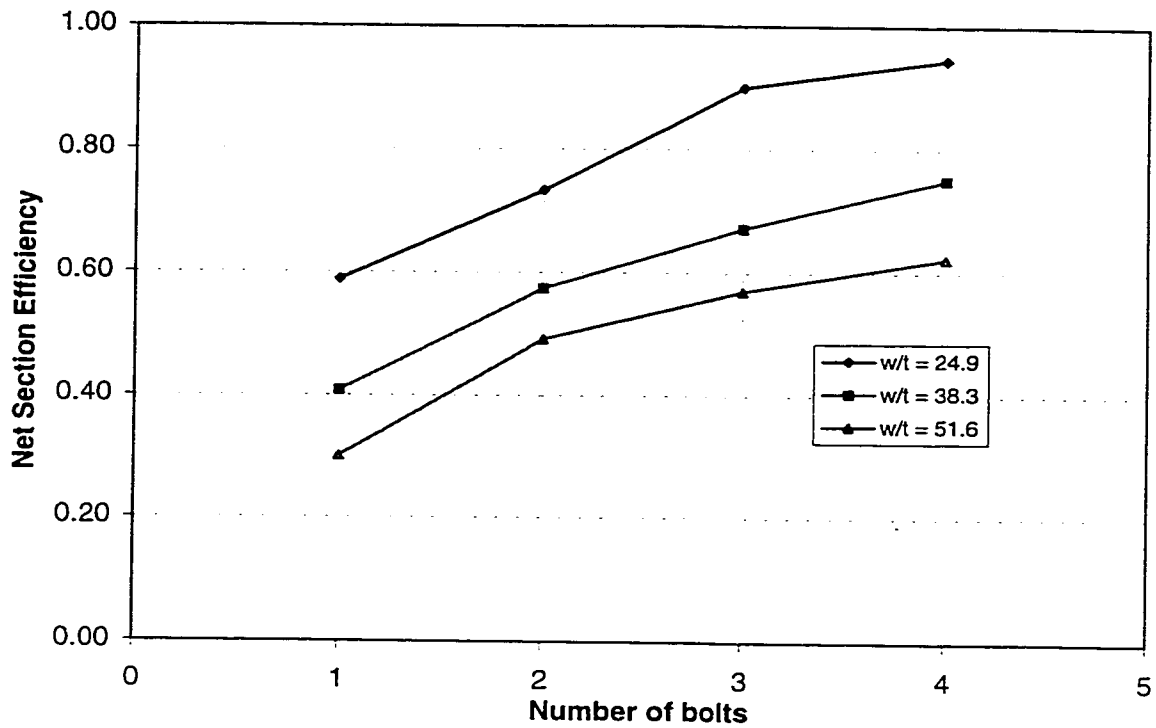
Figure 6.7 Effect of Bolt Number on the Net Section Efficiency of Angle Sections
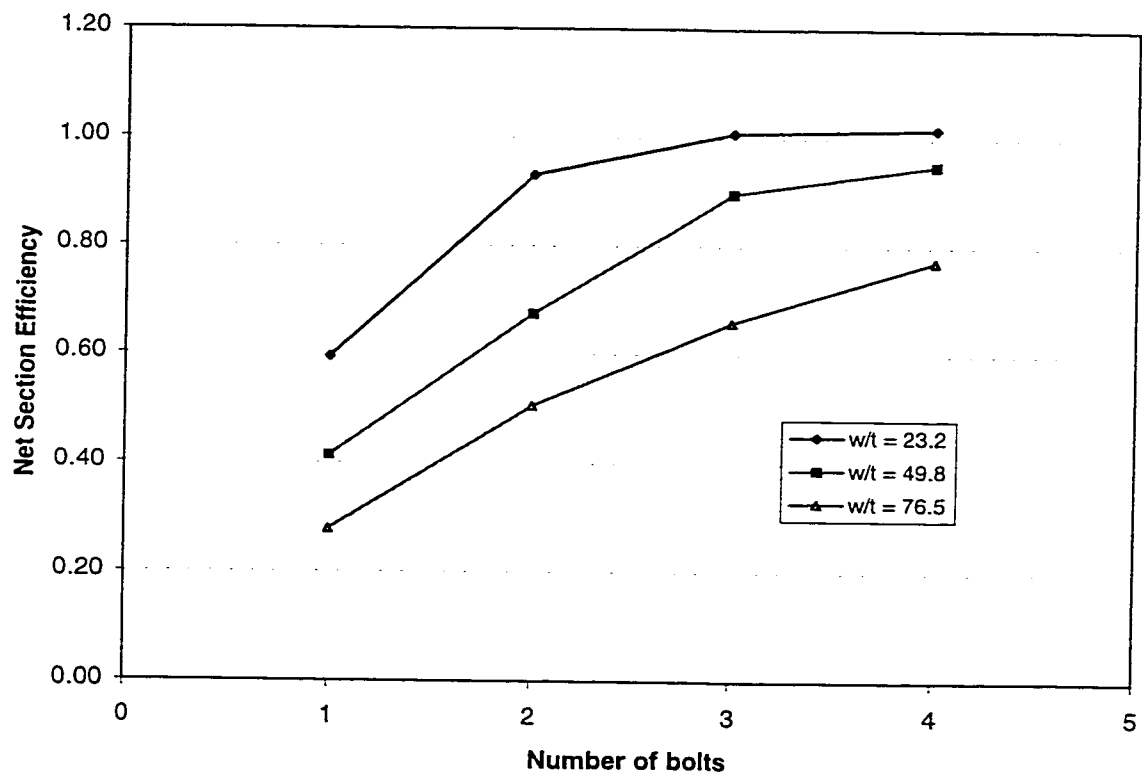
Figure 6.8 Effect of Bolt Number on the Net Section Efficiency of Channel Sections

122
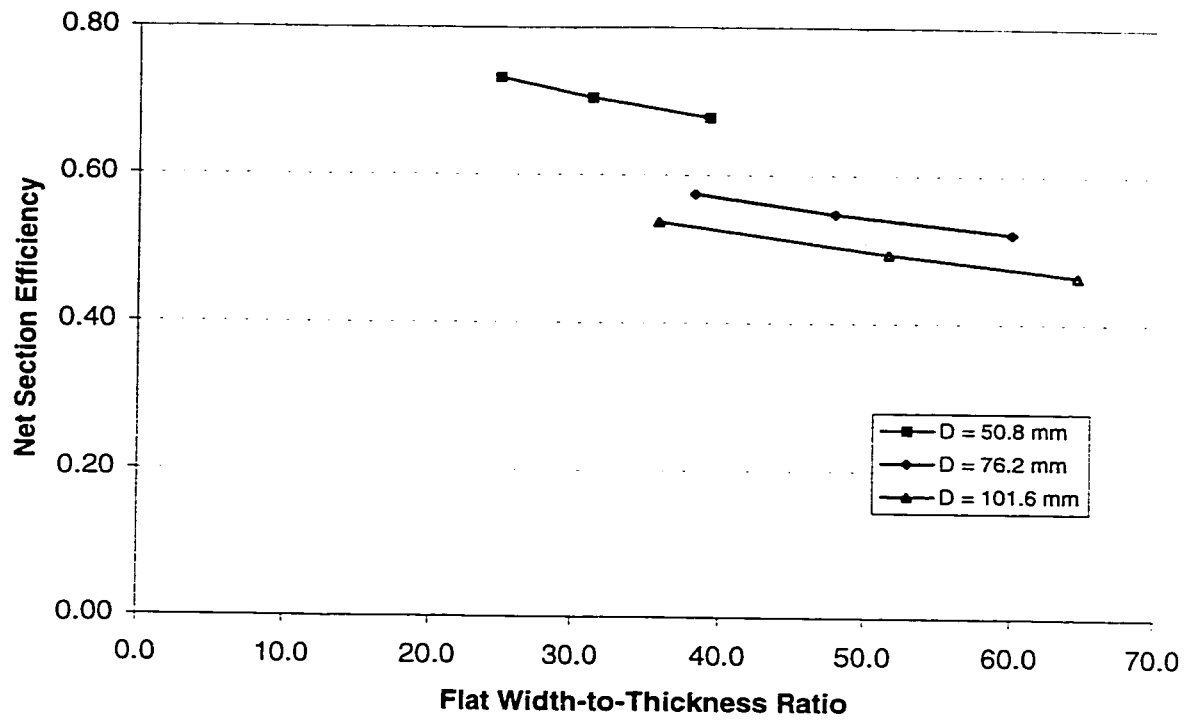
Figure 6.9 Effect of Flat Width-to-Thickness Ratio on Net Section Efficiency of Angle
Sections with 2 Bolts
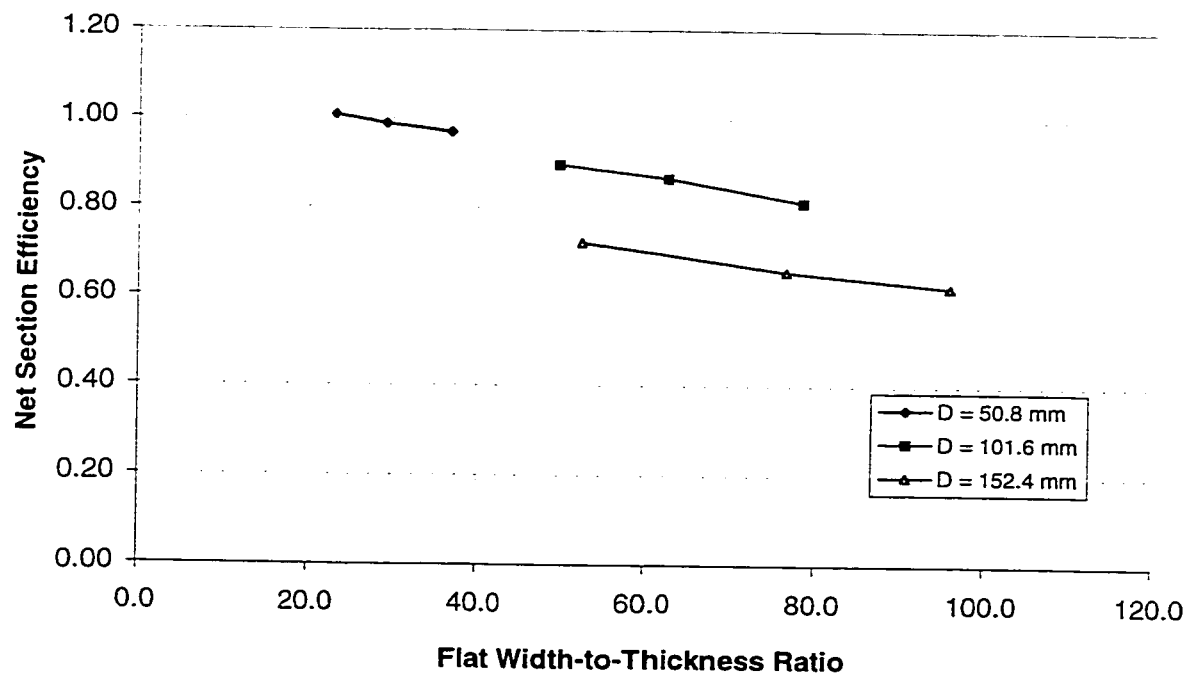
Figure 6.10 Effect of Flat Width-to-Thickness Ratio on Net Section Efficiency of
Channel Sections with 3 Bolts

123
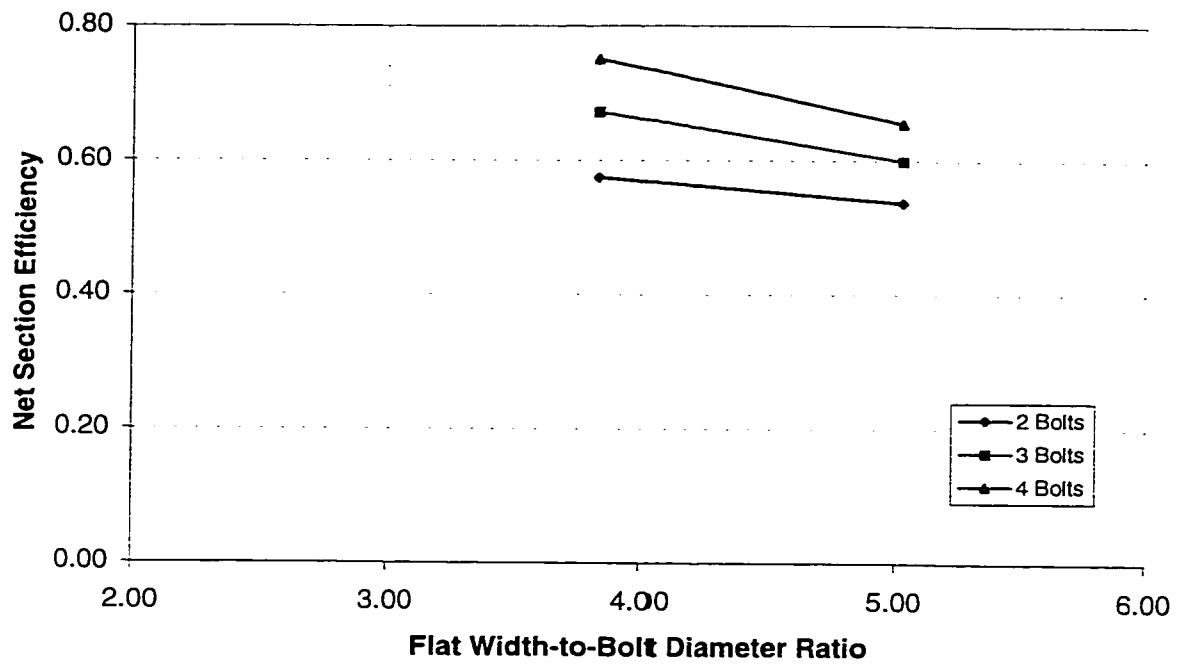
Figure 6.11 Effect of Flat Width-to-Bolt Diameter Ratio on the Net Section Efficiency of the Angle Sections
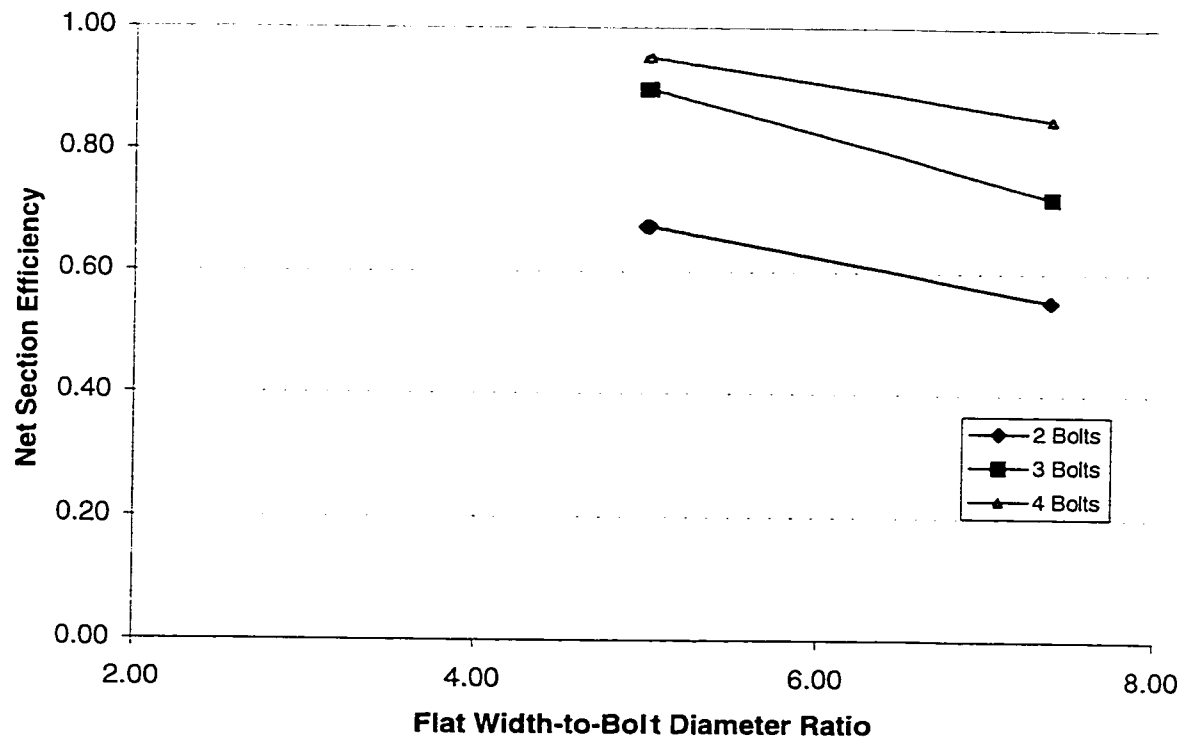
Figure 6.12 Effect of Flat Width-to-Bolt Diameter Ratio on the Net Section Efficiency of the Channel Sections

124
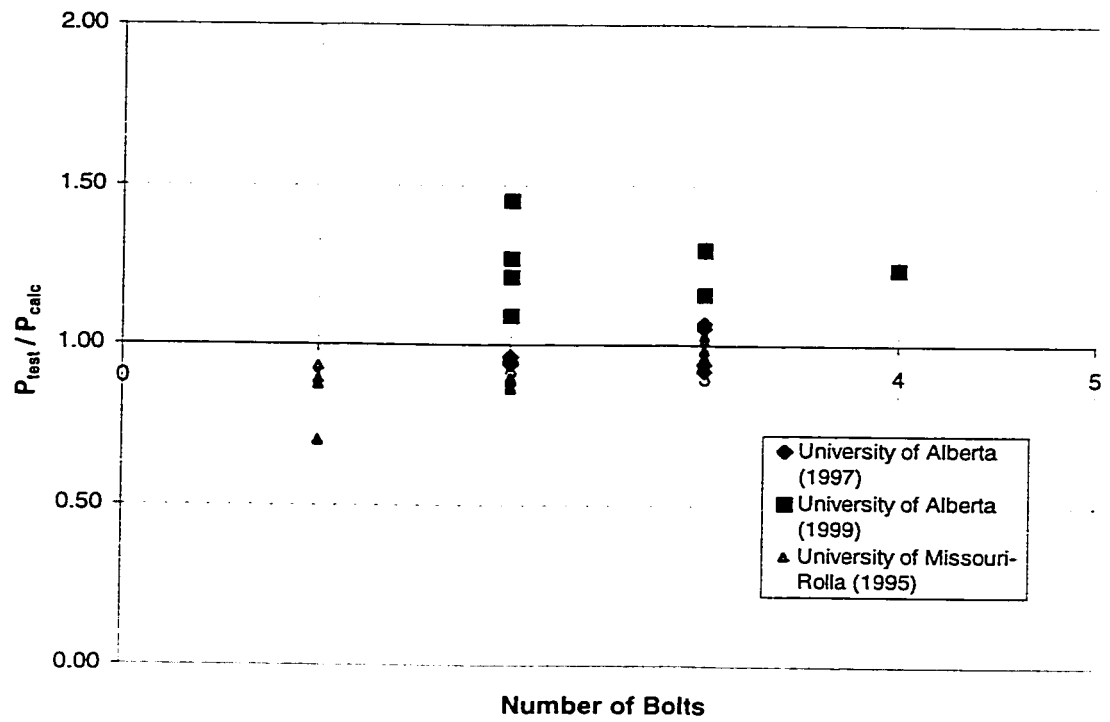
Figure 6.13 Evaluation of Equation 6.9 for Angle Sections
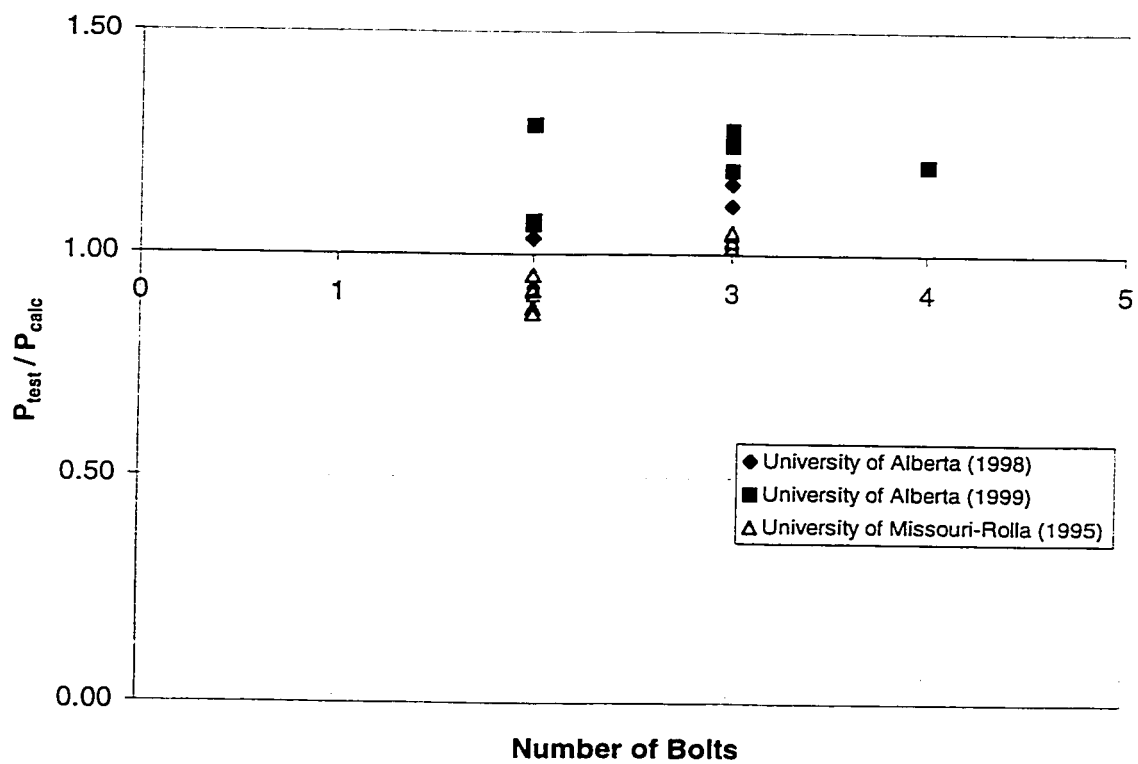
Figure 6.14 Evaluation of Equation 6.9 for Channel Sections

125

7. SUMMARY, CONCLUSIONS, AND RECOMMENDATIONS

7.1 Summary

This study was undertaken to investigate the effect of shear lag upon the net section efficiency of angle and channel cold-formed steel tension members with bolted connections. A total of twenty-three specimens were tested within test parameters that included number of bolts (or connection length), size of the specimen, and presence of washers. Two modes of failure were observed: bearing and net section fracture. The test results indicated that longer the connection and lower the flat width value, the less shear lag effects.

Finite element analysis was performed to predict the behavior of the connection and was able to provide a reasonable estimate of the ultimate load of the studied specimens. The stress and strain distributions at failure at the critical cross-section of the member were also evaluated using the finite element analysis. Based on the model obtained from finite element analysis, a parametric study with 100 tests was then conducted in order to develop the design criteria for cold-formed tension member with bolted connections. The factor $(1 - \bar{x}/L)$ and the geometric factors such as the flat width-to-thickness ratio and the flat width-to-bolt diameter ratio were found to have significant effects on the net section efficiency. Nonlinear regression equations were then derived for the net section efficiency of bolted angle and channel tension members. Existing test data was used to check the validity of the proposed equations. Good agreement was obtianed.

126

7.2 Conclusions

Based on the study presented herein and together with the results obtained by others, it can be concluded that:

1. The net section efficiency of both bolted angle and channel members in tension is affected by the connection length and cross-sectional geometry if only one element in the sections is connected by fasteners;

2. The factors found to have significant effects on the net section efficiency include eccentricity, connection length, slenderness of connected elements, size of bolt, and length of unconnected elements relative to length of connected element;

3. The amount of torque applied when tightening the bolt has been found to have effect on the net section fracture capacity of the connection and further investigation is required;

4. The Munse and Chesson's net section efficiency equation, $(U = 1 - \frac{\overline{x}}{L})$, was not able to provide a good prediction for the cold-formed angle sections with flat width-to-thickness ratio, w/t, greater than 30 and flat width-to-bolt diameter ratio, w/d, greater than 2.5, and for the channel sections with w/t ratio greater than 40 and w/d ratio greater than 5.

5. When there are two or more bolts in the line of force, it has been shown that Eqs. 6.2 and 6.3 accurately predict the net section efficiencies of equal leg angle members and channel members connected at the web, respectively.

6. For the cases with only one bolt in the line of force, Eqs. 6.6 and 6.7 are a good predictor for predicting the net section efficiencies of equal leg angle sections and channel sections connected at the web.

7. The available test results also indicate that the proposed net section efficiency equations can also be used for the stiffened sections and unequal leg angles with long leg connected. Further tests and analyses, however, are desirable in order to confirm these conclusions.

7.3 Design Recommendations of Net Section Fracture for Bolted Cold-Formed Members in Tension

For bolted cold-formed members, the factored tensile resistance, T_r, shall be taken as the lesser of

a) $T_r = \phi A_g F_y$ [7.1]

b) $T_r = \phi_u A_{ne} F_u$ [7.2]

where ϕ = resistance factor for gross yielding, taken as 0.9

ϕ_u = tensile fracture resistance factor, taken as 0.75

F_y = specified yield strength

F_u = specified ultimate strength

A_g = gross cross-sectional area

A_{ne} = effective net area accounting for shear lag

The effective net area can be calculated as follows:

$A_{ne} = U A_n$ [7.3]

where A_n = critical net area at a potential fracture section, calculated by reducing hole area from the gross area and the hole diameter is taken as 2 mm larger than the nominal size of bolt

U = net section efficiency factor to be determined as follows:

128

a) For equal leg angle members connected by one leg or unequal leg angles with long leg connected

   (i) with one bolt in the line of force

   $$U = 1 - 0.11(\frac{w}{t})^{0.3}(\frac{w}{d})^{0.42} \leq 1.0$$

   [7.4]

   (ii) with two or more bolts in the line of force

   $$U = 1 - 0.085(\frac{\overline{x}}{L})^{0.41}(\frac{w}{t})^{0.36}(\frac{w}{d})^{0.51} \leq 1.0$$

   [7.5]

b) For channel members connected by the web

   (i) with one bolt in the line of force

   $$U = 1 - 0.11(\frac{w}{t})^{0.4}(\frac{w}{d})^{0.07} \leq 1.0$$

   [7.6]

   (ii) with two or more bolts in the line of force

   $$U = 1 - 0.04(\frac{\overline{x}}{L})^{0.85}(\frac{w}{t})^{0.54}(\frac{w}{d})^{1.02} \leq 1.0$$

   [7.7]

REFERENCES

American Institute of Steel Construction (1993). Load and Resistance Factor Design Specification for Structural Steel Buildings. Chicago, Illinois.

American Iron and Steel Institute (1996). Specification for the Design of Cold-Formed Steel Structural Members. Washington, D.C..

American Society for Testing and Materials (1997). A370 Standard Test Methods and Definitions for Mechanical Testing of Steel Products. ASTM, Philadelphia, PA..

Canadian Standards Association (1994). CAN/CSA-S16.1-94 -- Limit States Design of Steel Structures. Canadian Standards Association, Rexdale, Ontario.

Canadian Standards Association (1994). CAN/CSA-S136-94 – Cold-Formed Steel Structural Members. Canadian Standards Association, Rexdale, Ontario.

Canadian Standards Association (1997). CAN/CSA-G40.21-97 – Structural Quality Steels. Canadian Standards Association, Rexdale, Ontario.

Chong, K. P. and Matlock, R. B. (1975). "Light-Gage Steel Bolted Connections without Washers." Journal of Structural Division, ASCE, Vol. 101(7), pp. 1381-1392.

Cheng, J. J. R., Grondin, G. Y., and Takai, N. (1998). "Shear Lag Effects on Bolted Cold-Formed Steel Angles in Tension." Proceedings of the Canadian Society of Civil Engineers Conference, Halifax, Nova Scotia, Vol. 3, pp. 147-156.

Cheng, J. J. R., Grondin, G. Y., and Estabrooks, B. (1999). "Shear Lag Effects on Bolted Cold-Formed Steel Channels in Tension." Proceedings of the Canadian Society of Civil Engineers Conference, Regina, Saskatchewan, Vol. 1, pp. 335-344.

Chesson, E. and Munse, W. H. (1963). "Riveted and Bolted Joints: Truss Type Tensile Connections." Journal of the Structural Division, ASCE, Vol. 89(1), pp. 67-106.

Chesson, E. and Munse, W. H. (1963). "Riveted and Bolted Joints: Net Section Design." Journal of the Structural Division, ASCE, Vol. 89(1), pp. 107-126.

Gilchrist, R. T. Jr. and Chong, K. P. (1979). "Thin Light-Gage Bolted Connections without Washers." Journal of Structural Division, ASCE, Vol. 105(1), pp. 175-184.

Hibbitt, Karlsson, & Sorenson, Inc. (HKS) (1997a). ABAQUS/Standard, Version 5.7-1 (Computer Software). Hibbitt, Karlsson, & Sorenson Inc., Pawtucket, Rhode Island.

Hibbitt, Karlsson, & Sorenson, Inc. (HKS) (1997b). ABAQUS/Standard Theory Manual. Version 5.7. Hibbitt, Karlsson, & Sorenson Inc., Pawtucket, Rhode Island.

Hibbitt, Karlsson, & Sorenson, Inc. (HKS) (1997c). ABAQUS/Standard User's Manual. Version 5.7. Hibbitt, Karlsson, & Sorenson Inc., Pawtucket, Rhode Island.

Kennedy, J. B. and Sinclair, G. R. (1969). "Ultimate Capacity of Single Bolted Angle Connections." Journal of the Structural Division, ASCE, Vol. 95(8), pp. 1645-1660.

Kulak, G. L., Adams, P. F., and Gilmor, M. I. (1995). Limit States Design in Structural Steel. Fifth Edition, CISC, Alliston, Ontario.

Kulak, G. L., Fisher, J. W., and Struik, J. H. A. (1987). Guide to Design Criteria for Bolted and Riveted Joints. John Wiley and Sons, New York, N. Y., pp. 99-100.

LaBoube, R. A. and Yu, W. W. (1995). "Tensile and Bearing Capacities of Bolted Connections." Final Summary Report, University of Missouri-Rolla, Rolla, Missouri.

March, C. (1969). "Single Angles in Tension and Compression." Journal of Structural Division, ASCE, Vol. 95(5), pp. 1043-1049.

McKibben, F. P. (1906). "Tension Tests of Steel Angles." Proceedings of the ASTM, Vol. 6, pp. 267-274.

McKibben, F. P. (1907). "Tension Tests of Steel Angles with Various Types of End-connections." Proceedings of the ASTM, Vol. 7, pp. 287-295.

Nelson, H. M. (1953). "Angles in Tension." Publication No. 7, British Constructional Steelwork Association, UK, pp. 8-18.

SPSS, Inc. (1999). SigmaPlot 5.0 (computer software). SPSS Inc., Chicago, Illinois.

Winter, G. (1956). "Tests on Bolted Connections in Light Gage Steel." Journal of the Structural Division, ASCE, Vol. 82(2), pp. 921-925.

Wu, Y. and Kulak, G. L. (1993). Shear Lag in Bolted Single and Double Angle Tension Members. Structural Engineering Report 187, Department of Civil Engineering, University of Alberta, Edmonton, Alberta.

Young, C. R. (1935). Elementary Structural Problems in Steel and Timber. John Wiley and Sons, New York, N. Y., pp. 7.

Yu, W. W. (1991). Cold-Formed Steel Design. Second Edition, John Wiley and Sons, New York, N. Y..

APPENDIX A

LOAD VS. DEFORMATION CURVES FOR THE TEST SPECIMENS
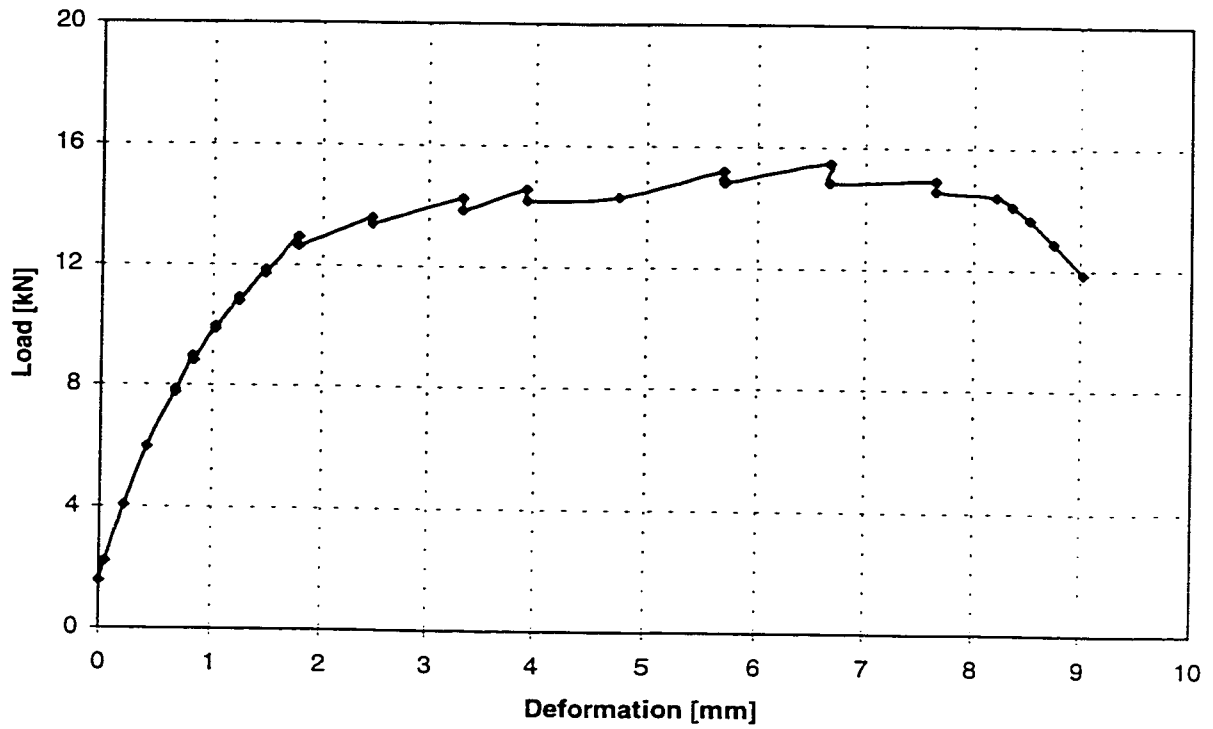
Figure A.1 Load vs. Deformation Curve for Specimen A2-1
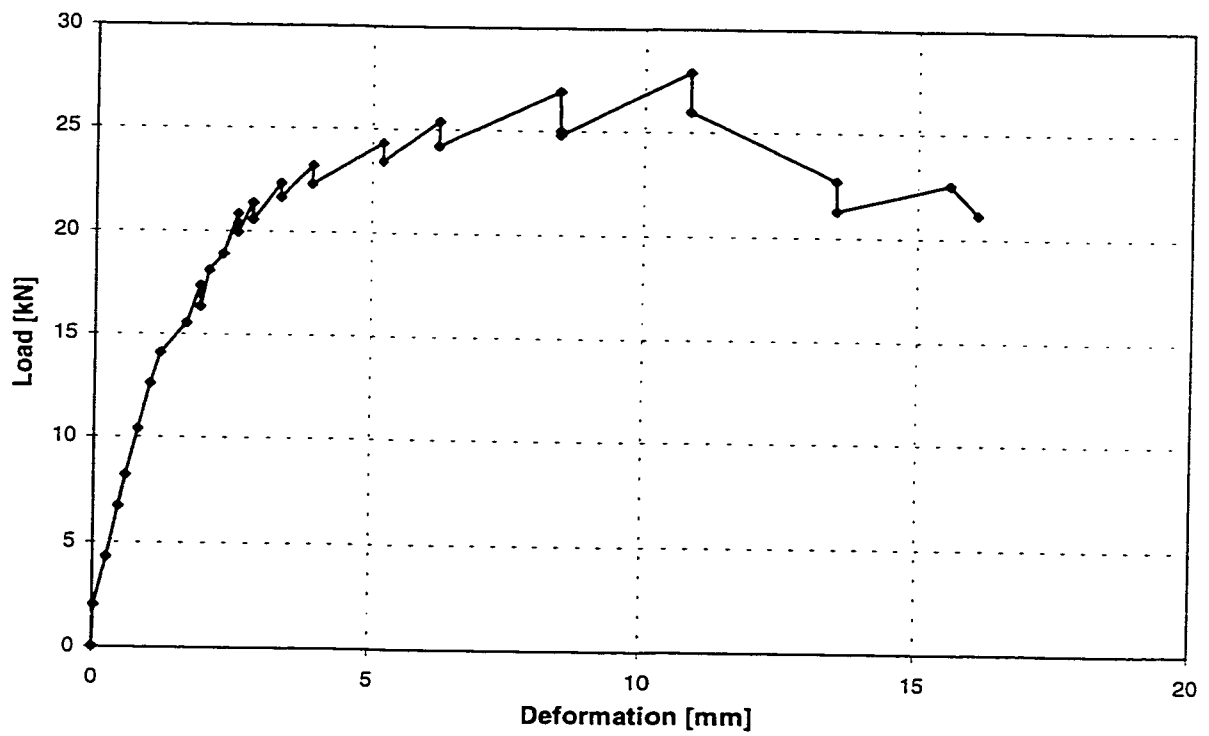
Figure A.2 Load vs. Deformation Curve for Specimen A2-2
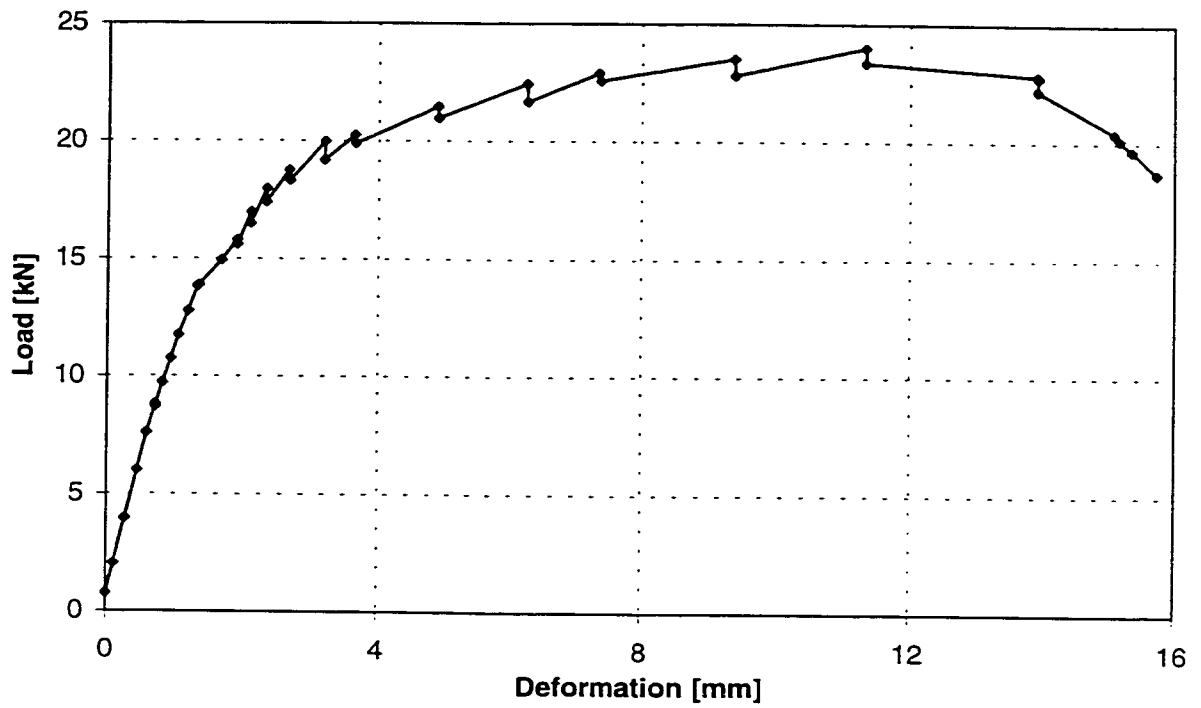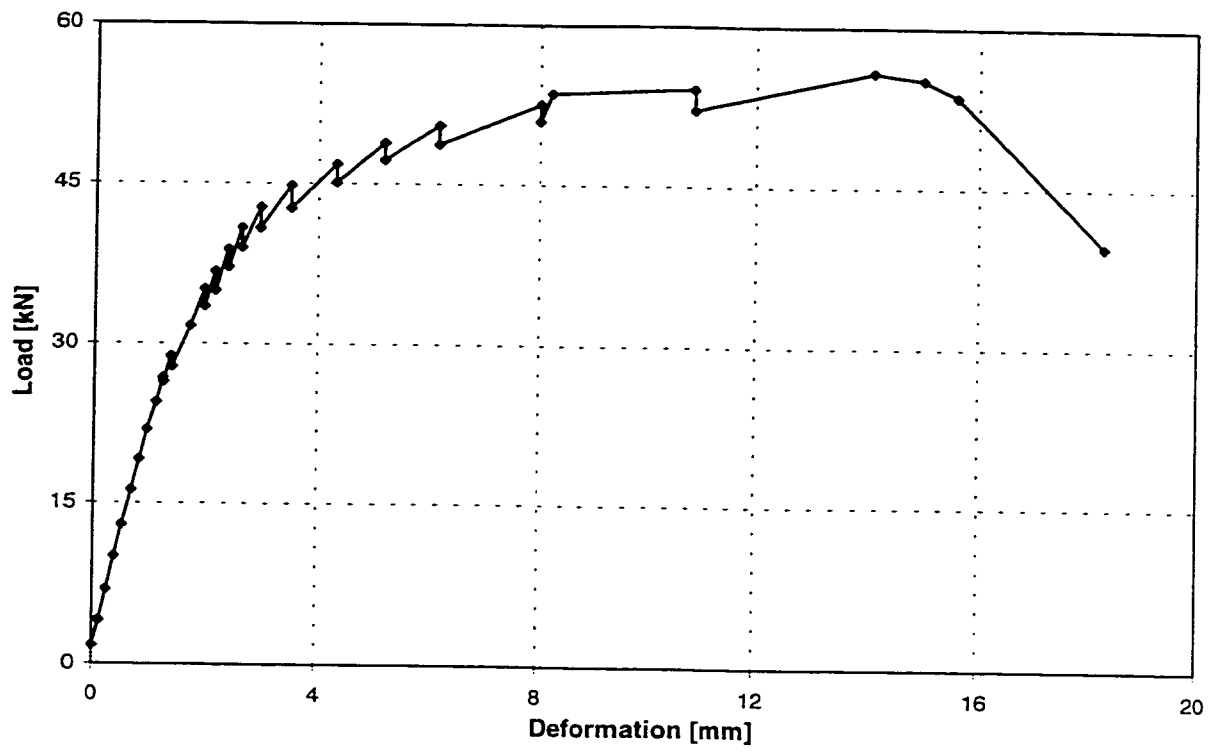
Figure A.3 Load vs. Deformation Curve for Specimen A2-2N
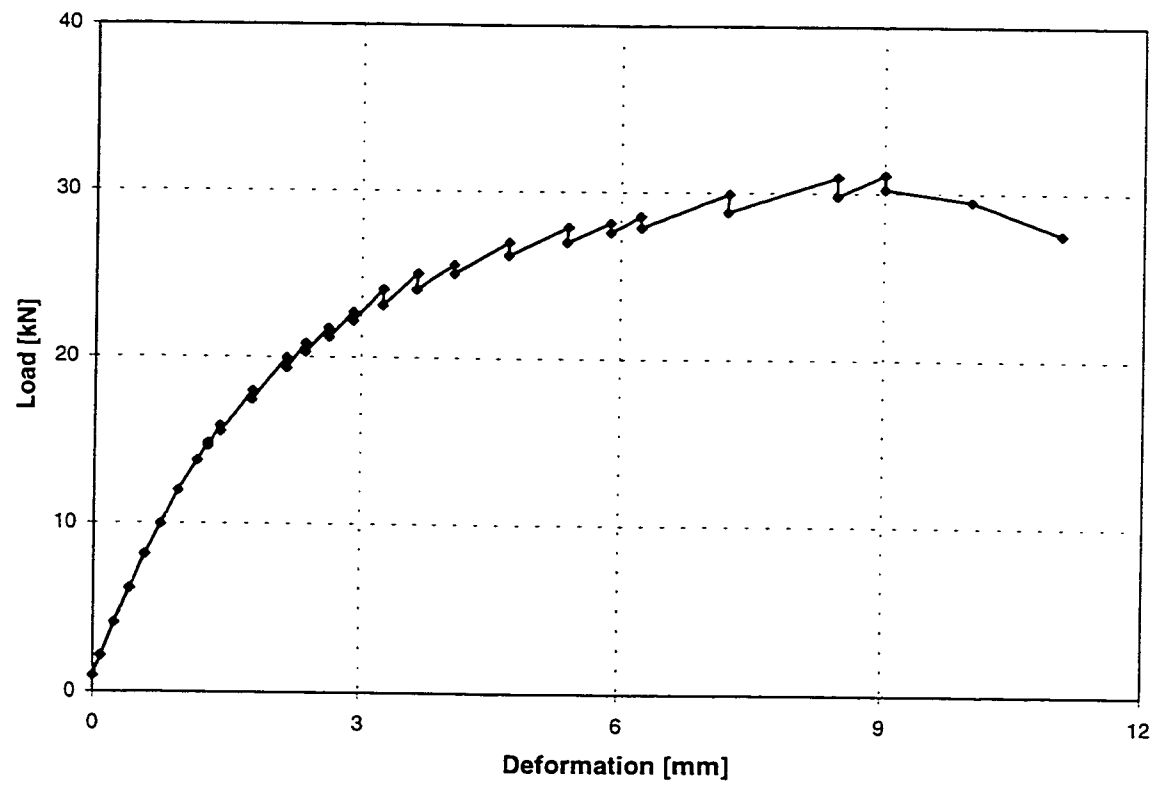
Figure A.4 Load vs. Deformation Curve for Specimen A2-3
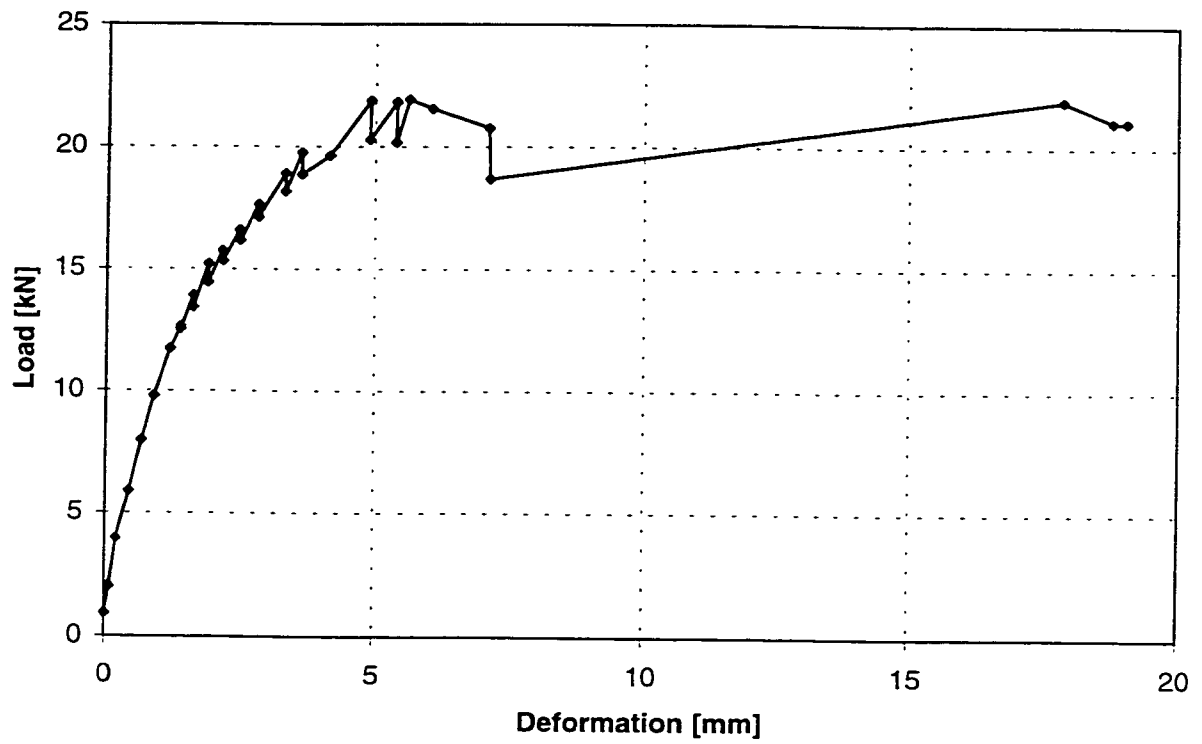
Figure A.5 Load vs. Deformation Curve for Specimen A3-1
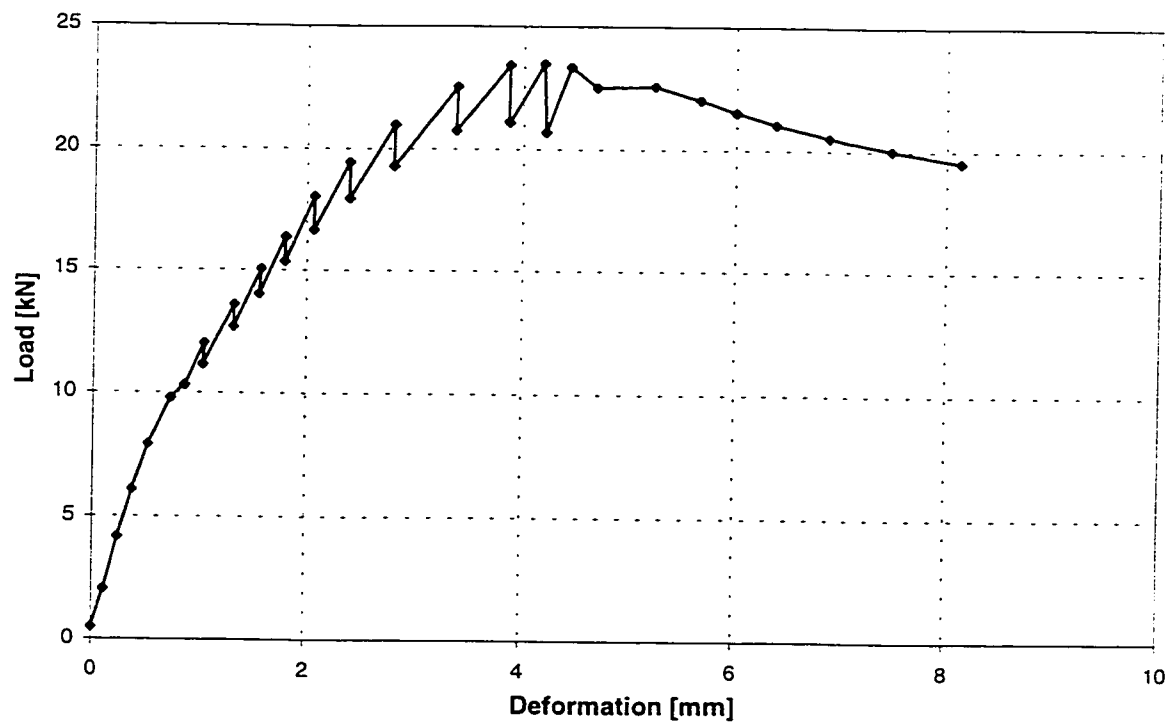
Figure A.6 Load vs. Deformation Curve for Specimen *A3-1

135
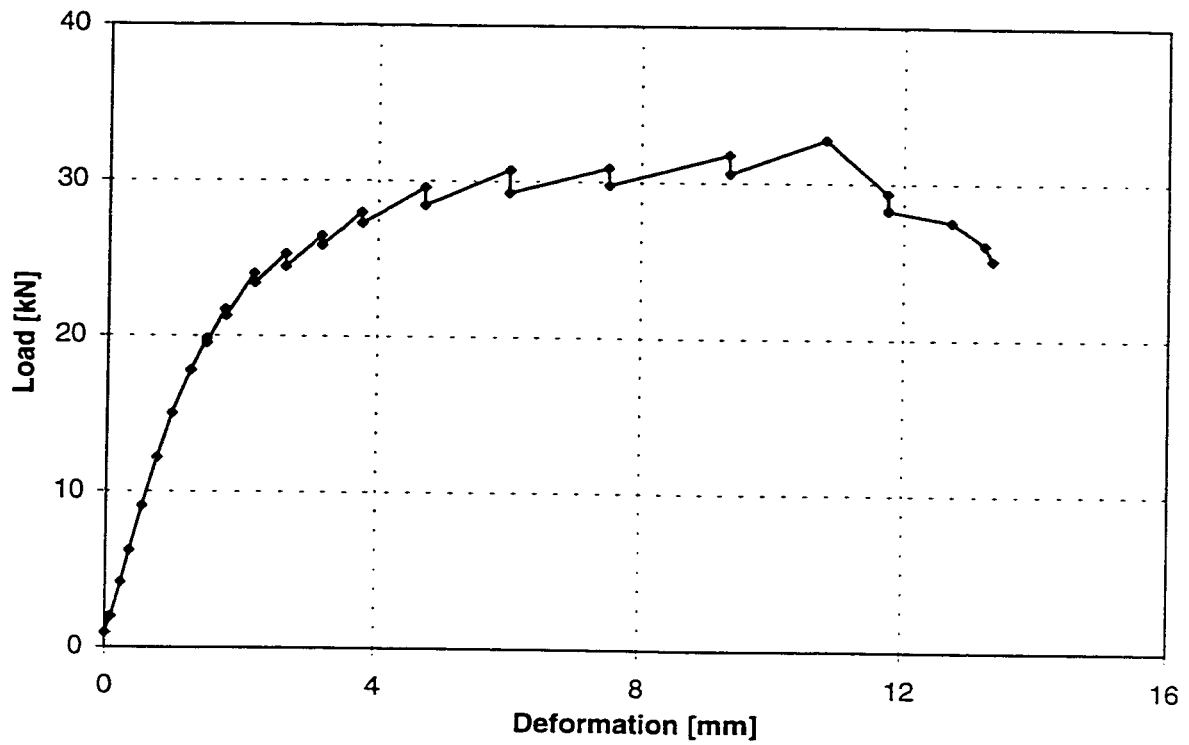
Figure A.7 Load vs. Deformation Curve for Specimen A3-2
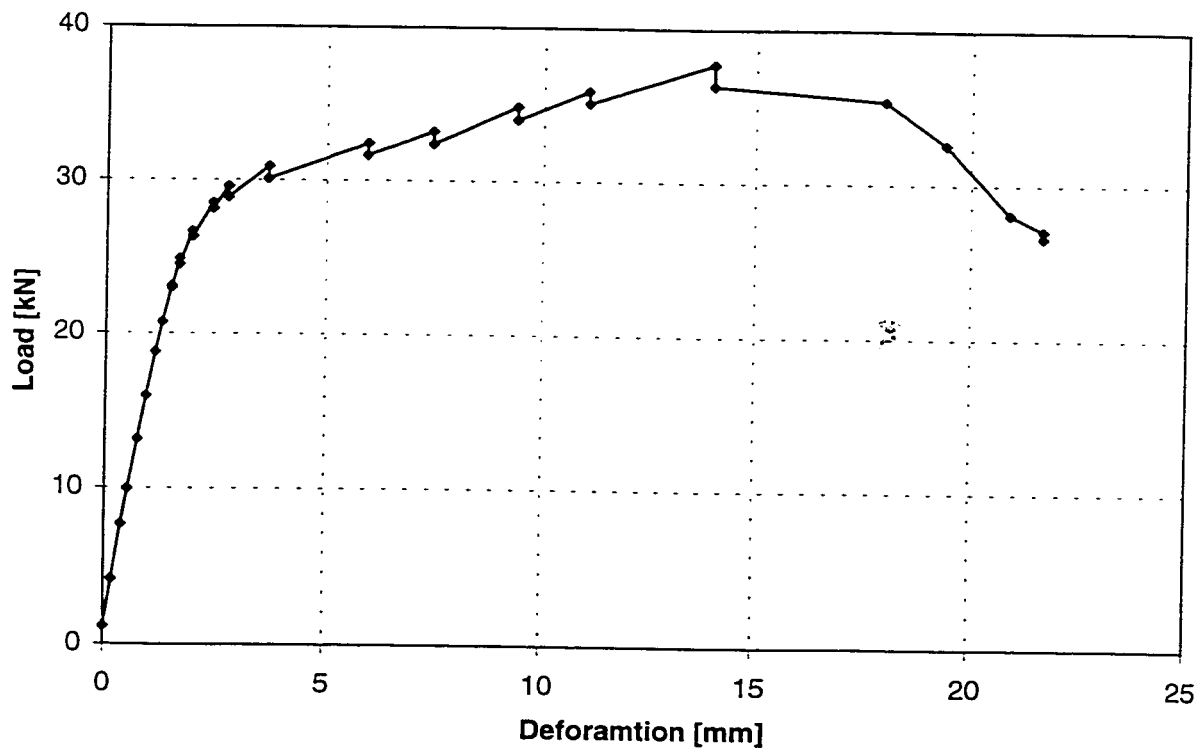
Figure A.8 Load vs. Deformation Curve for Specimen A3-3
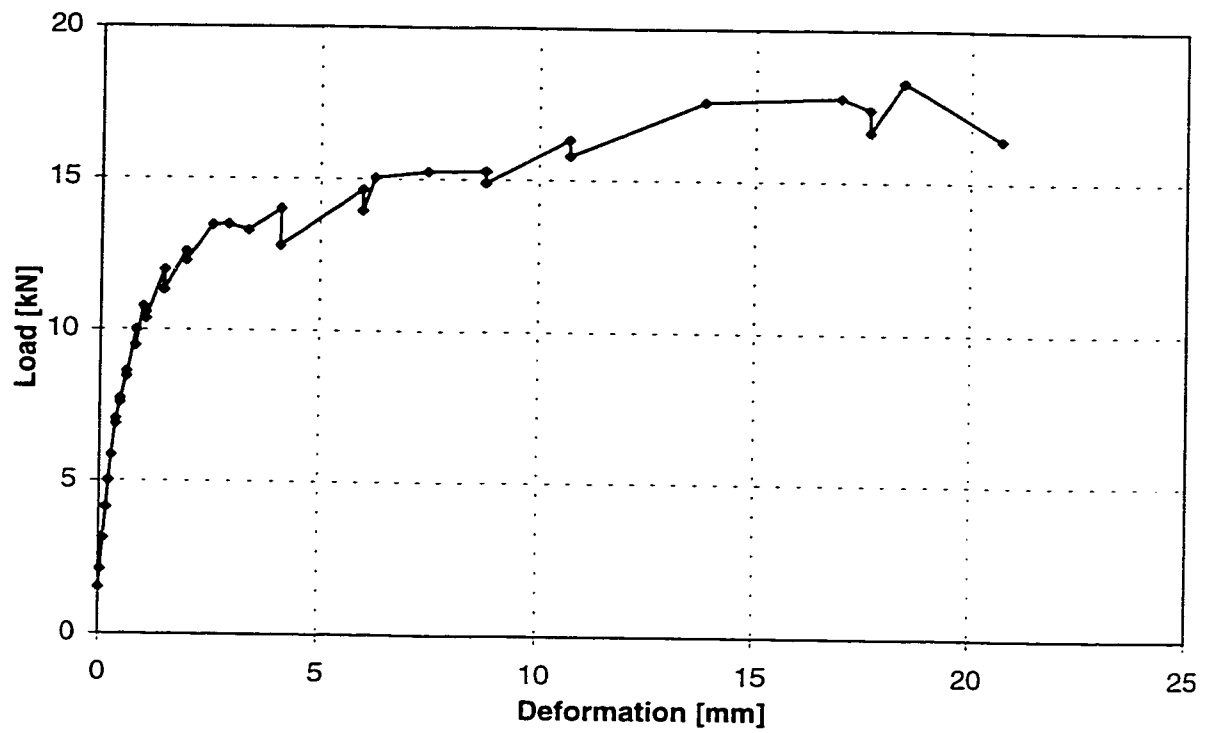
Figure A.9 Load vs. Deformation Curve for Specimen A4-1
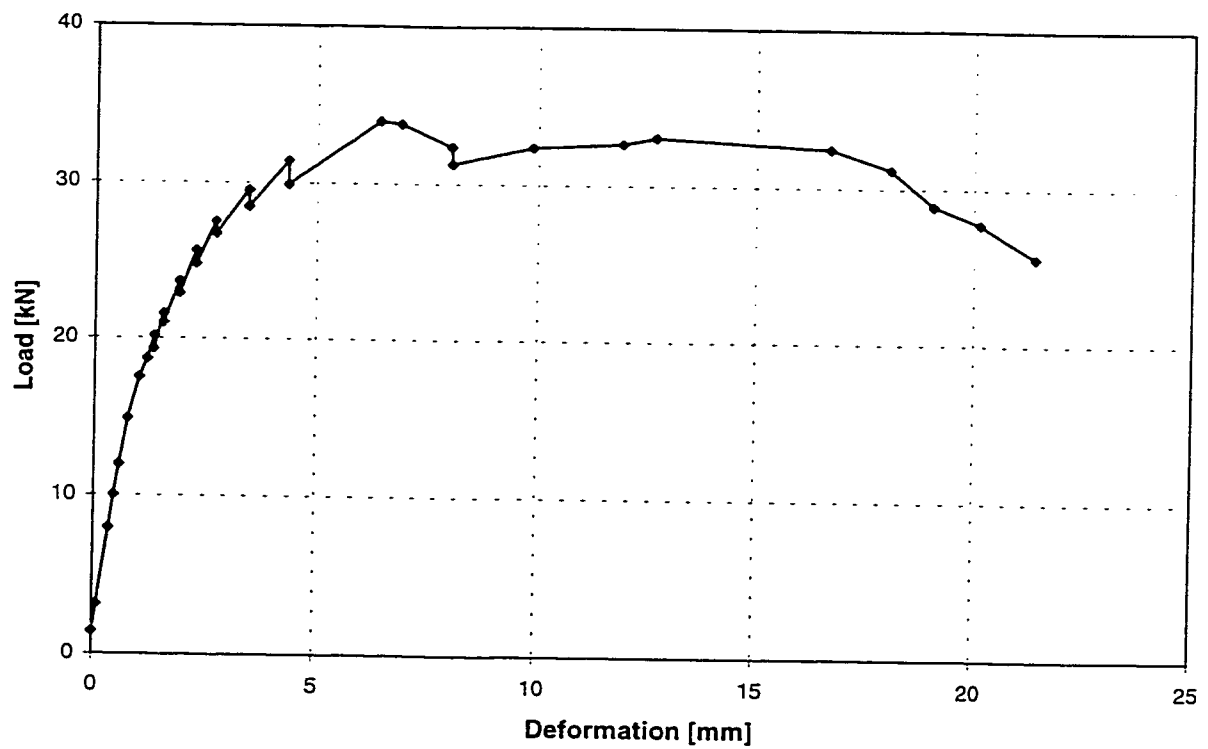
Figure A.10 Load vs. Deformation Curve for Specimen A4-2

137
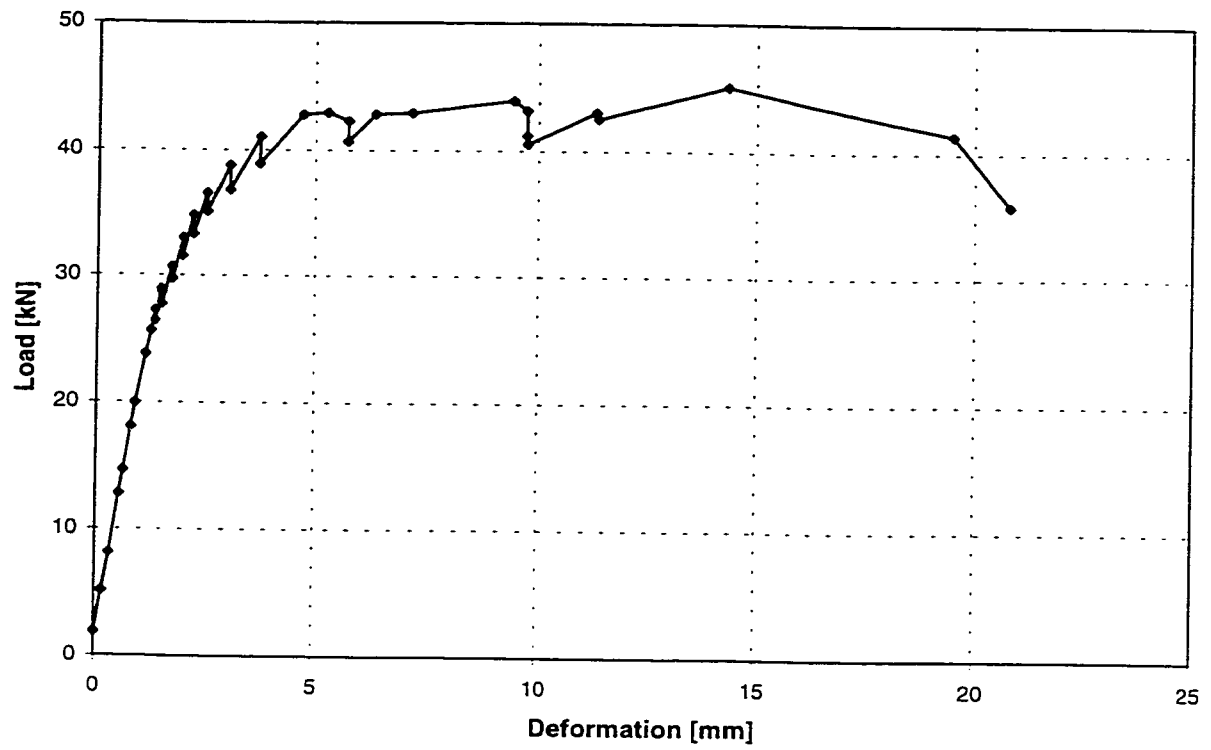
Figure A.11 Load vs. Deformation Curve for Specimen A4-3
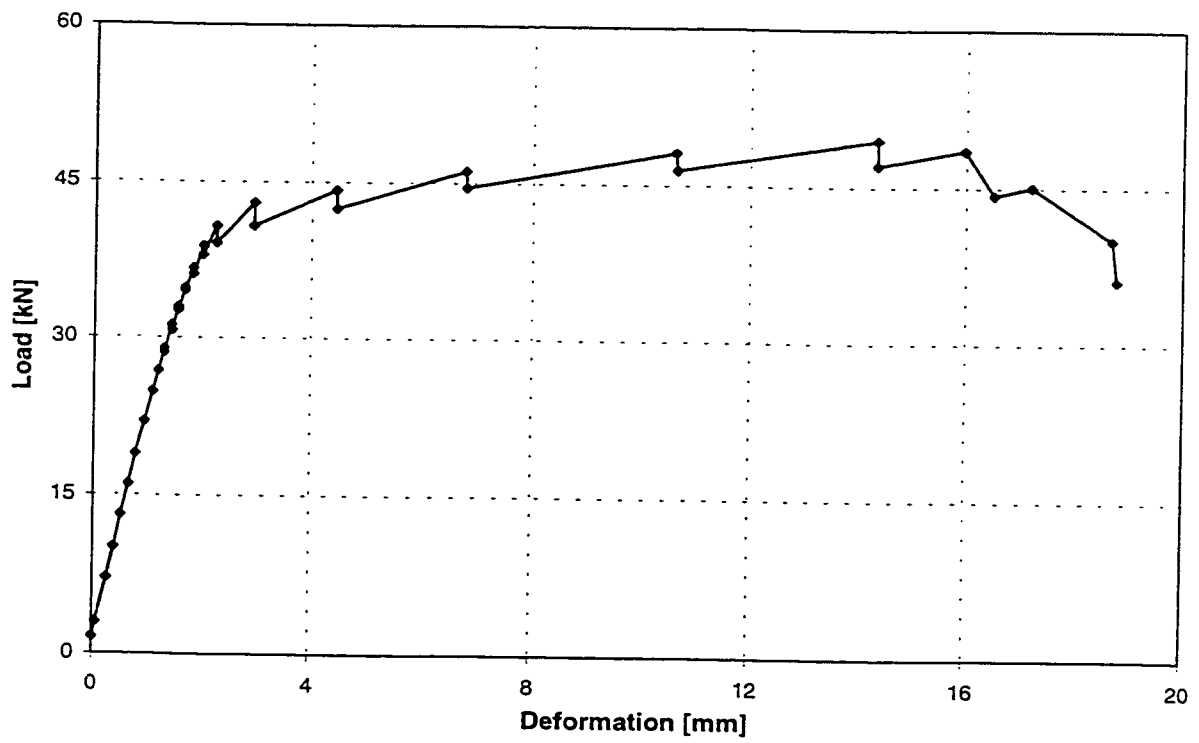
Figure A.12 Load vs. Deformation Curve for Specimen A4-4

138
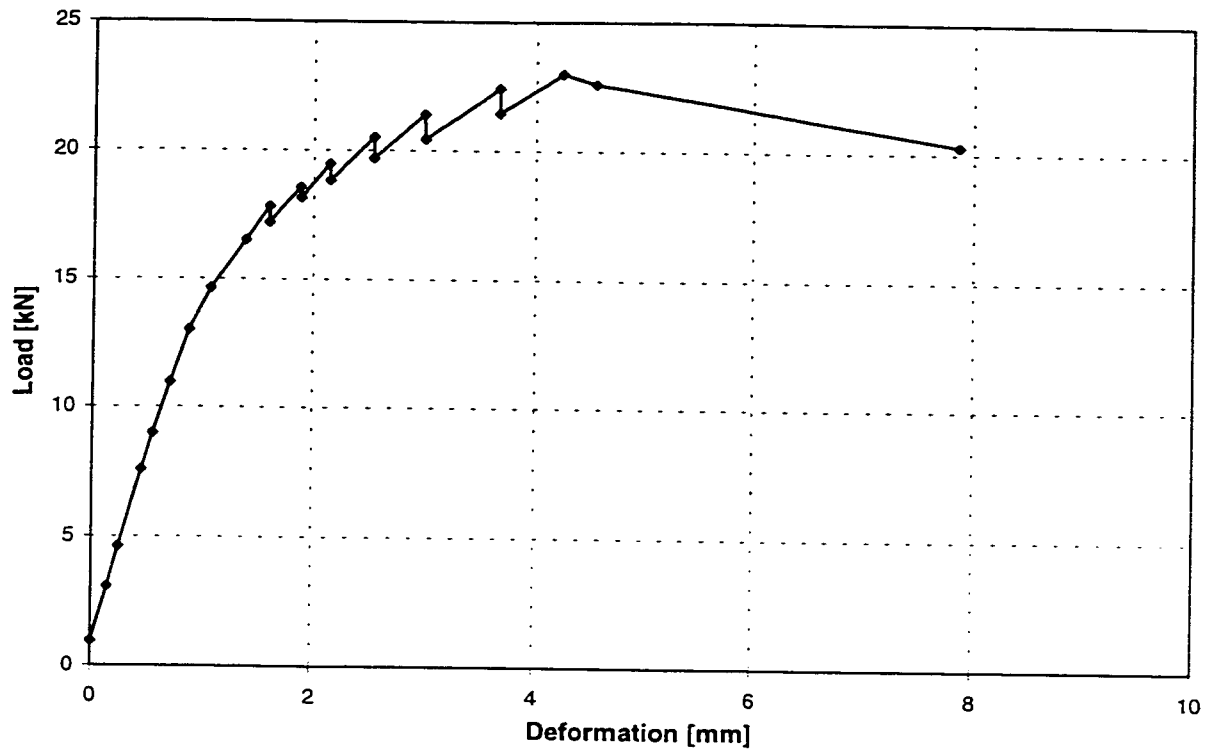
Figure A.13 Load vs. Deformation Curve for Specimen C2-1
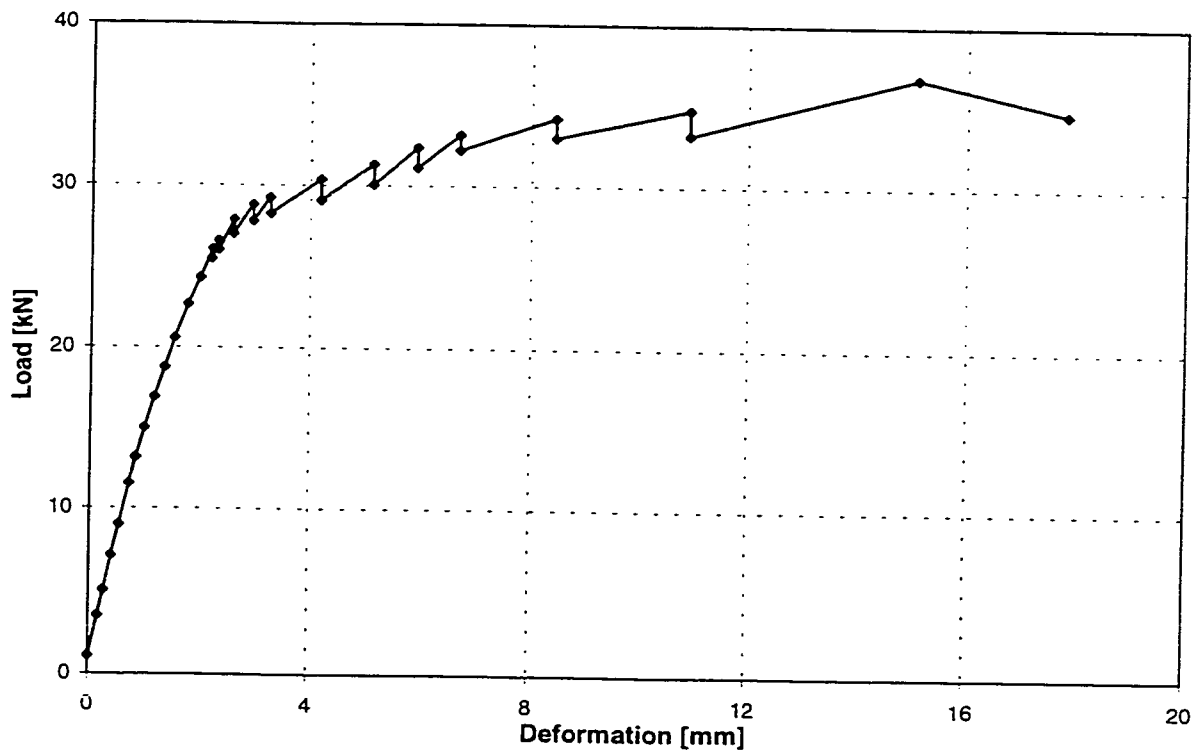
Figure A.14 Load vs. Deformation Curve for Specimen C2-2

139
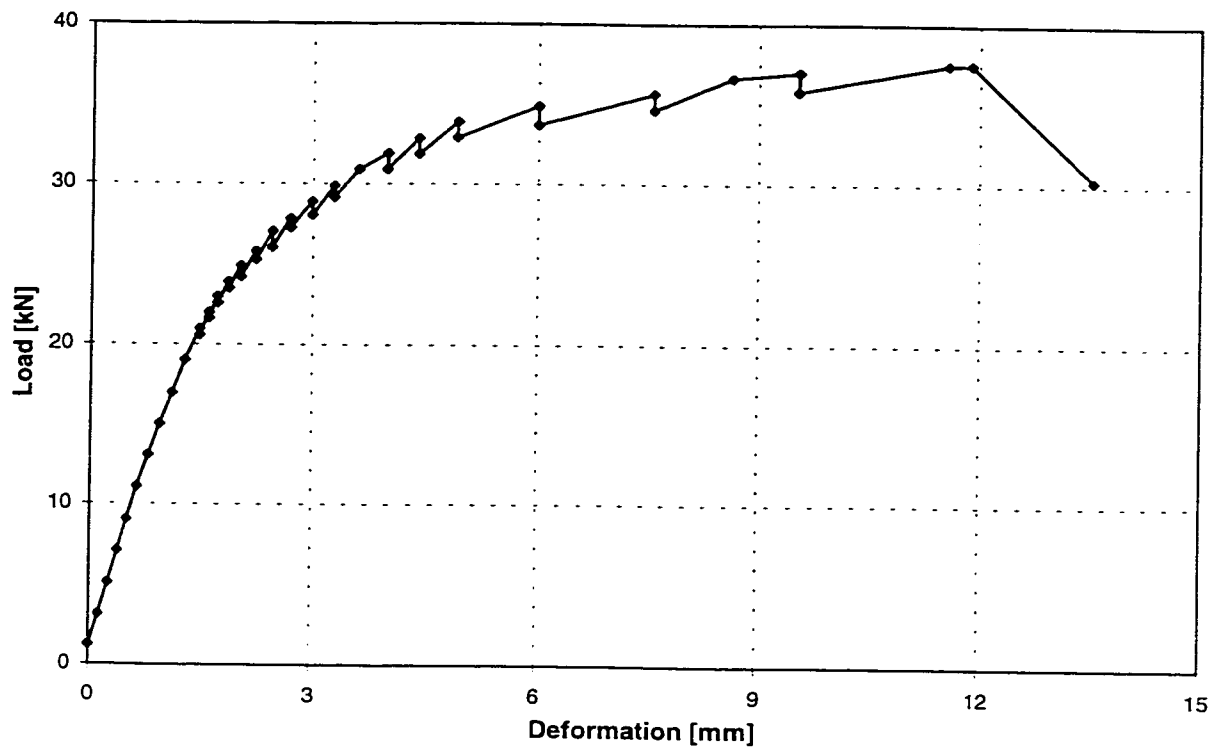
Figure A.15 Load vs. Deformation Curve for Specimen C2-3
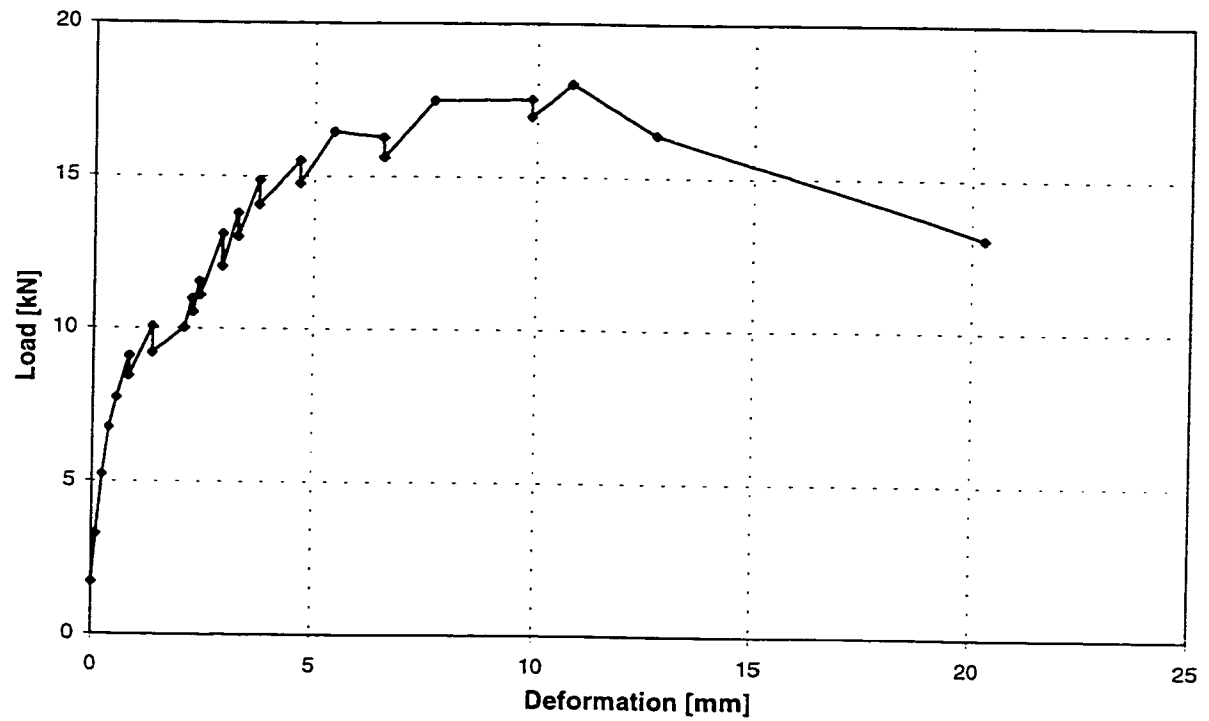
Figure A.16 Load vs. Deformation Curve for Specimen C3-1
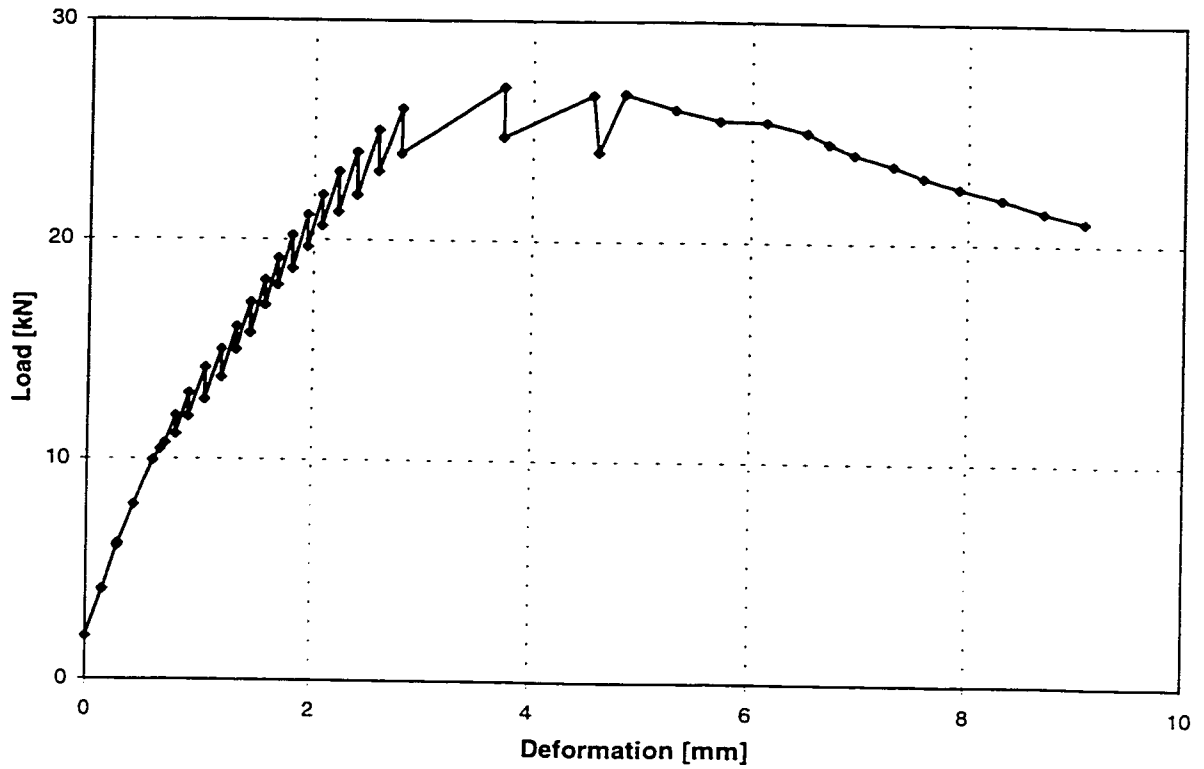
Figure A.17 Load vs. Deformation Curve for Specimen *C3-1
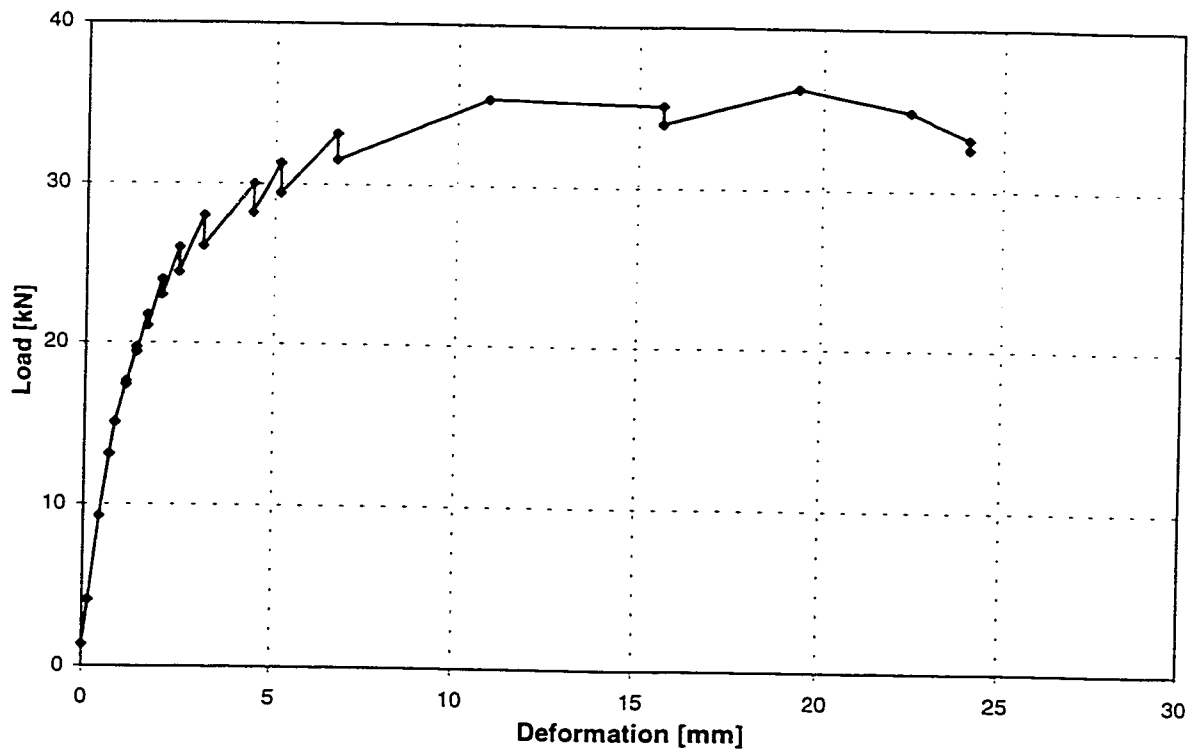
Figure A.18 Load vs. Deformation Curve for Specimen C3-2
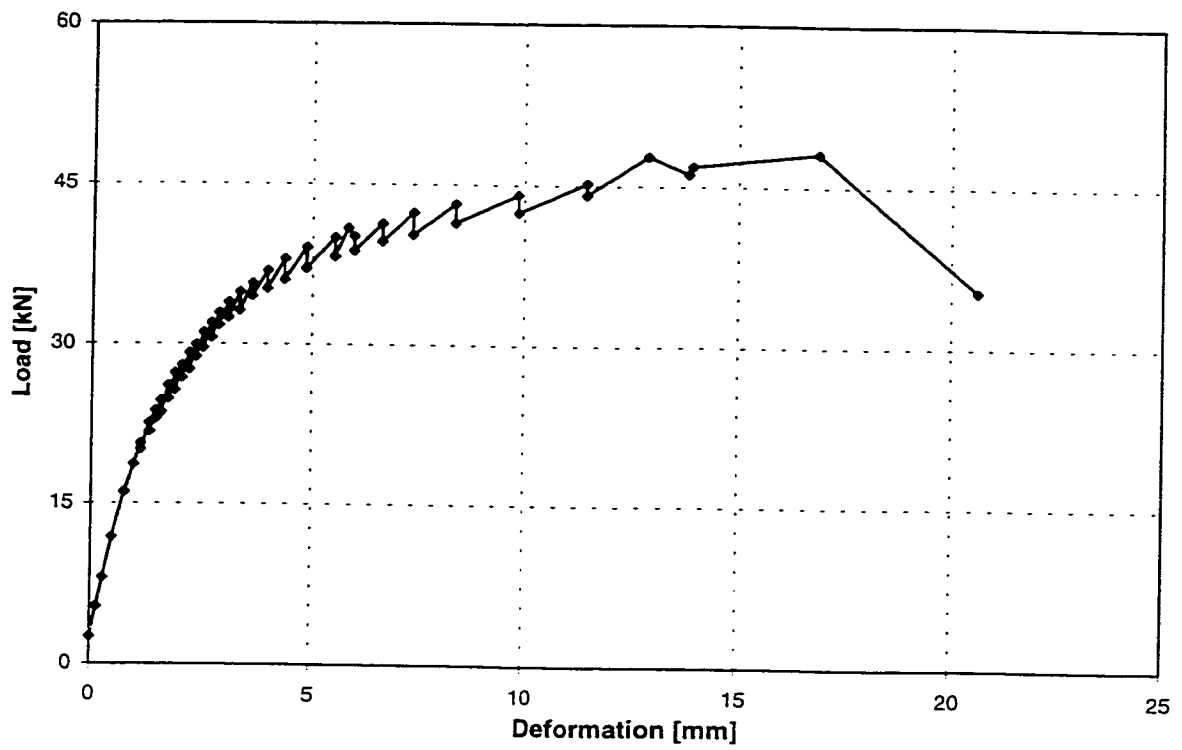
Figure A.19 Load vs. Deformation Curve for Specimen C3-3
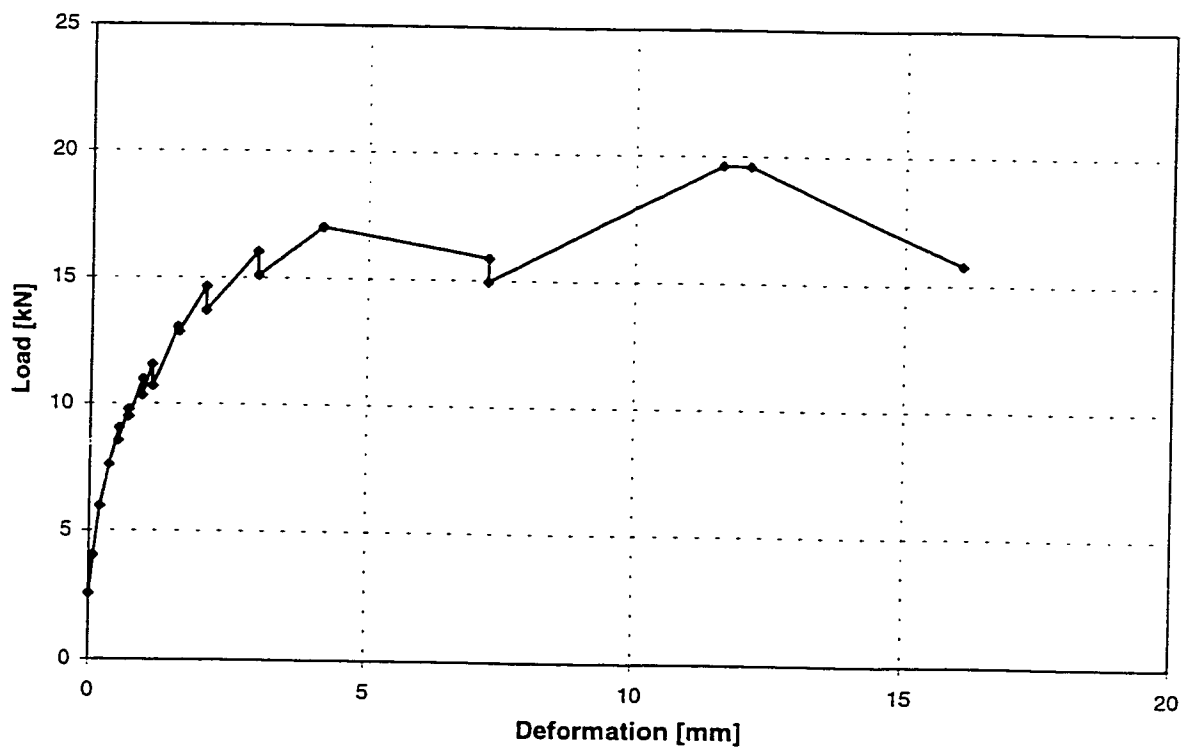
Figure A.20 Load vs. Deformation Curve for Specimen C4-1

142
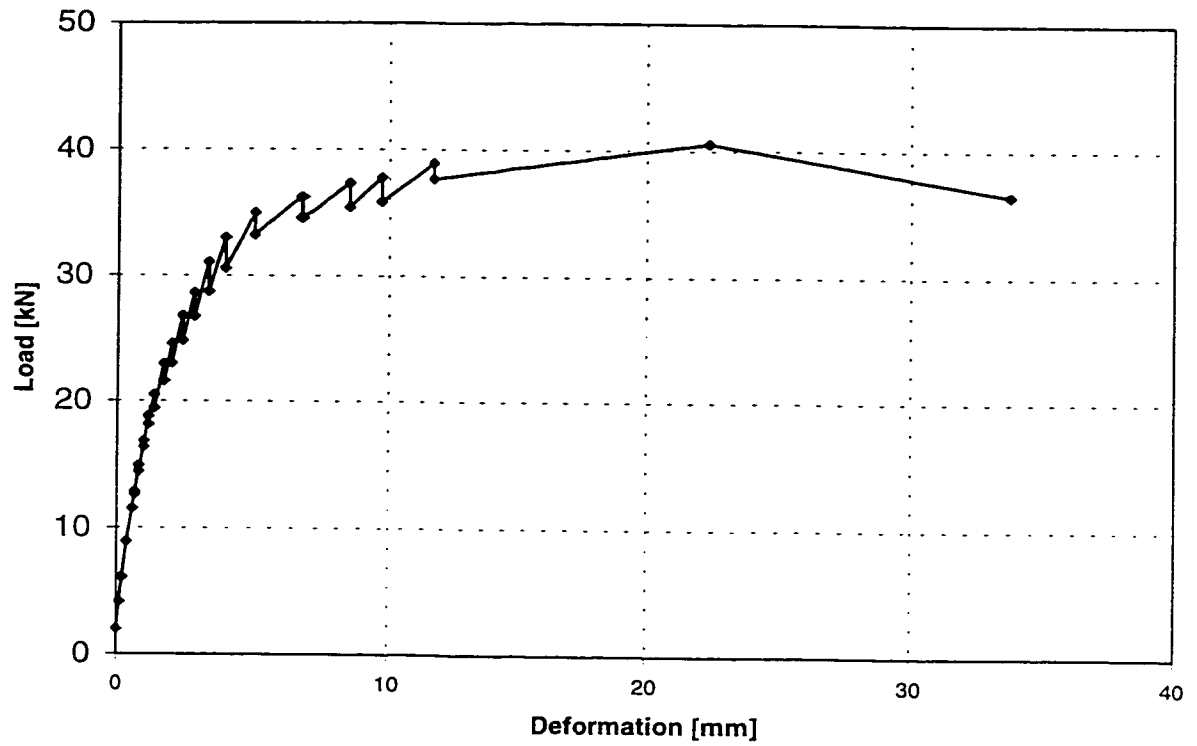
Figure A.21 Load vs. Deformation Curve for Specimen C4-2
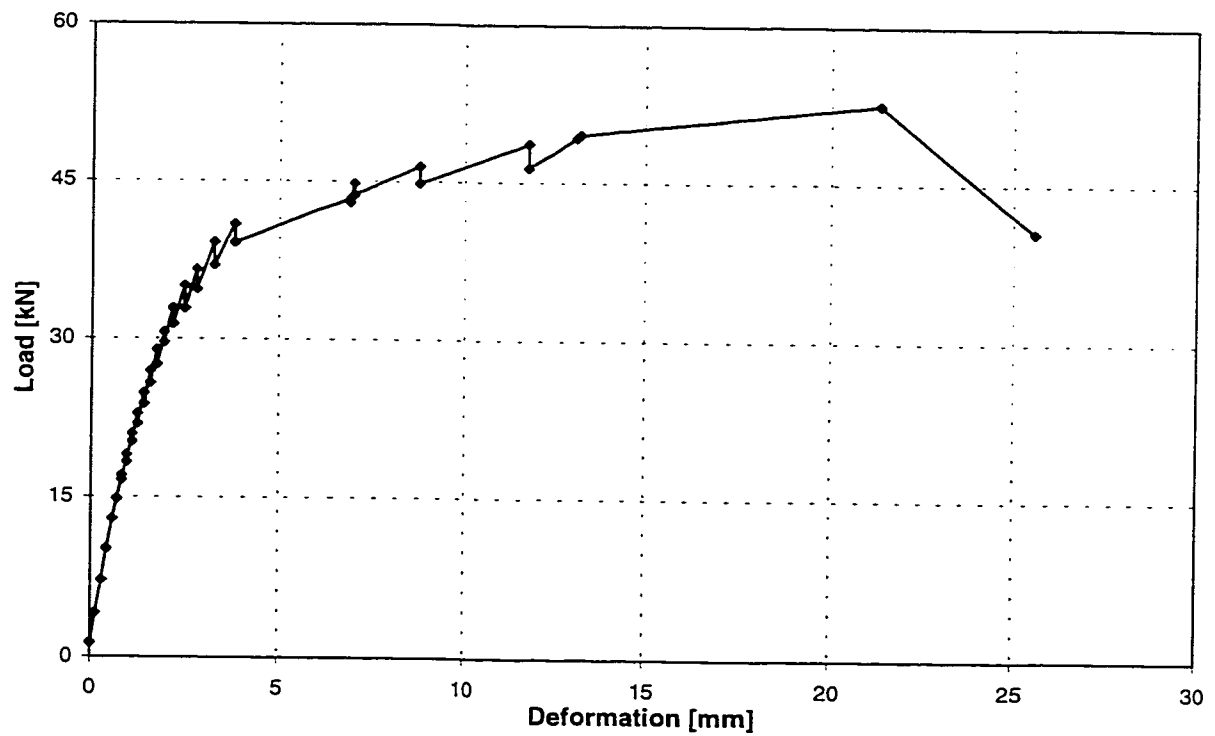
Figure A.22 Load vs. Deformation Curve for Specimen C4-3

143

Figure A.23 Load vs. Deformation Curve for Specimen C4-4

APPENDIX B

LOAD VS. DEFORMATION CURVES OBTAINED FROM THE FINITE

ELEMENT ANALYSIS
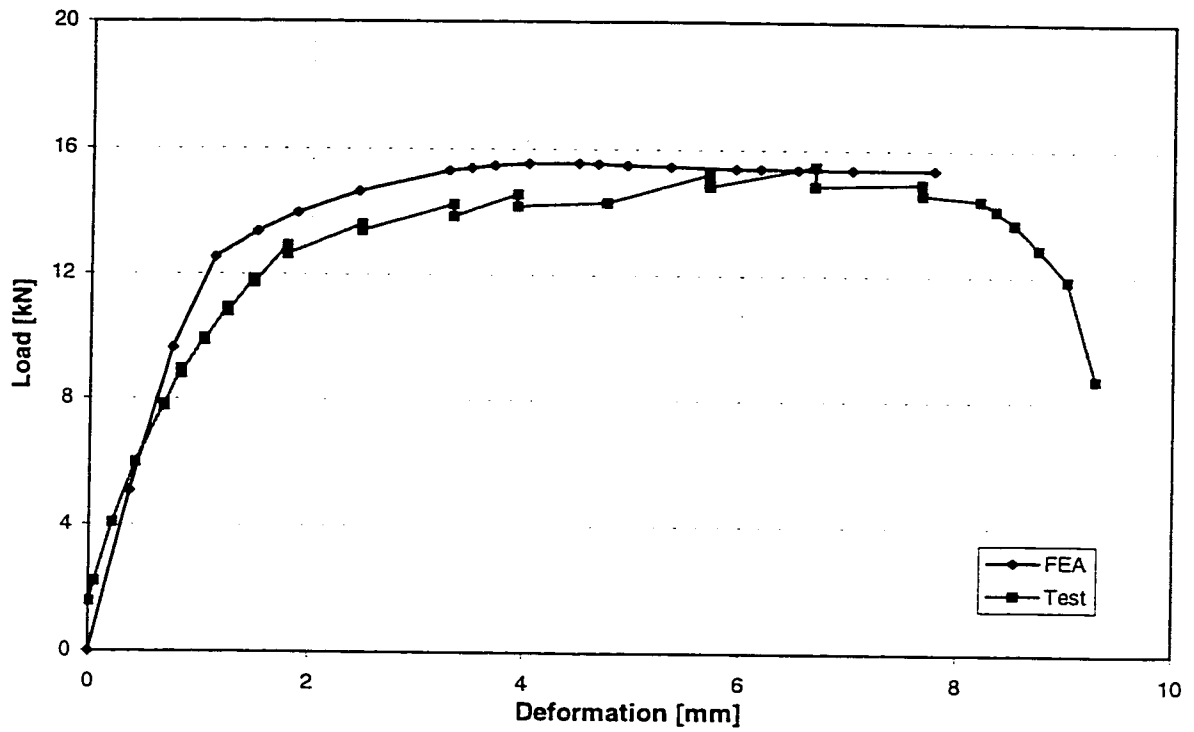
Figure B.1 Comparison of Load vs. Deformation Curves for A2-1
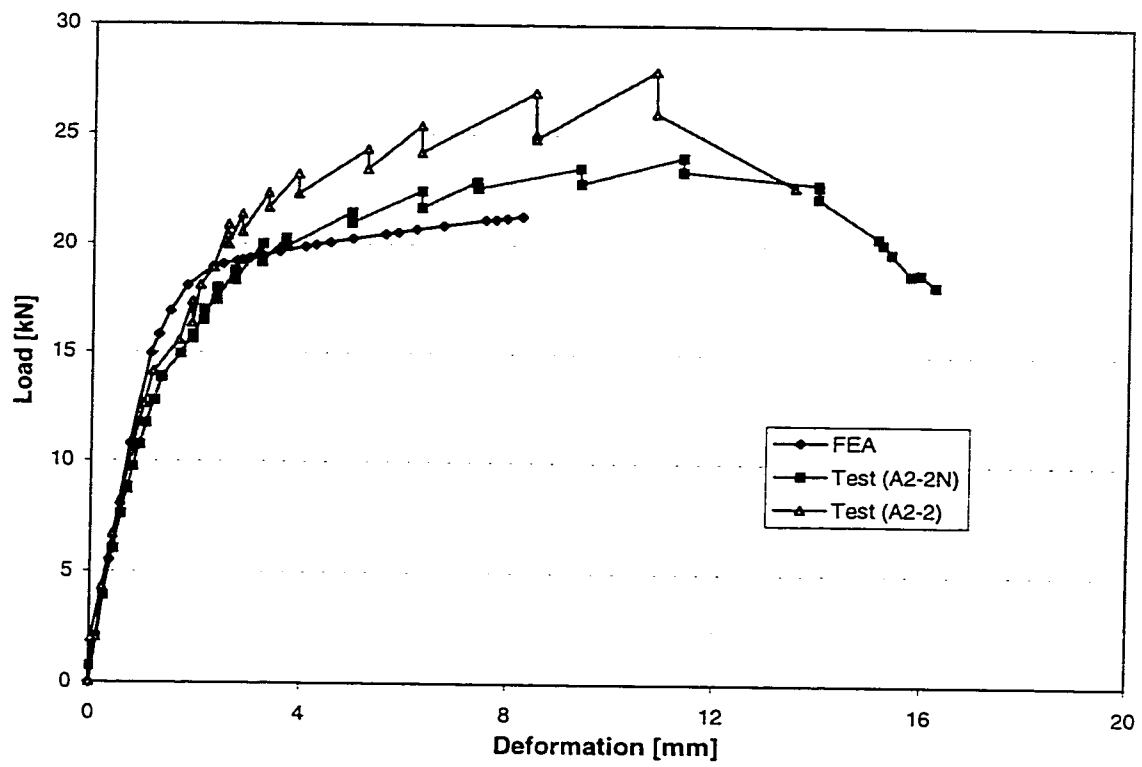
Figure B.2 Comparison of Load vs. Deformation Curves for A2-2

146
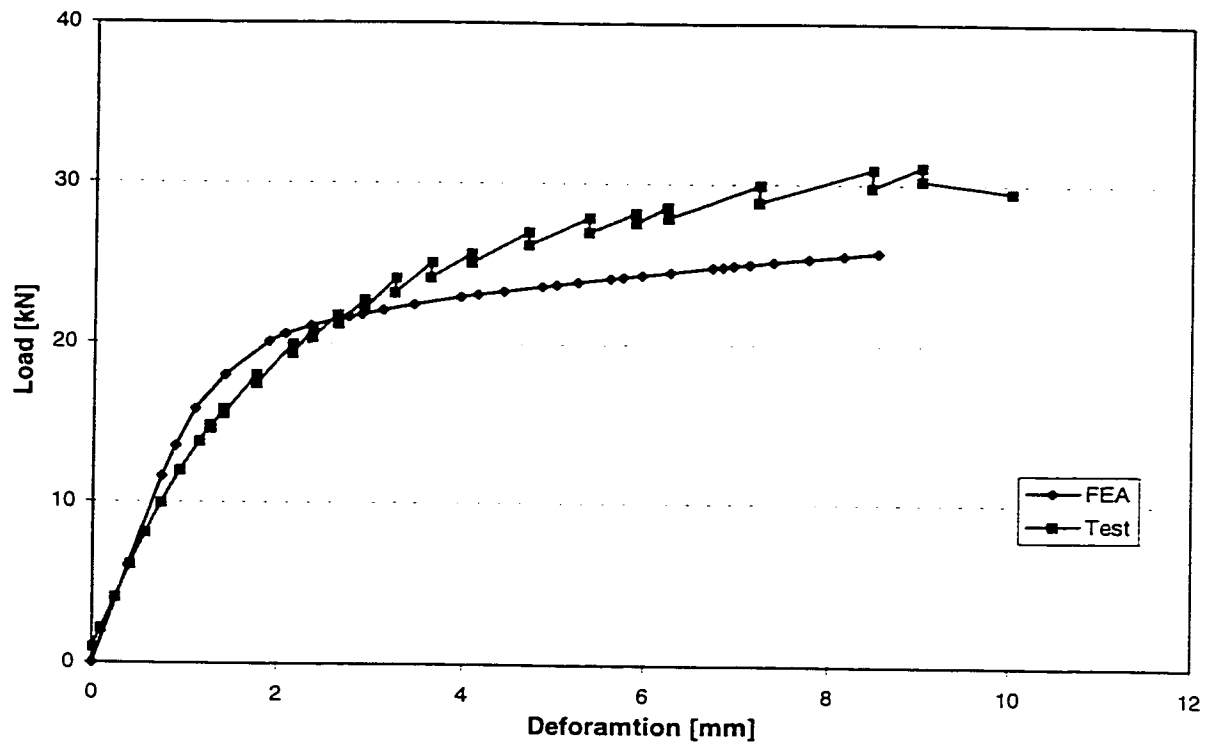
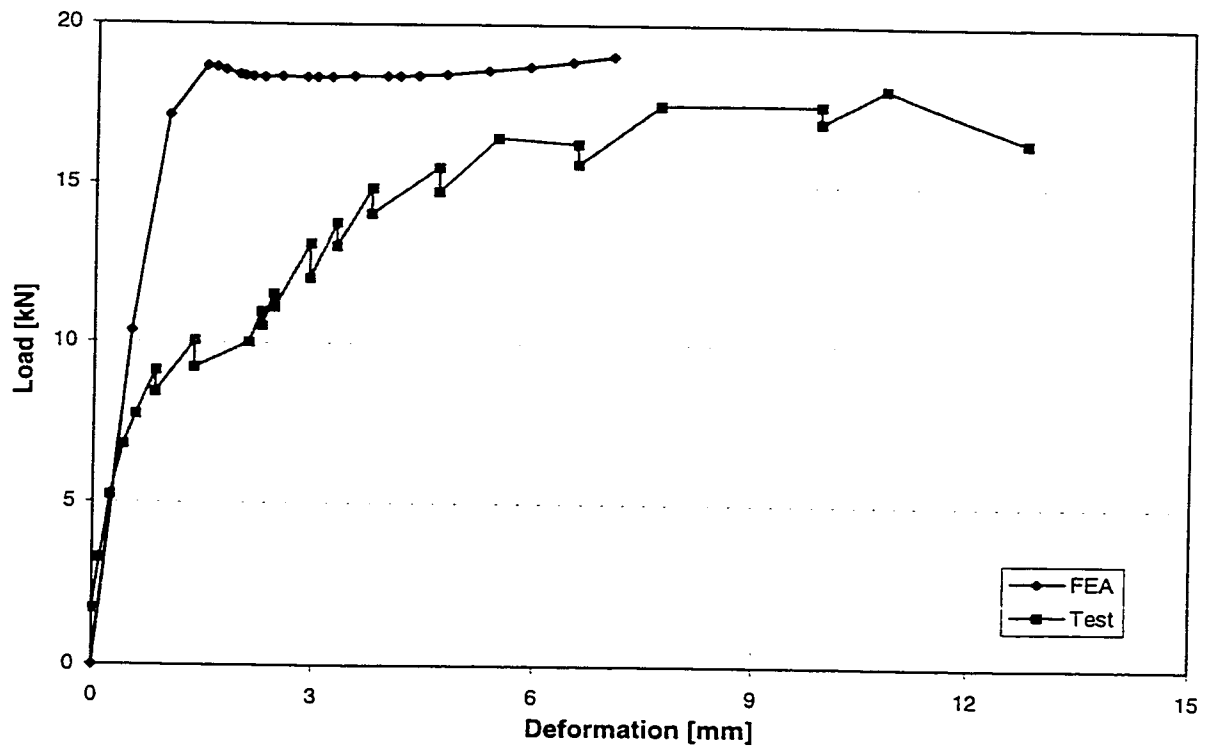Figure B.3 Comparison of Load vs. Deformation Curves for A2-3
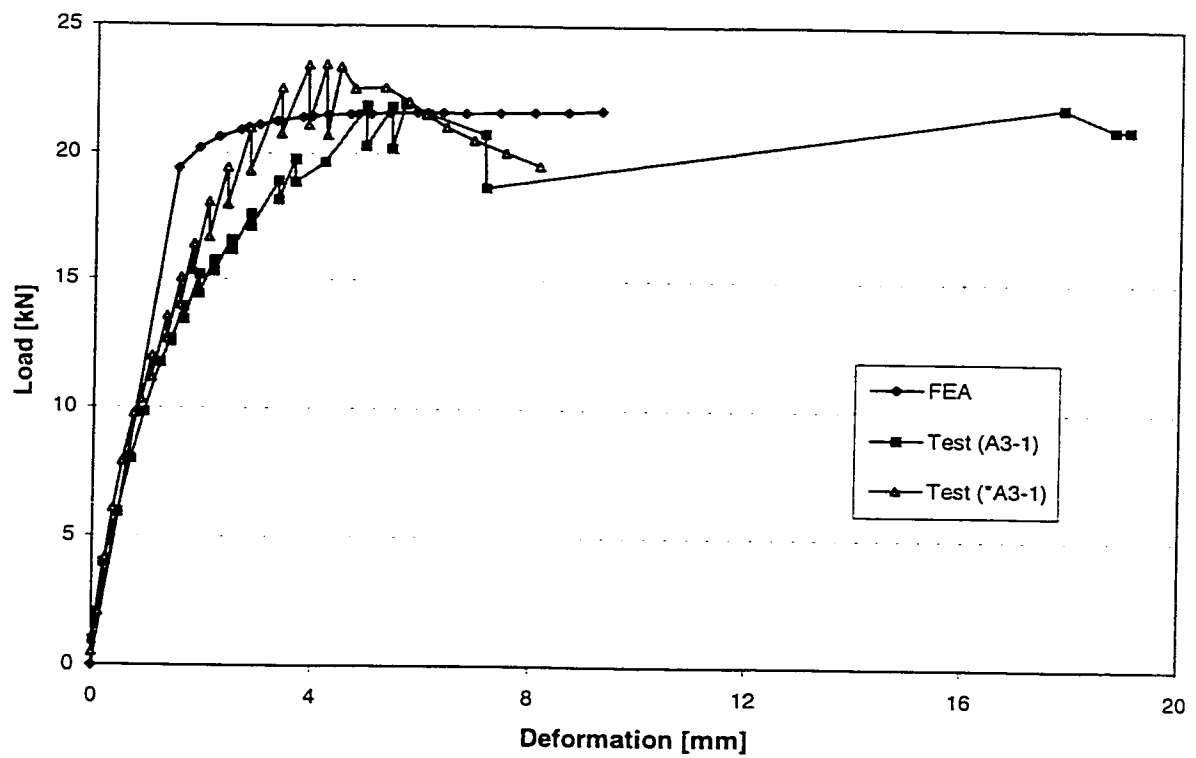
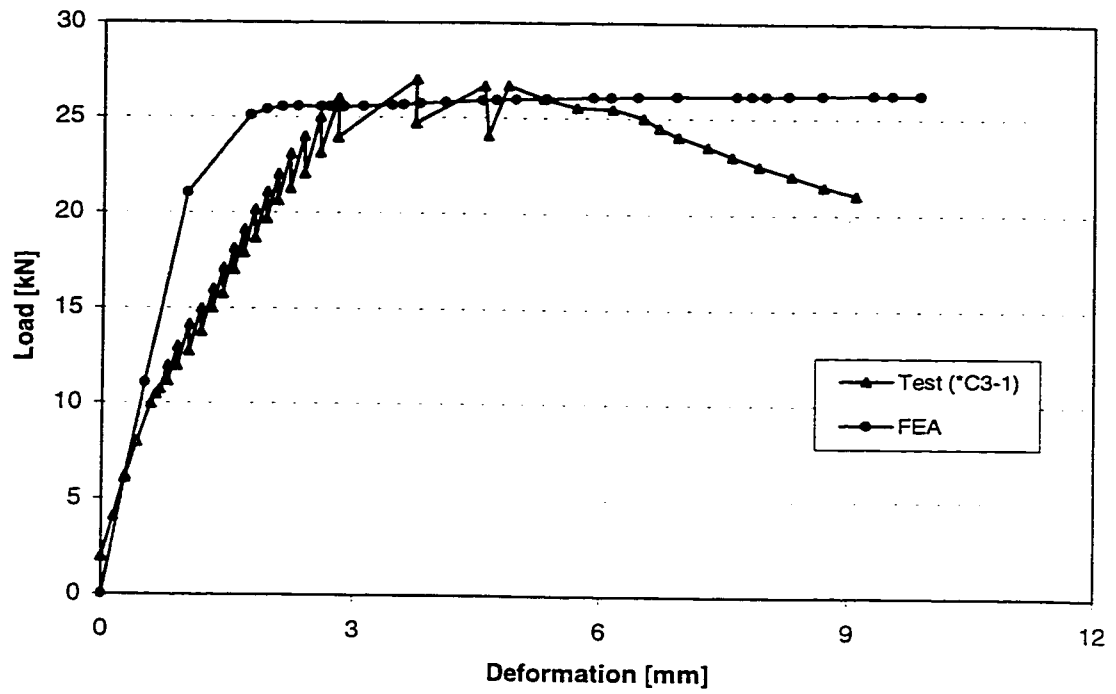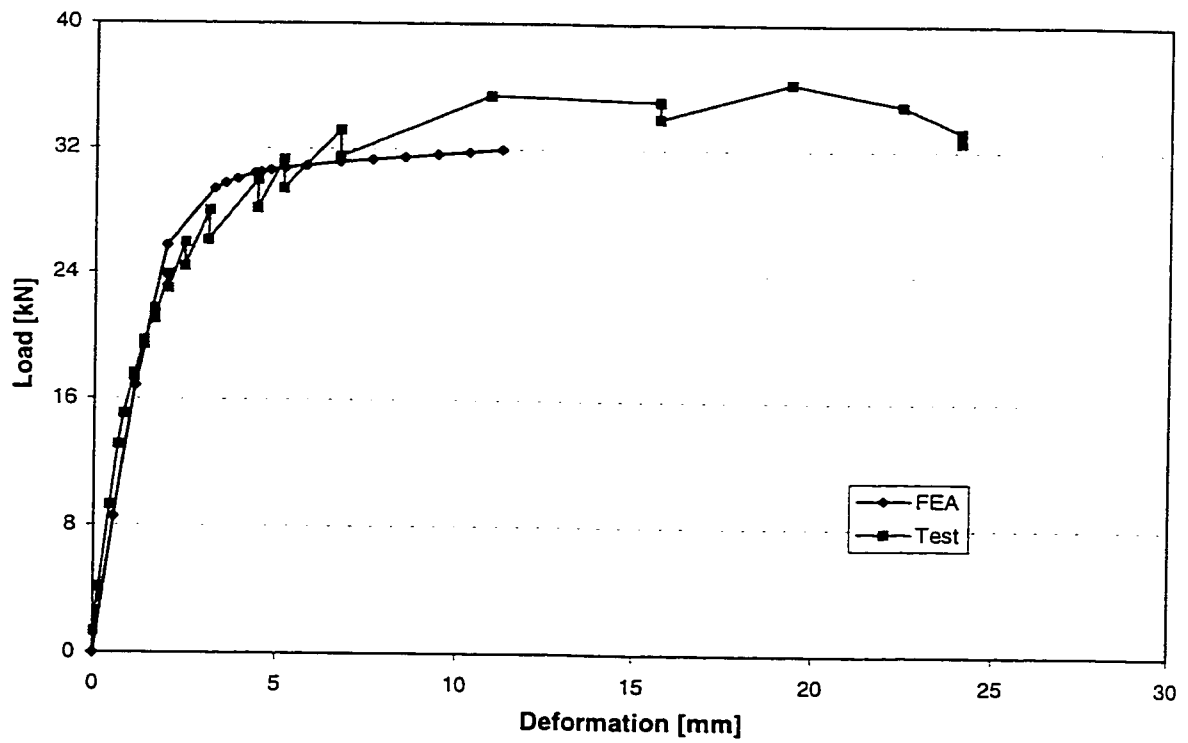Figure B.4 Comparison of Load vs. Deformation Curves for A3-1 and *A3-1

147
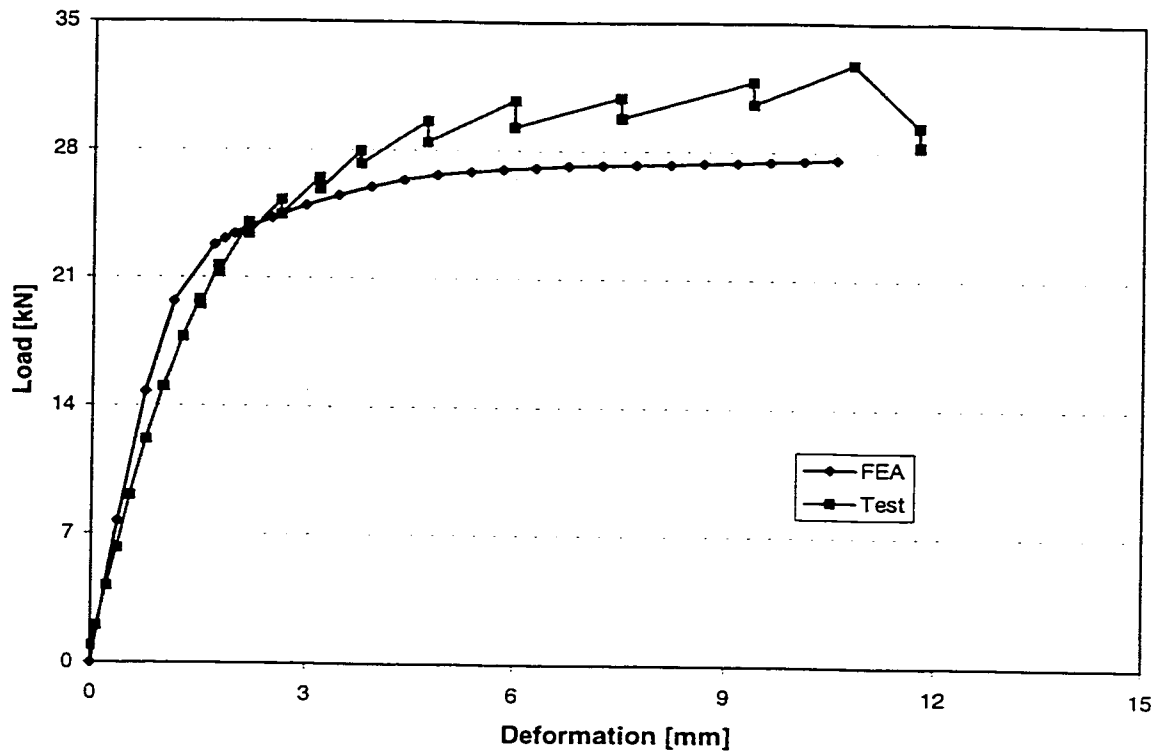
Figure B.5 Comparison of Load vs. Deformation Curves for A3-2
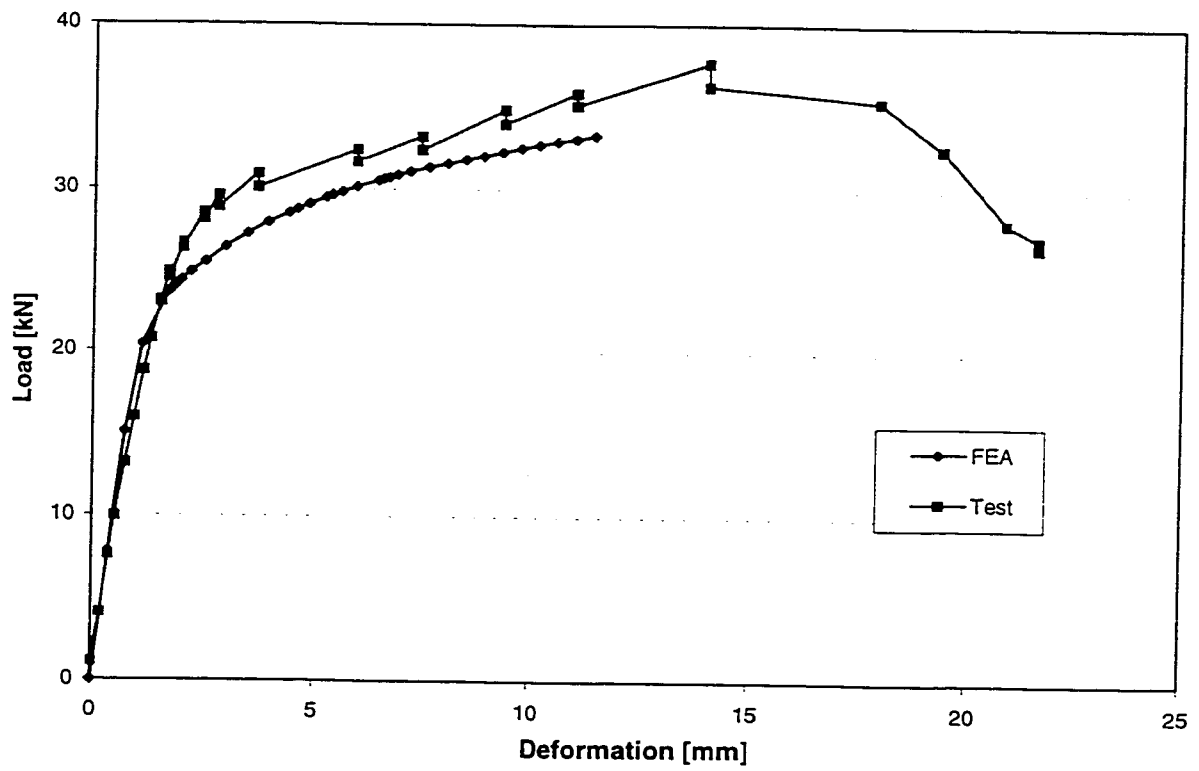
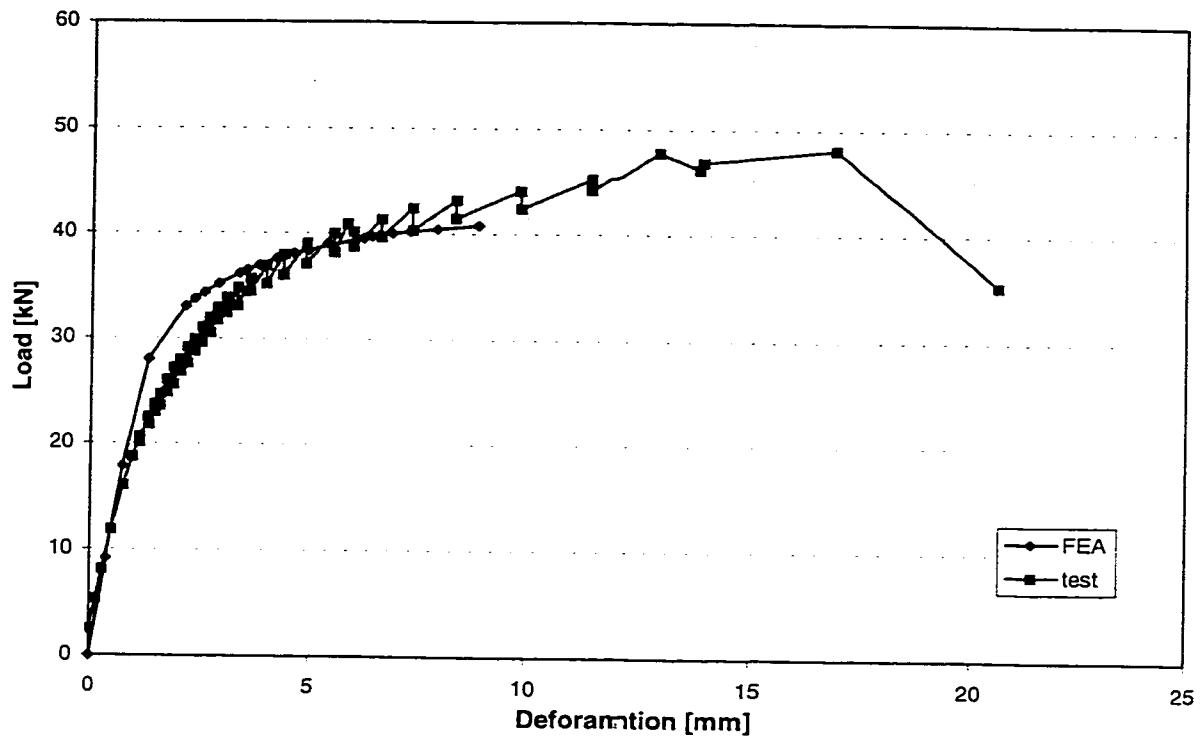Figure B.6 Comparison of Load vs. Deformation Curves for A3-3

148
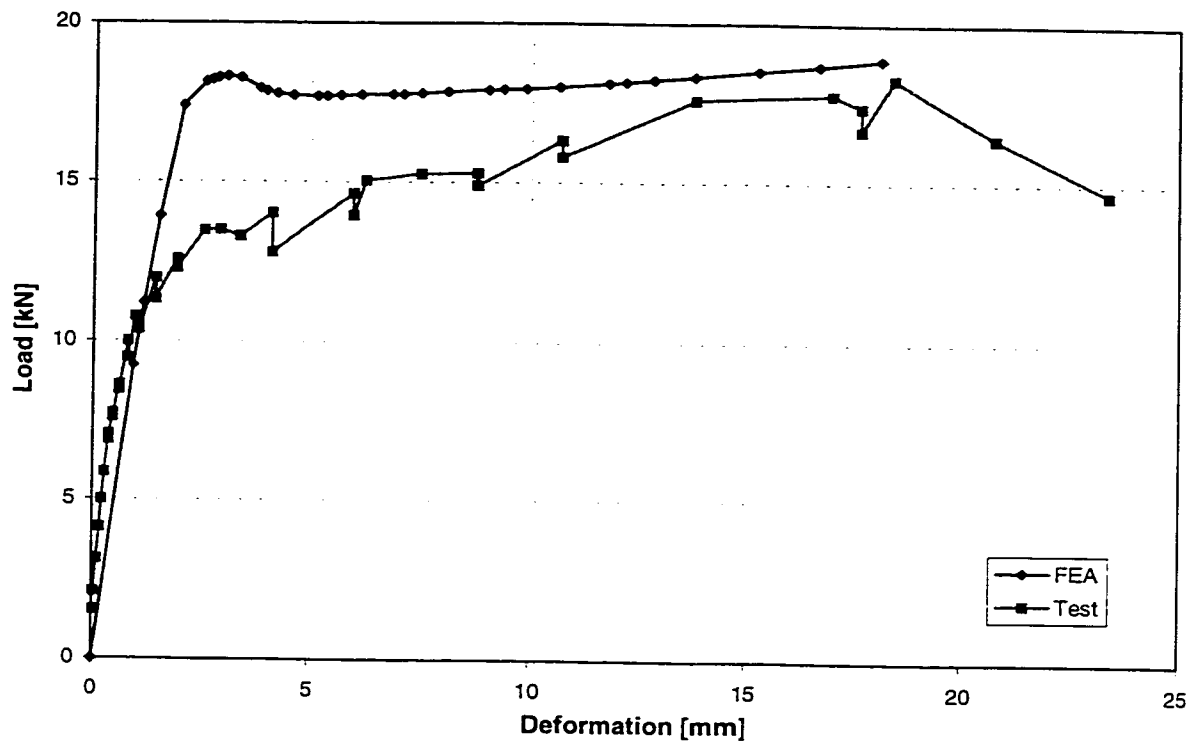
Figure B.7 Comparison of Load vs. Deformation Curves for A4-1
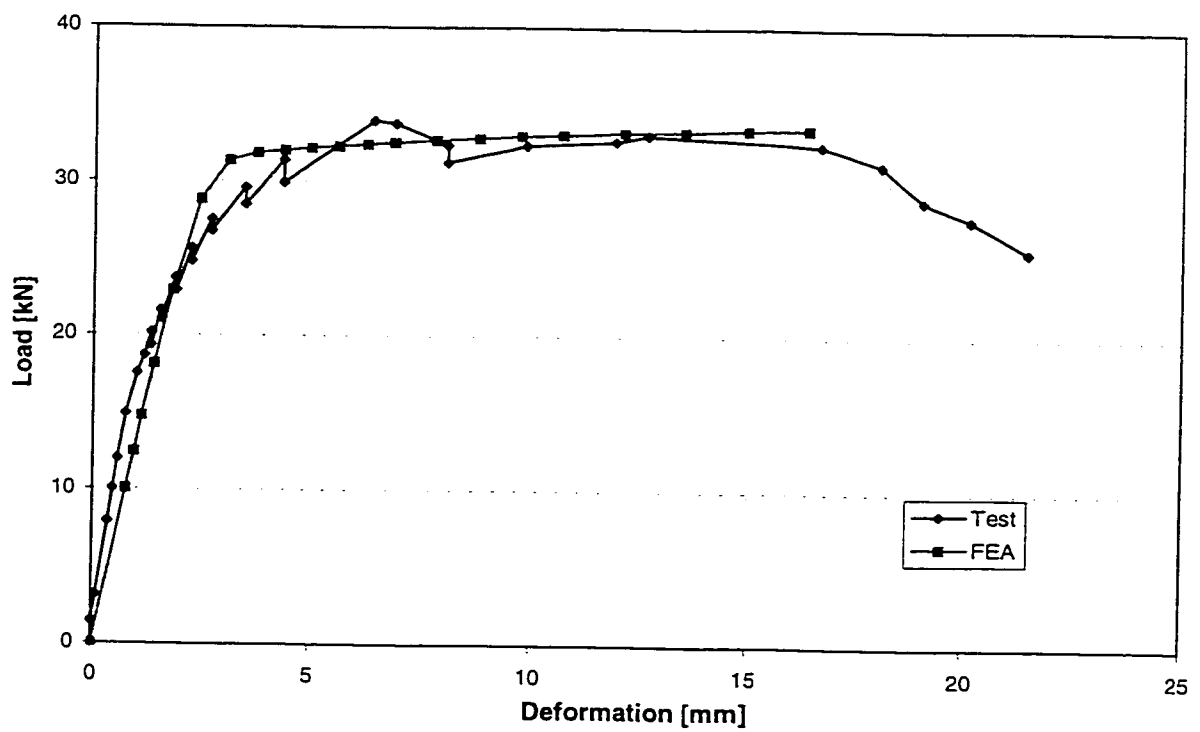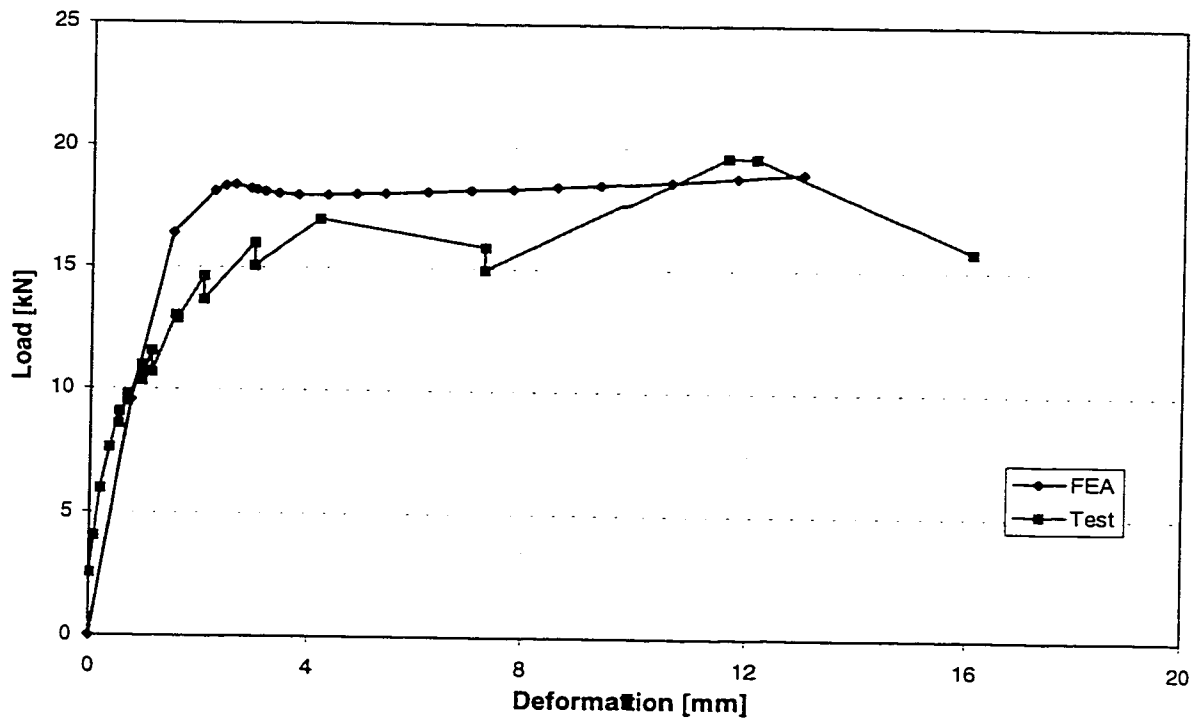

Figure B.8 Comparison of Load vs. Deformation Curves for A4-2

149
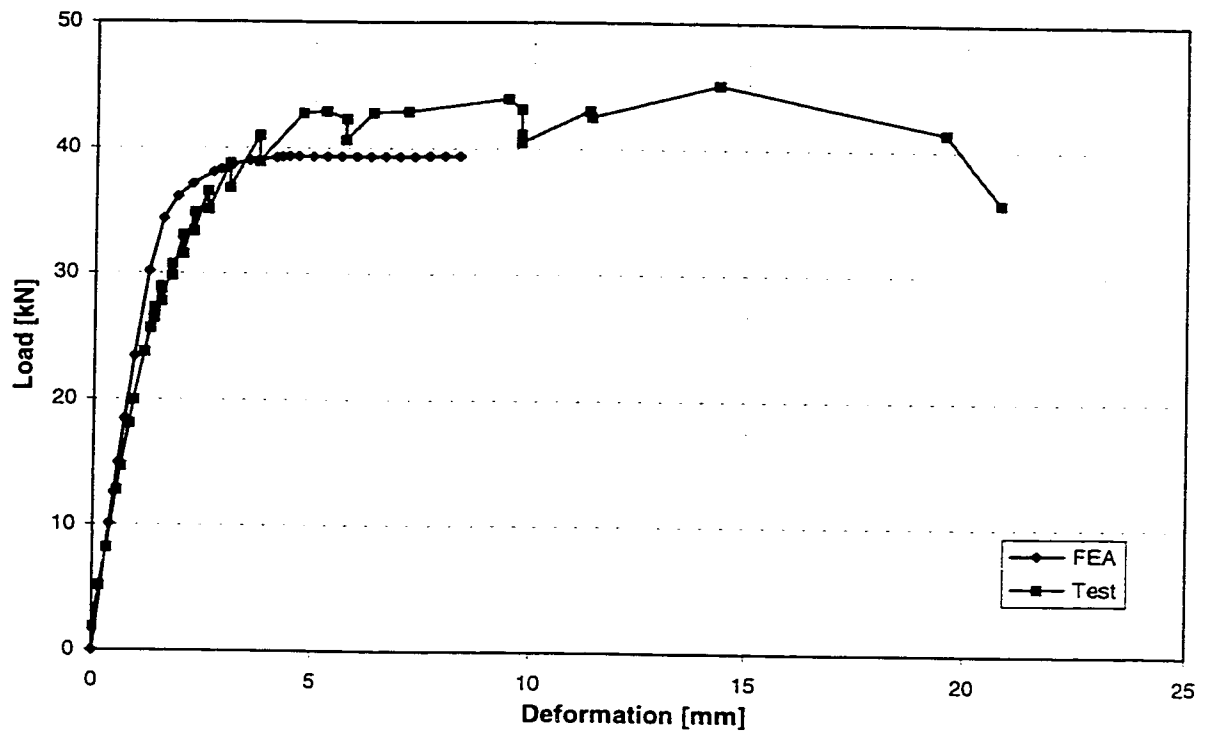
Figure B.9 Comparison of Load vs. Deformation Curves for A4-3
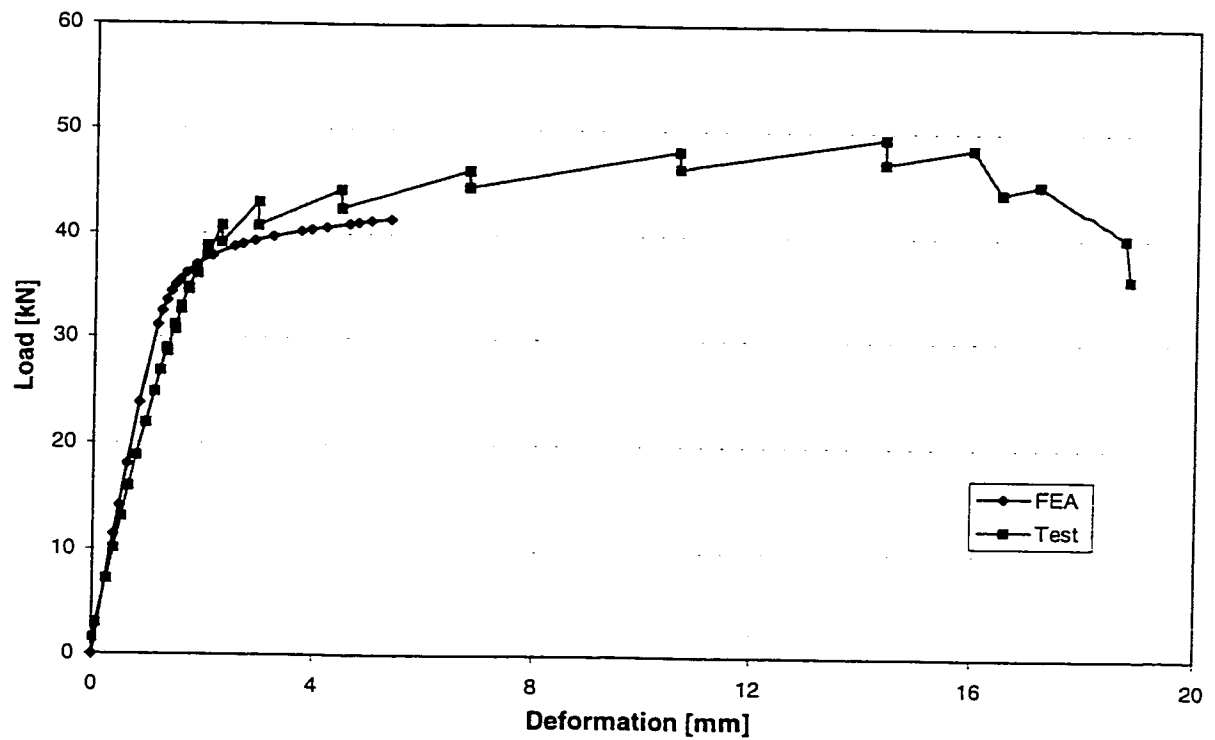
Figure B.10 Comparison of Load vs. Deformation Curves for A4-4

150
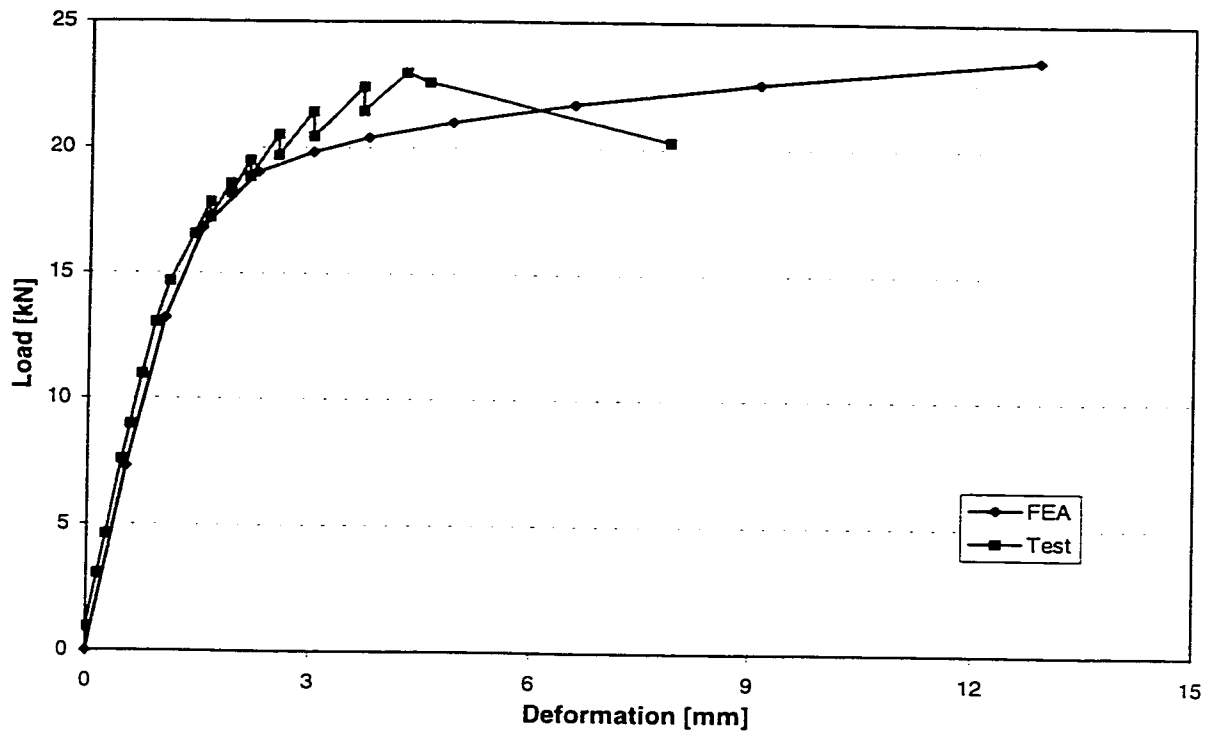
Figure B.11 Comparison of Load vs. Deformation Curves for C2-1
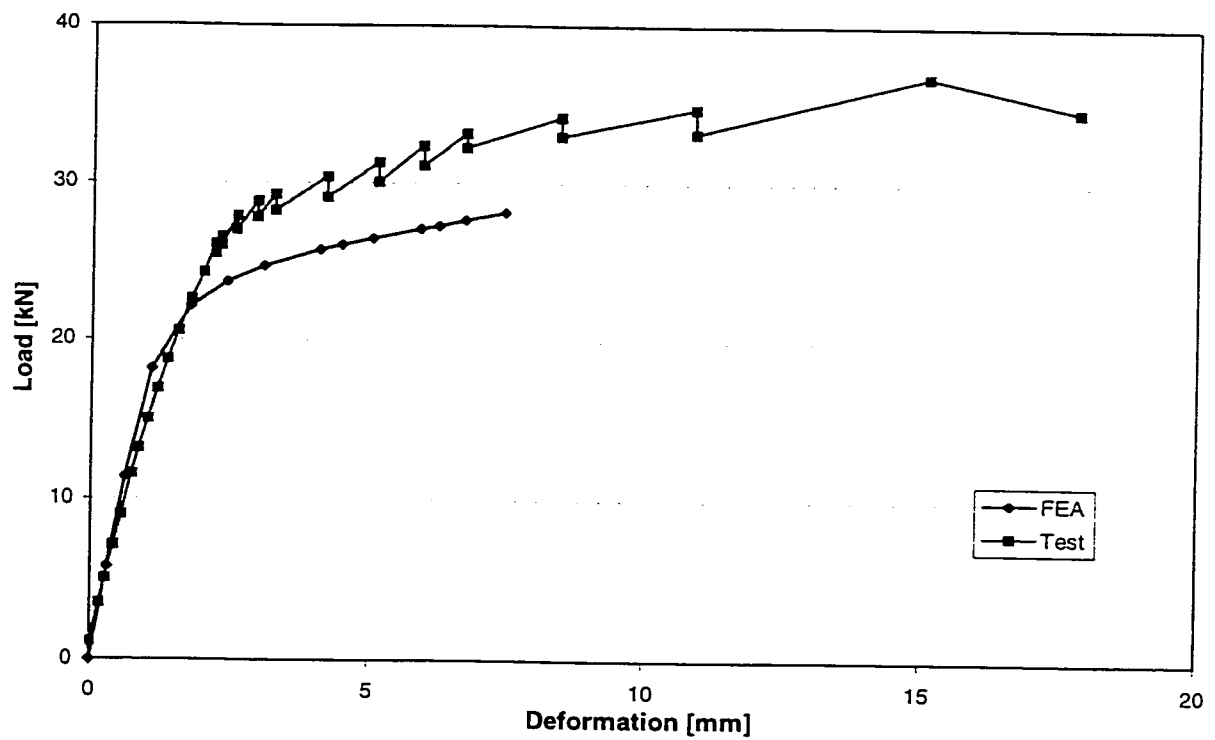
Figure B.12 Comparison of Load vs. Deformation Curves for C2-2

151
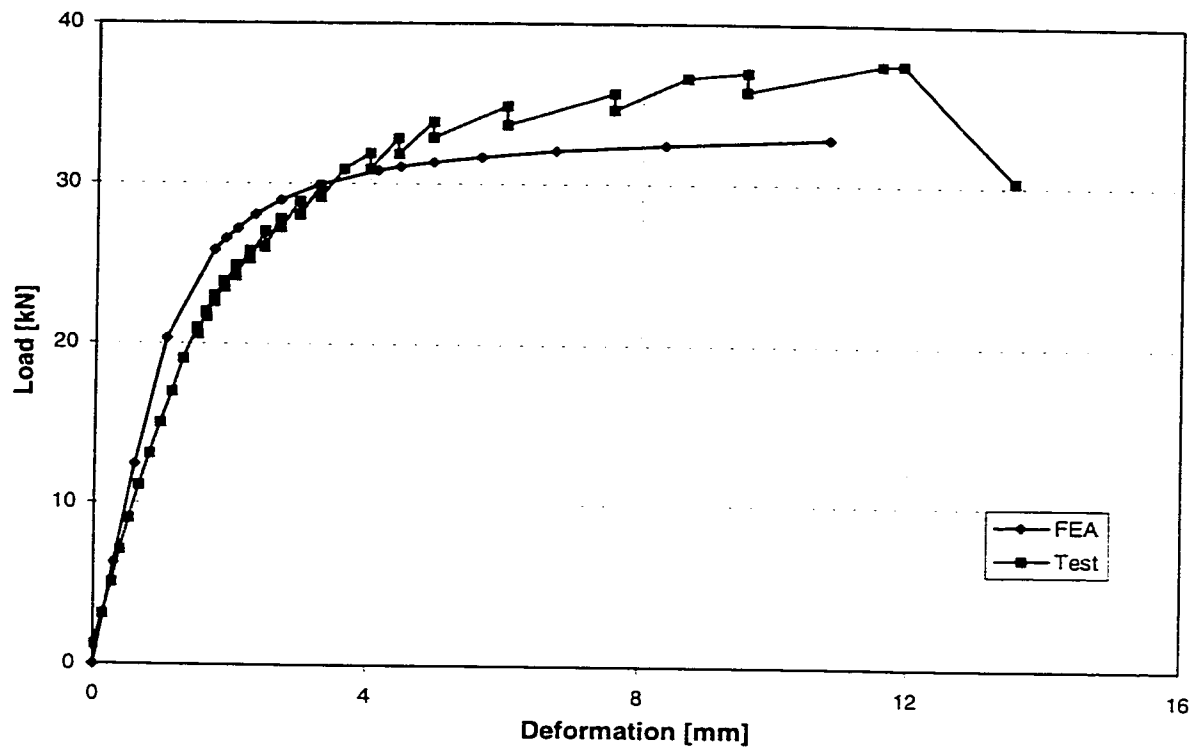
Figure B.13 Comparison of Load vs. Deformation Curves for C2-3

Figure B.14 Comparison of Load vs. Deformation Curves for C3-1

Figure B.15 Comparison of Load vs. Deformation Curves for *C3-1

Figure B.16 Comparison of Load vs. Deformation Curves for C3-2

153

Figure B.17 Comparison of Load vs. Deformation Curves for C3-3

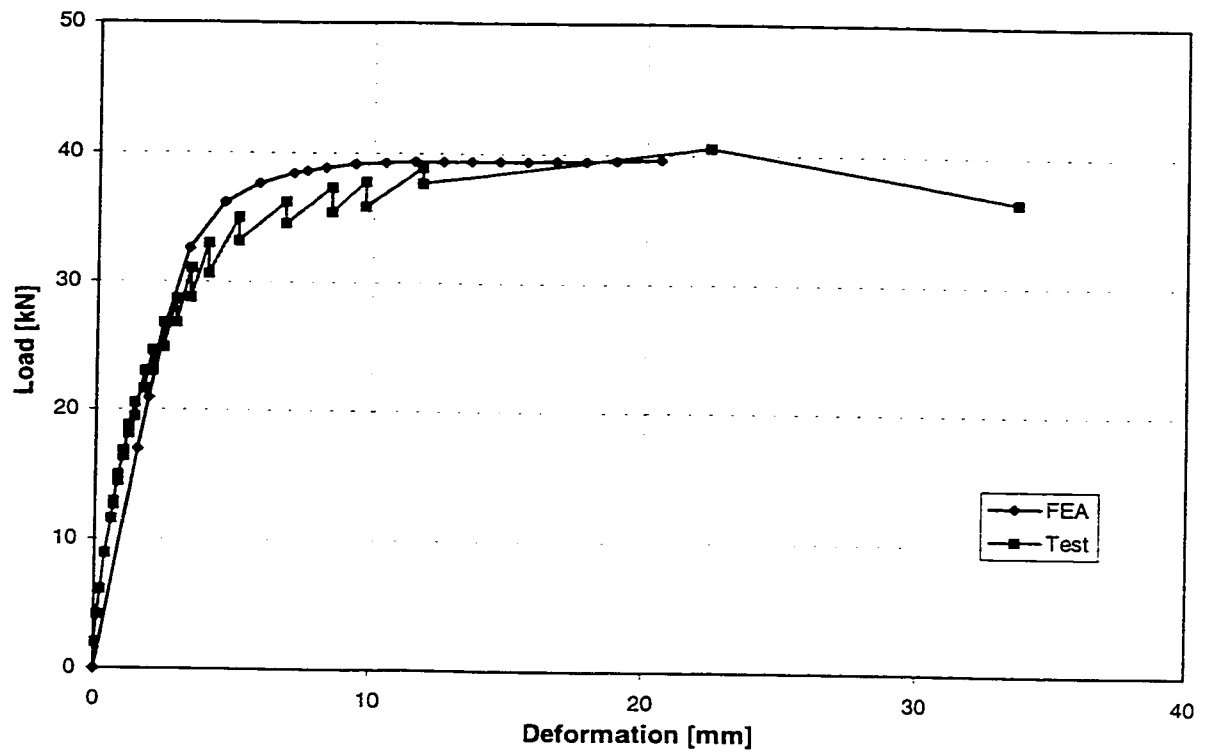Figure B.18 Comparison of Load vs. Deformation Curves for C4-1

154

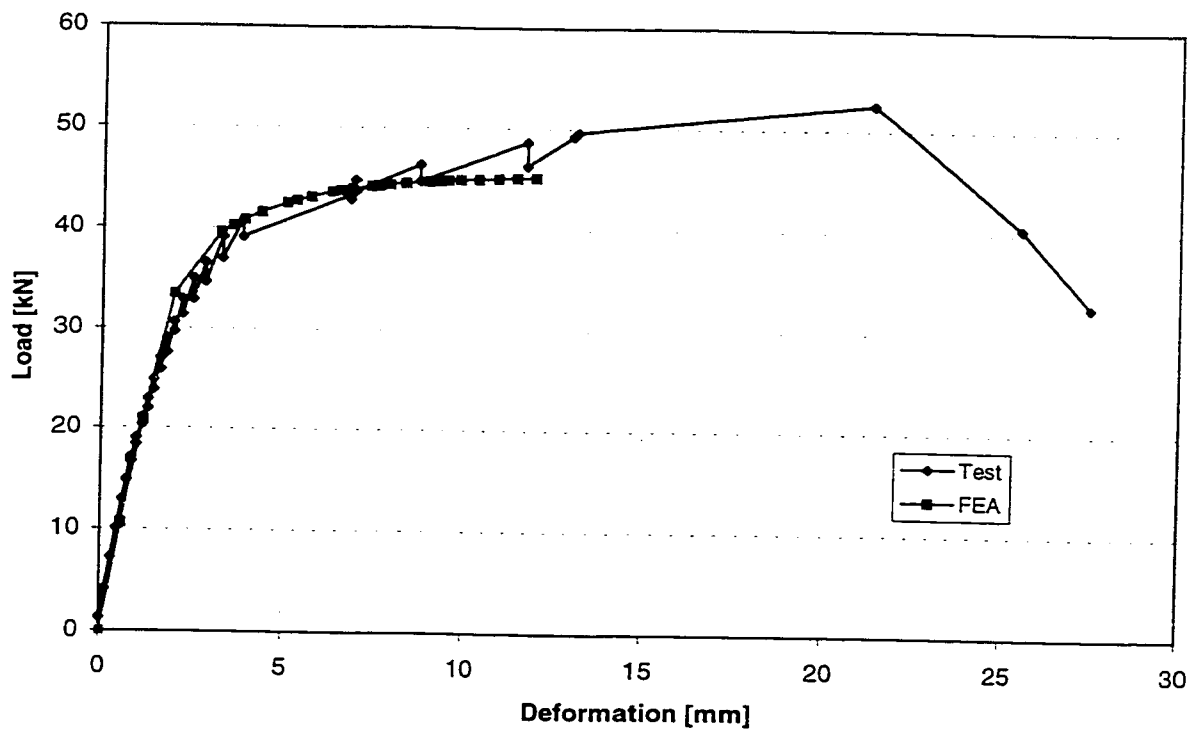Figure B.19 Comparison of Load vs. Deformation Curves for C4-2

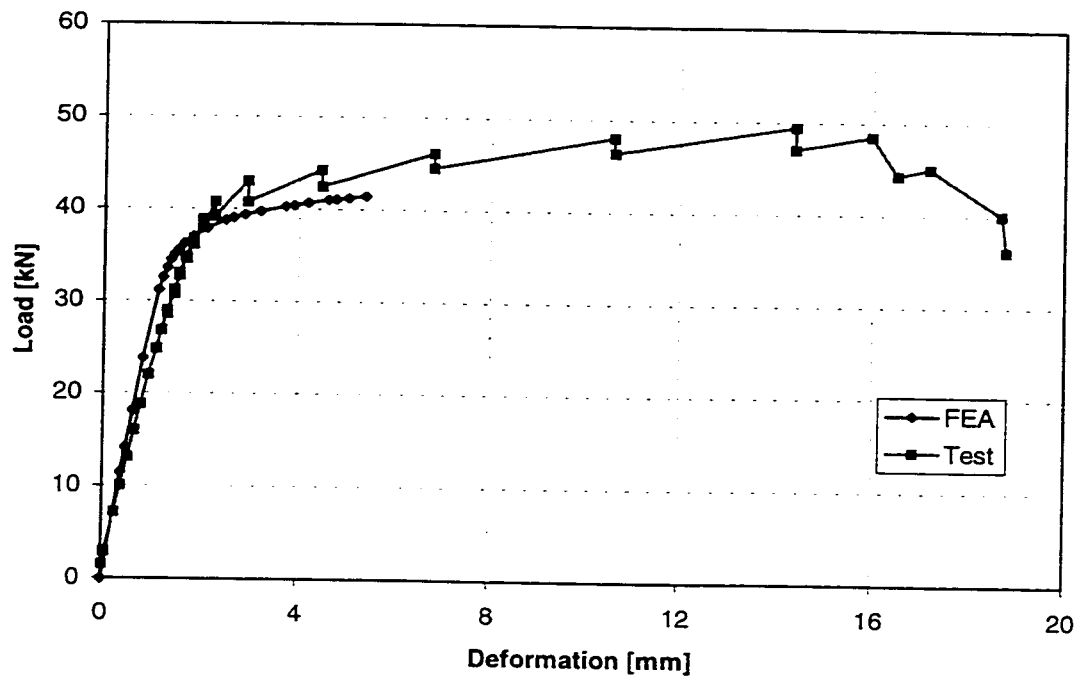Figure B.20 Comparison of Load vs. Deformation Curves for C4-3

155

Figure B.21 Comparison of Load vs. Deformation Curves for C4-4